REPORT DOCUMENTATION PAGE

Form Approved
OMB No. 0704-0188

1. AGENCY USE ONLY (Leave blank)	2. REPORT DATE 19.Oct.99	3. REPORT TYPE AND DATES COVERED DISSERTATION

4. TITLE AND SUBTITLE
THE TRANSIENT RESPONSE OF ROTARY DESICCANT WHEELS THROUGH EXPERIMENTATION AND NUMERICAL ANALYSIS

5. FUNDING NUMBERS

6. AUTHOR(S)
MAJ GRUMBACH STEPHEN D

7. PERFORMING ORGANIZATION NAME(S) AND ADDRESS(ES)
UNIVERSITY OF COLORADO AT BOULDER

8. PERFORMING ORGANIZATION REPORT NUMBER

9. SPONSORING/MONITORING AGENCY NAME(S) AND ADDRESS(ES)
THE DEPARTMENT OF THE AIR FORCE
AFIT/CIA, BLDG 125
2950 P STREET
WPAFB OH 45433

10. SPONSORING/MONITORING AGENCY REPORT NUMBER
FY99-297

11. SUPPLEMENTARY NOTES

12a. DISTRIBUTION AVAILABILITY STATEMENT
Unlimited distribution
In Accordance With AFI 35-205/AFIT Sup 1

12b. DISTRIBUTION CODE

13. ABSTRACT (Maximum 200 words)

19991108 132

14. SUBJECT TERMS

15. NUMBER OF PAGES
266

16. PRICE CODE

17. SECURITY CLASSIFICATION OF REPORT	18. SECURITY CLASSIFICATION OF THIS PAGE	19. SECURITY CLASSIFICATION OF ABSTRACT	20. LIMITATION OF ABSTRACT
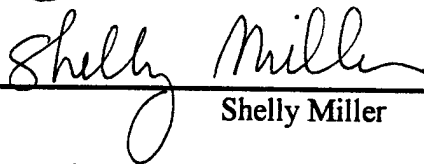
DTIC QUALITY INSPECTED 4

This thesis entitled

The Transient Response of Rotary Desiccant Wheels Through

Experimentation and Numerical Analysis

Written by Stephen Delbert Grumbach

Has been approved for the Department of Civil Engineering

_____
Michael J. Brandemuehl, chair

_____
Shelly Miller

_____
Peter Curtiss

_____
Jan Kreider

_____
Moncef Krarti

Date_____

The final copy of this thesis has been examined by the signatories, and we find that both the content and the form meet acceptable presentation standards of scholarly work in the above mentioned discipline.

i

ABSTRACT

Grumbach, Stephen Delbert (Ph.D. Civil Engineering)
The Transient Response of Rotary Desiccant Wheels: Heat and Mass Transfer
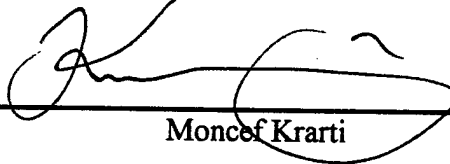Thesis directed by Professor Michael J. Brandemuehl

Rotary desiccant wheels are commonly used for industrial dehumidification systems and significant research has also been done to increase their application in other HVAC systems. The transient response is of concern because it can affect system overall performance and previous research efforts have indicated the transient response to be of substantial duration.

This research experimentally and analytically investigated the transient response of rotary desiccant wheels.

A model was developed to predict the transient response of rotary desiccant wheels with significant improvements to previous versions. The basic model uses fundamental principles of heat and mass transfer with the finite difference method. The parabolic concentration profile was used to approximate moisture gradients within the desiccant particle. This concept is fundamentally more correct than previous lumped capacitance models and avoids the computational difficulties of more rigorous models which include an extra second order differential equation. The NTU terms from the finite difference equations were also calculated at each point rather than as constants for a stream or wedge since they are significantly temperature and moisture dependent. The numerical solution techniques improved the speed and flexibility of the model by using a tri-diagonally

banded matrix solver for the difference equations and the bisection method was used for the parabolic concentration profile.

Experimental work was performed at the National Renewable Energy Laboratory (NREL) in Golden, CO on a commercially available rotary desiccant wheel made by NovelAire. Step changes to regeneration temperature, wheel speed, and flowrate were performed. The model validated very well using the experimental data through statistical and visual analysis of the outlet condition (temperature, humidity ratio) response curves. An alternative validation technique was also performed by statistically comparing thermographic images of the desiccant wheel surface with numerical calculations.

A parametric analysis was completed to observe the impact of different parameters on the transient response. Operational factors, ambient conditions, and wheel construction can have a substantial impact on the transient response by as much as 67%.

A control strategy comparison was done that determined cycling of rotary desiccant wheels can be an effective and efficient strategy to meet moisture removal requirements.

The Transient Response of Rotary Desiccant Wheels through Experimental and Numerical Analysis: Part I, Modeling and Validation.

Introduction

Desiccant systems have been a successful alternative to conventional air conditioning systems for certain dehumidification applications and are capable of "deep drying" air to very low humidity ratios. The most common desiccant system used is the rotary desiccant wheel as shown in . The psychrometric chart shows that the desiccant wheel exchanges latent load or moisture for sensible load or temperature with a very small change in enthalpy.

One concern with increasing the application of rotary desiccant wheels for dehumidification is the transient period of the wheel itself. In many cases cooling and dehumidification systems are configured to modulate or "cycle" in order to maintain setpoint and/or reduce energy consumption. A long transient period with the rotary desiccant wheel could significantly affect both the effectiveness and efficiency of the whole system. Previous research has not adequately quantified this phenomena and, as a result, there is significant variability in the estimates of the transient response for a given condition with the rotary desiccant wheel.

The purpose of this paper is therefore to quantify the transient response through experimental and numerical analysis.
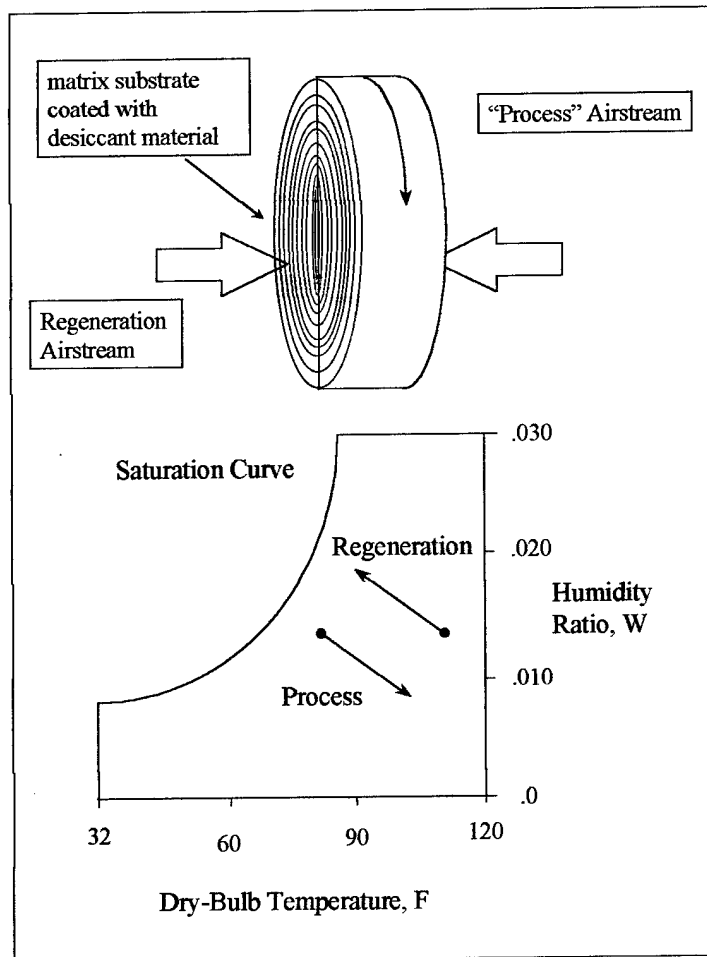
Figure 1. Simple Desiccant Schematic and Psychrometric Chart

Literature Review

The study of rotary desiccant wheels proceeds from the field of heat and mass regenerators. The dominant mechanisms are known to be convection for heat transfer and both convection and solid-side diffusion for the mass transfer. The basic differential equations governing conservation of mass and energy and the transfer rate equations for energy and mass have long been known. To date, there has been no complete analytical solution to these equations. In order to solve them, various numerical and simplification procedures have been created.

The different models that exist have been categorized several different ways. One division is between the models with complex mathematical detail (finite difference solutions) and those constructed for ease of computation (analogy, pseudo-steady-state, etc.). The simplified models have

primarily been constructed in order to minimize the complexity and computational time as well as to provide general insights. Within the finite difference models, there is also a division as to how to account for the modeling of the solid-side diffusion. The most fundamental models are known as the gas and solid side (GSS) models. They add a second order differential equation to account for the mass diffusion and moisture gradients within the particle. The extra second order equation adds complexity and computational time. A second type of model uses a "lumped capacitance" mass transfer coefficient for the overall mass transfer. These are known as the psudeo gas side (PGS) models. Essentially, this takes an analytically developed convective mass transfer coefficient and then empirically degrades it to account for the solid side diffusion. The trade-off has been decreased computational time and lower flexibility with the PGS method compared to increased complexity/flexibility and increased computation time for the more fundamental gas and solid-side model (GSS). This section will highlight some of the more significant developments that have been made in a chronological order.

Work by Hausen [1929] on sensible heat regenerators is considered the groundwork for rotary regenerators. He developed solutions to the governing equations for the periodic steady-state solution of a balanced and symmetric regenerator: first by graphical eigenfunctions and then by graphically solving central difference equations.

Rosen's [1951] paper on fixed bed sorption performed a rigorous solution of the surface and intraparticle diffusion. It is considered the classical solution to fixed bed sorption.

The article by Coppage and London [1953] describes the periodic flow rotary regenerator and compares it with other heat exchanger systems. This article is one of the first to model the differential element of the rotary heat exchanger as a crossflow heat exchanger. It summarizes the basic relations and describes some of these early solution techniques by Hausen, Nusselt, Boestad, Illiffe, and Saunders.

Lambertson [1958] presented a numerical, finite-difference solution to the sensible heat regenerator in periodic steady-state for use in calculating effectiveness, ε. He used a central-differencing scheme as proposed by Hausen and elaborated on by Dusinberre in the commentary section after the Coppage and London [1953] article

3

Carter [1966] derived the coupled rate and conservation equations for *transient* heat and mass transfer for a fluid stream passing through a fixed bed of adsorbent. He showed that the controlling mechanisms are the boundary-layer and adsorbed phase diffusion for the mass transfer and the boundary layer convection for the heat transfer. He used an additional diffusion equation to model the diffusion resistance in the desiccant solid. The differential equations were solved using a modified Euler method. The model was used for temperature and concentration prediction of the airflow.

Bullock and Threlkeld [1966] also derived the coupled heat and mass transfer equations for numerical solution. They used a modified Euler method with predictor-corrector routines.

Maclaine-Cross [1972] presented a finite-difference model known as MOSHMX (Method of Solving Heat and Mass Exchange) which has been used extensively by a number of researchers. He uses a gas-side controlled, lumped capacitance mass transfer coefficient that is typically referred to as a pseudo-gas side (PGS) coefficient. His solution technique uses a centrally differenced scheme solved by a matrix inversion technique.

Another method, commonly referred to as the "analogy" method was introduced by Banks [1985], and Maclaine-Cross and Banks [1972], based on earlier works by Henry [1939] and Cassie [1940]. The non-linear coupled heat and mass transfer equations are changed into two separate sets of de-coupled equations that are analogous to heat transfer alone. The basic differential equations are transformed by replacing the original dependent variables with new dependent variables called characteristic potentials. The characteristic potentials are based on temperature and humidity ratio. When the differential equations are written in terms of the characteristic potentials, they become uncoupled, hyperbolic wave equations. This model greatly simplifies the mathematics of the finite difference procedure and has been used for seasonal simulations.

Wilmott and Burns [1977] studied transient response of periodic flow thermal regenerators through step changes to the inlet gas temperature and flowrate. They found that reducing regenerator length and not reducing the period would affect the time required for steady-state.

Holmberg [1979] also presented a finite difference solution to the heat and mass transfer equations with the PGS coefficients. He used a staggered mesh, however, to account for steep

gradients within the matrix. He used an implicit Crank-Nicholson scheme for the equations and solved them using a Gauss-Seidel solution technique.

Mathiprakasam and Lavan[1980] produced linearized solutions from the basic equations in order to ease the computational requirements.

Barlow's [1982] "pseudo-steady-state" model proposed that discrete elements be treated as simple counterflow heat and mass exchangers. The equations are uncoupled at each step to allow easier computation. While the model is not as rigorous, it has been shown to have fair agreement with experimental data. Because of its ease of use, this program has also been used extensively by researchers.

Pesaran [1984, 1987] also developed the differential equation for diffusion within the desiccant particle. He showed that the amount of surface diffusion versus Knudsen diffusion varied significantly for different densities of silica gel (intermediate versus regular density). He also did a substantial amount of experimental work looking at the transient response of fixed bed adsorption with desiccants.

Jurinak [1982] compared two forms of the analogy method with a finite difference technique and concluded that the analogy method was reasonable for seasonal simulation with several caveats. A high thermal capacitance matrix or high Lewis number, high rotational speed, or unfavorable isotherm could cause significant errors with the analogy method. He also compared matrix properties (isotherms, heat of adsorption, water content, hysterisis, matrix diffusivity, thermal capacitance, and flow parameters) through a parametric analysis with a finite-difference technique.

Besides sensible heat regenerators, Brandemuehl [1982] applied both analogy and finite-difference methods to heat and mass regenerators. Specifically, he addressed nonuniform inlet conditions in a periodic steady-state and transient analysis through a step change to the periodic steady-state. Essentially, he found that non-uniform inlet conditions did cause significant effects on the performance of a heat and mass regenerator and the step change could require substantial time for a wheel (especially from a "cold" start). The adsorption isotherm he developed was used in this research as well. He also found that for certain values of the Lewis number, the analogy method did not show as good agreement.

Van Den Bulck et al., [1985] devised an equilibrium model that assumes the airstream and the desiccant are in equilibrium using wave theory and the analogy method. He used the results from this combined with finite difference results to devise another model: the effectiveness-NTU model (analogous to heat exchangers). With these, he has done some system studies as well.

Chant [1991] performed a steady-state and transient analysis of rotary desiccant regenerator using an assumed moisture profile within the desiccant particle to account for solid-side diffusion. The analysis then proceeds based on first principles. She tested both a parabolic and quartic profile of which she recommends the parabolic profile as an accurate, computationally efficient option to the solid-side diffusion equation. She used an ordinary differential equation technique combined with the Burlirsch-Stoer method for transient analysis and had mediocre success with validation. The transient model also appears to have had some stability problems. She used a finite difference approach combined with a sparse matrix solver for the steady-state analysis and had very good stability. She also examined the Cromer cycle and performed a second law analysis on it.

Based on a review of the literature, there has not been a study that compares the experimental transient response of a rotary desiccant wheel with a numerical model. The finite difference technique is recognized as the most accurate and most universal solution technique. The parabolic concentration profile appears to be the best compromise between fundamental principles, accuracy, and computational speed.

Mathematical Model

Coordinate System, Conventions, and Assumptions

Figure 2 represents the coordinate system for a desiccant wheel model used in this research. The wheel rotates between airstreams 1 and 2 (process and regeneration). The differential element is a "wedge" or a "fixed bed rotating in time" between the two airstreams.

Assumptions

The governing assumptions for the rotary desiccant wheel are as follows:

1. The thermal and mass transport resistance of the matrix material is infinite in both the tangential and axial direction and very small in the radial direction

2. There is no carryover, leakage or mixing of the airstreams. While there is a small amount of mixing between the two streams, the amount is assumed to be small because of improved seals and the overall effect negligible

3. The thermal and mass storage capacities of the air in the desiccant pores are negligible in the comparison with the convective heat and mass transport. The amount of air is relatively minor and the capacity of the convection transfer is large in comparison.

4. The fluids (process and regeneration) pass in counterflow directions.

5. The thermal properties of the matrix material are constant.

6. Temperature gradients within the desiccant particle are negligible (an isothermal particle).

7. The moisture content of a desiccant particle can be approximated by the parabolic concentration profile (PCP).

8. The moist air behaves as an ideal gas.

9. There is a layer of moist air at the surface of the desiccant that exists in equilibrium with the desiccant bed.

10. The mass transfer potential can be calculated using the local difference in humidity ratio (a modified Fick's Law approach) between the airstream and a theoretical airstream layer in equilibrium with the desiccant surface.
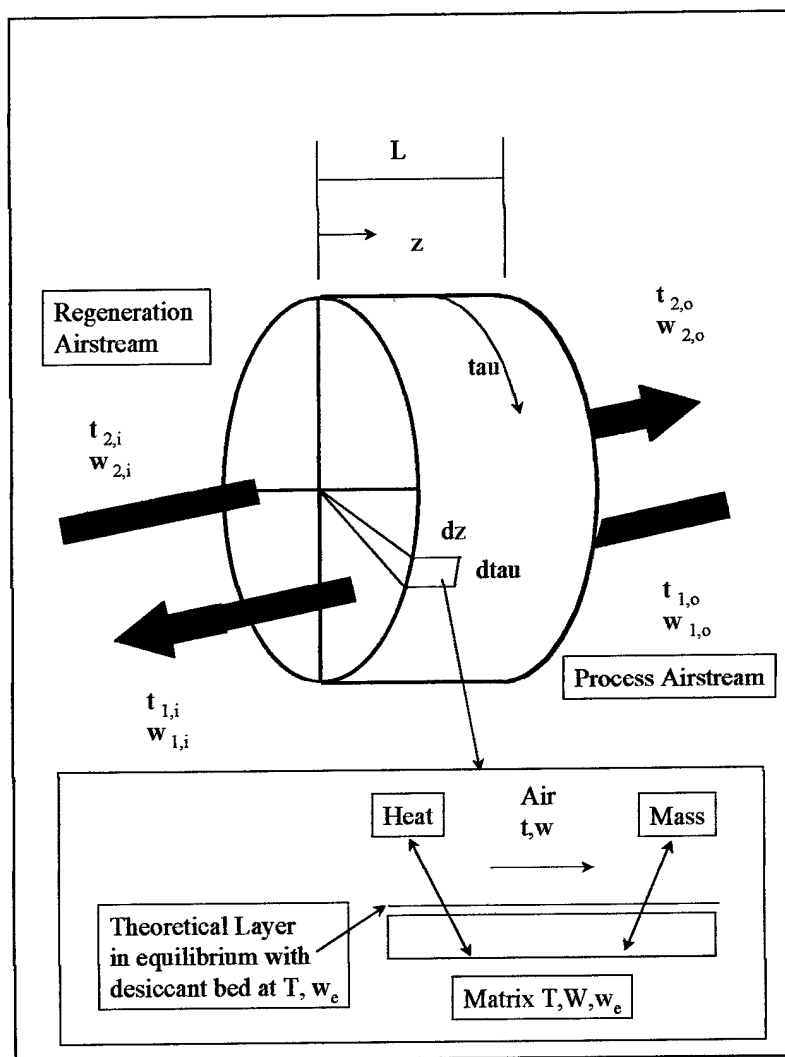
Figure 2. Nomenclature and Coordinate System for the
Rotary Desiccant Wheel

11. The hysteresis effect for sorption and de-sorption is assumed to be negligible. This means that the effective diffusivity is the same for both streams.

12. The binder and filler materials do not have hygroscopic properties and do not significantly interfere with mass transfer to the desiccant. According to the manufacturer, these materials are non-hygroscopic.

Governing Equations

The rotary wheel is treated as a fixed bed moving in time through two different airstreams or boundary conditions. Based on these conventions, the following are the transfer rate and conservation differential equations for a rotary desiccant wheel.

Mass Transfer rate
$$\frac{\partial w}{\partial x} = NTU_{m,jk}(w_e - w)$$

Mass Conservation
$$\frac{\partial w}{\partial x} + \beta_s \Gamma_s \frac{\partial W}{\partial \theta} = 0$$

Energy Transfer Rate
$$\frac{\partial i}{\partial x} = NTU_{q,jk} c_{p,ma}(T - t) + i_{fg}\frac{\partial w}{\partial x}$$

Energy Conservation
$$\frac{\partial i}{\partial x} + \beta_s \Gamma_s \frac{\partial I}{\partial \theta} = 0$$

In their initial form, the conservation equations are functions of the airstream properties (t,w) and the matrix itself (T,W). The rate equations are in terms of the airstream (t,w) and the theoretical layer (T, w_e) in equilibrium with the matrix.

The independent variables of axial distance and time have been non-dimensionalized as follows:

$$x = \frac{z}{L} \qquad\qquad \text{Equation 1}$$

$$\theta = \frac{\tau}{\tau_p} \qquad\qquad \text{Equation 2}$$

The time and rotation angle are related by:

$$\frac{\tau}{\tau_p} = \frac{\phi}{2\pi} \qquad\qquad \text{Equation 3}$$

The period fraction βj is the percentage of the period time and is defined by:

9

$$\beta_s = \frac{\tau_s}{\tau_p} = \frac{\phi_j}{2\pi} \qquad\qquad \text{Equation 4}$$

The mass capacity rate ratio Γ_j is the ratio of the desiccant mass "flow rate" to the mass flow rate of the airstream:

$$\Gamma_s = \frac{M_{dd}/\tau_p}{\dot{m}_{da,s}}$$

The NTU (Number of Transfer Units) term follows the classical definition ("UA/C$_{min}$") and in this context they are defined as:

$$NTU_{m,jk} = \frac{h_{m,jk}A_{s,s}}{\dot{m}_{da,s}} \qquad\qquad NTU_{q,jk} = \frac{h_{q,jk}A_{s,s}}{\dot{m}_{da,s}c_{p,ma}}$$

In Terms of Temperature

The computer model developed for this research works primarily in terms of temperature and humidity ratio. The differential equations are in terms of enthalpy and therefore must be converted to temperature.

Moist air is treated as an ideal gas mixture of dry air and water. The enthalpy of moist air is a function of the humidity ratio and the temperature. The moist air enthalpy is defined as:

$$i = i_{da} + w i_{wv} = c_{p,da}t + w(c_{p,wv}t + i_{fg})$$

rearranging and setting

$$c_{p,ma} = c_{p,da} + c_{p,wv}w$$

the result is

$$i = c_{p,ma}t + i_{fg}w$$

and its derivative with respect to axial distance, x, becomes

$$\frac{\partial i}{\partial x} = c_{p,ma}\frac{\partial t}{\partial x} + i_{fg}\frac{\partial w}{\partial x}$$

10

Inserting this definition into the energy transfer rate equation (**Error! Reference source not found.**, leaving the energy transfer differential equation:

$$\frac{\partial t}{\partial x} = NTU_{q,s}(T - t)$$

The enthalpy of the desiccant wheel is expressed as a function of the matrix, the desiccant, the water absorbed and the integral heat of wetting.

$$I = (c_{p,dm} + c_{p,wl}W)T + \Delta H_w$$

The integral heat of wetting, ΔH_w, is qualitatively the difference between the heat released by absorption and the vaporization of pure water. It is defined as:

$$\Delta H_w = i_{fg} \int_0^W (1 - \frac{i_{ad}}{i_{fg}})dW$$

The matrix enthalpy is defined as:

$$I = c_{p,m}T + W(i_{fg} - i_{ad})$$

where

$$c_{p,m} = c_{p,dm} + Wc_{p,wl}$$

Taking the derivative of **Error! Reference source not found.** with respect to normalized time

$$\frac{\partial I}{\partial \theta} = c_{p,m}\frac{\partial T}{\partial \theta} + (i_{fg} - i_{ad})\frac{\partial W}{\partial \theta}$$

Equation 5

Incorporating the air enthalpy equation (**Error! Reference source not found.**), the desiccant enthalpy equation (Equation 5) and the mass conservation equation (**Error! Reference source not found.**) into the energy conservation equation (**Error! Reference source not found.**). Canceling the enthalpy of vaporization from both sides and moving the matrix specific heat to the right hand side:

$$\frac{\partial T}{\partial \theta} = -\frac{1}{\beta_s \Gamma_s c_{p,m}}(c_{p,ma}\frac{\partial t}{\partial x} + i_{ad}\frac{\partial w}{\partial x})$$

In summary, the four basic differential equations are

The differential equations are all first order differential equations; therefore, one boundary condition or one initial condition is required. The boundary conditions state that the initial air states (temperature and moisture) of the different periods (hot and cold sides) are the same as the entering air for that period.

$$t(x = 0, 0 < \theta < \beta_1) = t_{1,i}$$

$$w(x = 0, 0 < \theta < \beta_1) = w_{1,i}$$

The initial conditions are required for the matrix states at $\tau=0$. After that, the initial condition for the next element is the exit condition from the previously solved element.

Psychometric Relationships

The differential equations above are non-linear and coupled. This is because the desiccant and moist air states are interrelated through the dependent variables (t,w,T,W,w_e). The equilibrium condition is a function of the isotherm relationships, effective diffusivity, and psychrometric relationships which are all non-linear. Mathematically, this is expressed as

$$W=W(T,w_e) \qquad I=I(T,W) \qquad i=i(t,w)$$

The relationships that define the desiccant and moist air states used in the equilibrium states above will follow.

Liquid water has been treated as an incompressible fluid and the enthalpy of liquid water is a function of temperature only.

$$i_{lw} = c_{p,lw}T$$

The absolute humidity of moist air in equilibrium with adsorbent is defined by:

$$w_e = 0.62198\frac{p_{va}}{p_t - p_{va}}$$

The vapor pressure is determined using the definition of relative humidity

$$RH(\%) = \frac{p_{va}}{p_{vs}}100$$

With further refinement ▌ can be changed to:

$$w_e = 0.62198 \frac{RH * p_{v,s}}{p_t - RH * p_{v,s}}$$

The saturation vapor pressure is given by an equation from the Hyland-Wexler equation in ASHRAE Fundamentals, [1993].

$$\ln(p_{vs}) = \frac{C_8}{T} + C_9 + C_{10}T + C_{11}T^2 + C_{12}T^3 + C_{13}LN(T)$$

<div align="center">Equation 6</div>

where

$C_8 = $ -5.8002206 E3

$C_9 = $ -5.5162560

$C_{10} = $ -4.8640239 E-2

$C_{11} = $ 4.1764768 E-5

$C_{12} = $ -1.4452093 E-8

$C_{13} = $ 6.5459673

and p_{ws} is in units of kilo Pascals and the temperature T, is in absolute units of degrees Kelvin.

Air and Moisture Parameters

In order to ensure that the model program is accurate over a significant range of temperatures and to improve flexibility, some parameters were put in the form of functions

The Specific Heat of Dry Air is a third order polynomial curve fit:

$$c_{p,da} = -4.37E^{-10}t^3 + 9.245t^2 - 4.077t + 1.057$$

The Specific Heat of water vapor is also a third order polynomial curve fit:

$$c_{p,wv} = 1.043E^{-7}t^3 - 8.499E^{-5}t^2 + 2.373t - 0.415$$

The Specific Heat of liquid water was assumed to be a constant because it typically varies less than 3% over the range of temperatures (273.15-430 °K) [Incropera and Dewitt, 1986] encountered in this research.

$c_{p,wf}$=4.186 kJ/(kg-K)

The thermal conductivity of air is necessary to solve for the convective heat and mass transfer. It is significantly affected by temperature (it can vary by more than 10% over the temperatures used) and is best represented by a second order polynomial:

$$k_f = -3.269E^{-11}t^2 + 9.799t - 1.668$$

Enthalpy of Vaporization

The enthalpy of vaporization is necessary along with the adsorption isotherm to solve for the enthalpy of adsorption. The expression for the enthalpy of vaporization is developed from a form of the Clapeyron equation:

$$i_{fg} = \left(\frac{dP}{dT}\right)_{sat}\frac{RT^2}{P_{vs}}$$

Adsorption Isotherm

The water content of the desiccant material in equilibrium with an air-vapor mixture at a given temperature and vapor pressure can be determined using the adsorption isotherm. The adsorption isotherm relations developed by Brandemeuhl [1982] as a function of moisture content and temperature for regular density silica gel are as follows:

$$RH = (2.112W)^{h*}(29.91p_{vs})^{h*-1}$$

where

$$h* = 1 + 0.2843e^{(-10.28W)}$$

and h* is also equal to:

$$h* = \frac{i_{ad}}{i_{fg}}$$

Parabolic Concentration Profile

The basic concept of the parabolic concentration profile (PCP) is that the moisture content within the desiccant particle is assumed to be parabolic, Figure 3. When the particle is in the process stream, there is a positive gradient. When the particle is in the regeneration stream, there is a negative gradient. The profile varies between these two extremes when it rotates between the airstreams.

Several studies have shown this assumption to be reasonably accurate [Do and Rice, 1986] except for a very small initial period when the profile is developing.
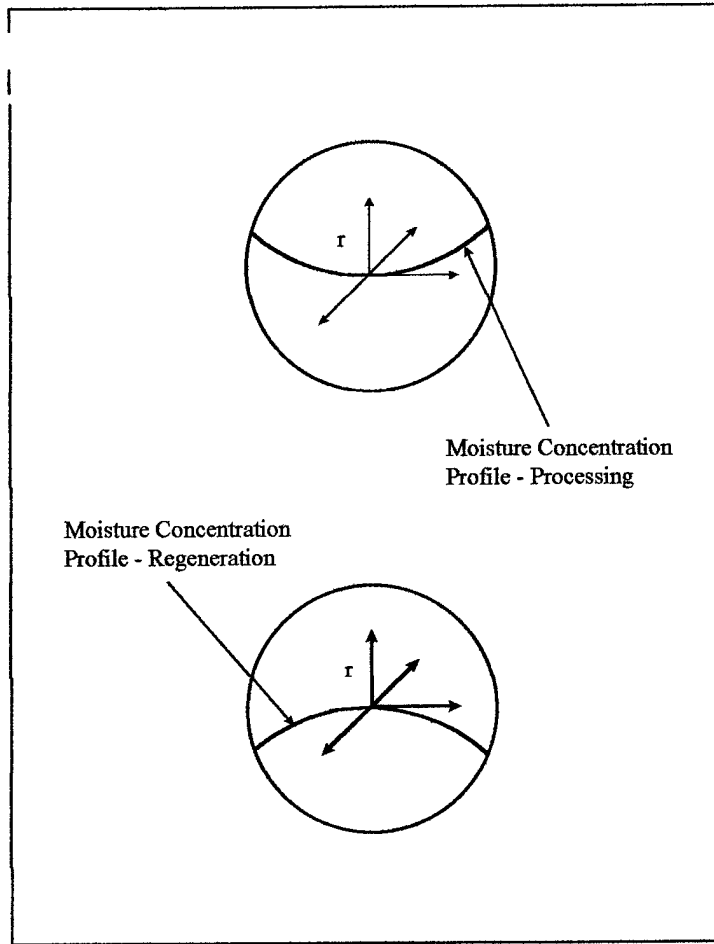

Figure 3. Parabolic Concentration Profile [Chant, 1991]

The PCP model evaluates the equilibrium humidity ratio, w_e, at the surface of the particle rather than at the average moisture concentration as with the typical PGS models. For a spherical particle, the following two expressions are needed to determine the moisture content at the surface, Ws [Chant, 1991]:

$$W_s = W + (2/5)a2$$

$$a2 = -(h_m R / 2\rho_p D_e)(w_e\{W_s, T\} - w)$$

In order to find the surface moisture content, the a2 term must be evaluated at each moist air grid point. The mass transfer coefficient can be analytically determined for the surface instead of the

PGS coefficient, which must be empirically altered to solve for the equilibrium at the average moisture content.

Effective Diffusivity

The effective diffusivity for regular density is primarily a function of surface diffusion [Pesaran, 1987]. The basic equation describing surface diffusivity used in this research is a "mechanistic hopping model" based on the heat of adsorption [Slaydek et al, 1974]:

$$D_s = D_o Exp(-a i_{st} / RT)$$

where $a = .45 / b$ and b is a function of the type of adsorption bond. For silica gel, b is equal to unity [Pesaran, 1987]. R is the gas constant for water vapor and R equal to 0.462 kJ/(kgK) is used. T is in degrees Kelvin. The D_o term is defined as: $\quad D_o = \frac{1}{4} v_o \lambda_s^2$

Pesaran [1987] also determined that D_o for silica gel is approximately equal to 1.6×10^{-6} m^{2}s^{-1}. The effective surface diffusivity is then found using:

$$D_{s,e} = D_s / \tau_s$$

For the surface tortuosity, τ_s, Pesaran [1987] used 2.8 in the case of regular density silica gel.

Heat and Mass Transfer Coefficients

According to Incropera and Dewitt, in *laminar* flow, the Nusselt number is a function of the geometry only. The heat transfer convection coefficient (h_q) can be analytically determined from established sources using the Nusselt number (Nu).. Mathematically, this is expressed as:

$$Nu = \frac{h d h}{k_{da}}$$

The Lewis Analogy, by extension, can be used to determine the heat or mass transfer coefficient given the other.

$$\frac{h_q}{h_m} = c_{p,ma} Le^{1-n}$$

Using typical values for n (1/3), Pr (0.705), and Sc (0.6) and placing these into the Lewis relation:

$$Le^{1-n} = \left(\frac{.6}{.705}\right)^{1-1/3} = 0.851^{2/3} = 0.898 \approx 1$$

so the heat and mass transfer coefficient ratio can be approximated by:

$$\frac{h_q}{h_m} = c_{p,\,ma}$$

Finite Difference Equations

The mathematical model of the rotary wheel is based on a two dimensional grid as shown in Figure 4. The rotary wheel is modeled as a fixed bed that rotates through time. Hence, the axial dimension is the abcissa and the time or angular position is the ordinate.
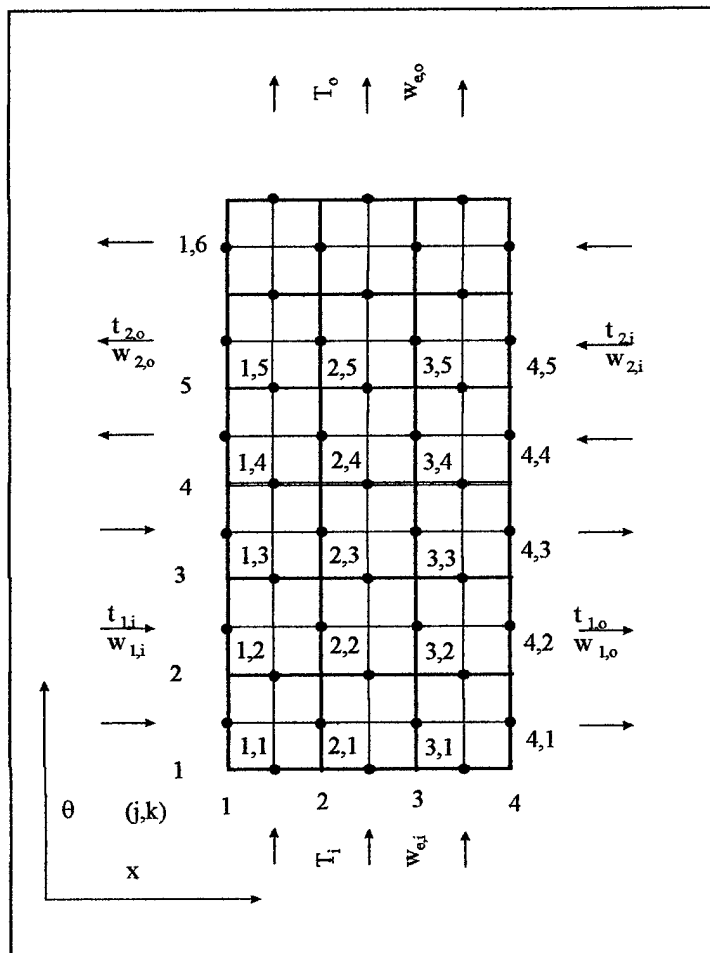
Figure 4. Schematic Representation of a Rotary Heat
Exchanger

Figure 5 shows the convention for the differential element. Based on the differential

equations and as shown in the differential element, a central differencing scheme was employed for the

first order equations as used by Holmberg [1977]. This central differencing scheme for a first order

differential equation is of second order accuracy.

The finite difference equations are:

Mass Rate Transfer

$$w(j+1,k) - w(j,k) = NTU_{m,j} \Delta x (w_e - w)_{av}$$

Where

$$(w_e - w)_{av} = \frac{1}{2}[(w_e(j,k+1) + w_e(j,k)] - \frac{1}{2}[(w(j+1,k) + w(j,k)]$$

Conservation of Mass

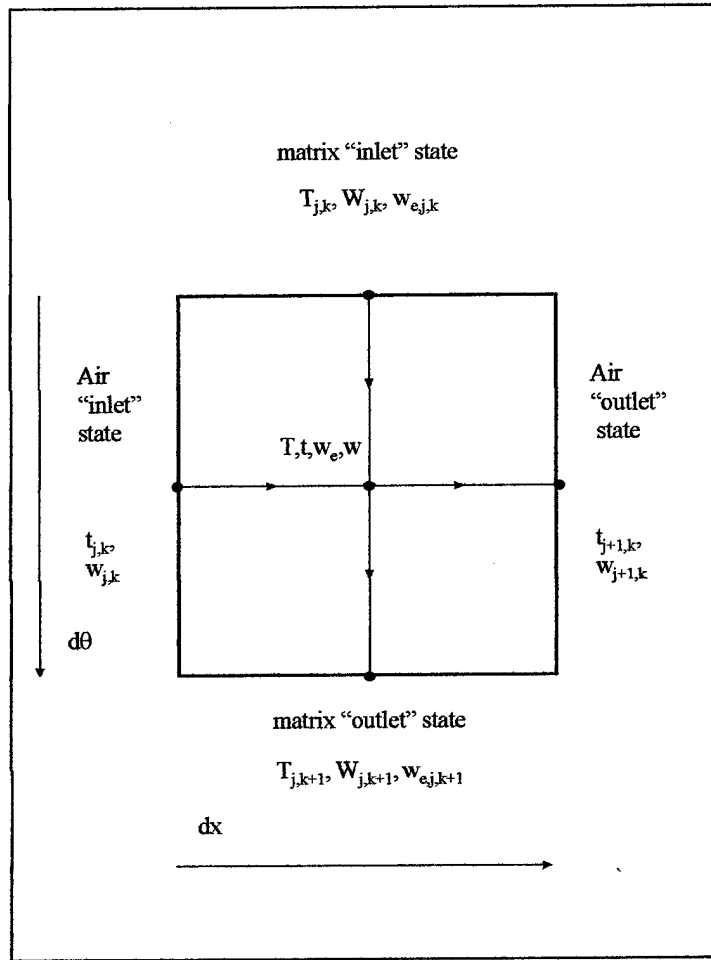$$W(j,k+1) - W(j,k) = -\frac{\Delta\theta}{\beta_j \Gamma_j \Delta x}[w(j+1,k) - w(j,k)]$$

Figure 5. Finite Difference Element

Energy Transfer Rate

$$t(j+1,k) - t(j,k) = NTU_{q,j}\Delta x(T-t)_{av}$$

where

$$(T-t)_{av} = \frac{1}{2}[T(j,k+1) + T(j,k)] - \frac{1}{2}[t(j+1,k) - t(j,k)]$$

Conservation of Energy

$$T(j,k+1) - T(j,k) = -\frac{\Delta\theta}{\Delta x \beta_j \Gamma_j c_{p,m}}[c_{p,ma}(t(j+1,k) - t(j,k)) + i_{ad}(w(j+1,k) - w(j,k))]$$

The variables of concern in this study are the specific properties transferred between the two airstreams: temperature and humidity ratio. The temperature and humidity ratio are direct solutions from the finite difference equations. The actual moisture transferred from the process stream is typically referred to by the industry as the Moisture Removal Capacity or MRC and is defined below:

$$MRC = \dot{m}_{da}(w_{p,\,in} - w_{p,\,out}),\, kg_w/hr$$

The non-dimensional transient response is of the same form used by Lambertson [1958] and Brandemuehl [1982]:

$$\eta_t = \frac{t - t_{\tau\,=\,0}}{t_{\tau\,=\,\infty} - t_{\tau\,=\,0}}$$

$$\eta_w = \frac{w - w_{\tau\,=\,0}}{w_{\tau\,=\,\infty} - w_{\tau\,=\,0}}$$

Numerical Scheme

The basic equations developed in the previous chapter must be numerically processed in a manner to optimize stability, speed, and accuracy.

MATRIX Format

In order to use various numerical solution techniques, a convenient way of expressing the equations is in a matrix format. The finite difference equations are first placed in a format where:

j ,k (+1 step) = current j,k

Using the finite difference equations, the matrix format is as follows:

$$A$$

$$
\begin{bmatrix}
1 & \dfrac{\Delta\theta}{\beta_s\Gamma_s\Delta x} & 0 & 0 \\[2mm]
0 & \left(1 + \dfrac{NTU_{m,\,jk}\Delta x}{2}\right) & 0 & 0 \\[2mm]
0 & \dfrac{\Delta\theta}{\Delta x\beta_s\Gamma_s C_{pm}} i_{ad} & 1 & \dfrac{\Delta\theta}{\Delta x\beta_s\Gamma_s C_{pm}} C_{pma} \\[2mm]
0 & 0 & -\dfrac{NTU_{q,\,jk}\Delta x}{2} & \left(\dfrac{NTU_{q,\,jk}\Delta x}{2} + 1\right)
\end{bmatrix}
\begin{array}{l}
MassConservation \\
MassRate \\
EnergyConservation \\
EnergyRate
\end{array}
$$

$$
\begin{matrix}
x \\
\begin{bmatrix} W(j,k+1) \\[1em] w(j+1,k) \\[1em] T(j,k+1) \\[1em] t(j+1,k) \end{bmatrix}
\end{matrix}
\quad
\begin{matrix}
b \\
\begin{bmatrix}
W(j,k) + \dfrac{\Delta\theta}{\beta_s\Gamma_s\Delta x}w(j,k) \\[1em]
NTU_{m,jk}\Delta x w_e + \left(1 - \dfrac{NTU_{m,jk}\Delta x}{2}\right)w(j,k) \\[1em]
T(j,k) + \dfrac{\Delta\theta}{\Delta x\beta_s\Gamma_s c_{pm}}\left((c_{pm,a}t(j,k) + i_{ad}w(j,k))\right) \\[1em]
\left(1 - \dfrac{NTU_{q,jk}\Delta x}{2}\right)t(j,k) + \dfrac{NTU_{q,jk}\Delta x}{2}T(j,k)
\end{bmatrix}
\end{matrix}
$$

Figure 6. Matrix Format

Numerical Techniques

To solve for the conditions of the rotary desiccant wheel, the following system of equations must be known:

1. Conservation of Mass

2. Conservation of Energy

3. Mass Transfer Rate

4. Energy Transfer Rate

5. Moist Air Enthalpy

6. Desiccant Wheel Enthalpy

7. The Adsorption Isotherm

8. Boundary Conditions (inlet states)

9. Initial Conditions (initial values or periodic steady-state)

There are now have five variables to solve for (t,w,T,W,w_e) at each location. However, the equilibrium temperature is clearly a function of w,W, and T. Using this relation, w_e can be solved and located on the "known" or right-hand of the matrix equation (matrix b). Thus, four unknowns will be solved at each element through iteration.

One substantial difference between this model and previous efforts is the calculation of NTU for each element. Previous efforts [Brandemuehl, 1982; Maclaine-cross, 1972; Chant 1991] have used a constant NTU for an entire stream or an entire wedge. The model developed in this thesis calculates a new NTU for *each* element. This involves determining various properties that are functions of temperature and moisture (specific heat, thermal conductivity) at each element as well in order to calculate NTU. The NTU is substantially dependent upon temperature and moisture and can vary by as much as 10.

An initial guess of the solution is made to start the procedure. The desiccant and moist air states for all axial positions are solved individually in a given wedge. For the transient case, this must be done for each wedge at every circumferential position. A step in the time direction is then made and the process repeats itself. At each element the mass and energy balances in the finite difference equations are checked to an epsilon criteria. The exiting condition of the airstream will be the average of the elements at the outlet axial positions.

The parabolic concentration profile (PCP) required solving a non-linear equation of one variable. The bisection method (while a little slower) was found to have very good stability and accuracy with reasonable speed and was therefore used in this research.

After manipulating the variables and equations into the matrix form shown above, it was observed that the matrix format was that of a tridiagonal matrix. The tridiagonal matrix solver was therefore used to solve the finite difference equations.

Step Size and Stability

Most of the work on step size and stability used in this work comes originally from Maclaine-Cross [1972] by way of Brandemuehl [1982]. The step sizes for both time and axial distance are critical so that the computer model will be stable and accurate while at the same time keeping computer run-time to a minimum. Grid sizes were considered of sufficient resolution when the model produced equivalent results with increasing grid sizes.

Maclaine-cross experimented with various step sizes for both the steady-state and transient responses and developed expressions for satisfactory stability and convergence. For the steady-state model, the number of axial steps is determined by:

$$N_x = 1.7\sqrt{MAX(NTU_p, NTU_r)} + 3.2$$

For the transient model, he determined the number of axial steps to be:

$$N_x = 2.8\sqrt{MAX(NTU_p, NTU_r)} + 5.6$$

The relationship between the number of axial steps, N_x, and the number of time steps, N_θ is provided by the following:

$$N_{\theta, total} = \frac{2N_x}{Minimum(\Gamma_p, \Gamma_r)}$$

There did not appear a significant difference in accuracy between the number of axial steps calculated with the steady-state equation and the transient equation. Because the steady-state equation generates significantly less steps, it was also much faster and most runs were done using this relation.

The equations for mass and energy balance are defined below:

$$mass - balance - ratio = \frac{\overset{\bullet}{m}_{p, da}(w_{p, out} - w_{p, in})}{\overset{\bullet}{m}_{r, da}(w_{r, out} - w_{r, in})}$$

$$energy - balance - ratio = \frac{\overset{\bullet}{m}_{p, da}(i_{p, out} - i_{p, in})}{\overset{\bullet}{m}_{r, da}(i_{r, out} - i_{r, in})}$$

In order to optimize the run time and still maintain accuracy, some trial and error runs were required. A sample of grid sizes and their associated run times using a 450 MHz PC is shown in Table 1 The wheel time refers to the actual time a desiccant wheel would be turning. The computer time is the corresponding run time of the computer. It can be seen that the runs for some of the more extreme

or stiff conditions are almost real time. Clearly this model would be unacceptable for seasonal simulation.

	Grid Size		Wheel Time	Computer Time	Computer / Wheel
Run	Axial	Circum	(hr)	(hr)	Ratio
1	5	200	1:38	1:23	0.8469
2	5	120	1:10	0:25	0.3571
3	5	80	1:10	0:16	0.2286
4	5	60	1:10	0:11	0.1571

Table 1. Grid Size and Run Times

Experimental Setup

Transient experiments for this research were done at the state-of-the-art desiccant research facility in the National Renewable Energy Laboratory (NREL) at Golden, CO. Small modifications were required to accommodate transient testing because the facility is primarily used for steady-state analysis.

A current, commercially available wheel, the NovelAire WSG, was used for the experiments. Details of the laboratory and the wheel are provided in Grumbach [1999]. This wheel uses silica gel as the desiccant material. The wheel heat transfer profile resembles sinusoidal openings much like corrugated cardboard. These openings were not uniform however and the profiles were modeled initially as triangle or rectangles.

A series of six runs were made to validate the model and to observe the actual transient response. These consisted of step increases and decreases to 1) regeneration temperature, 2) wheel speed, and 3) process flowrate. The step changes to regeneration temperature were made between the Air Refrigeration Institute (ARI) conditions at 35 C and the manufacturer's recommended operating conditions (140C). The step change to wheel speed was between 9 rph and the manufacturerer's recommended wheel speed of 18 rph. The process flowrate was changed between 400 fpm and the manufacturer's recommended 600 fpm.

Validation

Transient Validation

The statistical test used for the outlet validation portion of this research is the root mean square error or RMSE as shown in **Error! Reference source not found.**. The RMSE statistic can be interpreted as the average error between the two curves over the range of interest. The range was selected to focus on the transient response and minimize steady-state impact

$$RMSE = \sqrt{\frac{\sum (y_{pred,i} - y_i)^2}{n}}$$

The initial validation focused on the step change to regeneration temperature because the difference in process and regeneration temperature is the primary driving potential for moisture removal. At this point, both transfer profiles (triangular and rectangular) were used in transient response runs. Looking at the change in process outlet temperature (Figure 7), it can be seen that the rectangular profile follows the experimental curve with much greater fidelity than the triangular. The triangular profile clearly reached a steady-state much faster and at a much higher magnitude than the rectangular. Based on the steady-state graph (Figure 19) and the initial transient runs, the rectangular profile was chosen as the most representative of the average profile within the WSG wheel.

Looking at the figures, Figure 7 through Figure 10, the curves generally appear to be a close match. The RMSE (
Table 3) for these runs look relatively good. Process temperature RMSE is within a degree and the RMSE for the humidity ratios are both within 10%. The regeneration temperature curve shows a steady-state offset and has a correspondingly higher RMSE which will be discussed later.

The numerical curves of the process and regeneration humidity ratio (Figures 7 and 9) have a significant initial "overshoot" that does not greatly affect the statistical values. Intuitively, it would appear that a surface layer of moisture is quickly evaporated or condensing; however, there is no similar response from the experimental side. An explanation might be that the PCP numerical scheme needs some time to "set up" when there is excess moisture.

25

Although the steady-state response of the regeneration outlet temperature is a few degrees off (Figure 7), the curves are still nearly identical. A normalized graphing of the response would show very good agreement as with the other parameters.

The numerical results for the step decrease in regeneration temperature also exhibit very good agreement with the experimental results. The RMSE values for the graphs also reflect good correlation as with the step increase to regeneration temperature except for regeneration temperature.

The step increase and decrease to regeneration temperature clearly display a logarithmic response function. With this type of response, a time constant (or the time required to reach 63% of the st4ady-state value) for the system can be determined.

Run	Stream	Prop	Initial value	SS value (99%)	Time (min)	63%	time (min)
step increase	process	temp	308.15	333.4	22.1	324.06	5
"	process	humidity ratio	0.0177	0.0122	22.1	0.0142	5
"	regen	temp	308.15	320.5	22.0	315.93	3.25
"	regen	humidity ratio	0.0177	0.035	5.0	0.0286	0.5

Table 2. Summary of Time Constant Calculations for the Step Increase to Regeneration Temperature
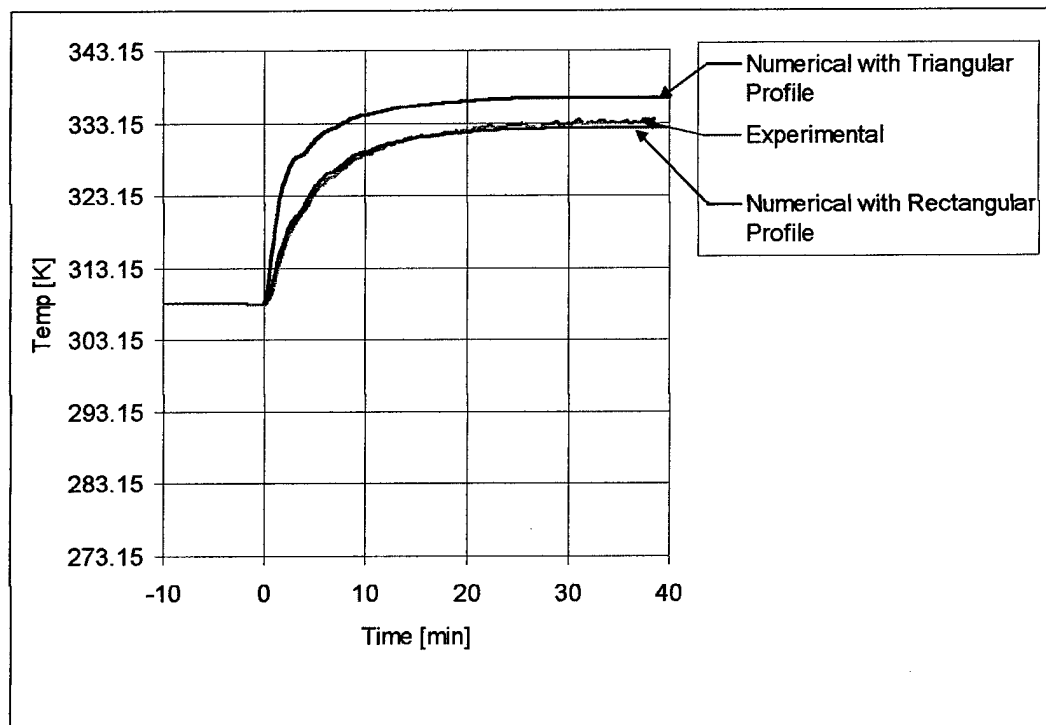
Figure 7. Process Outlet Temperature Versus Time With a
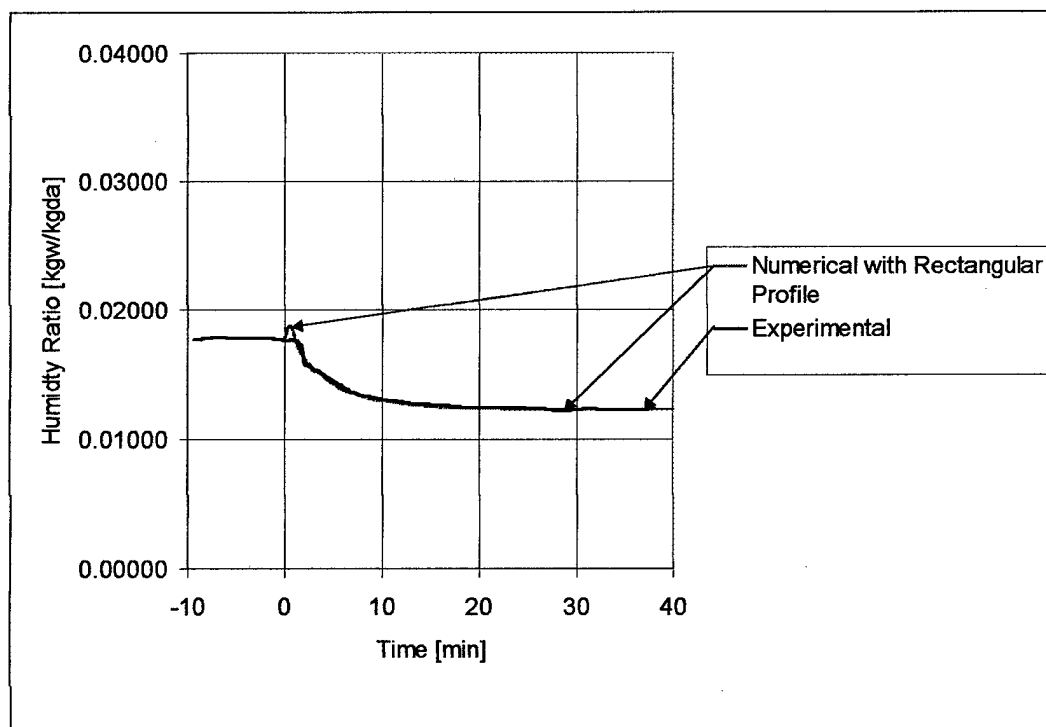Step Increase to Regeneration Inlet Temperature

Figure 8. Process Outlet Relative Humidity Versus Time
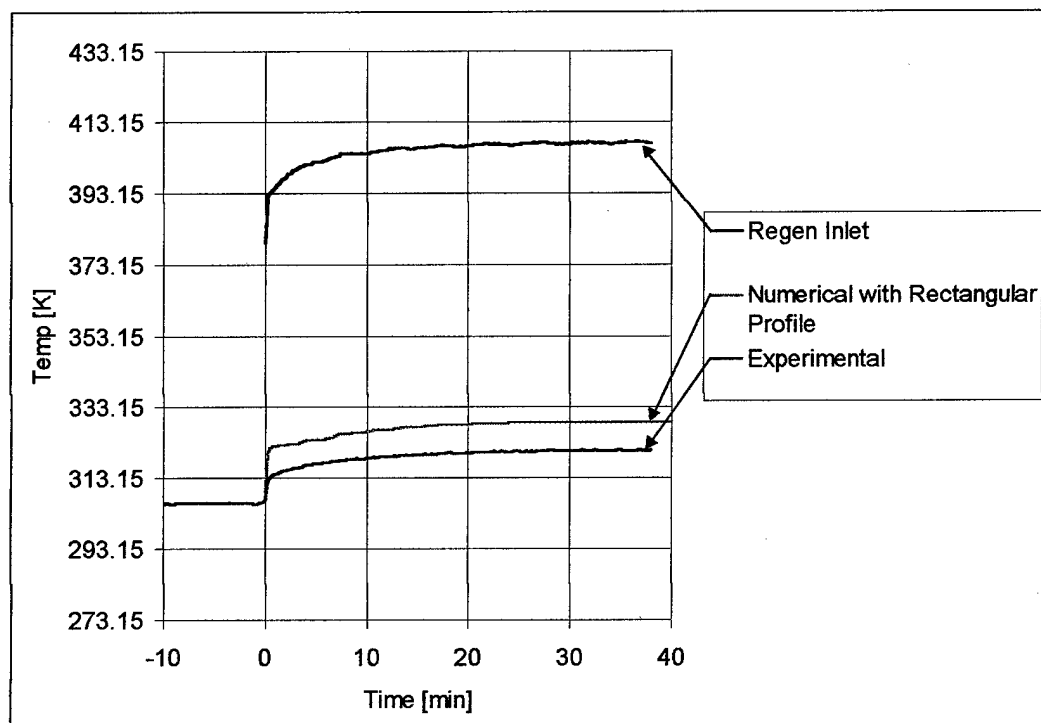with a Step Increase to Regeneration Inlet Temperature

Figure 9. Regeneration Outlet Temperature Versus Time
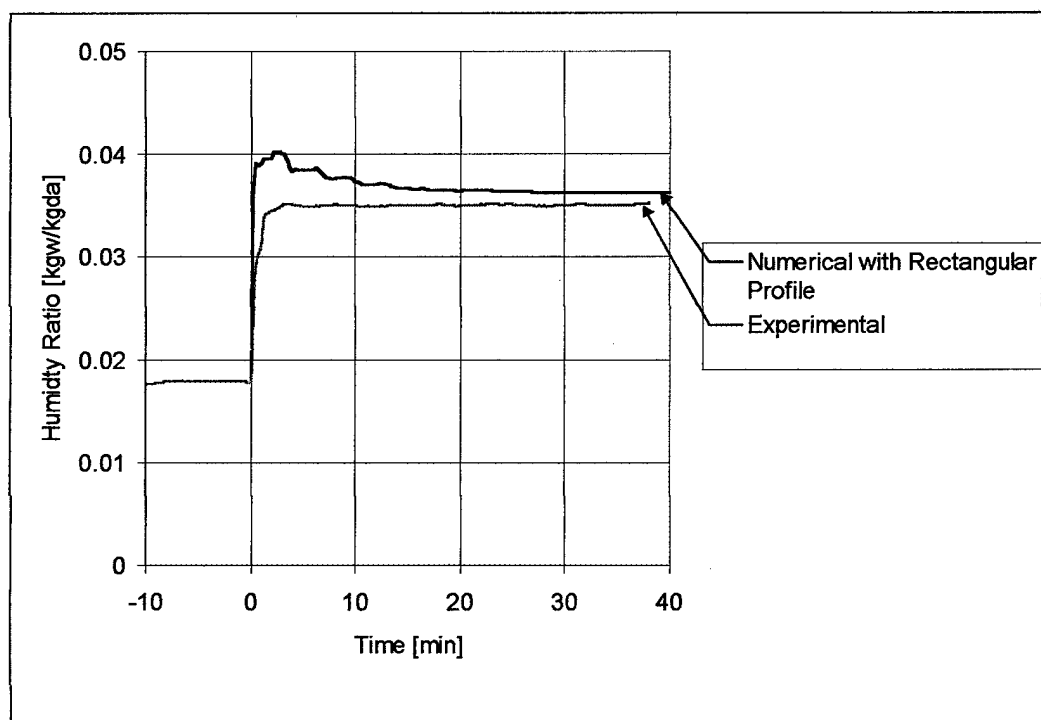with a Step Increase to Regeneration Inlet Temperature

Figure 10. Regeneration Outlet Humidity Ratio Versus Time
with a Step Increase to Regeneration Inlet Temperature

28

The graphs of the step increase to wheel speed are shown in Figure 11 through Figure 14. The numerical model curves generally look like those from the experiment. The RMSE (
Table 3) values tend to reflect this exactly as with the previous runs. The process temperature and humidity ratios appear fine. The regeneration temperature again has a slight steady-state offset while the regeneration humidity ratio looks reasonable.

One interesting point, and these can most clearly be seen in Figure 13, are the sinusoidally converging oscillations. The sinusoidal period corresponds to the wheel rotation speed. The step increase wheel rotation speed of 18 revolutions per hour corresponds to 3.3 minutes per revolution. Examining the graph in Figure 13, it can be seen that the period of the oscillations is indeed about 3.3 minutes. The temperature and moisture distributions, which form inside the desiccant wheel, are clearly a function of the wheel speed. When the step change occurs, the desiccant temperature and moisture gradients within the wheel do not change as quickly as the wheel speed. They produce the sinusoidal effect on the airstream temperature and humidity ratio until the new temperature and humidity ratio gradients are formed. The sinusoidal response is "damped" out as the transformation occurs.

The step decrease to wheel speed also appears to show that the numerical curves are close approximations of the experimental results. Again, the RMSE values are consistent with previous runs.

The oscillations in the graphs for step decrease are muted relative to the step increase. The oscillations apparently do not appear because with the slower wheel speed, the new temperature and humidity distributions have time to set up.
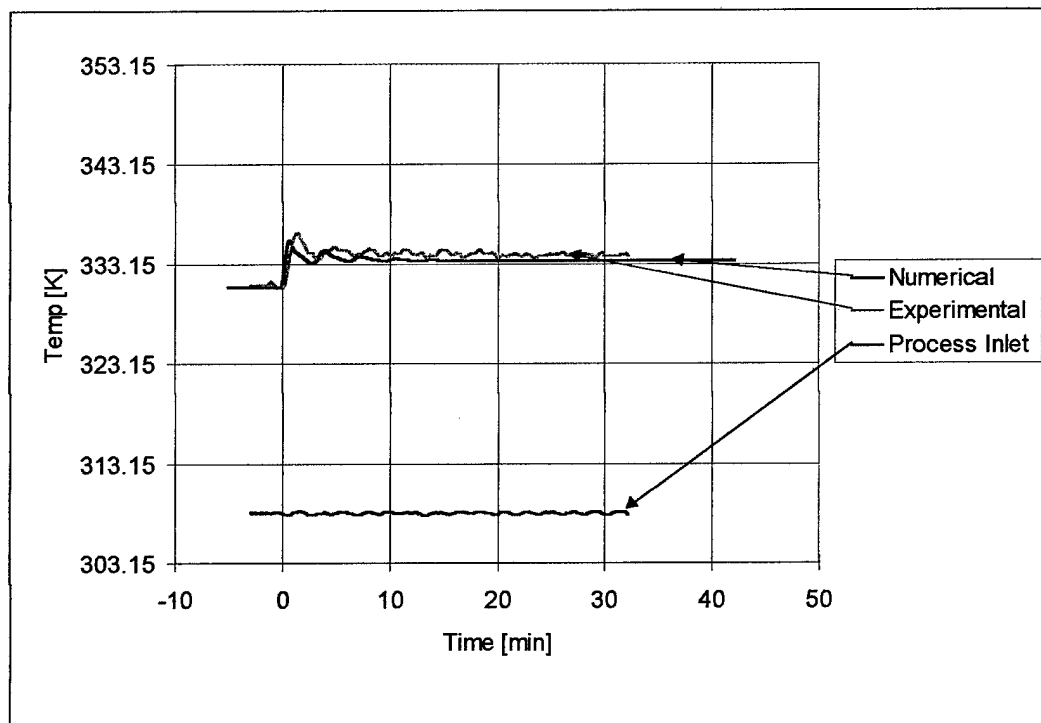
Figure 11. Process Outlet Temperature Versus Time with a
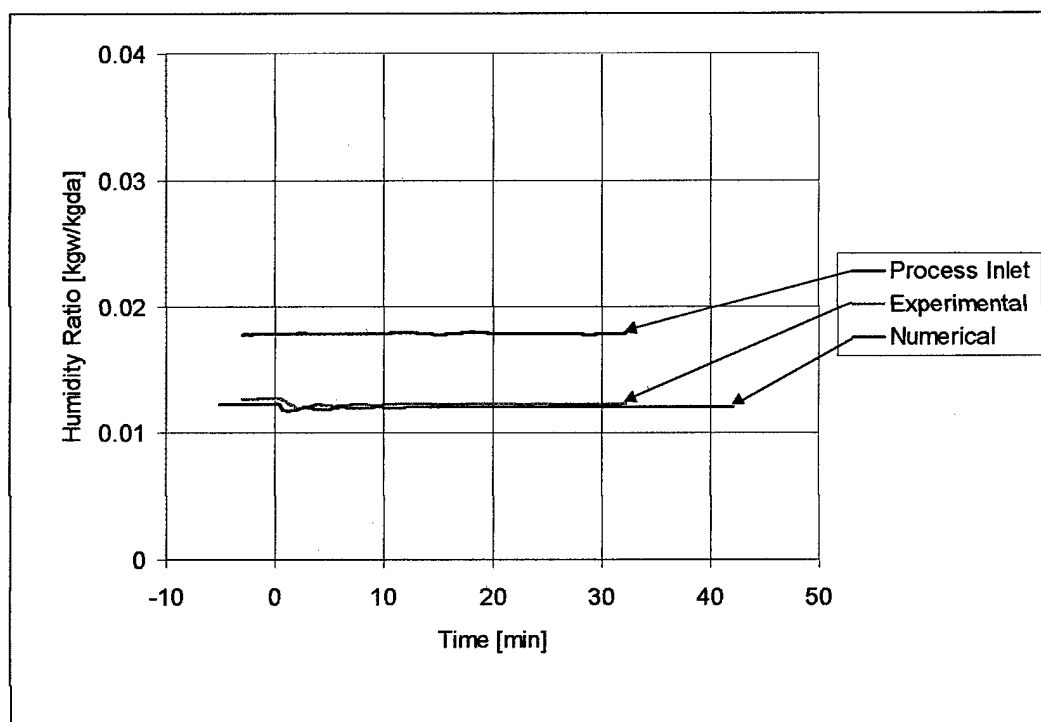Step Increase to Wheel Speed

Figure 12. Process Outlet Humidity Ratio Versus Time with
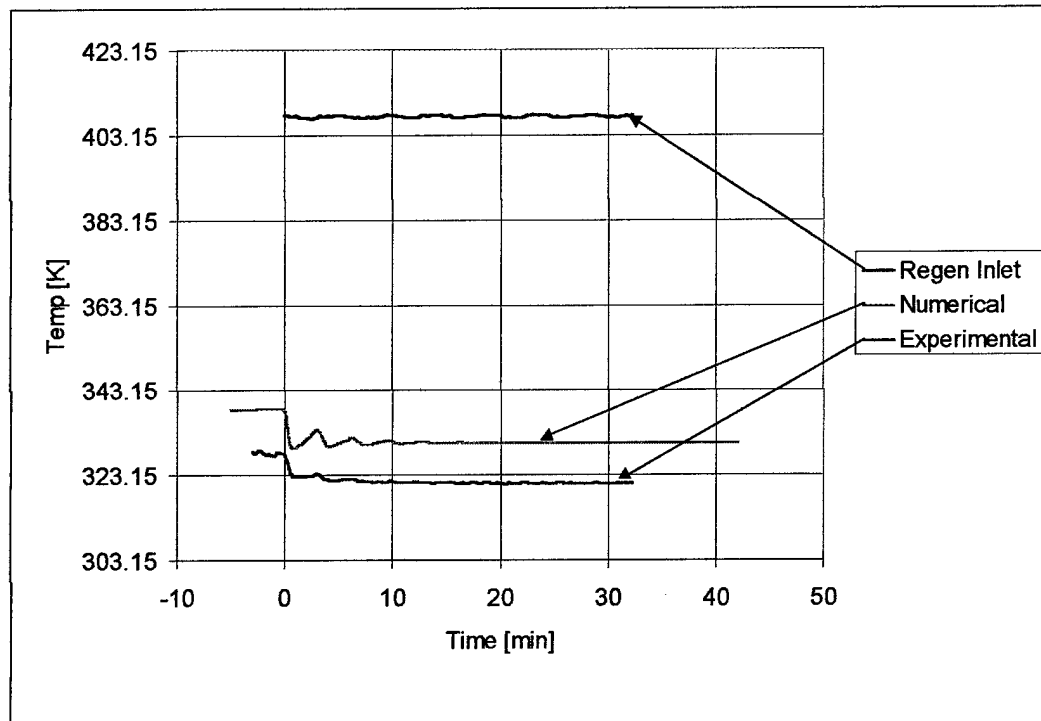a Step Increase to Wheel Speed

30

Figure 13. Regeneration Outlet Temperature Versus Time
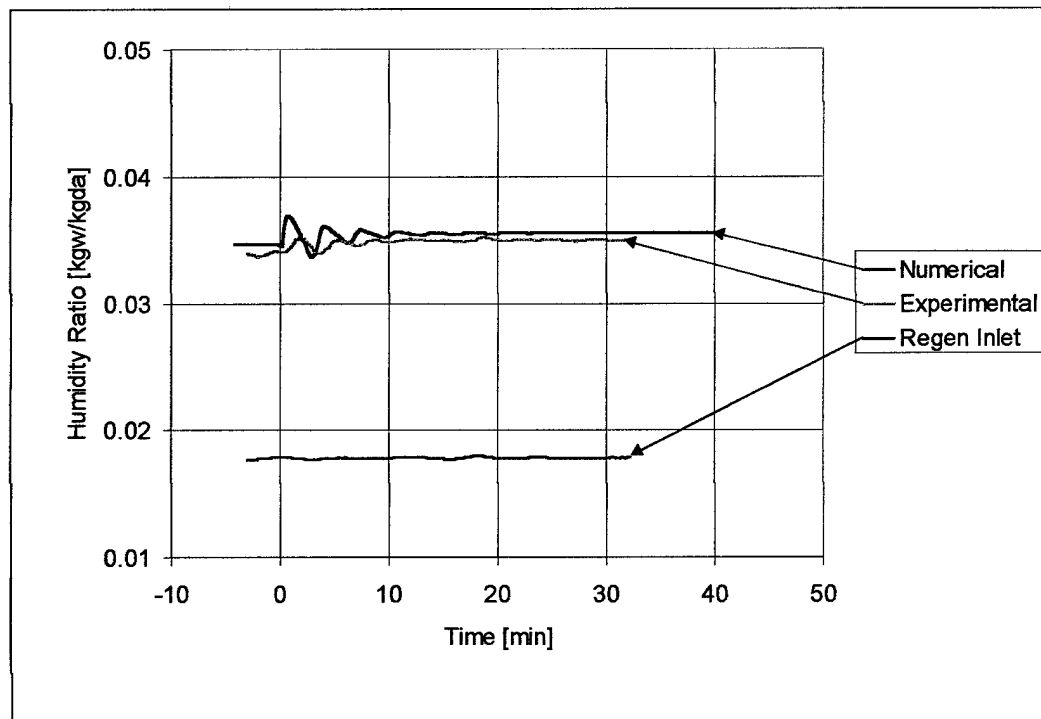with a Step Increase to Wheel Speed

Figure 14. Regeneration Outlet Relative Humidity Versus
Time with a Step Increase to Wheel Speed

31

The step increase to process flowrate (Figure 15 through Figure 18) also appears to show good agreement between the experimental and numerical solutions. The RMSE statistic (
Table 3) also showed good agreement as with previous runs. The curves for these step

changes also somewhat resemble a logarithmic function (in particular the process temperature)

although there is significantly more fluctuation than the step change to regeneration temperature and

the curve is less distinguishable. The fluctuation occurs as in the step change to wheel speed – without

the oscillations. This would make sense as the airstream flowrate is delivered as a constant while the

desiccant mass "flowrate" is sinusoidal.
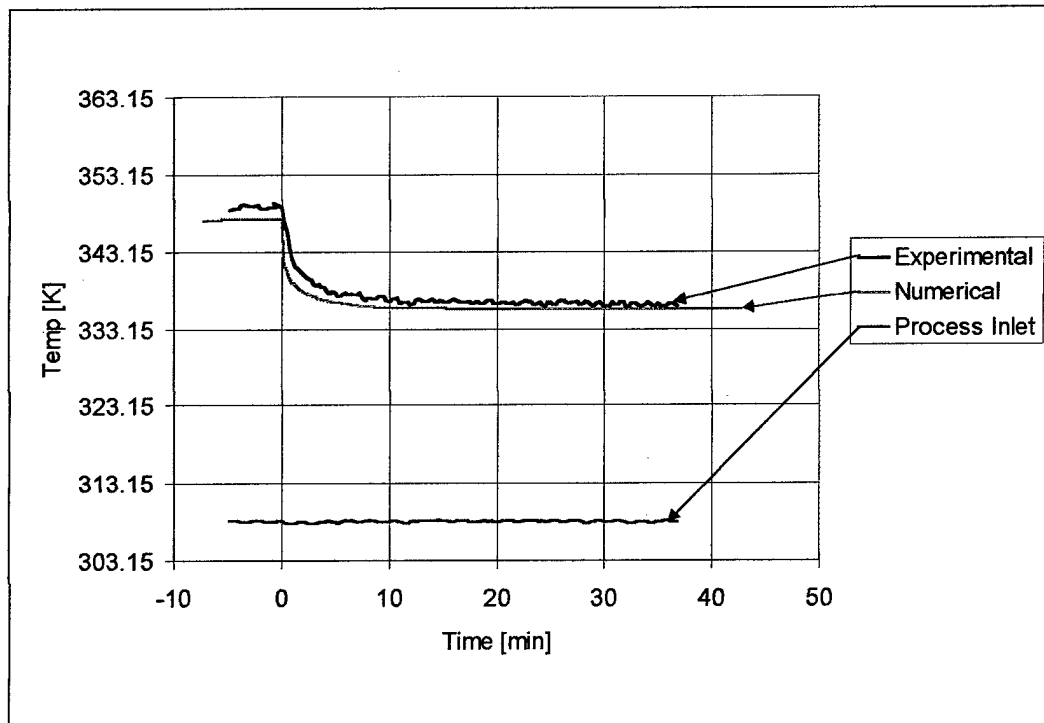
Figure 15. Process Outlet Temperature Versus Time with a
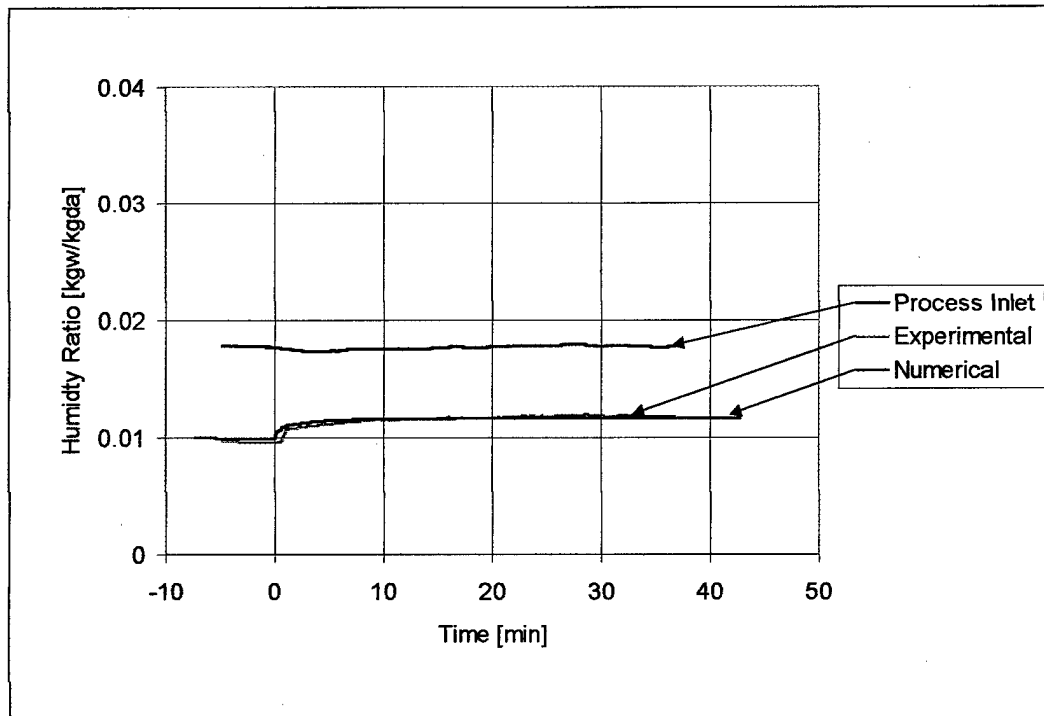Step Increase to Process Flowrate

Figure 16. Process Outlet Humidity Ratio Versus Time with
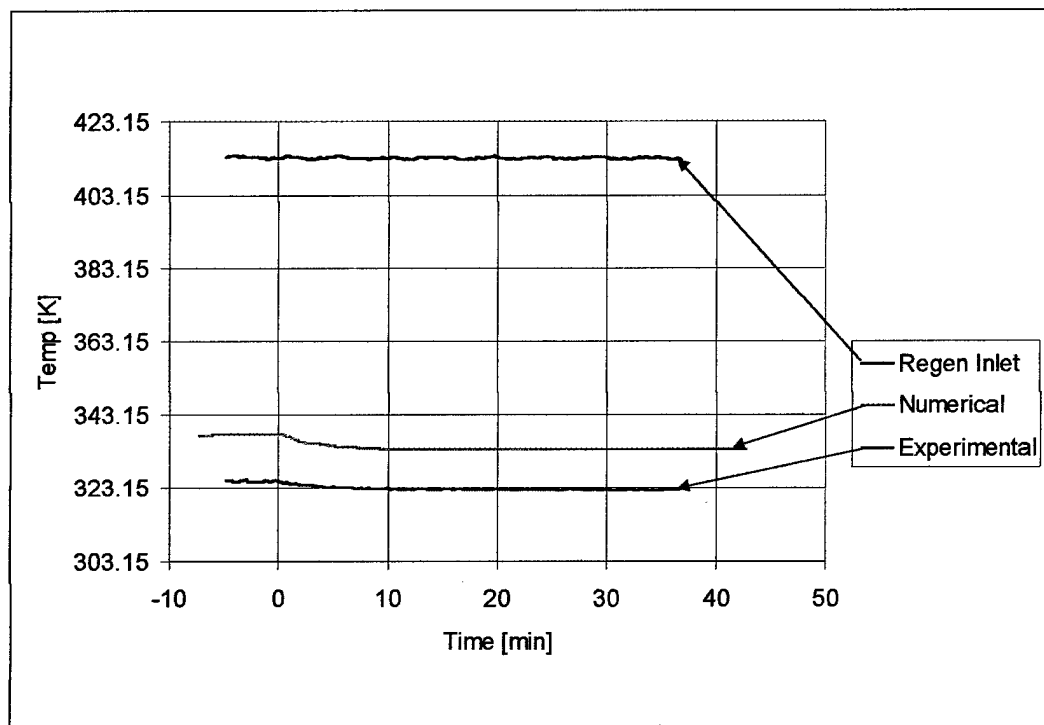a Step Increase to Process Flowrate

33

Figure 17. Regeneration Outlet Temperature Versus Time
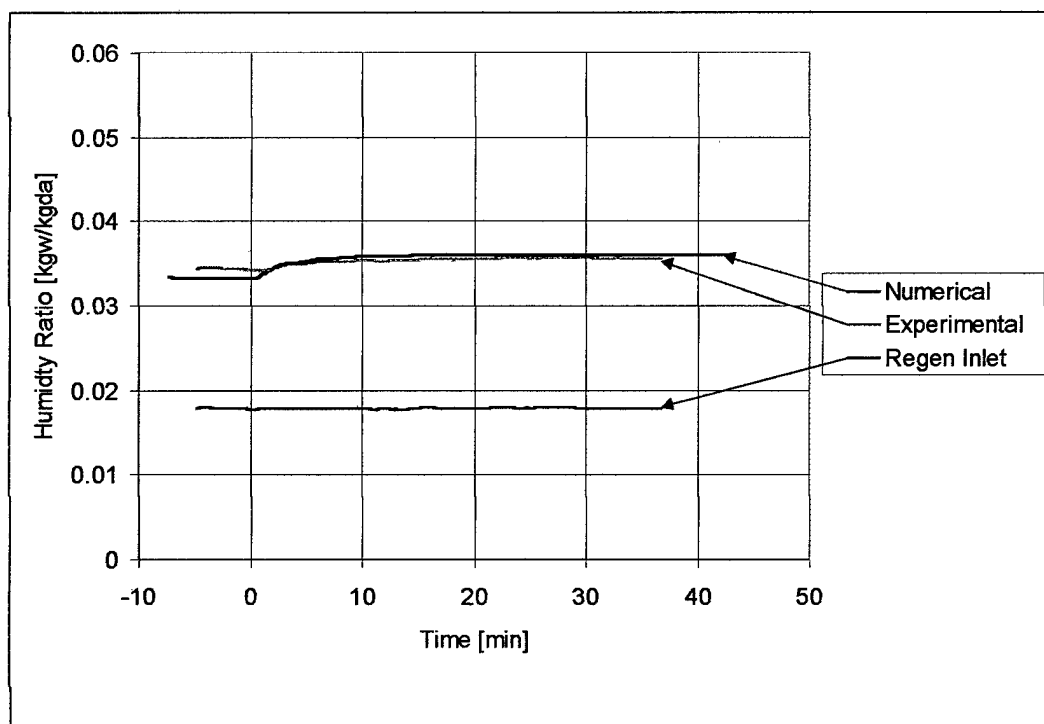with a Step Increase to Process Flowrate

Figure 18. Regeneration Relative Humidity Versus Time
with a Step Increase to Process Flowrate

Run	Stream	Parameter	Av Value	RMSE
step increase to regen temp	process	temp	320.7	0.62
"	process	humidity ratio	0.0150	0.0003
"	regen	temp	314.5	7.77
"	regen	humidity ratio	0.0264	0.0030
step decrease to regen temp	process	temp	319.9	1.09
"	process	humidity ratio	0.0147	0.0001
"	regen	temp	308.4	1.13
"	regen	humidity ratio	0.0230	0.0010
step increase to wheel speed	process	temp	332.5	0.62
"	process	humidity ratio	0.0123	0.0003
"	regen	temp	324.5	9.55
"	regen	humidity ratio	0.0343	0.0010
step decrease to wheel speed	process	temp	332.1	0.50
"	process	humidity ratio	0.0123	0.0006
"	regen	temp	324.5	11.16
"	regen	humidity ratio	0.0345	0.0011
step increase to process flowrate	process	temp	342.4	1.28
"	process	humidity ratio	0.0105	0.0002
"	regen	temp	324.0	11.04
"	regen	humidity ratio	0.0340	0.0004
step decrease to process flowrate	process	temp	342.0	1.36
"	process	humidity ratio	0.0108	0.0005
"	regen	temp	323.8	12.49
"	regen	humidity ratio	0.0351	0.0012

Table 3. Summary of Root Mean Square Error for All Runs
and Parameters

Steady-state Validation

A good way of looking at the steady-state conditions is to use a psychometric

chart for comparison, Figure 19. In this case, the steady-state values of the first run

are used. The two profiles for heat and mass transfer, the rectangle and triangle,

appear to follow a linear extension from the inlet conditions. This corresponds to

their NTU values: greater NTU magnitudes of the triangular profile translate into

greater heat and mass transfer as one might expect.

Clearly, the process outlet values are in very good agreement with all three

sources of data. Only the numerical solution with the triangular profile appears to

slightly deviate from the pack. On the regeneration side; however, there is significant

separation between the experimental data and the numerical and/or historical. The

triangular and rectangular points are about equidistant from the experimental data.

The triangular point is closer in temperature while the rectangular point is closer in

humidity ratio. The historical curve fit point is substantially closer to the numerical
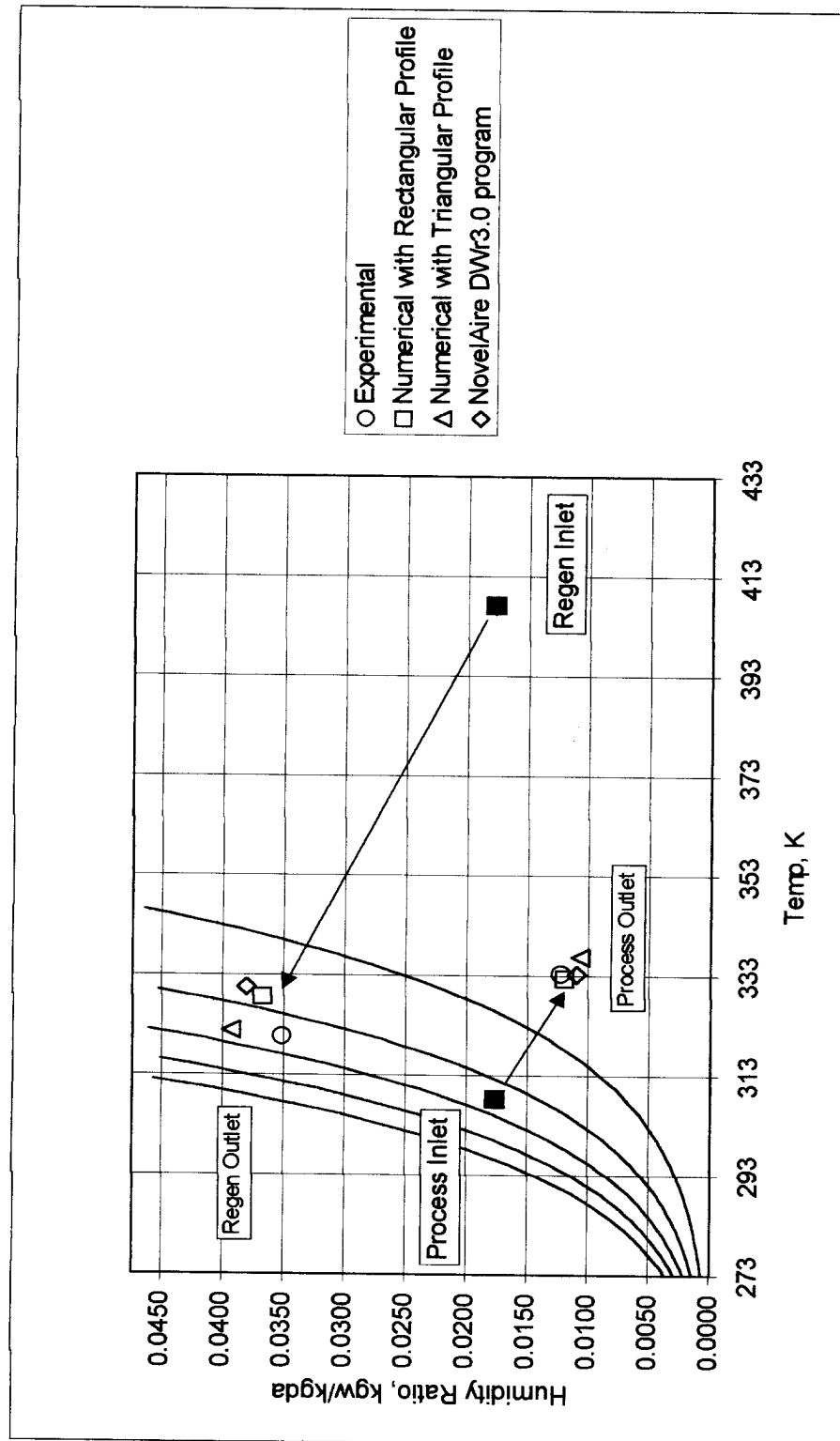
run with the rectangular profile.

Figure 19. Steady-State Comparison of Process and Regeneration Outlet States Using Experimental, Numerical, and Historical Data (NovelAire DWr3.0)

Mass and energy balances, using Error! Reference source not found. and Error! Reference source not found., are much better for the numerical and historical points than with the experimental points for all cases. Specifically, the energy balances for the experimental runs give ratios of approximately 0.6-0.8. The numerical runs and the program based on historical data conserve mass and energy implicitly and their balances are typically between 0.98 and 1.0. Because the experimental runs do not appear to conserve both mass and energy well, the numerical results cannot be expected to validate perfectly with the experimental results.

There are several possible explanations for the deviation of the mass and energy balances of the experimental data. They will be reviewed here.

1. The inaccuracy associated with the sensors themselves. An uncertainty analysis was performed using the accuracies provided by the laboratory as listed in Chapter 5 (Experimental Setup) with the steady-state inlet and outlet parameters (flowrate, temperature, and humidity ratio). A mass and energy balance was done on the wheel using the steady-state conditions from the step increase to regeneration temperature.

The uncertainty analysis used the procedure presented by Kline-McClintock [Holman, 1989]. This analysis calculates a combined uncertainty error that takes into account the error of all variables. The result of this analysis is an absolute energy balance ratio error of 0.22. The accuracy bounds of the sensors can therefore significantly impact the energy balance and agreement with the numerical results.

$$ErrorR = \left[\left(\frac{\partial R}{\partial x_1} err_1 \right)^2 + \left(\frac{\partial R}{\partial x_2} err_2 \right)^2 + \ldots + \left(\frac{\partial R}{\partial x_3} err_3 \right)^2 \right]^{1/2}$$

2. Leakage. Leakage occurs when air from one stream enters the other stream through openings between the casing and the wheel itself or releases air straight to the atmosphere as shown in Figure 20. Some leakage does occur during normal operation and previous researchers have quantified the leakage percentages for the different pathways using other systems to be in the range of 1-4.3% [Schultz, 1987].

Experimental Pressure Readings indicate a difference of approximately 2.4 inWG between the Process Inlet and Regeneration Outlet Streams and 1.8 in WG between the Regeneration Inlet and Process Outlet Streams. This pressure difference clearly indicates that some leakage must occur since there are openings in the plenum where this is possible.

Another indication of leakage within the experimental wheel runs are the mass flowrates. The input values used in **Error! Reference source not found.** for the computer model indicate the mass flowrates are constant from inlet to outlet because the computer model uses a constant flowrate. The actual experimental values for inlet and outlet flowrates differed in some cases by as much as 6%. The values listed in **Error! Reference source not found.** are the lower flowrates which were assumed to have made it through the wheel and were used by the numerical model. The difference in flowrates also indicate carryover and possible leakage to the atmosphere.

The disagreement in the energy balance of the experimental results and the discrepancy with numerical regeneration temperature is believed to be the result of combined sensor accuracy and carryover/leakage within the experimental apparatus.
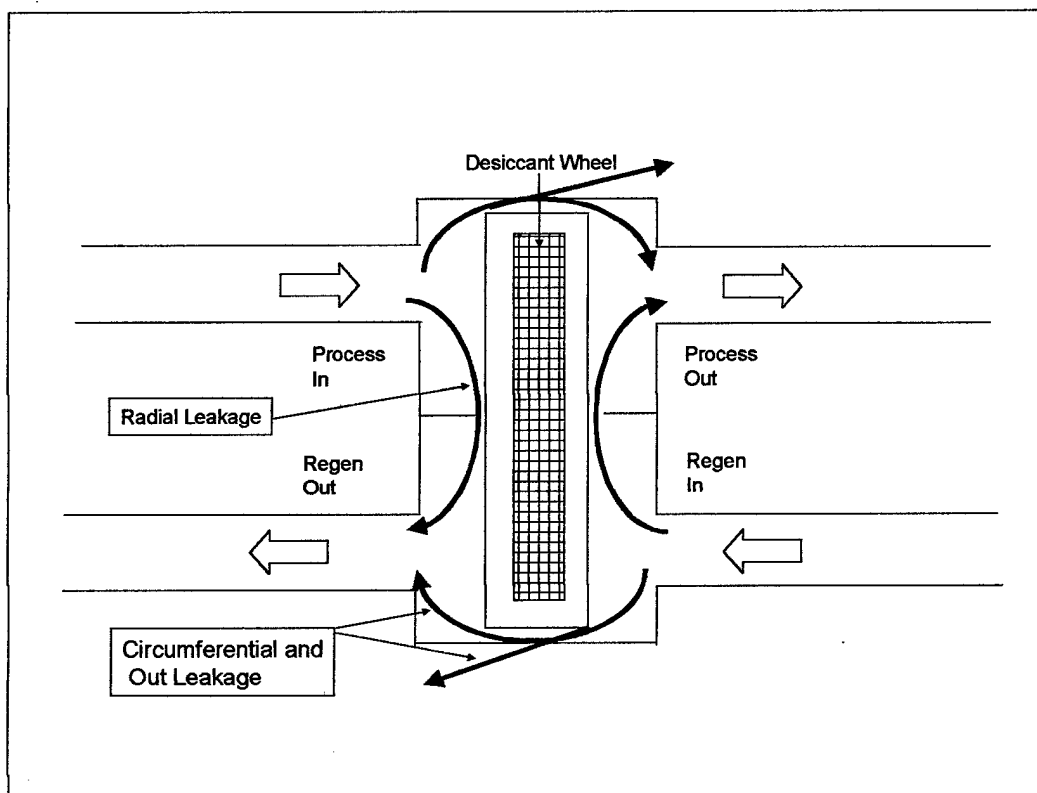
Figure 20. Schematic Showing Possible Leakage Sites

Summary

It can be seen from the transient graphs and the summary (

Table 3) that the numerical finite difference scheme with the PCP model does, in

fact, reasonably represent the transient response of a rotary heat and mass desiccant

wheel.

The summary of transient response times (Table 4) shows that the transient

response of the WSG rotary desiccant wheel under these conditions is significant relative

to the response time of a typical cooling coil. The steady-state values were calculated at

a point removed from the transient phase. The transient times were essentially

determined using 99% of the steady-state value or almost the full transient period.

Run	Stream	Parameter	initial	SS value	time (min)
step increase to regen temp	process	temp	308.15	333.4	22.1
"	process	humidity ratio	0.0177	0.0122	22.1
"	regen	temp	308.15	320.5	22.0
"	regen	humidity ratio	0.0177	0.035	5.0
step decrease to regen temp	process	temp	333.4	306	38.9
"	process	humidity ratio	0.0122	0.0177	38.9
"	regen	temp	320.5	300	36.8
"	regen	humidity ratio	0.035	0.01	26.8
step increase to wheel speed	process	temp	330.7	334.1	5.0
"	process	humidity ratio	0.0126	0.011	3.5
"	regen	temp	327	321	12.5
"	regen	humidity ratio	0.034	0.035	10.0
step decrease to wheel speed	process	temp	333	331	10.0
"	process	humidity ratio	0.0117	0.0127	4.0
"	regen	temp	321	327	10.0
"	regen	humidity ratio	0.035	0.034	9.0
step increase to process flowrate	process	temp	348	336	12.0
"	process	humidity ratio	0.0096	0.011	10.0
"	regen	temp	325	323	10.0
"	regen	humidity ratio	0.034	0.035	10.0
step decrease to process flowrate	process	temp	336	348	15.0
"	process	humidity ratio	0.0118	0.0095	13.0
"	regen	temp	322.5	325.5	15.0
"	regen	humidity ratio	0.0357	0.0344	15.0

Table 4. Summary of Full Transient Time for All Runs And Parameters

41

The Transient Response of Rotary Desiccant Wheels Through

Experimentation and Numerical Analysis

by
Stephen Delbert Grumbach

B.S. Clemson University, 1984

M.S. Air Force Institute of Technology, 1989

A thesis submitted to the

Faculty of the Graduate School of the

University of Colorado in partial fulfillment

of the requirement for the degree of

Doctor of Philosophy

Department of Civil Engineering
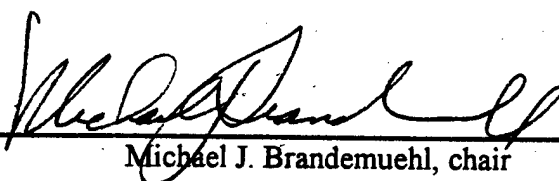
1999

This thesis entitled

The Transient Response of Rotary Desiccant Wheels Through

Experimentation and Numerical Analysis

Written by Stephen Delbert Grumbach

Has been approved for the Department of Civil Engineering

_____

Michael J. Brandemuehl, chair

_____

Shelly Miller

_____

Peter Curtiss

_____

Jan Kreider

_____

Moncef Krarti

Date   19 Jul 99

The final copy of this thesis has been examined by the signatories, and we find that
both the content and the form meet acceptable presentation standards of scholarly
work in the above mentioned discipline.

ABSTRACT

Grumbach, Stephen Delbert (Ph.D. Civil Engineering)
The Transient Response of Rotary Desiccant Wheels Through Experimentation and
Numerical Analysis
Thesis directed by Professor Michael J. Brandemuehl
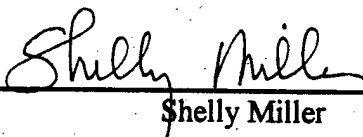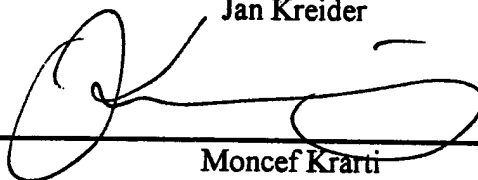
Rotary desiccant wheels are commonly used for industrial dehumidification
systems and significant research is being done to increase their application in other
HVAC systems. The transient response is of concern because it can affect overall
system performance and previous research efforts have indicated the transient
response to be of substantial duration.

This research experimentally and analytically investigated the transient
response of rotary desiccant wheels.

A model was developed to predict the transient response of rotary desiccant
wheels with significant improvements to previous versions. The basic model uses
fundamental principles of heat and mass transfer with the finite difference method.
The parabolic concentration profile was used to approximate moisture gradients
within the desiccant particle. This concept is fundamentally more correct than
previous lumped capacitance models and avoids the computational difficulties of
more rigorous models which include an extra second order differential equation. The
NTU terms from the finite difference equations were also calculated at each point
rather than as constants for a stream or element since they are significantly
temperature and moisture dependent. The numerical solution techniques improved
the speed and flexibility of the model by using a tridiagonally banded matrix solver

for the difference equations and the bisection method was used for the parabolic concentration profile.

Experimental work was performed at the National Renewable Energy Laboratory (NREL) in Golden, CO on a commercially available rotary desiccant wheel made by NovelAire. Step changes to regeneration temperature, wheel speed, and flowrate were performed.

The model was validated by comparing the experimental data to model predictions using statistical and visual analysis of the outlet condition (temperature, humidity ratio) response curves. An alternative validation technique was also performed by statistically comparing thermographic images of the desiccant wheel surface with numerical calculations.

A parametric analysis was completed to observe the impact of different parameters on the transient response. Operational factors, ambient conditions, and wheel construction can have a substantial impact on the transient response time. Ambient temperature, for example, can increase transient time by up to 97% from a baseline of 16 minutes.

A control strategy comparison was done that determined cycling of rotary desiccant wheels could be an effective and efficient strategy to meet moisture removal requirements.

ACKNOWLEDGEMENTS

I would like to thank several people who have contributed to this effort and helped make my journey a little easier in preparing it. To say that I was challenged in this endeavor is an understatement.

I would like to express my gratitude and appreciation to my advisor, Dr Michael Brandemuehl for his guidance, excellent advice, teaching, and patience. His knowledge and experience helped me understand the concepts and frame the problem that I needed to solve. Despite his busy schedule, he managed to find time. Even when I would repeatedly ask a basic question...

I would also like to thank the members of my proposal and defense committee who have taken the time to help me complete this project.

I am also indebted to Steve Slayzak and Joe Ryan of NREL who allowed me to do the experimental work there. They provided a professional laboratory that was able to run the experiments quickly and precisely.

To my mom and dad. Thank you for the encouragement. Your support never wavered.

To my brother Robert, thanks for coming out on the ski trips.

To my wonderful family: Sue, Jasmine and Laura. Thank you for this opportunity. You supported me and understood when I had to work. This has not been easy because of the time involved and I appreciate your patience. Thank you very much.

Finally, thank God.

TABLE OF CONTENTS

LIST OF FIGURES

LIST OF TABLES

NOMENCLATURE

a_2 coefficient for parabolic concentration profile [kg$_{water}$/kg$_{desiccant}$]

a constant representing adsorption bonding in surface diffusion model

ADP   apparatus dew point [ ]

a_K average pore radius [m]

A_s exchanger transfer area [m^2]

b surface diffusion parameter describing type of adsorption bond

COP   coefficient of performance [ ]

$c_{p,da}$ specific heat of dry air at constant pressure [kJ/kg$_{da}$K]

$c_{p,dm}$ specific heat of dry desiccant matrix [kJ/kg$_{dd}$K]

$c_{p,lw}$ specific heat of liquid water [kJ/kg$_{lw}$K]

$c_{p,m}$ total specific heat of desiccant matrix

$c_{p,ma}$ specific heat of moist air at constant pressure [kJ/kg$_{da}$K]

$c_{p,wv}$ specific heat of water vapor at constant pressure [kJ/kg$_{wv}$K]

D_{AB} mass diffusivity with subspecies A and B [m2/s]

dh hydraulic diameter [m]

D_o uncorrected surface diffusivity

$D_{s,eff}$ effective surface mass diffusivity [m^2/s]

E number of trials for Chi-Square statistical test

h^* ratio of enthalpy of adsorption to enthalpy of vaporization [ ]

h_m mass transfer coefficient [kg$_w$/(m^2·s·kg$_w$/kg$_{da}$)]

h_q heat transfer coefficient [W/(m^2·K°)]

ΔHw	integral heat of wetting [kJ/kg_{dd}]
i	enthalpy of the airstream on a dry mass basis, [kJ/kg_{da}]
i_{ad}	heat of adsorption [kJ/kg_w]
i_{fg}	latent heat of vaporization of water [kJ/kg_w]
i_{lw}	enthalpy of liquid water [kJ/kg_{lw}]
I	enthalpy of the desiccant per unit mass dry desiccant [kJ/kg_{DD}]
i_{st}	isosteric enthalpy of adsorption[kJ/kg]
k_{da}	thermal conductivity of air [$W/(mK)$]
Kn	Knudsen diffusion [m^2/s]
L	axial length of the rotary wheel [m]
Le	Lewis number [Le]
$\dot{m}_{da}$	mass flowrate of dry air [kg_{da}/s]
M_{dd}	mass of dry desiccant [kg]
MRC	moisture removal capacity [kg_w/hr or lbm_w/hr]
n	number of occurences for the Chi-Square statistical test
n	parameter for Lewis analogy [ ]
NTU_m	number of transfer units, mass [ ]
NTU_q	number of transfer units, thermal [ ]
Nu	Nusselt Number [ ]
N_x	number of steps in the axial direction [ ]
$N_{\theta,s}$	number of circumferential steps [ ]
Pr	Prandtl number [ ]
p_t	total pressure [Pa]

p_v	vapor pressure [Pa]
p_{vs}	saturation vapor pressure [Pa]
R, r	radius of desiccant particle [m]
R	universal gas constant [kJ/(kg-K)]
Re	Reynolds number [ ]
RH	relative humidity [%]
RHe	equilibrium relative humidity [%]
RMSE	root mean square error [ ]
Sc	Schmidt number [ ]
SH, SH_L	Sherwood number [ ]
SHR	Sensible Heat Ratio [ ]
t	air temperature [°K]
T	matrix temperature [°K]
T_H	high temperature heat sink of a Carnot cycle [°K]
T_L	low temperature heat sink of a Carnot cycle [°K]
V, v	velocity [m/s]
v_{fg}	specific volume difference between vapor and liquid [m³/kg]
w	humidity ratio of moist air [kg water/kg dry air]
W	mass fraction of desiccant, [kg water/kg dry desiccant]
w_e	equilibrium humidity ratio of air [kg water/kg dry air]
Ws	surface mass fraction desiccant [kg water/kg dry desiccant]
x	non-dimensionalized axial length [ ]
z	axial distance [m]

Greek

β ratio of stream period to the wheel period [ ]

χ^2 Chi Squared Statistic [ ]

ε effectiveness [ ]

Γ mass capacity rate ratio [ ]

η non-dimensional response [ ]

ϕ rotation angle [radians]

λ_K Knudsen mean free path [m]

λ_s surface mean free path or jump distance [m]

μ viscosity [Ns/m^2]

ν dynamic viscosity [m^2/s]

θ non-dimensionalized time [ ]

ρ_p density of particle [kg/m^3]

τ time [s]

τ_j duration of period j [s]

τ_p rotational period [s]

τ_s tortuosity factor for intraparticle surface diffusion [ ]

Subscript

av	average
i	initial
j	axial position
k	circumferential position
p	process stream
r	regeneration stream
s	stream, process or regeneration
t	temperature
w	humidity

CHAPTER 1. INTRODUCTION

Problem Description

Heating, ventilating, and air conditioning (HVAC) engineers have grown

more concerned with issues of humidity control over the last several decades.

Increasing ventilation requirements and energy costs make the total cost of removing

ambient moisture a significant issue/concern. In addition, damage to facilities,

materials, and furnishings due to exposure to moisture can also be costly and time

consuming. Possible adverse health effects and discomfort from excess moisture or

humidity are clearly a concern as well.

Excessive moisture within buildings can cause significant, long term damage

to assets within the building and to the structure itself. The damage manifests itself in

two main forms: the growth of molds and mildews and simple, excessive moisture.

The molds and mildews cause peeling of vinyl wall coverings, fungal growth and

stains, odors, surface mildew on interior finishings, and adverse health reactions. The

excessive moisture can by itself cause corrosion, crumbling gypsum board, paint de-

lamination, stains, and a cold, clammy feeling within the interior environment

[Banks, 1992][Odom et al., 1992].

Motels, hotels, and dormitories are facility types where these problems are

most notable because of the low internal heat gain and the relatively high ventilation

rates required. A survey done in 1990 by the members of the American Hotel and

Motel Association revealed that moisture, mold, and mildew cost approximately $68

million each year in lost revenue and damage repair. A second survey was done to

estimate customer dissatisfaction. Seventy percent of those who responded complained of musty, stale rooms caused by mold and mildew. Rust and mildew stains were also mentioned as significant problems [Banks, 1992]. Certainly, excessive moisture can have significant maintenance costs and decrease revenues and profits.

The moisture in buildings comes from four main sources: diffusion through walls, infiltration through openings, internal gains (people, equipment), and ventilation air. Moisture diffusion through materials accounts for a small portion of the moisture load. The majority (at least 90%) of the moisture gain comes from the other three sources. Most air conditioning systems are supposed to be designed to handle these moisture gains. If not, the room will have an excessively high relative humidity or moisture may condense directly on room surfaces if they are below dewpoint. The recent increase in ventilation rates to satisfy indoor air quality requirements as specified by ASHRAE Standard 62-1989 also exacerbated the moisture removal problem.

Within the ventilation load, the moisture or "latent load" can be significant. Figure 1 [Kosar et al., 1998] demonstrates the sensible heat ratio (SHR) of a 100% outside air ventilation load for three different U.S. locations. The sensible heat ratio is simply defined as the sensible load divided by the total load (sensible + latent). These SHRs mean that under design conditions more than half of the total load is required for moisture removal for systems with 100% outside air.

SHR=.17

SHR=.46

SHR=.22   SHR=.18

SHR=.48   SHR=.58

60000
50000
40000
30000
20000
10000
0

Load per 1000 SCFM of Outdoor Air (Btu/hr)

■ Latent
■ Sensible

| 2.5% dry bulb | 2.5% dew point | 2.5% dry bulb | 2.5% dew point | 2.5% dry bulb | 2.5% dew point |

Chicago

89F DB/74F MCWB
(31.7C/23.3C)

103 gr/lb (14.7 g/kg)

72.7F DP/83F MCDB
(22.6C/28.3C)

122 gr/lb
(17.4g/kg)

Atlanta

92F DB/74F MCWB
(33.3C/23.3C)

98 gr/lb (14.0 g/kg)

72.7F DP/83F MCDB
(22.9C/27.2C)

124 gr/lb (17.7g/kg)

Houston

94F DB/77F MCWB
(34.4C/25.0C)

113 gr/lb (16.1 g/kg)

77.0F DP/83F MCDB
(25.0C/28.3C)

141 gr/lb (20.1g/kg)

Mean Coincident Wet Bulb = MCWB
Mean coincident Dry bulb = MCDB

Figure 1. Ventilation (100% Outside Air) Loads at Design Conditions (Kosar et al., 1998)

The energy cost of conditioning ventilation air can also be substantial. For example, a field test completed in 1992 on a hotel wing in Miami with about 75 rooms and a cool/reheat system determined the annual energy cost for the ventilation air alone to be around $25,000 for the year[Banks, 1992]. The ventilation load is

3

usually a significant portion of the total building load and is a direct function of the number of people, operational schedule, and temperature and relative humidity of the location. The ventilation air that is brought into a facility consists of dry air and moisture that must be conditioned to an acceptable level.

Typical air conditioning arrangements for comfort cooling commonly rely on the dehumidification capabilities of vapor compression cooling coils. Some applications of vapor compression (VC) equipment simply cannot remove sufficient moisture without overcooling the building or excessive re-heating costs. While there are a number of solutions to this dehumidification problem, they generally pay a penalty of increased equipment size, or significant additional energy, increased fan power, lower performance efficiency, or a combination of these.

One solution that has been implemented successfully in many dehumidification applications is the use of desiccant materials. Desiccant systems have been primarily applied to industrial systems for dry storage conditions or special processes which require an airstream of very low humidity. The desiccant industry is currently looking for increased application in the comfort cooling HVAC market. Desiccant systems are an alternative to conventional air conditioning systems for dehumidification and are capable of "deep drying" air to very low humidity ratios.

The two primary forms of desiccant dehumidification are through liquid absorbents and solid adsorbents. The most common form of the solid adsorbent is the desiccant wheel, Figure 2. As shown in Figure 2, the airstream that will lose moisture and transfer it to the wheel is called the "process" stream. This stream is typically the one used for the process of concern such as ventilation or a manufacturing process.

4

The other airstream, called the "regeneration" stream, will gain moisture from the wheel and functions as the "waste" stream. The psychrometric chart (also Figure 2) shows that the process stream decreases its humidity ratio and increases in temperature. The regeneration stream increases its humidity ratio and decreases in temperature. Essentially, the desiccant wheel exchanges latent load or moisture for sensible load or temperature with a very small change in enthalpy.

There are two basic types of desiccant systems: those designed for both cooling and dehumidification and those designed to work with vapor compression systems. While the desiccant and evaporative cooling systems hold promise, the combined or "hybrid" systems using vapor compression and desiccants have already been used successfully. In these systems, the vapor compression equipment is generally responsible for the "sensible" or heat energy load. The desiccant component is responsible for the latent load or dehumidification.
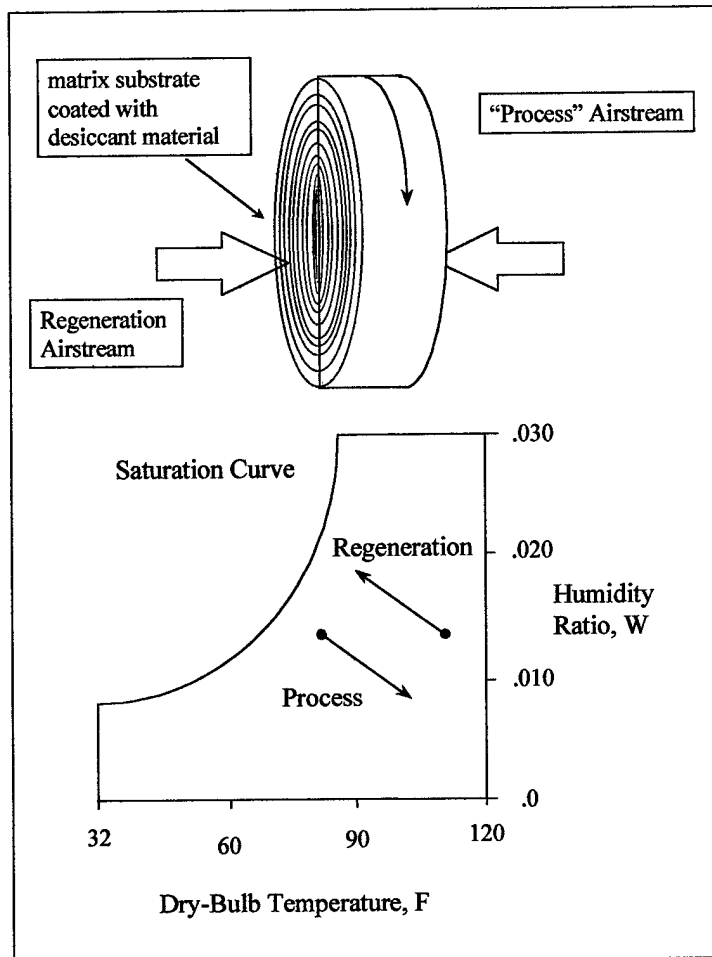
Figure 2. Simple Desiccant Schematic and Psychrometric Chart

Transient Response

A simple definition of transient operation or response is defined as the period of time required for the output variable(s) of a system to reach a constant or steady-state value in response to a change in the input variable(s). The transient response of the rotary desiccant wheel has been previously estimated to require approximately one hour of time to reach steady-state [Brandemuehl, 1982]. The typical HVAC system can reach steady-state in a few minutes. The transient response period of the rotary desiccant wheel suggests several issues that need to be addressed regarding their control.

6

The first issue is the effectiveness of the system. This is qualitatively defined here as how well the system provides air at a given temperature and moisture level. One current practice is to run desiccant dehumidification systems continuously to avoid the transient response altogether. Therefore, the transient response has no impact on the effectiveness of the system. If the system operates on a cyclical basis, the transient response of the rotary desiccant wheel could be a significant factor. For example, a cooling coil can reach steady-state normally within 1 to 2 minutes. Assuming the cooling coil reaches steady-state much faster than the desiccant wheel, problems can occur depending upon the type of feedback control. If the system is temperature controlled and the cooling coil reaches steady-state quicker than the desiccant wheel, it could also satisfy the load before the desiccant wheel has reached steady-state. A substantial amount of air that has not been satisfactorily dehumidified could reach the conditioned space. This excess humidity could damage materials within the space or make occupants within it uncomfortable. Frequent cycling can compound the problem.

The second issue is the efficiency of the system or how much energy is consumed for a given amount of dehumidification. As stated above, one current practice for desiccant dehumidification is to run them almost continuously in order to ensure meeting ventilation requirements and avoid the transient response of the desiccant wheel. It can be quite expensive, however, to have a system running continuously. Cycling the unit can lower the energy cost but also lower the moisture removal capacity. In order to compare systems, it is also interesting and necessary to see how much energy is consumed over some operational period with the transient

7

response. Therefore, there is a trade-off: cycling the wheel can reduce the operational cost but the transient response of the desiccant wheel could also cause a significant amount of overly humid air to enter the space. This would imply that significant gains maybe found if the characteristics of the transient response and its impact upon the ventilation system can be found.

What makes the desiccant wheel unique when used in combination with a vapor compression coil is the time to reach steady-state conditions. Several studies have indicated that the time to reach steady-state for desiccant wheels is significant. Pesaran [1987] shows graphs of transient fixed-bed response with the system requiring approximately 12 minutes to reach steady-state. Figures from Brandemuehl [1982] have shown that the wheel may, in fact, need as long as one hour to reach steady-state. Charles Cromer [1998] indicated that his cycle started substantial dehumidification almost immediately. Discussions with engineers at the National Renewable Energy Laboratory (NREL) who regularly work with desiccants say the average is around fifteen minutes. This small sample is indicative of the variance in the behavior of desiccant wheel transient response.

Assessment

Of the studies done on transient response of rotary desiccant wheels, none has actually compared experimental data with analytical data in the time domain for a rotary heat and mass desiccant wheel. Wilmott and Burns [1977] did a transient analysis on a sensible only rotary regenerator. Brandemuehl [1982] calculated analytic transient results but he did not have experimental data to compare with the analytical results. Pesaran [1987] showed results comparing experimental data with

analytic models; however, the geometry was a fixed bed. While the fixed bed is similar to the rotary wheel, there has not been a study that actually compares and shows experimental and analytic transient response data of a rotary heat and mass desiccant wheel. The rotary wheel is significantly more complicated than a fixed bed and there could be interactions that affect the transient response differently.

Current wheel technology has also improved significantly since previous studies. Current technology uses a homogeneous mixture of substrate and desiccant; previous technology used desiccant attached to the surface of a substrate. The agreement between experimental results and analytical results could be impacted with this improvement in wheel construction.

Certainly the capability to predict desiccant wheel behavior is desirable and a number of models have been developed to analyze and predict its behavior under different circumstances [Carter, 1966; Maclaine-cross, 1972; Barlow, 1982]. The most accurate of these models; however, requires either excessive experimental data (lumped capacitance transfer coefficients) or excessive computational effort for the moisture gradients within the particle. The parabolic concentration profile (PCP) is a concept that provides model flexibility and ease of application because it is based on fundamental principles. It assumes a parabolic profile of the moisture gradients within the desiccant particle and then proceeds based on first law principles. Individual experimental values are not required as with lumped capacitance models. It has a lower computational requirement; however, than more rigorous models with an additional second order differential equation. Until this research, the PCP concept

9

had not been successfully used and validated in the transient response of rotary desiccant wheels.

There is currently no direct solution of the governing equations because all methodologies have either been a numerical solution or a simplification of the governing equations. The finite difference solution is currently the most rigorous and accurate although it has a substantial computational cost. The finite difference solution is also the most capable of dealing with the coupling and non-linearities between the differential equations. Simplified models for doing seasonal simulations of a desiccant wheel such as the analogy method and the pseudo steady-state modes are more computationally efficient but not as flexible or as fundamentally sound as the finite difference techniques that have been used.

Improved numerical techniques are also now available for solving single non-linear equations and simultaneous finite difference equations. These routines could substantially improve the performance and robustness of a rotary desiccant model.

The impact of input variables on the transient response of the rotary desiccant wheel has also not been studied in detail. Clearly, it would be beneficial to know how certain variables affect the transient response and to have some idea of the boundaries of that response.

Finally, there is very little research that specifically addresses control strategies for desiccant wheels in order to optimize their performance. Once the transient response time of the wheel has been quantified, it would be advantageous to know how to maximize the effectiveness and efficiency of the system with the transient response incorporated.

Thesis Objective

The primary objective of this research is to predict, verify, and analyze the transient response of the rotary desiccant wheel. Based on the previous assessment, several specific goals have been developed for this research.

1. Build a computer model to predict the transient response of rotary desiccant wheels.

2. Perform experiments to quantify actual transient response

3. Validate the computer model with experimental results

4. Compare and evaluate factors that affect the desiccant wheel transient response.

5. Compare and analyze control strategies

CHAPTER 2. BACKGROUND AND LITERATURE REVIEW

Air Conditioning Concepts

The latent potion of the outside air ventilation load can be significant depending upon the location and type of facility. In the United States for example, these problems are most prevalent in the fast-growing southeast region where the weather is typically warm and humid. The standard convention to describe the moisture portion of the cooling load is called the sensible heat ratio (SHR). The following example illustrates a typical cooling/dehumidifying process that a designer might see for an application of 100% outside air in a humid environment.

In a typical vapor compression air conditioning cycle, both sensible and latent cooling can be done by the cooling coil. Sensible cooling will be accomplished if the coil temperature is simply below the dry bulb temperature of the entering air. The cooling coil must also be at a temperature lower than the dew point temperature of the entering air in order to remove moisture by condensation. A cooling coil, like the load, has a sensible heat ratio as well. Using the coil sensible heat ratio (CSHR) and the entering air state (EA), a line can be drawn to the saturation curve and label this point the apparatus dew point (ADP), as shown in Figure 3. The ADP is not simply the surface temperature of the coil but, for given inlet conditions, represents the theoretical dew point of the air leaving the coil. It is a function of coil temperature, coil geometry, airflow velocity and airflow states. In fact, it represents the maximum temperature of the coil under ideal conditions. The actual path of the air is also shown: the air is initially sensibly cooled and moisture removal begins when it

reaches the saturation curve and then proceeds down the saturation curve. For simplicity purposes, the CSHR is represented as a line on the psychrometric chart although it is actually a ratio by definition.
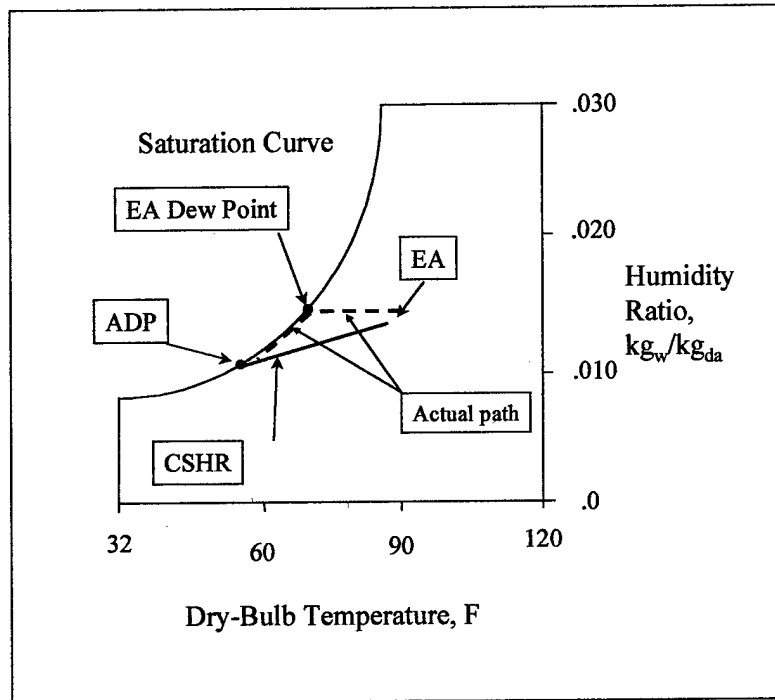
Figure 3. Psychrometric Chart Showing Load SHR Line

COP is defined as the ratio of the amount of energy transferred to the amount of energy input to the system. Based on the Carnot definition of refrigeration:

$$COP_{R,rev} = \frac{1}{\dfrac{T_H}{T_L} - 1}$$

Equation 1

For a refrigeration system, the ADP is related to the low temperature reservoir (T_L). Decreasing the ADP or T_L will lower the COP. The ADP can have a significant effect on the Coefficient of Performance (COP).

An engineer must look at the psychrometrics involved to make sure the cooling coil can handle the particular load. The sensible heat ratio of the coil (CSHR) may not always be equal to that of the load (LSHR) and be capable of handling the humidity load, Figure 4.

When the difference is unadjusted, the room and air streams will settle into an equilibrium and the room conditions will be above the design criteria (if CSHR>LSHR) making the humidity level potentially unacceptably high, Figure 5. The SHR of a conventional vapor compression cooling coil is about 0.75 [Kosar et al, 1998] under typical design conditions.

For commercial facilities, there are several options for dehumdification with varying degrees of effectiveness and cost that have been implemented. For residential facilities, the disparity between coil and load SHR is typically ignored [Chant, 1991].
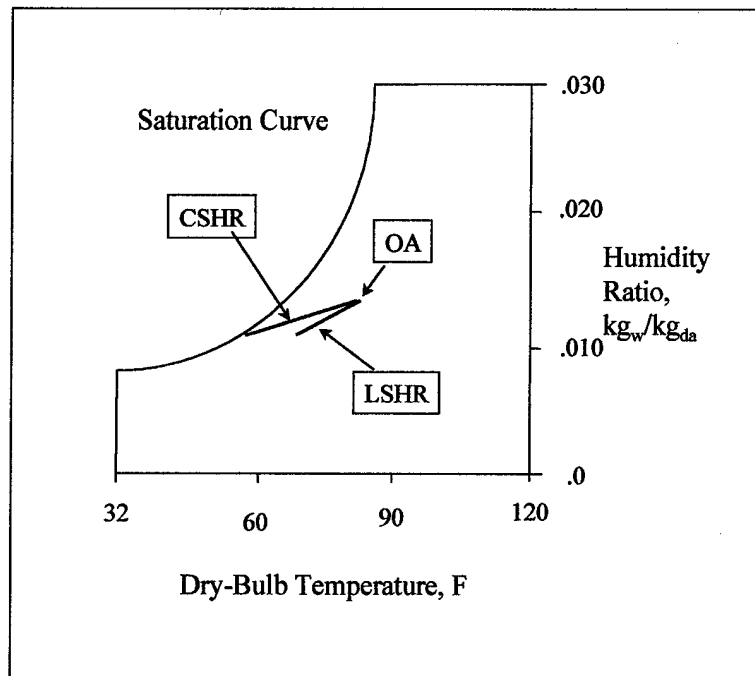
Figure 4. Comparison of Ventilation Load and Coil Sensible Heat Ratios
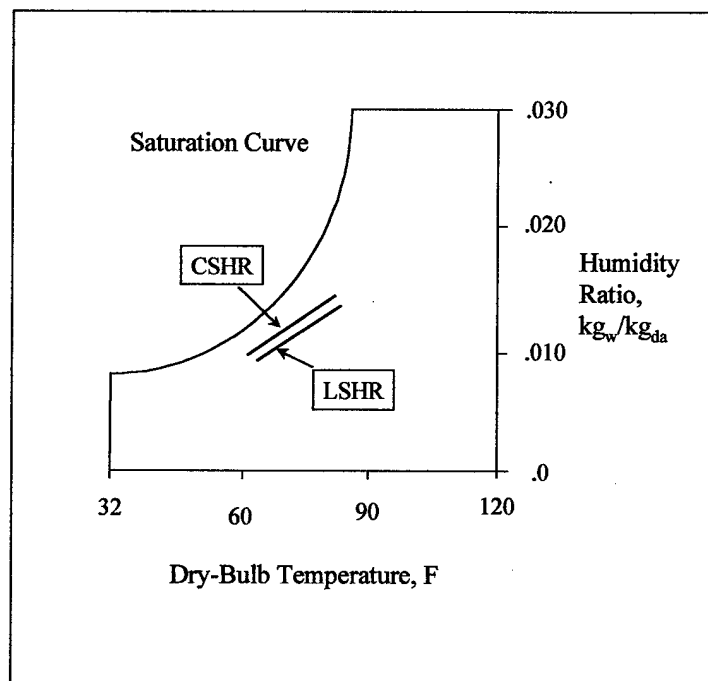
Figure 5. Equilibrium State of Coil and Ventilation Load SHRs

15

Current Air Conditioning Applications

There are several strategies for designing the HVAC system to fit the building load that are well presented by Gatley [1992]: new energy reheat, reheat with refrigerant hot gas, treated air, heat pipes, run-around coils, dual-path air conditioning, return air face and bypass, cool storage, cold air distribution, and desiccant dehumidification. All of these strategies will reduce the space relative humidity; some can use less energy and operate at a lower cost.

One of the strategies used to provide the supply air at a satisfactory temperature is simply to add reheat. Basically, heat is added to the supply air after it leaves the cooling coil. This has the effect of decreasing the relative humidity of the supply airstream and allows the system to "fit" the load profile or SHR, Figure 6. The heat can be a separate source such as electric resistance or natural gas. This has a triple penalty, however, of 1) increasing the equipment size, 2) the cost of heating the air and, 3) the additional over-cooling required [Gatley, 1992].

A variation of this approach is to use waste condenser or compressor heat from the vapor compression system. This improves on the reheat system by removing the penalty for additional heat; however, the other two penalties still remain.

Treated and filtered air that is recycled is another option and has been shown to be cost effective [Gatley, 1992]. Essentially, the return air is simply treated, filtered, and re-circulated back to the building. Both gases and particulates are filtered. There is no or very little outside air required and therefore the OA energy

cost is minimal. The primary cost for this system is the up-front filtration equipment cost.

Heat pipes or run-around coil systems are other options for aiding the vapor compression system with dehumdification. Essentially, sensible energy is transferred between the supply and return air streams to match the load, Figure 7. Because the air going over the cooling coil is closer to saturation, increased dehumidification can be achieved with condensation on the coil. There is no penalty for the heat energy as with the new energy system. However, for direct expansion (DX) systems the ADP is lowered and the COP suffers slightly as well. Additional fan power is also required due to the increased pressure drop. The heat pipe is a simple heat exchanger with no additional energy requirement. There is an additional cost for the piping and pump as well as the energy cost to operate the pump.
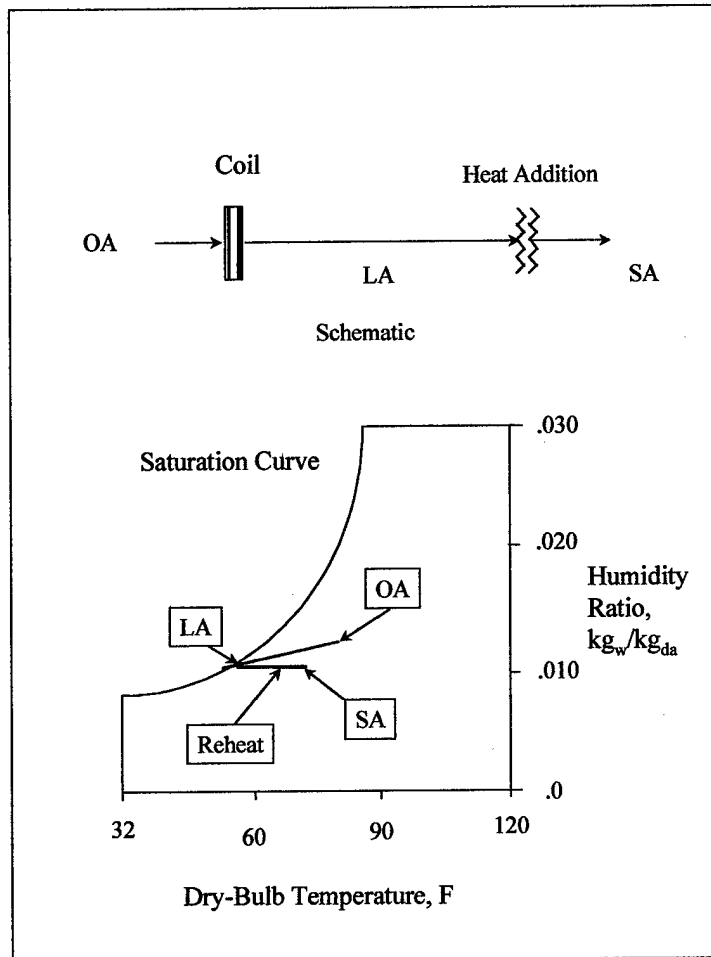
Figure 6. Schematic and Psychrometric Chart of Reheat Strategy

The dual path air conditioning strategy and the return air face and bypass systems basically involve dedicating a cooling coil to dehumidifying the outside air. The dual path uses a completely separate coil. The Face and Bypass system uses a controlled damper with a single coil. Reheat may still be required at part load conditions however.
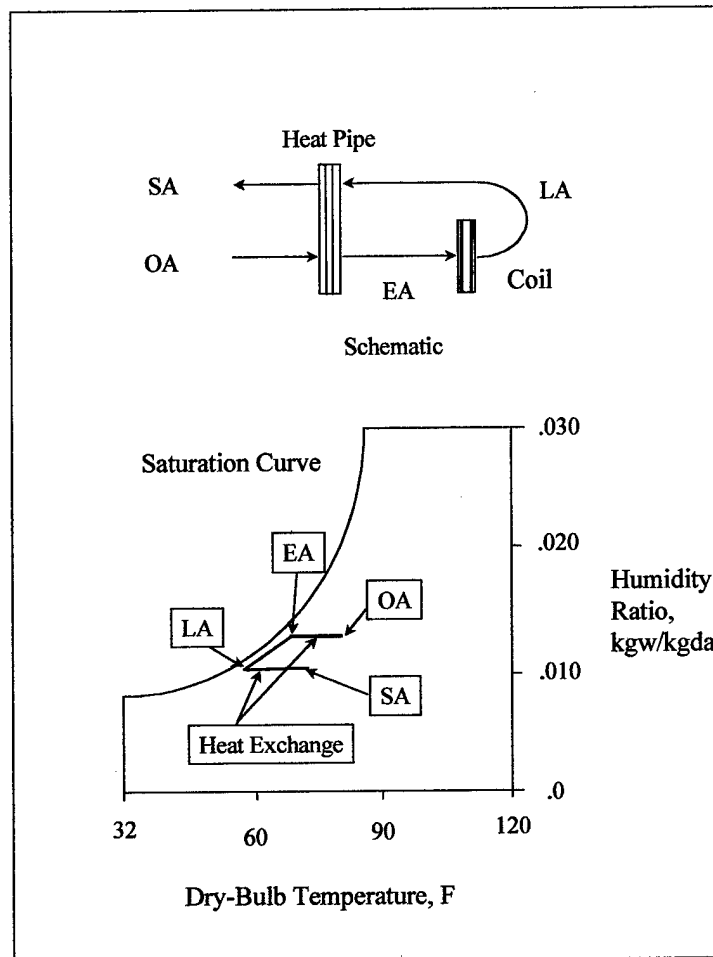
Figure 7. Heat Pipe Schematic and Psychrometric Chart

Current Desiccant Dehumidification Applications

An alternative technology available for dehumidification is to use desiccants

with regeneration. Specifically, the rotary desiccant wheel as shown in Chapter 1 is

the most common.

While the main thrust of this research is for desiccant dehumidification, there

are systems made entirely of desiccant components for both cooling and

dehumidification. Both the Pennington cycle and ventilation cycle are complete

cooling systems. They have been researched because of the potential renewable

energy source that desiccants can utilize [Maclaine-Cross, 1972; Brandemuehl, 1982;

19

Jurinak, 1982; Banks, 1992]. These systems use desiccant wheels to remove the latent portion of the air and then evaporatively cool the air. Any of the above listed references has a well-developed description of these systems.

Because this research is focused on using desiccant wheels for dehumidification, it is appropriate to look at complete cycles that use desiccants for dehumidification. There are two cycles where the desiccant portion is dedicated strictly to dehumidification. The first is the relatively common cycle referred to as the typical desiccant enhanced cooling cycle (DEC), the second is a relatively new cycle that was first proposed in 1988 called the Cromer cycle [Cromer, 1988].

The DEC cycle is shown in Figure 8. The system shown includes options to increase the efficiency of the system through heat recovery. The process stream begins as ambient air at point 1 and is dehumidified by a desiccant wheel. It emerges at point 2 with a lower humidity ratio and higher temperature. Passing through a sensible heat exchanger connected to the ambient air of the regeneration stream, the process stream is sensibly cooled, point 3. The process stream is further cooled by a vapor compression coil down to design conditions at point 4. The regeneration stream begins as ambient air at point 5. It is slightly heated by the sensible heat exchanger (point 6). The regeneration stream is then heated to full regeneration temperature by new thermal energy or a waste heat source (point 7). After passing through the desiccant wheel (point 8), the regeneration stream has absorbed moisture from the wheel and decreased in temperature.

The heat source can be either waste condenser heat from the vapor compression system or new heat from another source such as a boiler or directly from

a burner. The regenerated desiccant wheel allows this system to achieve deeper

drying and to separate sensible cooling from dehumidification.
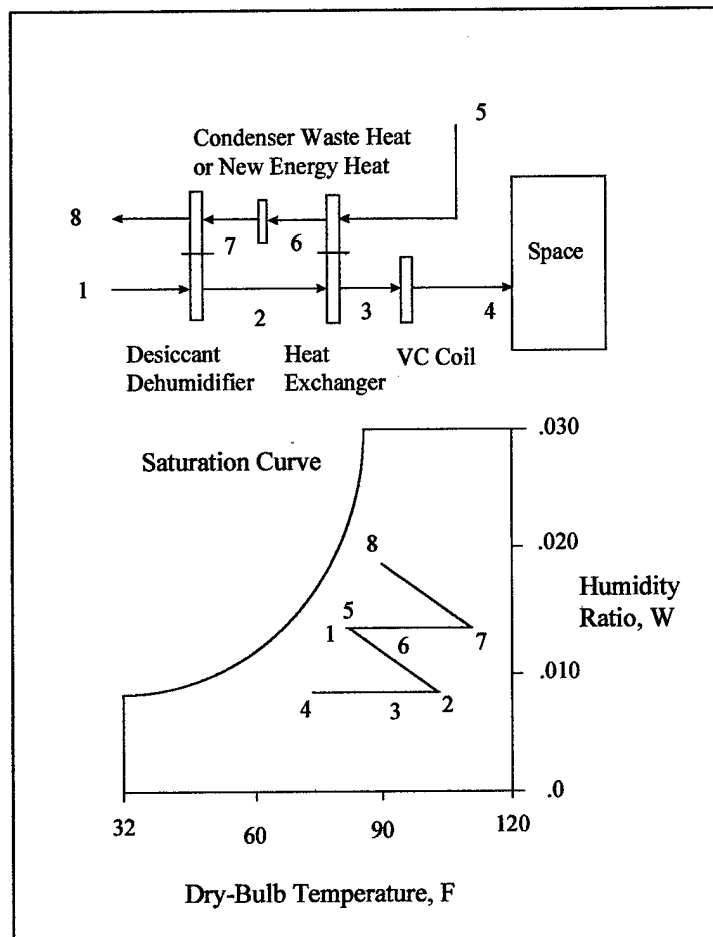
Figure 8. Typical Desiccant Enhanced Cooling (DEC) Cycle

The Cromer cycle is another desiccant cycle that has been recently proposed

and has received attention because of its simplicity and possible low energy

consumption, Figure 9. Essentially, the Cromer cycle uses the difference in relative

humidity between the supply and return airstreams as the driving potential for the

desiccant wheel. The desiccant wheel adsorbs humidity from the leaving airstream

(LA) which is typically around 95% RH and transfers it to the incoming outside

airstream (OA) at 50-60% RH. The airstream entering the coil (EA) now has a higher

relative humidity and the coil does substantially more condensation/dehumidification

(LA). The goal of the Cromer cycle is to maximize moisture removal or mass

transfer and minimize heat transfer so there is minimal drop in the ADP of the coil

and hence the COP remains higher than for a heat pipe application.
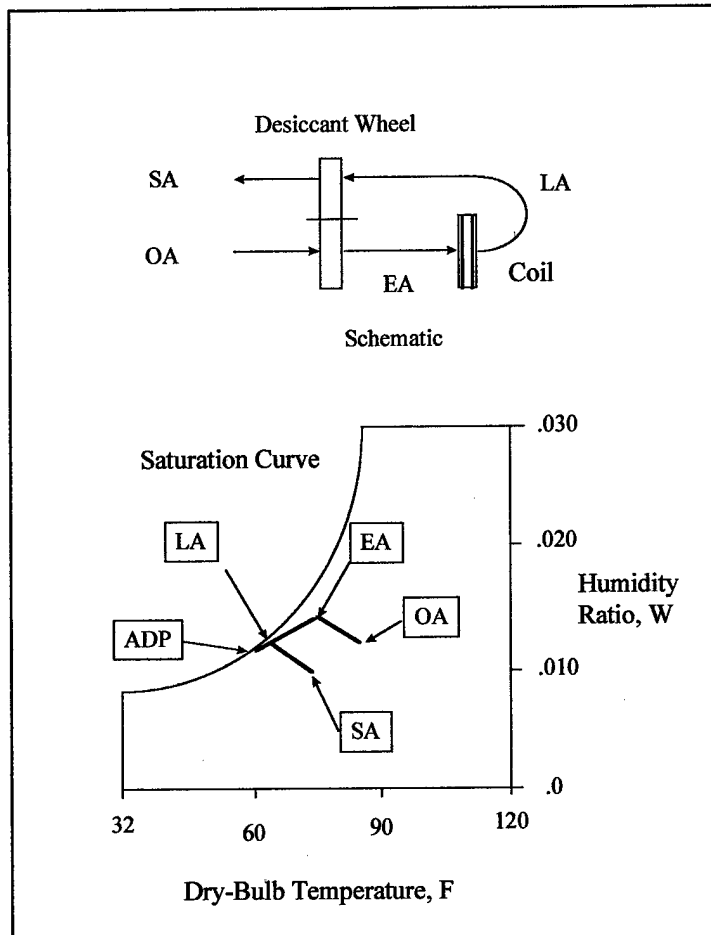
Figure 9. Cromer Cycle Schematic and Psych Chart

In order to be able to quantify the amount of moisture removed by a rotary

desiccant wheel system, the industry standard parameter for Moisture Removal

Capacity or MRC has been defined in Equation 2.

$$MRC = \overset{\bullet}{m}_{da}(w_{p,\,in} - w_{p,\,out}), kg_w / hr$$

This term has recently been listed in ARI 940 [1998] and is currently included

in an ASHRAE draft standard on desiccant dehumidification [ASHRAE 139P, 1995].

Another industry parameter is the MRC per the energy used (MRC/kW). This

benchmark typically ignores the energy requirement of rotating the wheel and focuses

on the thermal energy added to the regeneration stream. This "efficiency" can be

calculated as shown in   Equation 3:

$$MRC / ThermalEnergy = MRC / \overset{\bullet}{m}_r(i_{r,\,in} - i_{amb}), kg_w / hr / kW$$

Desiccant Concepts

This section discusses general desiccant concepts and parameters applicable to

rotary desiccant wheels.

Desiccant dehumidification has a great capacity for drying air due to a strong

affinity of desiccants for water or moisture. Sorption is the term given to the binding

of one substance to another and refers to both adsorption and absorption. Desiccants

are a particular subset of sorbents that have a particular affinity for water.

"Adsorption is the adherence of atoms, molecules, or ions (the adsorbate) to a surface. It is called physical adsorption (or physisorption) when the forces between surfaces are van der Waals forces and it is called chemical adsorption (or chemisorption) when the forces between adsorbate and surface are of the magnitude of chemical bond forces" [Moeller et. al., 1980].

Adsorption occurs when the desiccant does not physically or chemically change shape or composition. Absorption occurs when there is a physical or chemical change to the desiccant, as for example, when salt absorbs water and becomes a liquid [ASHRAE Fundamentals, 1993]. Chemical adsorption and absorption will not be considered in this research.

Adsorption is a phenomena that takes place in the pores of the desiccant material as "capillary condensation." The desiccant solid must have some wetting for adsorption to occur. The surfaces of this condensed liquid within the desiccant pores are concave due to surface tension. This concavity causes a lower vapor pressure over these surfaces. The drop in vapor pressure can be quite low depending upon the radius of curvature of the surface. The moisture in the airstream moves to the surfaces in the pores of the desiccant because of the lower vapor pressure.

To give an indication of the scale of the material used in desiccant adsorption, the average pore radius of regular density and intermediate density silica gel are 11 Å and 68 Å respectively [Pesaran, 1987]. A molecule of water has a diameter of approximately 2 Å. A cubic inch of regular density silica gel has been calculated to have 90,000 square feet of surface area within its pores.

The materials that are commonly used for desiccants in the commercial world are silica gels, activated carbon, zeolytes, and molecular sieves (which include synthetic zeolites). For many air conditioning applications, silica gels have been the desiccant of choice because of their relatively high capacity for moisture at low temperatures and moderate vapor pressures [Ruthven, 1984]. Pesaran [1989] has performed experimental testing using several different materials and determined that

microporous silica gel powder has highest storage capacity. Much research is still underway in materials selection and researchers are looking at various polymers and desiccant materials paired with other compounds such as epoxies.

The amount of moisture that a desiccant can hold is typically a function of its "adsorption isotherm." An adsorption isotherm is an equilibrium relationship that relates the amount of moisture adsorbed into a desiccant to the local airstream, as a function of temperature and pressure. The Brunauer Type system, Figure 10, was developed to roughly categorize the types of isotherms into five major groups, I through V [Hougen, 1943].

Typically the abscissa is the relative humidity and the ordinate is the water content of the desiccant, expressed as the mass of water per mass of dry desiccant. The different types were developed to reflect the types of desiccant appropriate for a given application. In many cases, a desiccant material can be fabricated to give a desired isotherm shape.

Collier [1989] has shown that a Type I isotherm is generally preferable for desiccant cooling (ventilation cycle) using a staged regeneration and where increased temperature (160 °F) is used for the regeneration stream. The Cromer cycle, which uses the difference in relative humidities of typical HVAC airstreams, has been postulated to operate better with a Type III isotherm [Cromer, 1988]. Desiccants with a Type III isotherm transfer more mass at the higher relative humidities where the Cromer cycle operates (at 50-60% RH).

As stated above, the adsorption isotherm provides the moisture content under equilibrium conditions. For a periodic rotary desiccant wheel, the desiccant bed

"element" is constantly in a transient mode. In order to solve for the moisture loading

at a given time, an equation expressing the rate of mass transfer is also necessary.
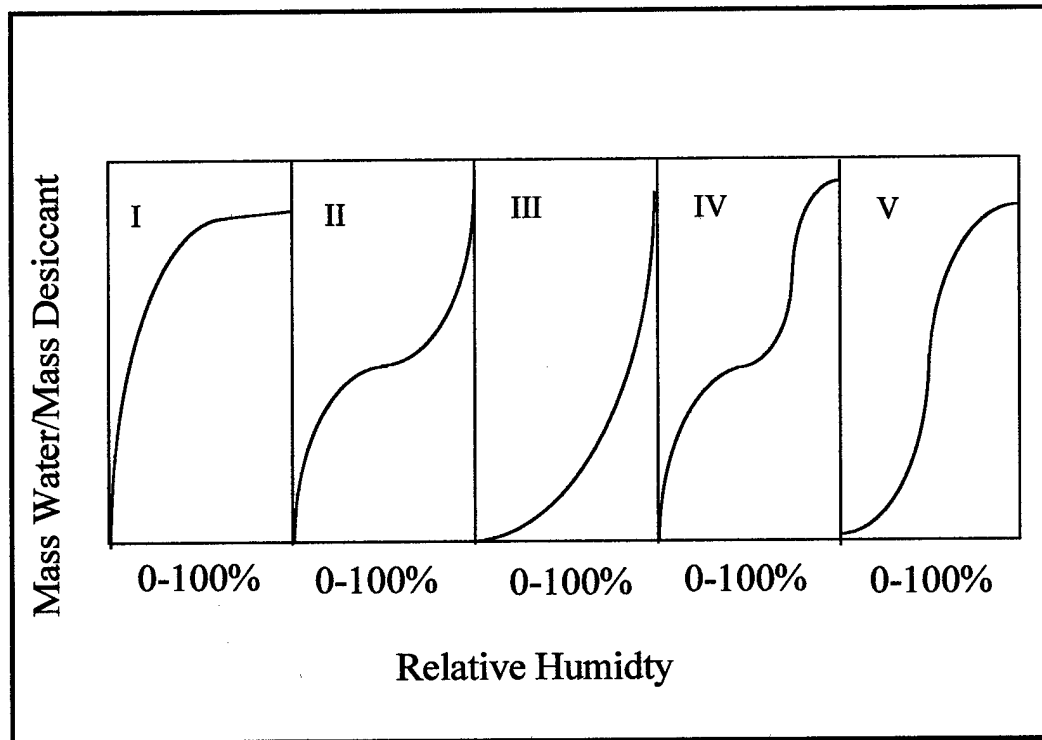
Figure 10. Brunauer Type System

The majority of models calculate the mass transfer based on a theoretical layer

of air above the desiccant that is in equilibrium with the desiccant bed itself. The

mass transfer is then based upon the difference in absolute humidity between the

airstream and the equilibrium layer. The mass transfer can also be based upon molar

concentration; however, relative humidity is a more common psychrometric

parameter.

The desiccant wheel is essentially a form of a rotary heat and mass

regenerator that transfers a heat and mass between two air streams. Regenerators can

be configured however through material selection and geometry to optimize a

26

combination: heat transfer priority, mass transfer priority, or both heat and mass transfer priority [Brandemuehl, 1982].

Desiccant systems have another benefit besides their sorption capability. They can significantly improve the air quality by acting as a filter and removing unwanted contaminants such as carbon monoxide, nitrogen dioxide, and sulfur dioxide [Relwani, 1986]. Their longevity is estimated at approximately 20 years and their maintenance is relatively simple [MaClaine-Cross, 1988].

There have been a variety of designs over the years. As stated in the introduction, earlier designs were simply packed with desiccant beads or a substrate that is coated with desiccant material. Current designs also use a homogenous mixture of desiccant, binder, and filler. These are shown in Figure 11. The impetus for this is the material science development of binders that allow the flow of moisture through them. This presented an interesting question as to whether the existing convection-based equations could adequately model the adsorption. Using a homogenous mixture for surface and substrate, there will be desiccant particles that are not in "direct" contact with the airstream as they are below the surface.

How much the binder or the filler materials interfere with the mass transfer of the rotary desiccant wheel was unknown prior to this research.
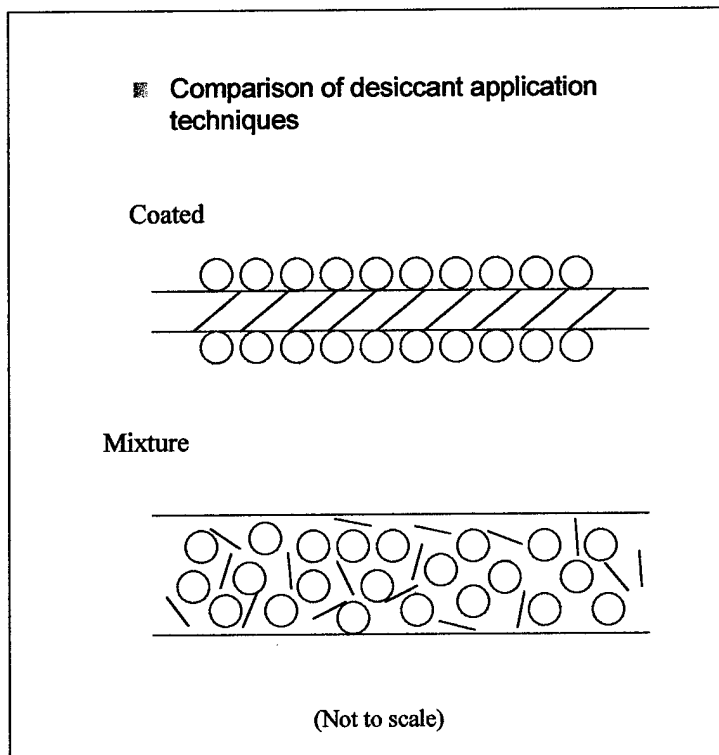
Figure 11. Comparison of Desiccant Material Application
Techniques

The desiccant wheel geometry is primarily a function of the convective

transfer profile or the shape of the openings in the desiccant wheel face. Table 1

compares the various channel geometries with a ratio of the Stanton number to the

pressure drop friction factor. The Stanton number is defined as the ratio of the

convection transfer to momentum and viscosity. The ratio of Stanton number to

pressure drop factor provides an indication of the amount of convective thermal or

mass transfer provided relative to the pressure drop or fan energy required to move

the air through that geometry. Early designs appeared to favor the parallel plate,

probably because of its high transfer to pressure drop ratio. Current designs have

shifted to other profiles such as the circular, triangular and rectangular. This is

probably due to improved manufacturing techniques and the increased structural

support these profiles provide.

Channel Geometry	Stanton Number/Pressure Drop Friction Factor, (St/f)
Packed Bed	.060
Triangle	.321
Square	.366
Circle	.390
Parallel Plate	.489
Staggered parallel Strip	.520

Table 1. Ratio of Heat-Transfer Rate to Pressure Drop for Various Dehumidifier Geometries (Pesaran, et.al. 1992)

Model Literature Review

The study of rotary desiccant wheels proceeds from the field of heat and mass

regenerators. The dominant mechanisms are known to be convection for heat transfer

and both convection and solid-side diffusion for the mass transfer. The basic

differential equations governing conservation of mass and energy and the transfer rate

equations for energy and mass have long been known. To date, there has been no

complete analytical solution to these equations. In order to solve them, various

numerical and simplification procedures have been created.

The different models that exist have been categorized several different ways.

One division is between the models with complex mathematical detail (finite

difference solutions) and those constructed for ease of computation (analogy, pseudo-

steady-state). The simplified models have primarily been constructed in order to

minimize the computational complexity and computational time and provide general

insights. In a number of cases, the simplified models perform adequately; however, they are not as fundamentally correct or as universal. Within the finite difference models, there is also a division as to how to account for the modeling of the solid-side diffusion. The most fundamental models are known as the gas and solid side (GSS) models. They add a second order differential equation to account for the mass diffusion and moisture gradients within the particle. The extra second order equation adds considerable complexity and computational time. A second type of model uses a "lumped capacitance" mass transfer coefficient for the overall mass transfer. These are known as the psudeo gas side (PGS) models. Essentially, this takes an analytically developed convective mass transfer coefficient and then empirically degrades it to account for the solid side diffusion. The trade-off has been decreased computational time and lower flexibility with the PGS method compared to increased complexity/flexibility and increased computation time for the more fundamental gas and solid-side model (GSS). This section will highlight some of the more significant and current developments that have been made in a chronological order.

Work by Hausen [1929] on sensible heat regenerators is considered the groundwork for rotary regenerators. He developed solutions to the governing equations for the periodic steady-state solution of a balanced and symmetric regenerator: first by graphical eigenfunctions and then by graphically solving central difference equations.

Rosen's [1951] paper on fixed bed sorption performed a rigorous solution of the surface and intraparticle diffusion. It is considered the classical solution to fixed bed sorption.

The article by Coppage and London [1953] describes the periodic flow rotary regenerator and compares it with other heat exchanger systems. This article is one of the first to model the differential element of the rotary heat exchanger as a crossflow heat exchanger. It summarizes the basic relations and describes some of these early solution techniques by Hausen, Nusselt, Boestad, Illiffe, and Saunders.

Lambertson [1958] presented a numerical, finite-difference solution to the sensible heat regenerator in periodic steady-state for use in calculating effectiveness, ε. He used a central-differencing scheme as proposed by Hausen and elaborated on by Dusinberre in the commentary section after the Coppage and London [1953] article. His solution was one of the first to use a digital computer to solve for the solution.

Carter [1966] derived the coupled rate and conservation equations for transient heat and mass transfer for a fluid stream passing through a fixed bed of adsorbent. He showed that the controlling mechanisms are the boundary-layer and adsorbed phase diffusion for the mass transfer and the boundary layer convection for the heat transfer. He used an additional diffusion equation to model the diffusion resistance in the desiccant solid. The differential equations were solved using a modified Euler method. The model was used for temperature and concentration prediction of the airflow.

Bullock and Threlkeld [1966] also derived the coupled heat and mass transfer equations for numerical solution. Their model, however, ignored the solid side diffusion mass transfer. They used a modified Euler method with predictor-corrector routines.

Maclaine-Cross [1972] presented a finite-difference model known as MOSHMX (Method of Solving Heat and Mass Exchange) which has been used extensively by a number of researchers. He uses a gas-side controlled, lumped capacitance mass transfer coefficient that is typically referred to as a pseudo-gas side (PGS) coefficient. His solution technique uses an explicit finite difference technique solved by a matrix inversion technique.

Another method, commonly referred to as the "analogy" method was introduced by Banks [1985], and Maclaine-Cross and Banks [1972], based on earlier works by Henry [1939] and Cassie [1940]. The non-linear coupled heat and mass transfer equations are changed into two separate sets of de-coupled equations that are analogous to heat transfer alone. The basic differential equations are transformed by replacing the original dependent variables with new dependent variables called characteristic potentials. The characteristic potentials are based on temperature and humidity ratio. When the differential equations are written in terms of the characteristic potentials, they become uncoupled, hyperbolic wave equations. This model greatly simplifies the mathematics of the finite difference procedure and has been used for seasonal simulations.

Wilmott and Burns [1977] studied transient response of periodic flow thermal regenerators through step changes to the inlet gas temperature and flowrate. They found that reducing regenerator length and not reducing the period would affect the time required for steady-state. They also looked at unbalanced flow and found that it reduces the time to reach steady-state.

Pla-Barby, [1978] and Barker and Kettleborough [1980a] have also used the finite-difference technique to model packed bed dehumidifiers.

Holmberg [1979] also presented a finite difference solution to the heat and mass transfer equations with the PGS coefficients. He used a staggered mesh, however, to account for steep gradients within the matrix. He used an implicit Crank-Nicholson scheme for the equations and solved them using a Gauss-Seidel solution technique.

Mathiprakasam and Lavan[1980] produced linearized solutions from the basic equations in order to ease the computational requirements.

Barlow's [1982] "pseudo-steady-state" model proposed that discrete elements be treated as simple counterflow heat and mass exchangers. The equations are uncoupled at each step to allow easier computation. While the model is not as rigorous, it has been shown to have fair agreement with experimental data. Because of its ease of use, this program has also been used extensively by researchers.

Pesaran [1984, 1987] also developed the differential equation for diffusion within the desiccant particle. He showed that the amount of surface diffusion versus Knudsen diffusion varied significantly for different densities of silica gel (intermediate versus regular density). He also did a substantial amount of experimental work looking at the transient response of fixed bed adsorption with desiccants.

Jurinak [1982] compared two forms of the analogy method with a finite difference technique and concluded that the analogy method was reasonable for seasonal simulation with several caveats. A high thermal capacitance matrix or high

33

Lewis number, high rotational speed, or unfavorable isotherm could cause significant errors with the analogy method. He also compared matrix properties (isotherms, heat of adsorption, water content, hysterisis, matrix diffusivity, thermal capacitance, and flow parameters) through a parametric analysis with a finite-difference technique. Finally, he looked at recirculation of purged flow.

Besides sensible heat regenerators, Brandemuehl [1982] applied both analogy and finite-difference methods to heat and mass regenerators. Specifically, he addressed nonuniform inlet conditions in a periodic steady-state and transient analysis through a step change to the periodic steady-state. Essentially, he found that non-uniform inlet conditions did cause significant effects on the performance of a heat and mass regenerator and the step change could require substantial time for a wheel (especially from a "cold" start). The adsorption isotherm he developed was used in this research as well. He also found that for certain values of the Lewis number, the analogy method did not show as good agreement.

Van Den Bulck et al., [1985] devised an equilibrium model that assumes the airstream and the desiccant are in equilibrium using wave theory and the analogy method. He used the results from this combined with finite difference results to devise another model: the effectiveness-NTU model (analogous to heat exchangers). With these, he has done some system studies as well.

Schultz [1987] did a comparison of Barlow's model with Maclaine-cross's MOSHMX and found some significant deficiencies both from an analytical evaluation of the differential equations and a comparison of the numerical output. He also compared the finite difference model output to experimental data and found

reasonable agreement. Non-uniform passage sizes however caused difficulty using analytic heat and mass transfer coefficients.

Chant [1991] performed a steady-state and transient analysis of rotary desiccant regenerator using an assumed moisture profile within the desiccant particle to account for solid-side diffusion. The analysis then proceeds based on first principles. She tested both a parabolic and quartic profile of which she recommends the parabolic profile as an accurate, computationally efficient option to the solid-side diffusion equation. She used an ordinary differential equation technique combined with the Burlirsch-Stoer method for transient analysis and had mediocre success with validation. The transient model also appears to have had some stability problems. She used a finite difference approach combined with a sparse matrix solver for the steady-state analysis and had very good stability. She also examined the Cromer cycle and performed a second law analysis on it.

Based on a review of the literature, there has not been a study that compares the measured transient response of a rotary desiccant wheel with a numerical model. The finite difference technique is recognized as the most accurate and most universal solution technique. The parabolic concentration profile appears to be the best compromise between fundamental principles, accuracy, and computational speed. Because of interactions with other HVAC components, different types of feedback control, and newer control strategies associated with indoor air quality, the transient response of desiccant wheels may have a significant impact.

CHAPTER 3. THE MATHEMATICAL MODEL

Coordinate System, Conventions, and Assumptions

Figure 12 represents the coordinate system for a desiccant wheel model used in this research. The wheel rotates between airstreams 1 and 2 (process and regeneration). The differential element is a "wedge" with a radius, r, and two independent variables. The spatial independent variable, z, is function of the axial distance of the wheel. The time independent variable, τ, is essentially a function of the number of "grid steps" and the rotational speed of the wheel. The basic model concept is to approximate the wheel rotation by treating a wedge as a "fixed bed rotating in time" between the two airstreams.

Assumptions

The governing assumptions for the rotary desiccant wheel are as follows:

1. The thermal and mass transport resistance of the matrix material is infinite in both the tangential and axial direction and very small in the radial direction. The axial and circumferential dimensions therefore use a finite grid.

2. There is no carryover, leakage or mixing of the airstreams. While there is a small amount of mixing between the two streams, the amount is assumed to be small because of improved seals and the overall effect negligible. The amount of leakage is a function of the individual housing construction and would have to be determined by experiment. In order to keep the model relatively simple, leakage was ignored for the model.

3. The thermal and mass storage capacities of the air in the desiccant pores are negligible in the comparison with the convective heat and mass transport. The amount of air is relatively minor and the capacity of the convection transfer is large in comparison.

4. The fluids (process and regeneration) pass in counterflow directions.

5. The thermal properties of the matrix material are constant. Most of the properties obtained from the material manufacturers were constants and this makes the model significantly simpler and more flexible.

6. Temperature gradients within the desiccant particle are negligible (an isothermal particle).

7. The moisture content of a desiccant particle can be approximated by the parabolic concentration profile (PCP). The PCP concept has previously been validated by Do and Rice [1986] and Chant [1991].

8. The moist air behaves as an ideal gas.

9. There is a layer of moist air at the surface of the desiccant that exists in equilibrium with the desiccant bed. This provides the basis for the adsorption isotherm to be used in calculating the equilibrium humidity ratio. This is a fundamental assumption of boundary layer theory.

10. The mass transfer potential can be calculated using the local difference in humidity ratio (a modified Fick's Law approach) between the airstream and a theoretical airstream layer in equilibrium with the desiccant surface.
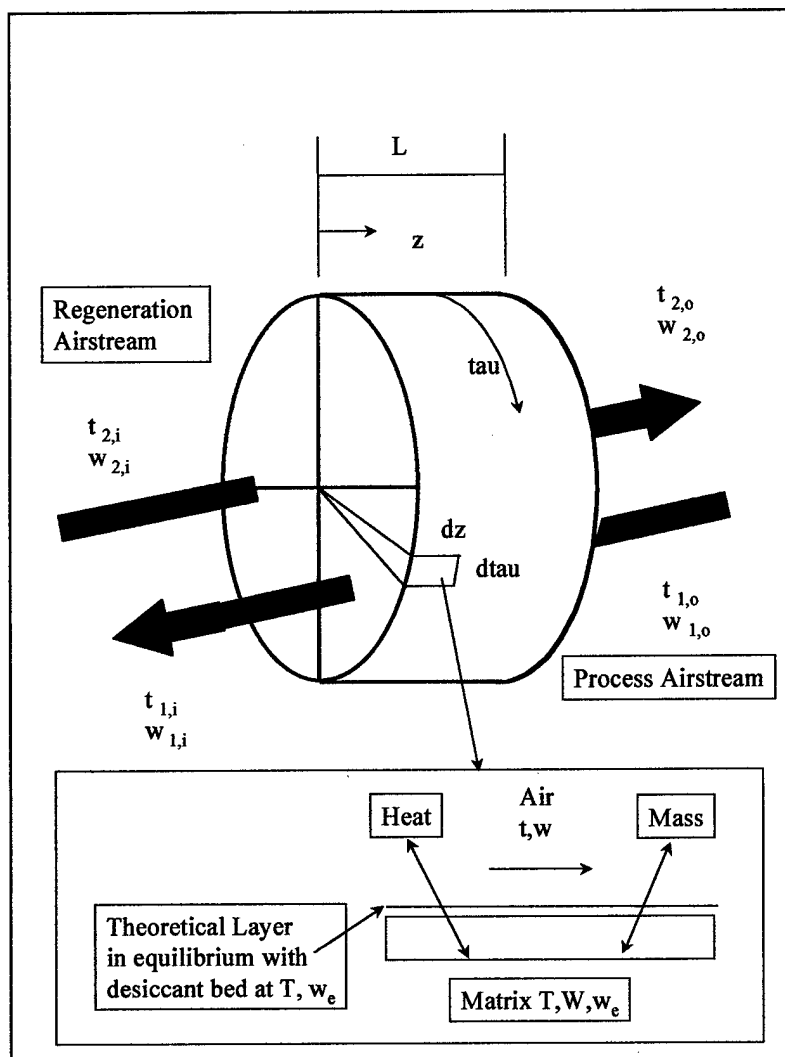
Figure 12. Nomenclature and Coordinate System for the Rotary
Desiccant Wheel

11. The hysteresis effect for sorption and de-sorption is assumed to be
negligible. This means that the effective diffusivity is the same for both streams.
While some actual amount of hysteresis effect is clearly present, including it in the
model makes the model less flexible and requires an additional experimentally
derived parameter (de-sorption).

12. The binder and filler materials do not have hygroscopic properties and do not significantly interfere with mass transfer to the desiccant. According to the manufacturer, these materials are non-hygroscopic.

Governing Equations

As explained by Brandemuehl [1982], there are two points of reference by which the differential element may be "tracked" through the airstream and matrix. One method is to hold the element in place and let the matrix rotate through it. The other, which these equations are based on, is to let the element rotate around the matrix in time. The rotary wheel then is treated as a fixed bed moving in time through two different airstreams or boundary conditions. Based on these conventions, the following are the transfer rate and conservation differential equations for a rotary desiccant wheel.

Mass Transfer rate

$$\frac{\partial w}{\partial x} = NTU_{m,jk}(w_e - w)$$

Equation 4

Mass Conservation

$$\frac{\partial w}{\partial x} + \beta_s \Gamma_s \frac{\partial W}{\partial \theta} = 0$$

Equation 5

Energy Transfer Rate

$$\frac{\partial i}{\partial x} = NTU_{q,jk} c_{p,ma}(T-t) + i_{fg}\frac{\partial w}{\partial x}$$

Energy Conservation

$$\frac{\partial i}{\partial x} + \beta_s \Gamma_s \frac{\partial i}{\partial \theta} = 0$$

In their initial form, the conservation equations are functions of the airstream properties (t,w) and the matrix itself (T,W). The rate equations are in terms of the airstream (t,w) and the theoretical layer (T, w_e) in equilibrium with the matrix.

The independent variables of axial distance and time have been non-dimensionalized as follows:

$$x = \frac{z}{L}$$

$$\theta = \frac{\tau}{\tau_p}$$

The time and rotation angle are related by:

$$\frac{\tau}{\tau_p} = \frac{\phi}{2\pi}$$

The period fraction βj is the percentage of the period time. It may not sum to zero if there are structural members blocking a small portion of the opening [Schultz, 1987]. It is defined by:

$$\beta_s = \frac{\tau_s}{\tau_p} = \frac{\phi_j}{2\pi}$$

Equation 11

The mass capacity rate ratio Γ_j is the ratio of the desiccant mass "flow rate" to the mass flow rate of the airstream:

$$\Gamma_s = \frac{M_{dd} / \tau_p}{\dot{m}_{da,s}}$$

Equation 12

The NTU (Number of Transfer Units) term follows the classical definition ("UA/C$_{min}$") and in this context they are defined as:

$$NTU_{m,jk} = \frac{h_{m,jk}A_{s,s}}{\dot{m}_{da,s}}$$

Equation 13

$$NTU_{q,jk} = \frac{h_{q,jk}A_{s,s}}{\dot{m}_{da,s}C_{p,ma}}$$

Equation 14

In Terms of Temperature

The computer model developed for this research works primarily in terms of temperature and humidity ratio. The differential equations are in terms of enthalpy and therefore must be converted to temperature.

Moist air is treated as an ideal gas mixture of dry air and water. The enthalpy of moist air is a function of the humidity ratio and the temperature. The moist air enthalpy is defined as:

$$i = i_{da} + w i_{wv} = c_{p,da} t + w(c_{p,wv} t + i_{fg})$$

Equation 15

rearranging and setting

$$c_{p,ma} = c_{p,da} + c_{p,wv} w$$

Equation 16

the result is

$$i = c_{p,ma} t + i_{fg} w$$

Equation 17

and its derivative with respect to axial distance, x, becomes

$$\frac{\partial i}{\partial x} = c_{p,ma} \frac{\partial t}{\partial x} + i_{fg} \frac{\partial w}{\partial x}$$

Equation 18

Inserting this definition into the energy transfer rate equation (Equation 6), the enthalpy of vaporization term and the specific heat of moist air cancel out.

$$c_{p,ma} \frac{\partial t}{\partial x} + i_{fg} \frac{\partial w}{\partial x} = NTU_{q,s} c_{p,ma}(T-t) + i_{fg} \frac{\partial w}{\partial x}$$

leaving the energy transfer differential equation:

$$\frac{\partial t}{\partial x} = NTU_{q,s}(T-t)$$

Equation 19

42

The enthalpy of the desiccant wheel is expressed as a function of the matrix, the desiccant, the water absorbed and the integral heat of wetting.

$$I = (c_{p,dm} + c_{p,wl}W)T + \Delta H_w$$

Equation 20

The integral heat of wetting, ΔH_w, is qualitatively the difference between the heat released by absorption and the vaporization of pure water. It is defined as:

$$\Delta H_w = i_{fg} \int_0^W (1 - \frac{i_{ad}}{i_{fg}})dW$$

Equation 21

The matrix enthalpy is defined as:

$$I = c_{p,m}T + W(i_{fg} - i_{ad})$$

Equation 22

where

$$c_{p,m} = c_{p,dm} + Wc_{p,wl}$$

Equation 23

Taking the derivative of Equation 22 with respect to normalized time

$$\frac{\partial I}{\partial \theta} = c_{p,m}\frac{\partial T}{\partial \theta} + (i_{fg} - i_{ad})\frac{\partial W}{\partial \theta}$$

Equation 24

Incorporating the air enthalpy equation (Equation 18), the desiccant enthalpy equation (Equation 24) and the mass conservation equation (Equation 5) into the energy conservation equation (Equation 7):

$$c_{p,m}\frac{\partial T}{\partial \theta} + (i_{fg} - i_{ad})(-\frac{1}{\beta_j \Gamma_j}\frac{\partial w}{\partial x}) = -\frac{1}{\beta_j \Gamma_j}(c_{pma}\frac{\partial t}{\partial x} + i_{fg}\frac{\partial w}{\partial x})$$

Canceling the enthalpy of vaporization from both sides and moving the matrix specific heat to the right hand side:

$$\frac{\partial T}{\partial \theta} = -\frac{1}{\beta_s \Gamma_s c_{p,m}}(c_{p,ma}\frac{\partial t}{\partial x} + i_{ad}\frac{\partial w}{\partial x})$$

Equation 25

In summary, the four basic differential equations are: Equation 4, Equation 5, Equation 19, and Equation 25.

Boundary and Initial Conditions

The differential equations are all first order differential equations; therefore, one boundary condition or one initial condition is required. The following boundary conditions for the differential equations apply to both the transient and periodic steady-state solutions.

The first two boundary conditions state that the initial air states (temperature and moisture) of the different periods (hot and cold sides) are the same as the entering air for that period.

$$t(x = 0, 0 < \theta < \beta_1) = t_{1,i}$$

Equation 26

$$w(x = 0, 0 < \theta < \beta_1) = w_{1,i}$$

Equation 27

44

The initial conditions are required for the matrix states at $\tau=0$. After that, the initial condition for the next element is the exit condition from the previously solved element.

$$T(x, \theta = 0) = T_0$$

Equation 28

$$W(x, \theta = 0) = W_0$$

Equation 29

The third and fourth boundary conditions reflect periodic steady-state conditions. The first set (Equation 30 and Equation 31) reflects the condition that a given wedge in a specific circumferential position will have constant values (temperature and water content) over time. This can be solved quickly by setting the trailing edge of the matrix leaving the regeneration period equal to the leading edge of the matrix in the process period. This is also known as the "reversal condition."

$$T(x, \theta_0) = T(x, \theta_1)$$

Equation 30

$$W(x, \theta_0) = W(x, \theta_1)$$

Equation 31

Another way to express the steady-state condition is that the outlet variables (process and regeneration streams) do not vary with time (Equation 32 and Equation 33).

$$t(x = 1, \theta) = t(x = 1, \theta + 1)$$

Equation 32

$$w(x = 1, \theta) = w(x = 1, \theta + 1)$$

Equation 33

Note the difference between the steady-state and transient situation boundary conditions: the outlet conditions (temperature and humidity) and matrix conditions (temperature and humidity) for a given wedge are constant with time in the periodic steady-state.

Equilibrium Conditions

The differential equations above are non-linear and coupled. This is because the desiccant and moist air states are interrelated through the dependent variables (t, w, T, W, w_e). The equilibrium condition is a function of the isotherm relationships, effective diffusivity, and psychrometric relationships which are all non-linear. Mathematically, this is expressed as

$W = W(T, w_e)$

$I = I(T, W)$

$i = i(t, w)$

Equation 34

The relationships that define the desiccant and moist air states used in the equilibrium states above will follow.

Liquid water has been treated as an incompressible fluid and the enthalpy of liquid water is a function of temperature only.

$$i_{lw} = c_{p,lw} T$$

Equation 35

The absolute humidity of moist air in equilibrium with adsorbent is defined by:

$$w_e = 0.62198 \frac{p_{va}}{p_t - p_{va}}$$

Equation 36

The vapor pressure is determined using the definition of relative humidity

$$RH(\%) = \frac{p_{va}}{p_{vs}} 100$$

Equation 37

With further refinement Equation 36 can be changed to:

$$w_e = 0.62198 \frac{RH * p_{v,s}}{p_t - RH * p_{v,s}}$$

Equation 38

The saturation vapor pressure is given by an equation from the Hyland-Wexler equations in ASHRAE, [1993].

$$\ln(p_{vs}) = \frac{C_8}{T} + C_9 + C_{10}T + C_{11}T^2 + C_{12}T^3 + C_{13}LN(T)$$

Equation 39

where

$C_8 = -5.8002206 \text{ E3}$

$C_9 = -5.5162560$

$C_{10} = -4.8640239 \text{ E-2}$

$C_{11} = 4.1764768 \text{ E-5}$

$C_{12} = -1.4452093 \text{ E-8}$

$C_{13} = 6.5459673$

and p_{ws} is in units of kilo Pascals and the temperature T, is in absolute units of degrees Kelvin.

The relative humidity is related to the water content of the desiccant matrix through the adsorption isotherm, which will be discussed in that section.

Air and Moisture Parameters

In order to ensure that the model program is accurate over a significant range of temperatures and to improve flexibility, some parameters were put in the form of functions. The basic equations will be shown here; the supporting data [Incropera and DeWitt, 1986] is shown in Appendix A.

The Specific Heat of Dry Air is a third order polynomial curve fit:

$$c_{p,\,da} = -4.37E^{-10}t^3 + 9.245t^2 - 4.077t + 1.057$$

Equation 40

The Specific Heat of water vapor is also a third order polynomial curve fit:

$$c_{p,\,wv} = 1.043E^{-7}t^3 - 8.499E^{-5}t^2 + 2.373t - 0.415$$

Equation 41

The Specific Heat of liquid water was assumed to be a constant because it typically varies less than 3% over the range of temperatures (273.15-430 °K) [Incropera and Dewitt, 1986] encountered in this research.

$c_{p,wl}$=4.186 kJ/(kg-K)

The thermal conductivity of air is necessary to solve for the convective heat and mass transfer. It is significantly affected by temperature (it can vary by more

48

than 10% over the temperatures used) and is best represented by a second order polynomial:

$$k_f = -3.269E^{-11}t^2 + 9.799t - 1.668$$

<div align="right">Equation 42</div>

Enthalpy of Vaporization

The enthalpy of vaporization is necessary along with the adsorption isotherm to solve for the enthalpy of adsorption. The expression for the enthalpy of vaporization is developed from a form of the Clapeyron equation:

$$\left(\frac{dP}{dT}\right)_{sat} = \frac{i_{fg}}{Tv_{fg}}$$

<div align="right">Equation 43</div>

The Clapyeron equation can be simplified for liquid vapor phase changes by making an approximation. Because v_g is much greater than v_f, it can be assumed that v_{fg} is approximately equal to v_g. The vapor can be treated as an ideal gas and calculated with:

$$v_g = RT / P$$

<div align="right">Equation 44</div>

where the water vapor gas constant, R = .462 kJ/(kg-K). Substituting into the Clapeyron equation:

$$i_{fg} = \left(\frac{dP}{dT}\right)_{sat} \frac{RT^2}{P_{vs}}$$

<div align="right">Equation 45</div>

Adsorption Isotherms

Desiccant materials adsorb water. In doing so, it releases an amount of heat (internal energy) known as the heat of sorption. It is like the heat of vaporization for pure liquid water in magnitude; however it is slightly larger. A small amount of additional energy must be given up for the adhesion to the pores versus the vaporization of pure water by itself. The heat of sorption must be known in order to complete the heat and mass balance equations. Brandemuehl [1982] used the following procedure based on a suggestion from Othmer. Given pressure, temperature, and water content data for a particular desiccant, a relationship for the heat of sorption can be built with a form of the Clausius-Clapyron equation:

$$\frac{d \ln p_v}{d \ln p_{vs}} = \frac{i_{ad}}{i_{fg}}$$

Equation 46

As stated earlier, the adsorption isotherm is a function relating the water content of the desiccant material to the temperature and pressure of a hypothetical equilibrium layer above the desiccant. Using curves calculated from the Clausius-Clapeyron equation, two expressions can be derived.

$$\frac{i_{ad}}{i_{fg}} = f(W)$$

Equation 47

$$RH_e = f(W, p_{vs}, \frac{i_{ad}}{i_{fg}})$$

Equation 48

50

With these two expressions, the water content of the desiccant material in equilibrium with an air-vapor mixture at a given temperature and vapor pressure can be determined. The relations developed by Brandemeuhl [1982] are as follows:

$$RH = (2.112W)^{h^*}(29.91p_{vs})^{h^*-1}$$

<div align="right">Equation 49</div>

here

$$h^* = 1 + 0.2843e^{(-10.28W)}$$

<div align="right">Equation 50</div>

and h* is also equal to:

$$h^* = \frac{i_{ad}}{i_{fg}}$$

<div align="right">Equation 51</div>

Graphs of this isotherm are located in Appendix C.

Parabolic Concentration Profile

The basic concept of the parabolic concentration profile (PCP) is that the moisture content within the desiccant particle is assumed to be parabolic, Figure 13. When the particle is in the process stream, there is a positive gradient. When the particle is in the regeneration stream, there is a negative gradient. The profile varies between these two extremes when it rotates between the airstreams. Several studies have shown this assumption to be reasonably accurate [Do and Rice, 1986] except for a very small initial period when the profile is developing.
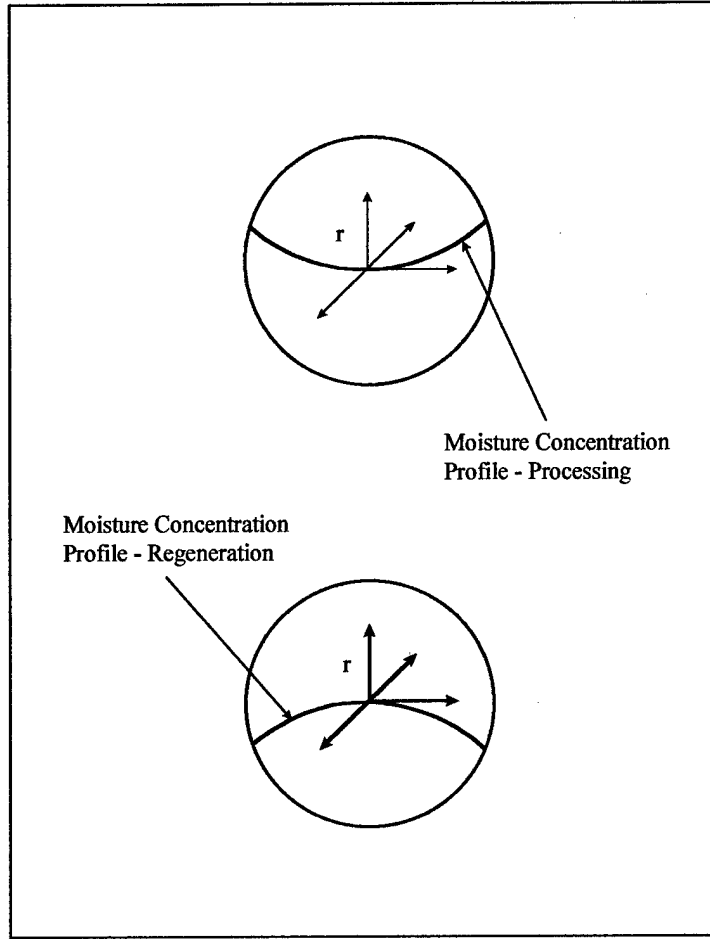
Figure 13. Parabolic Concentration Profile [Chant, 1991]

The PCP model evaluates the equilibrium humidity ratio, w_e, at the surface of the particle rather than at the average moisture concentration as with the typical PGS models. For a spherical particle, the following two expressions are needed to determine the moisture content at the surface, Ws [Chant, 1991]:

$$W_s = W + (2/5)a2$$

Equation 52

$$a2 = -(h_m R / 2\rho_p D_e)(w_e\{W_s, T\} - w)$$

Equation 53

52

The derivation for these equations is in Appendix B. The first part of the a2 equation is essentially the Sherwood number, Equation 54. This non-dimensional variable is the ratio of the mass convection to mass solid-side diffusion.

$$Sh = -\frac{h_m R}{2\rho_p D_e}$$

In order to find the surface moisture content, the a2 term must be evaluated at each moist air grid point. The mass transfer coefficient can be analytically determined for the surface instead of the PGS coefficient, which must be empirically altered to solve for the equilibrium at the average moisture content. The expressions above are then used in the mass transfer rate and mass conservation equations:

$$\frac{\partial w}{\partial x} = NTU_{m,j}(w_e[W + 2/5a2, T_e] - w)$$

$$\frac{\partial W}{\partial \theta} = \frac{1}{\beta_j \Gamma_j} NTU_{m,j}(w_e[W + 2/5a2, T_e] - w)$$

Effective Diffusivity

There are three types of diffusion for mass transfer: surface, ordinary, and Knudsen diffusion. Ordinary diffusion occurs as the water vapor in moderate concentrations of moist air moves through the pores of the desiccant. Most of these

molecular collisions are with other water molecules because the pores are relatively large and the moisture concentration high.

Knudsen diffusion occurs when the ratio of the "path" to pore radius is relatively high and the moisture concentration is low: the water molecules tend to collide more often with the pore walls. The Knudsen number is defined as

$$Kn = \frac{\lambda_K}{a_K}$$

<div align="right">Equation 57</div>

where λ is the mean free path and a_K is the pore radius. When the Knudsen number is high, ordinary diffusion can safely be ignored.

Surface diffusion is the movement of the water molecules into the pore openings. For regular density silica gel, Pesaran [1987] found surface diffusion to be the dominant factor. A surface diffusion model based on the "hopping" of adsorbed molecules between adjacent sites of different adsorption strength has been proposed and verified for physical adsorption [Gilliland et al, 1974] and chemisorption [Slaydek et al., 1974] for more than 30 adsorbate-adsorbent pairs. The basic equation describing surface diffusivity is based on the heat of adsorption and is:

$$D_s = D_o Exp(-ai_{st} / RT)$$

<div align="right">Equation 58</div>

where $a = .45 / b$ and b is a function of the type of adsorption bond. For silica gel, b is equal to unity [Pesaran, 1987]. R is the gas constant for water vapor and R

equal to 0.462 kJ/(kgK) is used. T is in degrees Kelvin. The D_o term is defined as:

$$D_o = \frac{1}{4} v_o \lambda_s{}^2$$

<div align="right">Equation 59</div>

Pesaran [1987] also determined that D_o for silica gel is approximately equal to $1.6 \times 10^{-6} \ m^2 s^{-1}$.

The effective surface diffusivity is then found using:

$$D_{s,e} = D_s / \tau_s$$

<div align="right">Equation 60</div>

For the surface tortuosity, τ_s, Pesaran [1987] used 2.8 in the case of regular density silica gel.

$$D_{s,e} = D_o / \tau Exp(-.974 i_{st} / T)$$

<div align="right">Equation 61</div>

The parabolic concentration profile (PCP) of moisture content of the desiccant particle has been recommended by Do and Rice [1986] and Chant [1991] as an accurate methodology to account for solid-side diffusion. The methodology makes an assumption of the profile of the moisture content within the particle under a set of conditions and then proceeds based on first principles. Using the average water content for the particle, the water content at the surface can be easily calculated. This is a straight algebraic calculation and therefore adds a minimal amount to the computation time. Another advantage is that the analytic mass transfer coefficient (the effective diffusivity) can be easily calculated. The less rigorous PGS method uses the empirically degraded "lumped capacitance" coefficient which must be

empirically determined for each material. Currently this has primarily been done for silica gels. Using a coefficient which does not require the empirical validation would allow greater flexibility with a working model. The more rigorous alternative (the GSS model) requires the addition of a second order differential equation. This raises the number of differential equations to be solved at each point from four to five and substantially increases the computational effort. The parabolic concentration profile (PCP) appears to be a reasonable compromise between fundamental accuracy and computational expense.

Heat and Mass Transfer Coefficients

The heat transfer convection coefficients (h_q) can be determined from established sources using non-dimensionalized parameters such as the Nusselt number (Nu), the Reynolds number (Re), and the Prandtl number (Pr). These incorporate the phenomena of momentum, viscosity, and thermal diffusivity for various geometries and fluids. Mathematically, this is expressed as:

$$Nu = \frac{hdh}{k_{da}}$$

Equation 62

where $Nu = f(\text{Re}, \text{Pr})$. According to Incropera and Dewitt, in *laminar* flow, the Nusselt number is a function of the geometry only. A curve fit was therefore done using the Nusselt number data from Incropera and Dewitt [1986] versus the geometry (cross-sectional area ratio) and is located in Appendix D.

$$\text{Re} = \frac{VL}{\nu}$$

<div align="right">Equation 63</div>

$$\text{Pr} = \frac{c_p \mu}{k} = \frac{\nu}{\alpha}$$

<div align="right">Equation 64</div>

The convection geometry for rotary desiccant wheels is typically a triangular, circular, square, or rectangular profile.

The mass transfer coefficient (h_m) can also be expressed in analogous equations using the Sherwood number (Sh_L), Reynolds, and the Schmidt number (Sc). These parameters relate momentum, viscosity, and mass diffusivity. They are expressed as:

$$Sh_L = \frac{h_m L}{D_{AB}} \quad \text{where } Sh_L \text{ is also a function: } \quad Sh_L = f(\text{Re}, Sc)$$

where Reynolds has already been defined and the Schmidt number is defined as:

$$Sc = \frac{\nu}{D_{AB}}$$

<div align="right">Equation 65</div>

Again, the relationship is determined by the geometries of the given system. Another method, and the one used in this research, is to use the Lewis analogy. The Lewis analogy is the ratio of the thermal diffusivity to that of the mass diffusivity. By extension, it can also be used to determine the heat or mass transfer coefficient given the other.

$$Le = \frac{\alpha}{D_{AB}} = \frac{Sc}{\text{Pr}}$$

Equation 66

and

$$\frac{h_q}{h_m} = c_{p,ma} Le^{1-n}$$

Equation 67

where, typically, n=1/3 for most applications. The Prandtl number varies by less than 1% over the range of temperatures of most HVAC applications for moist air and can safely be considered as a constant [Schultz, 1987].

$\text{Pr} = 0.705$

The Schmidt number is also treated in a like manner.

Sc=0.6

Placing these into the Lewis relation:

$$Le^{1-n} = \left(\frac{.6}{.705}\right)^{1-1/3} = 0.851^{2/3} = 0.898 \approx 1$$

and the heat and mass transfer coefficient ratio is sometimes approximated by:

$$\frac{h_q}{h_m} = c_{p,ma}$$

Equation 68

While using the calculated value for the Lewis number is technically correct, ASHRAE Fundamentals [1993] states that setting the Lewis number equal to one is a relatively standard convention. The convention with the Lewis number equal to one was typically used in this research because it appeared to validate slightly better. The

58

difference in outlet variables for either approach is relatively small however and not very significant (<1%).

Finite Difference Equations

The mathematical model of the rotary wheel is based on a two dimensional grid as shown in Figure 14. The rotary wheel is modeled as a fixed bed that rotates through time. Hence, the axial dimension is the abcissa and the time or angular position is the ordinate.
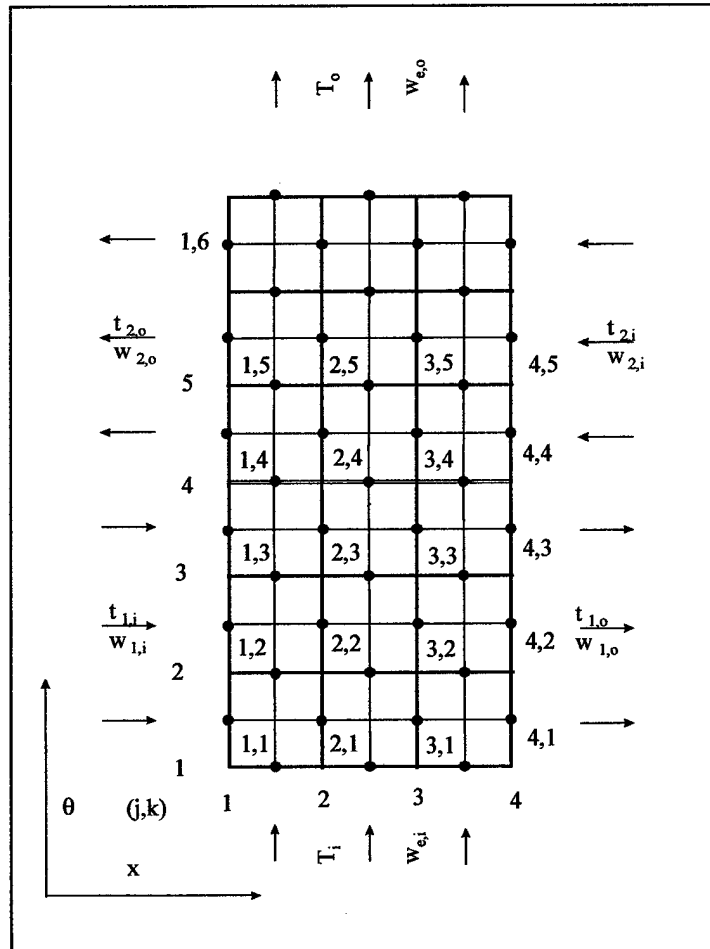
Figure 14. Schematic Representation of a Rotary Heat Exchanger

Figure 15 shows the convention for the differential element. Based on the differential equations and as shown in the differential element, a central differencing scheme was employed for the first order equations as used by Holmberg [1977]. This central differencing scheme for a first order differential equation is of second order accuracy.

Backward differencing techniques are normally referred to as an implicit solution - they rely on the simultaneous solution of equations at the same value of an independent variable. Forward differencing techniques for finite differences are typically an "explicit" technique. They solve at the next step strictly based on the single previous point. Central differencing techniques are neither fully implicit or fully explicit. Because this is a staggered grid, it works intuitively best with a central differencing technique

The finite difference equations are:

Mass Rate Transfer
$$w(j+1,k) - w(j,k) = NTU_{m,j}\Delta x(w_e - w)_{av}$$

Where

$$(w_e - w)_{av} = \frac{1}{2}[(w_e(j,k+1) + w_e(j,k)] - \frac{1}{2}[(w(j+1,k) + w(j,k)]$$

Equation 69

Conservation of Mass
$$W(j,k+1) - W(j,k) = -\frac{\Delta\theta}{\beta_j\Gamma_j\Delta x}[w(j+1,k) - w(j,k)]$$

Equation 70

60

matrix "inlet" state

$T_{j,k}$, $W_{j,k}$, $w_{e,j,k}$

Air "inlet" state

T,t,w_e,w

Air "outlet" state

$t_{j,k}$, $w_{j,k}$

$t_{j+1,k}$, $w_{j+1,k}$

$d\theta$

matrix "outlet" state

$T_{j,k+1}$, $W_{j,k+1}$, $w_{e,j,k+1}$

dx
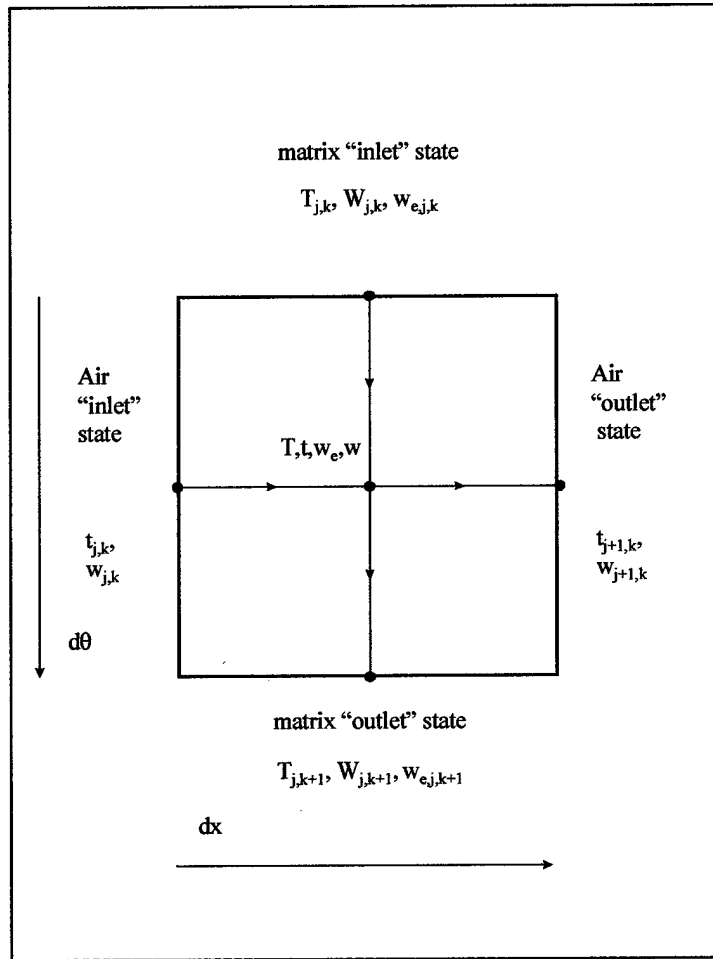
Figure 15. Finite Difference Element

Energy Transfer Rate

$$t(j+1,k) - t(j,k) = NTU_{q,j}\Delta x(T-t)_{av}$$

where

$$(T-t)_{av} = \frac{1}{2}[T(j,k+1) + T(j,k)] - \frac{1}{2}[t(j+1,k) - t(j,k)]$$

Equation 71

Conservation of Energy

61

$$T(j,k+1) - T(j,k) = -\frac{\Delta\theta}{\Delta x \beta_j \Gamma_j c_{p,m}}[c_{p,ma}(t(j+1,k) - t(j,k)) + i_{ad}(w(j+1,k) - w(j,k))]$$

<div align="right">Equation 72</div>

Chant [1991] found that her transient model suffered from stability/convergence problems. It appears that is because of the equations themselves which mathematicians would call "stiff" equations.

"Stiffness occurs in a problem where there are two or more very different scales of the independent variable on which the dependent variables are changing" [Press et al., 1992].

The step size chosen may not be optimal for all equations. Typically, implicit integration techniques are supposed to be the cure. For this reason, a fully implicit finite differencing scheme was also completed. This is shown in Appendix E. The fully implicit solution solves for all the values at the future time step. In order to preserve the second order accuracy, this methodology required using values from two previous time steps. The bulk of this research was done using the central differencing scheme because of its speed and the grid sizes required were not extreme.

Parameters of Concern

The variables of concern in this study are the specific properties transferred between the two airstreams: temperature, humidity ratio, moisture transfer (mass rate), and enthalpy. The temperature and humidity ratio are direct solutions from the finite difference equations. The moist air enthalpy can be determined from a previous expression (Equation 15)

Effectiveness is typically defined as the ratio of actual transfer to the maximum possible transfer rate and normally it is used for the steady-state. The effectiveness of the rotary desiccant wheel in terms of the above listed parameters needs to be calculated in order to compare it with other comparable components. Unlike a typical heat exchanger or evaporative cooler, the rotary desiccant wheel exchanges both heat and mass. The effectiveness definitions would therefore follow that of an air-to-air energy recovery device rather than a sensible-only heat exchanger or an evaporative cooler [ASHRAE, 1993]. The following definitions are used in this dissertation:

for temperature: $\quad \varepsilon_T = \dfrac{\dot{m}_j(t_{p,in} - t_{p,out})}{\dot{m}_{min}(t_{p,in} - t_{r,in})}$

Equation 73

for humidity ratio: $\quad \varepsilon_w = \dfrac{w_{p,out}}{w_{p,in}}$

Equation 74

for enthalpy: $\quad \varepsilon_i = \dfrac{\dot{m}_p(i_{p,in} - i_{p,out})}{\dot{m}_{MIN}(i_{p,in} - i_{r,in})}$

Equation 75

Note that the moisture definition of effectiveness is unusual: the denominator is not the difference of the inlet conditions. Typically process and regeneration air come from the same source: ambient air. The effectiveness value would therefore be infinite at all times because the difference in the humidity ratios would be zero. The

63

maximum possible transfer has therefore been designated as the maximum moisture flowrate of either stream.

The non-dimensional transient response is of the same form used by Lambertson [1958] and Brandemuehl [1982]:

$$\eta_t = \frac{t - t_{\tau = 0}}{t_{\tau = \infty} - t_{\tau = 0}}$$

Equation 76

$$\eta_w = \frac{w - w_{\tau = 0}}{w_{\tau = \infty} - w_{\tau = 0}}$$

Equation 77

These essentially relate the difference between the current outlet value and the initial outlet value to the difference between the initial outlet and steady-state outlet values.

A simple qualitative uncertainty analysis was performed to achieve some idea as to the potential inaccuracy of the model. This is located in Appendix H.

CHAPTER 4. NUMERICAL TECHNIQUE

The basic equations developed in the previous chapter must be processed in a manner to optimize stability, speed, and accuracy. This is primarily a function of the numerical scheme chosen and how it is implemented. This chapter explains how the finite difference technique is implemented numerically.

MATRIX Format

In order to use various numerical solution techniques, a convenient way of expressing the equations is in a matrix format. The finite difference equations are first placed in a format where:

j ,k (+1 step) = current j,k

Mass Rate

$$w(j+1,k) - w(j,k) = NTU_{m,jk}\Delta x(w_e - w)_{av}$$

where

$$(w_e - w)_{av} = \frac{1}{2}[(w_e(j,k+1) + w_e(j,k)] - \frac{1}{2}[(w(j+1,k) + w(j,k)]$$

multiplying and expanding

$$w(j+1,k) - w(j,k) = NTU_{m,jk}\Delta x w_e - \frac{NTU_{m,jk}\Delta x}{2}(w(j,k) + w(j+1,k))$$

consolidating terms

$$(1+\frac{NTU_{m,\,jk}\Delta x}{2})w(j+1,k) = NTU_{m,\,jk}\Delta x w_e + (1-\frac{NTU_{m,\,jk}\Delta x}{2})w(j,k)$$

<div align="right">Equation 78</div>

Mass Conservation

$$W(j,k+1)+\frac{\Delta\theta}{\beta_s\Gamma_s\Delta x}w(j+1,k) = W(j,k)+\frac{\Delta\theta}{\beta_s\Gamma_s\Delta x}w(j,k)$$

<div align="right">Equation 79</div>

Energy Rate

$$t(j+1,k)-t(j,k) = NTU_{q,\,jk}\Delta x(T-t)_{av}$$

where

$$(T-t)_{av} = \frac{1}{2}[T(j,k+1)+T(j,k)]-\frac{1}{2}[t(j+1,k)+t(j,k)]$$

multiplying and expanding

$$t(j+1,k)-t(j,k) = NTU_{q,\,jk}\Delta x\frac{1}{2}[T(j,k+1)+T(j,k)]-\frac{1}{2}[t(j+1,k)+t(j,k)]$$

consolidating terms

$$(\frac{NTU_{q,\,jk}\Delta x}{2}+1)t(j+1,k)-\frac{NTU_{q,\,jk}\Delta x}{2}T(j,k+1) = (1-\frac{NTU_{q,\,jk}\Delta x}{2})t(j,k)+\frac{NTU_{q,\,jk}\Delta x}{2}T(j,k)$$

<div align="right">Equation 80</div>

Energy Conservation

$$T(j,k+1)-T(j,k) = -\frac{\Delta\theta}{\Delta x\beta_s\Gamma_s c_{p,m}}[c_{p,ma}(t(j+1,k)-t(j,k))+i_{ad}(w(j+1,k)-w(j,k))]$$

multiplying and expanding

$$T(j,k+1)-T(j,k) =$$

$$= -\frac{\Delta\theta}{\Delta x\beta_s\Gamma_s c_{p,m}}[c_{p,ma}(t(j+1,k)+i_{ad}w(j+1,k)]+\frac{\Delta\theta}{\Delta x\beta_d\Gamma_s c_{p,m}}[c_{p,ma}t(j,k)+i_{ad}w(j,k)]]$$

consolidating terms

<div align="center">66</div>

$$T(j,k+1)+\frac{\Delta\theta}{\Delta x\beta_s\Gamma_s c_{p,m}}c_{p,mat}(j+1,k)+\frac{\Delta\theta}{\Delta x\beta_s\Gamma_s c_{p,m}}i_{ad}w(j+1,k)=$$

$$=T(j,k)+\frac{\Delta\theta}{\Delta x\beta_s\Gamma_s c_{p,m}}[c_{p,mat}(j,k)+i_{ad}w(j,k)]$$

Equation 81

These equations are then placed in a matrix notation:

$$Ax=b$$

where A is the matrix of coefficients for the variables to be solved; x is the matrix of the variables to be solved, and b is the right hand side of the equation. The right hand side of the equation is primarily composed of "known" values determined from the previous finite element. These are shown placed in their respective matrices in Figure 16. Moving the order of the variables and the equations around, the matrix format can be made sparse yet banded. This proved to be quite useful with various matrix solution techniques.

$$A$$

$$\begin{bmatrix} 1 & \dfrac{\Delta\theta}{\beta_s\Gamma_s\Delta x} & 0 & 0 \\ 0 & (1+\dfrac{NTU_{m,jk}\Delta x}{2}) & 0 & 0 \\ 0 & \dfrac{\Delta\theta}{\Delta x\beta_s\Gamma_s c_{pm}}i_{ad} & 1 & \dfrac{\Delta\theta}{\Delta x\beta_s\Gamma_s c_{pm}}c_{pma} \\ 0 & 0 & -\dfrac{NTU_{q,jk}\Delta x}{2} & (\dfrac{NTU_{q,jk}\Delta x}{2}+1) \end{bmatrix} \begin{array}{l} \textit{MassConservation} \\ \textit{MassRate} \\ \textit{EnergyConservation} \\ \textit{EnergyRate} \end{array}$$

$$
\underset{x}{
\begin{bmatrix}
W(j,k+1) \\[2mm]
w(j+1,k) \\[2mm]
T(j,k+1) \\[2mm]
t(j+1,k)
\end{bmatrix}}
\quad
\underset{b}{
\begin{bmatrix}
W(j,k) + \dfrac{\Delta\theta}{\beta_s \Gamma_s \Delta x} w(j,k) \\[4mm]
NTU_{m,jk}\Delta x\, w_e + \left(1 - \dfrac{NTU_{m,jk}\Delta x}{2}\right)w(j,k) \\[4mm]
T(j,k) + \dfrac{\Delta\theta}{\Delta x \beta_s \Gamma_s c_{pm}}\left((c_{pm,a}t(j,k) + i_{ad}w(j,k))\right) \\[4mm]
\left(1 - \dfrac{NTU_{q,jk}\Delta x}{2}\right)t(j,k) + \dfrac{NTU_{q,jk}\Delta x}{2}T(j,k)
\end{bmatrix}}
$$

Figure 16. Matrix Format

Numerical Techniques

To solve for the conditions of the rotary desiccant wheel, the following system of equations must be known:

1. Conservation of Mass

2. Conservation of Energy

3. Mass Transfer Rate

4. Energy Transfer Rate

5. Moist Air Enthalpy

6. Desiccant Wheel Enthalpy

7. The Adsorption Isotherm

8. Boundary Conditions (inlet states)

9. Initial Conditions (initial values or periodic steady-state)

There are now have five variables to solve for (t, w, T, W, w_e) at each location. However, the equilibrium temperature is clearly a function of w, W, and T. Using this relation, w_e can be solved and located on the "known" or right-hand of the matrix equation (matrix b). Thus, four unknowns will be solved at each element through iteration.

One substantial difference between this model and previous efforts is the calculation of NTU for each element. Previous efforts [Brandemuehl, 1982; Maclaine-cross, 1972; Chant 1991] have used a constant NTU for an entire stream or an entire wedge. The model developed in this thesis calculates a new NTU for *each* element. This involves determining various properties that are functions of temperature and moisture (specific heat, thermal conductivity) at each element as well in order to calculate NTU. This clearly increases the computational cost; however, the NTU is substantially dependent upon temperature and moisture. This can most clearly be seen in the inlet NTU values for process and regeneration calculated in the parametric analysis, Chapter 8.

An initial guess of the solution is made to start the procedure. The desiccant and moist air states for all axial positions are solved individually in a given wedge. For the transient case, this must be done for each wedge at every circumferential position. A step in the time direction is then made and the process repeats itself. At each element the mass and energy balances in the finite difference equations are checked to an epsilon criteria. Typically, the epsilon criteria used was 10^{-6}. The exiting condition of the airstream will be the average of the elements at the outlet axial positions.

The parabolic concentration profile (PCP) required solving a non-linear equation of one variable. Initially, the secant method was chosen based on previous research efforts. This technique proved relatively unstable; however, and initial runs showed the outlet conditions with dips and oscillations in what should have been the steady-state as shown in Figure 17. The "a2" curve has some relatively flat portions that apparently caused the derivative used in the secant method to search for a solution outside of the bracketed solution interval. At least one portion of the a2 equation has a discontinuous section as shown in Figure 18. When the equation solver "found" the discontinuous section, the value calculated for a2 caused instability in the outlet variables. A subroutine using Brent's method also exhibited the same phenomena and for probably the same reason. The bisection method (while a little slower) was found to have very good stability and accuracy with reasonable speed and was therefore used in this research.
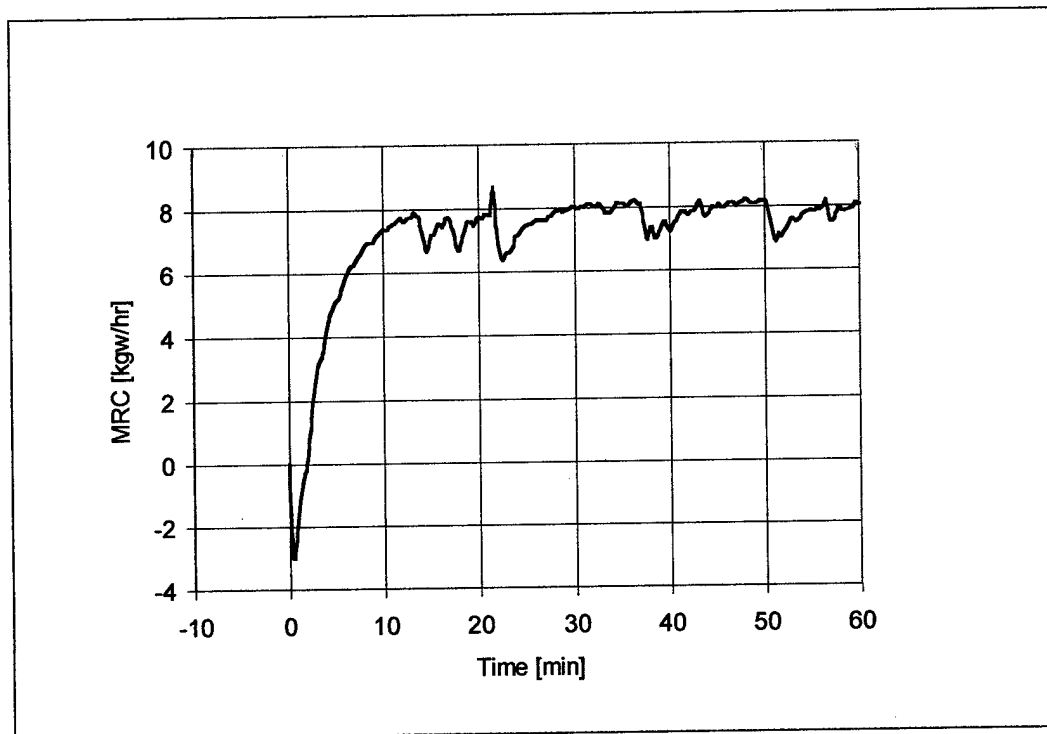
Figure 17. Sample Output with Instabilities Caused by PCP Solver
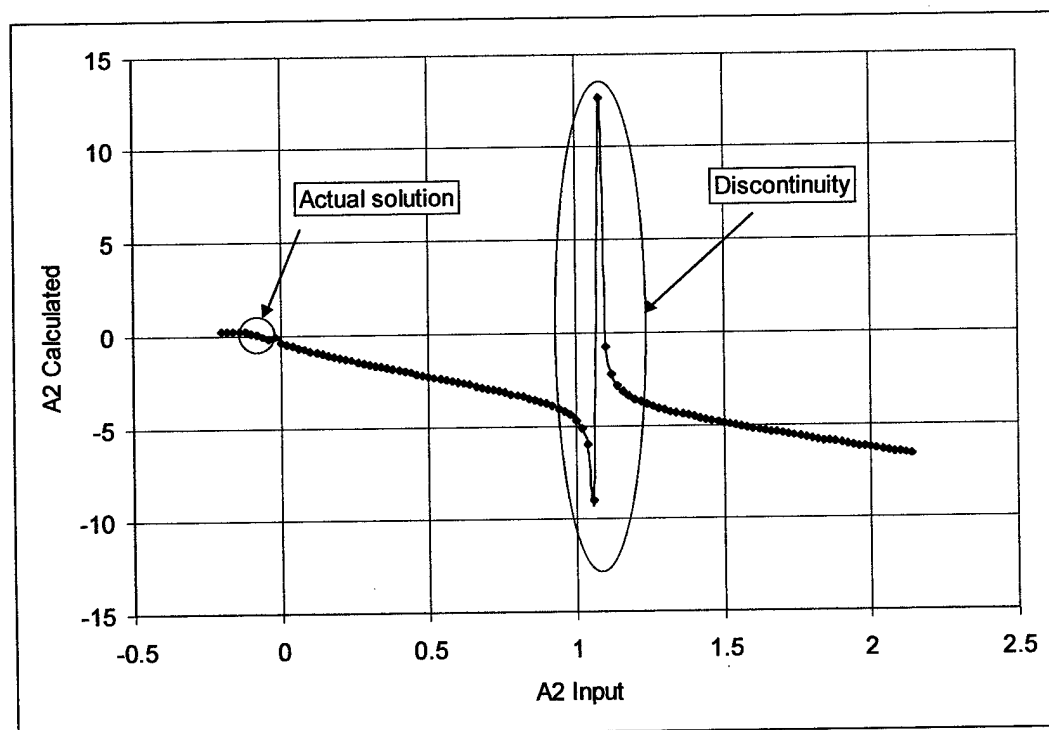
Figure 18. A2 Function Showing Discontinuity

A number of numerical techniques have been used to solve the finite difference equations: modified Euler method, matrix inversion techniques, Gauss-Seidel, etc.. Initial runs were done using a Gauss-Seidel technique because it is powerful, stable, and simple. After manipulating the variables and equations into the matrix form shown above, it was observed that the matrix format was that of a tridiagonal matrix with the form shown in Figure 19.
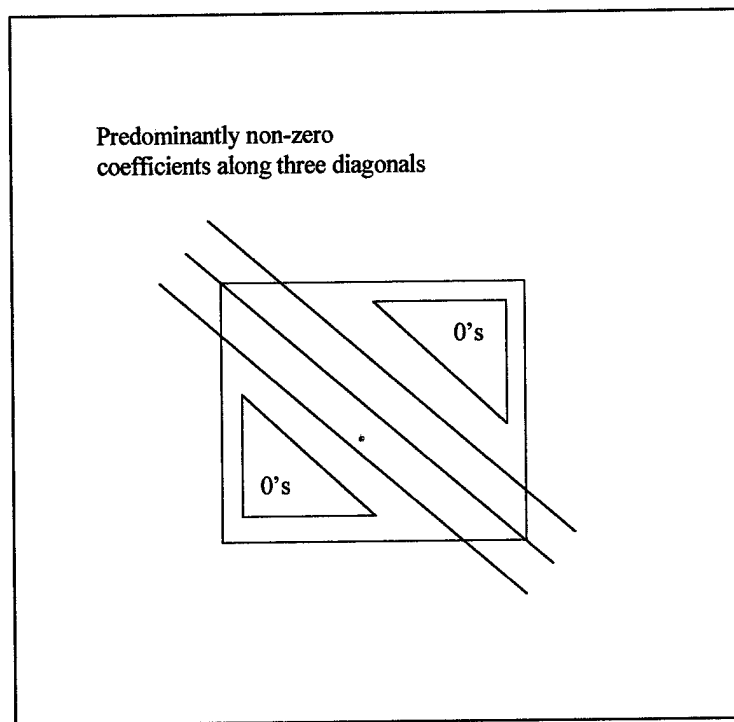
Figure 19. Tridiagonal Matrix Form

The tridiagonal matrix solver allowed for a faster solution for two reasons: the tridiagonal is a direct solution, not iterative, and the triangles with the zero coefficients are avoided. The Gauss-Seidel subroutine was from Ozisik [1994] and the tridiagonal matrix solver was from Press et. al. [1992]. Several runs with both the Gauss-Seidel and the tridiagonal matrix concluded that the tridiagonal solver was

indeed much faster. For most runs, the tridiagonal matrix solver was almost three times as fast. The tridiagonal solver should also be faster than a standard matrix solver or a generally banded matrix solver.

Step Size and Stability

Most of the work on step size and stability used in this work comes originally from Maclaine-Cross [1972] by way of Brandemuehl [1982]. The step sizes for both time and axial distance are critical so that the computer model will be stable and accurate while at the same time keeping computer run-time to a minimum. Accuracy was assumed to be obtained when the model produced consistent results for various grid sizes. A grid size that was not "fine" enough would not produce consistent or results equal with finer grid sizes.

Maclaine-cross experimented with various step sizes for both the steady-state and transient responses and developed expressions for satisfactory stability and convergence. For the steady-state model, the number of axial steps is determined by:

$$N_x = 1.7\sqrt{MAX(NTU_P, NTU_r)} + 3.2$$

Equation 82

For the transient model, he determined the number of axial steps to be:

$$N_x = 2.8\sqrt{MAX(NTU_P, NTU_r)} + 5.6$$

Equation 83

By using Dusinberre's original equations [Coppage, et. al., 1953], it can be shown that his equations were stable when $\Delta\theta \approx \Delta x$. This specifies a relationship

between the number of axial steps, N_x, and the number of time steps, N_θ. The finite

element figure implies the following relationship [Brandemuehl, 1982]:

$$N_{\theta,s} = \frac{N_x}{\Gamma_j}$$

For the entire grid (both streams), the relationship specifying the total number

of time steps would be as follows:

$$N_{\theta,total} = \frac{N_x}{\Gamma_p} + \frac{N_x}{\Gamma_r}$$

These relations worked for all but a few of the validation and parametric runs.

Runs where the grid size was insufficient were detected by observing the mass and

energy balances at a point where the system should have been in steady-state.

Generally, these step size relations produced mass and energy balances closely

approaching one. The runs with insuffcient grid sizing had mass and energy balances

much less than one($<.98$). In order to ensure adequate grid size, a more conservative

relation was also developed using the stream with the minimum flowrate ratio, Γ.

This has the effect of increasing the number of time steps.

$$N_{\theta,total} = \frac{2N_x}{Minimum(\Gamma_p, \Gamma_r)}$$

For many runs there was no significant difference in accuracy between the

number of axial steps calculated with the steady-state equation and the transient

equation. Because the steady-state equation generates significantly less steps, it was also much faster and most runs were done using this relation

The equations for mass and energy balance are defined below:

$$mass-balance-ratio = \frac{\dot{m}_{p,da}(w_{p,out} - w_{p,in})}{\dot{m}_{r,da}(w_{r,out} - w_{r,in})}$$

<div align="right">Equation 87</div>

$$energy-balance-ratio = \frac{\dot{m}_{p,da}(i_{p,out} - i_{p,in})}{\dot{m}_{r,da}(i_{r,out} - i_{r,in})}$$

<div align="right">Equation 88</div>

In order to optimize the run time and still maintain accuracy, some trial and error runs were required. A sample of grid sizes and their associated run times using a 450 MHz PC is shown in Table 2. The wheel time refers to the actual time a desiccant wheel would be turning. The computer time is the corresponding run time of the computer. It can be seen that the runs for some of the more extreme or stiff conditions are almost real time.

	Grid Size		Wheel Time	Computer Time	Computer / Wheel
Run	Axial	Circum	(hr)	(hr)	Ratio
1	5	200	1:38	1:23	0.8469
2	5	120	1:10	0:25	0.3571
3	5	80	1:10	0:16	0.2286
4	5	60	1:10	0:11	0.1571

Table 2. Grid Size and Run Times

When the system is in a configuration requiring a relatively fine grid size the model appears simply too slow for seasonal simulation. Unfortunately, today's

conventional operation is also the configuration requiring a fine grid size (high

regeneration temperature, unbalanced wheel split). Therefore, for most simulations,

seasonal lengths do not appear feasible.

CHAPTER 5. EXPERIMENTAL SETUP

To observe the actual behavior of a system and ensure that the computer model can produce accurate results, it was necessary to perform experiments of the desiccant wheel transient response phenomena and record the outcome.

The experimental work of this research was done at the National Renewable Energy Laboratory (NREL) located in Golden, Colorado. The desiccant laboratory located there is a state-of-the-art facility with high precision equipment that can accurately simulate a large variety of air conditions (flowrate, temperature, humidity, and pressure). The equipment and air conditions are also computer controlled and monitored. A picture of the laboratory at NREL is shown in Figure 20. A schematic of the desiccant laboratory is shown at Figure 21.

The NREL desiccant lab is normally set up for steady-state testing. A small amount of alteration was required in order to perform transient testing.

Desiccant Lab Components

The desiccant lab facility consists of the testing apparatus itself, the sensing equipment, and the computer monitoring and data storage.

The testing apparatus consists of the intake fans, ductwork, the heat and moisture generating equipment, the plenum section to hold the desiccant wheel, and the desiccant wheel itself. As can be seen from the schematic in Figure 21, each stream (process and regeneration) has its own set of components in order to allow for
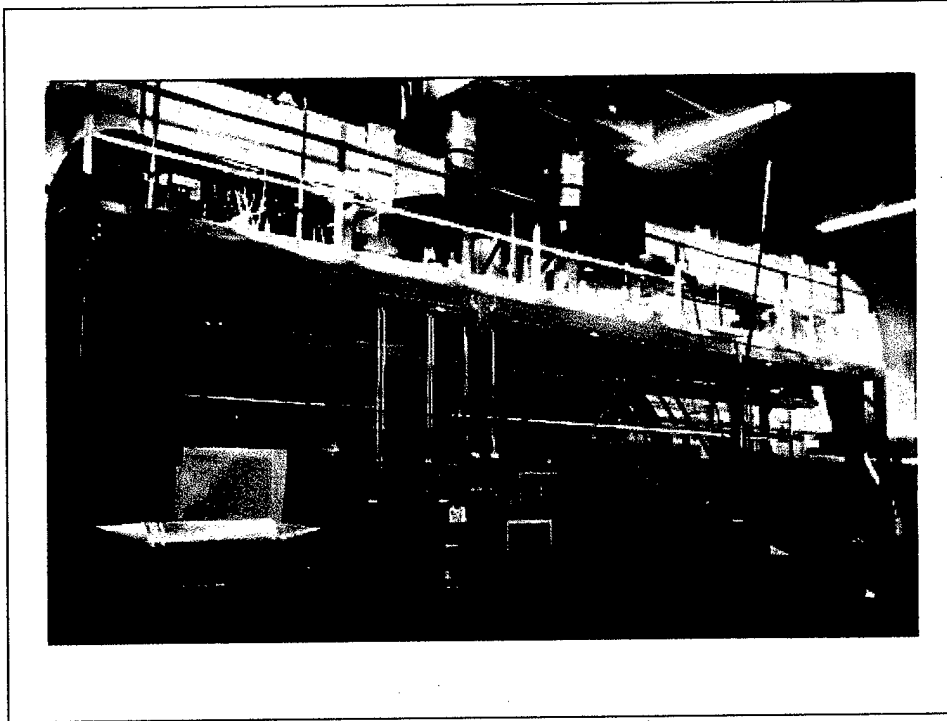
Figure 20. Photograph of the Desiccant Laboratory at NREL

independent control. Variable speed fans control the airflow rates and dynamic

pressures. Each fan is capable of air volumes of up to 4000 cfm. The ductwork

sections consist of 12 inch round galvanized steel with all sections wrapped in 2 inch

insulation to minimize heat losses. The heat is generated primarily through hot water

coils from a boiler and "topped off" with electrical resistance coils as needed. These

provide air at temperatures up to 120 °F in the process stream and up to 400 °F in the

regeneration stream. The moisture is entered into the airstream through water fed

evaporative cooling pads. They can generate airstream humidity levels in the range

of 35-250 grains/lb (.005-.0357 kg_w/kg_{da}). A plenum section around the desiccant

wheel is used to ensure mixed, laminar flow enters the test section and also provides a

portal for viewing. The plenum section has been designed to connect with flex duct

for quick connect/disconnect and secure connections.
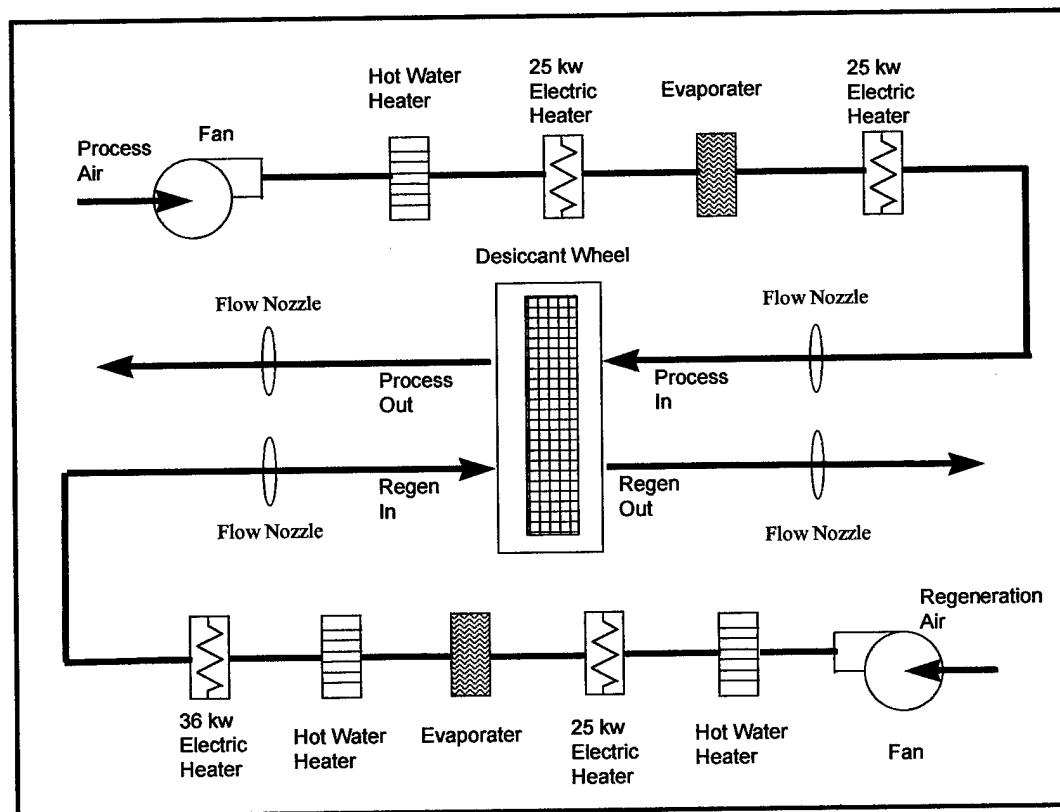
Figure 21. Schematic of Desiccant Laboratory at NREL

The sensing equipment is shown in Figure 22. The temperature sensors are

type-T thermocouples of copper/constantan with an absolute accuracy of +/- 0.3 °F.

Four thermocouples are used in a "t" shaped grid to obtain an average reading and

minimize temperature stratification. The humidity measurements are made with a D-

2 General Eastern chilled mirror hygrometer with a dewpoint accuracy in the range of

+/- 0.3 °F. The inlets for the humidity sensor are also arranged in a grid fashion to

minimize stratification. Flowrate measurements are made across flow nozzles made

to ASME specifications using capacitance type pressure transducers. Flowrates are

subsequently calculated by standard AMSE procedures with an absolute accuracy of

+/- 3%. Differential pressures are also measured across the wheel to determine the

fan power necessary for a given airflow. Baffles and mixing vanes are used within

the plenum to ensure a uniform flow. [Slayzak and Ryan, 1998]
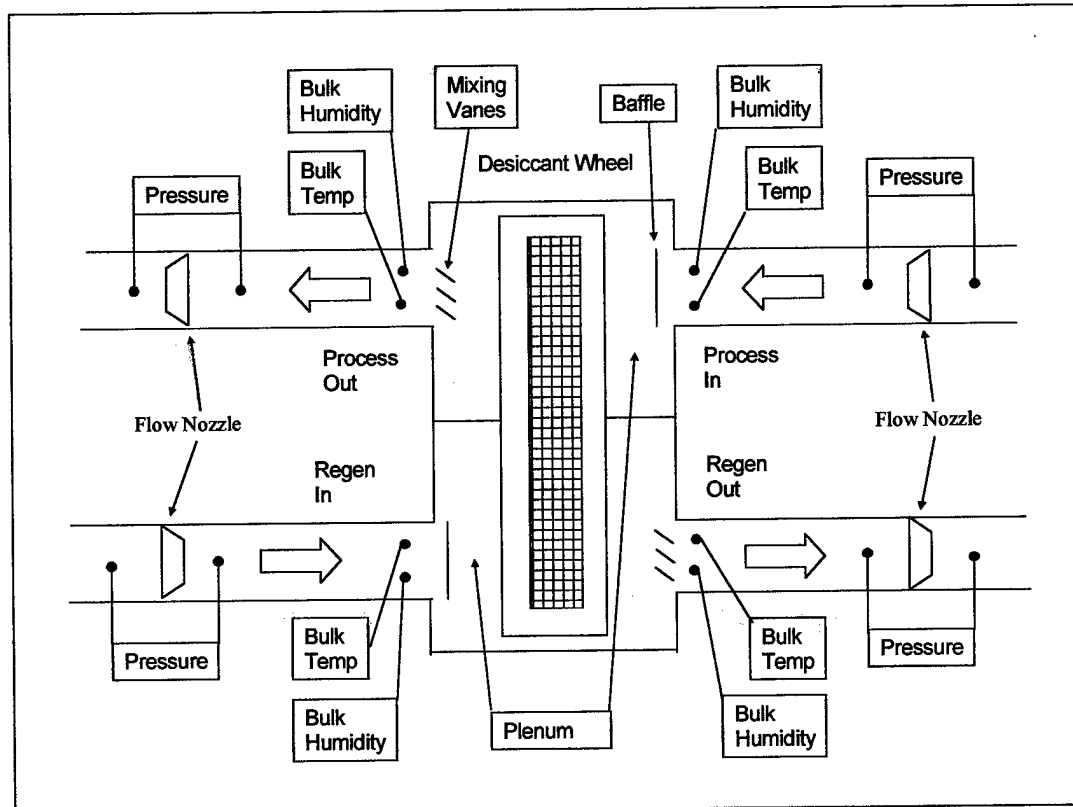
Figure 22. Schematic of Sensor Locations at NREL Desiccant Lab

The control console is shown in Figure 23. The system can be monitored and

controlled from this location through personal computers and manual controls. The

signals are interfaced with the PCs through a Hewlett-Packard data acquisition

system. Data can be easily logged, stored, and retrieved through electronic media.

Currently, these data can then be collected and stored every fifteen seconds. A

summary of the NREL desiccant lab capabilities was provided by Ryan [1999] and is

located at Table 3.
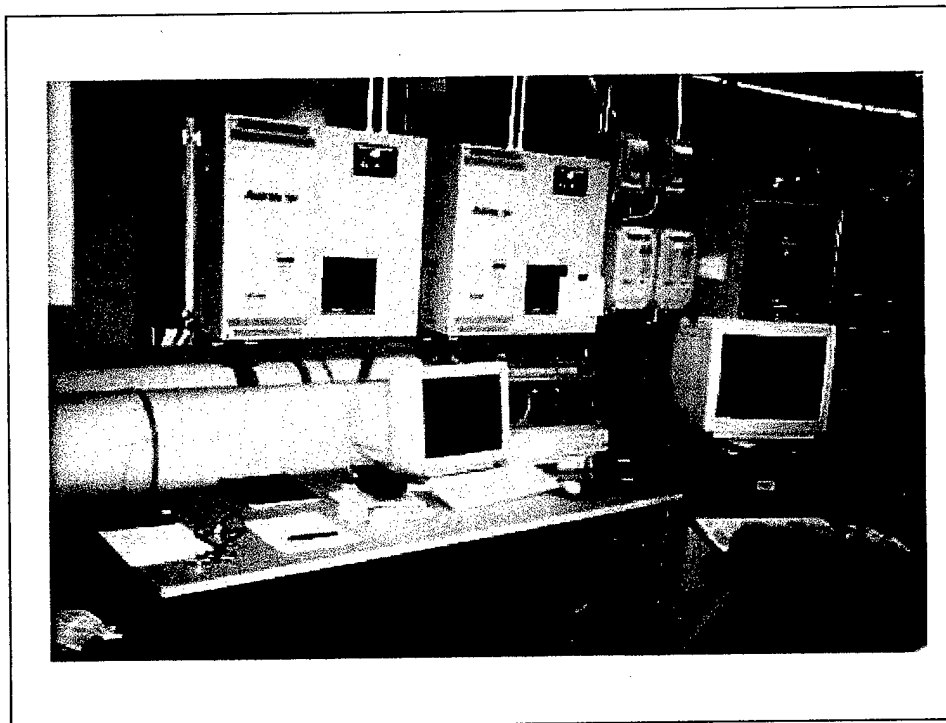
Figure 23. Control Console at the Desiccant Laboratory at NREL

	Process Loop	Regeneration Loop
Hardware		
Inlet blower horsepower	15	15
Outlet blower	n/a	5
Electric resistance	25 kW (2)	25 kW, 36 kW
Hot water coils	1	2
Evaporative pads	1" depth	1" depth
Temperature measurement	Type-T thermocouples, 4 each in the inlet and outlet	Type-T thermocouples, 4 each in the inlet and outlet
Flow measurement	ASME nozzle	ASME nozzle
Humidity measurement	General Eastern M4/Sim-12H Vaisala HMP 223 Vaisala HMD 50Y Aspirated Psychrometer (inlet)	General Eastern M4/Sim-12H
Capacities:		
Flow rate	4000 cfm	4000 cfm
Temperature	120 °F	400 °F

	Process Loop	Regeneration Loop
Humidity ratio	35-250 grains/lb	35-250 grains/lb
Accuracies:		
Flow rate	+/- 3%	+/- 3%
Temperature	+/- 0.3 °F	+/- 0.3 °F
Humidity (dew point)	+/- 0.3 °F	+/- 0.3 °F
MRC/MRR	+/- 4%	+/- 4%
Moisture Mass Balance	-5%	-5%
Control Tolerance:		
Flow rate	+/- 10 cfm	+/- 10 cfm
Temperature	+/- 0.3 °F	+/- 0.3 °F
Humidity (dew point)	+/- 2 grains/lb	+/- 2 grains/lb

Table 3. Summary of NREL Desiccant Laboratory Capabilities

Experimental Desiccant Wheel

The computer model in this research was built using data from the Solar

Energy Research Institute (now NREL) Microbead wheel. This data has been listed

in the works of several researchers [Chant, 1991][Schultz, 1987]. This wheel has

become dated, however, and does not represent the state of the art. For this research,

a current, commercially available desiccant wheel sold by NovelAire Co was used.

The model is referred to as the WSG or wound silica gel model. A summary of the

wheel input values for the SERI and NovelAire wheels is shown at Table 4.

Comparing the SERI microbead and the NovelAire wheel, one can see that the

amount of desiccant mass has increased while the transfer surface area appears to

have decreased significantly. The microbead wheel uses a parallel plate profile while

the WSG wheel uses a triangular/rectangular profile. The newer wheel also has a

much smaller particle radius.

In validating the performance of the NovelAire Wheel, two different types of

profiles were used for the flutes where the heat and mass transfer take place. The

profiles in the wheel face closely resemble the edge of simple corrugated cardboard. The profiles seen in the experimental wheel itself, however, had significant variability. Some flutes appeared to barely touch the surface above and looked relatively triangular. In others, the top triangular point was "mashed" down a bit and the profile appeared rectangular. The detail calculations for the rectangular and triangular profiles are located in Appendix F. These two profiles represent the extremes for possible heat and mass transfer profiles. The rectangular profile has a minimum of surface area, maximum hydraulic diameter, and maximum amount of desiccant mass. The triangular profile has a maximum amount of surface area, minimum hydraulic diameter, and the minimum amount of desiccant mass. This translates into a higher Number of Transfer Units for the triangular profile and a lower number of NTUs for the rectangular. These two profiles were used in the validation portion as a starting point in order to determine the best fit.

description	Seri microbead	NovelAire WSG	UNITS
particle radius	.0000475	.0000035	m
particle density	1129	1129	Kg/m^3
total transfer surface area, both periods	82	38.5	m^2
mass of dry desiccant	4.01	8.1	Kg
specific heat of the matrix per mass of dry desiccant	3.1	1.82	kJ/kg_{DD}-K
thetap	.5	.75	-
thetar	1.0	1.0	-
cross-sectional flow area	.162	.167	m^2
hydraulic diameter of flute	.0016	.00136	m

description	Seri microbead	NovelAire WSG	UNITS
length or thickness of the wheel	.1	.2	m
height of the flute	small	.00159	m
width of the flute	very wide	.003387	m
shape of the flute	infinite parallel plates	Rectangular/triangular	-

Table 4. Input Data for SERI Microbead and the NovelAire WSG Desiccant Wheels

A picture of the WSG wheel is shown in Figure 24. The wheel is contained inside the "structural cassette" used when the wheel is to be operated.

Perhaps the largest difference between older desiccant wheels and newer models as represented by the NovelAire WSG wheel is how the desiccant is attached to a substrate material in order to give the matrix a rigid structure. Older wheels, like the SERI microbead, attached the desiccant material to the substrate surface in a "layered" effect. The desiccant has direct contact with the airstream. Newer desiccant wheels typically combine the desiccant and a substrate into a homogenous mixture that can be fabricated into a rigid matrix. The substrate material uses binders and/or fillers that are capable of letting the water vapor pass through to the desiccant.

Experimental runs

The experimental tests to be performed were selected for two purposes: 1) to observe the actual transient response to various inputs and 2) to validate the computer model. The tests were done on the assumption that for the majority of HVAC systems with desiccant dehumidification, the following items were the most likely

and most feasible to be used in controlling the system. Step changes (as opposed to graduated changes) were selected in order to be consistent across the tests and because they actually represent the optimum or fastest possible change. The following cases were selected for the experimental work.
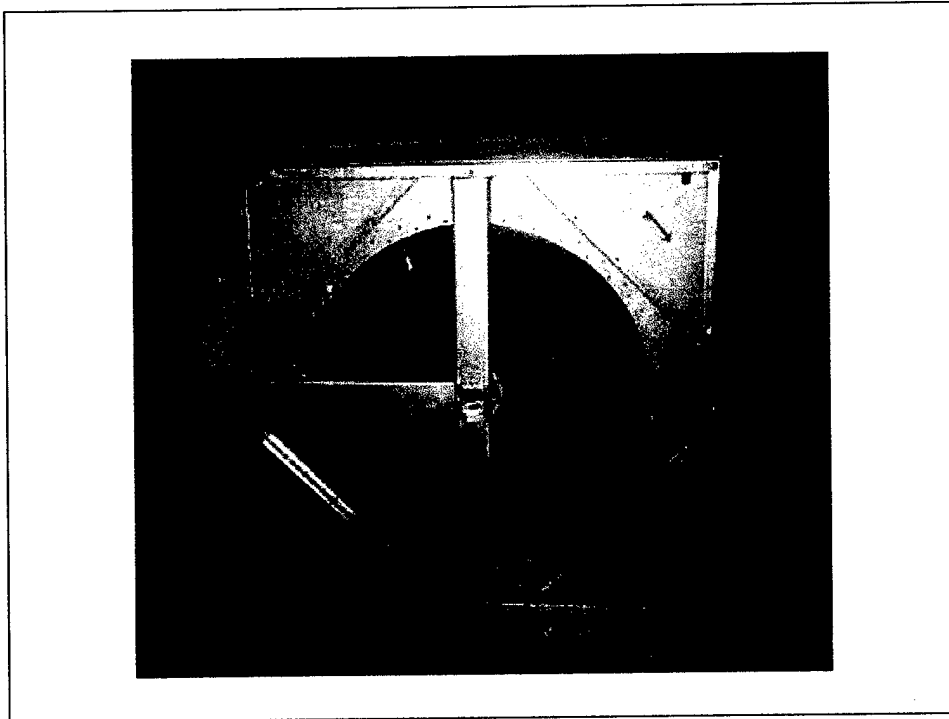
Figure 24. Photo of the NovelAire WSG Wheel

Step increase to regeneration temperature/step decrease to regeneration temperature. For most desiccant systems, the wheel is primarily regenerated through raising the temperature of the regeneration stream. The step change in temperature is not normally instantaneous, but it is relatively quick. The step change decrease will measure how long the wheel takes to return to a non-adsorbing steady-state. The step increase and decrease can then be compared.

Step increase to process flowrate/step decrease to process flowrate. This is to simulate modulated airflow to a space. Typical, current HVAC designs use variable air volume systems that modulate airflow. A desiccant wheel could be expected to see changing air flowrates. Again, the step increase can be compared to the step decrease.

Step increase to the wheel speed. The step increase to wheel speed of the desiccant wheel was performed to see if changing the wheel speed would have a significant effect on the transient response. This is also a relatively easy step increase to implement.

Run	Description
1	step increase from ambient temperature to full regen design temperature
2	step decrease from full regen design temperature to ambient temperature
3	step increase from one half process design flowrate to full process design flowrate
4	step decrease from full process design flowrate to one half process design flowrate
5	step increase from one half design wheel speed to full design wheel speed
6	step decrease from full design wheel speed to one half design wheel speed

Table 5. List of Experimental Step Changes

The initial and step conditions for ambient temperature and humidity ratio were selected based on applicability to the industry and apparent optimized performance of the wheel. Accordingly, the initial conditions were based on the Air Refrigeration Institute (ARI) Standard 940 [1998], which provides four such possible conditions. Ambient conditions at 95F and 40% relative humidity are one of the four possible conditions and also the typical standard for most cooling coil testing. They

were therefore selected as the ambient conditions for this research. The step change conditions (wheel speed, flowrate, regeneration temperature) consisted of the manufacturer's (NovelAire) recommended design ratings for the WSG wheel as shown in Table 6.

Wheel Speed	Flowrate (in velocity)	Regeneration Temperature
18 rph	600 ft per minute	140 °C

Table 6. Manufacturer's Recommended Operating Conditions for the NovelAire WSG Wheel

Physical Implementation

The following section describes the physical implementation of the experiments or how they were accomplished in the laboratory.

Step Increase To Regeneration Temperature. The schematic for this step change is Figure 26. The step change to temperature was accomplished by initially running the wheel where it saw only the process stream at given ambient conditions and nothing from the regeneration stream. This simulated the wheel operating under steady-state ambient conditions since the process and regeneration are normally at the same temperature and humidity level. The regeneration stream was raised to the transient step change temperature while it diverted from the wheel. When the wheel reached steady-state at the "ambient conditions" and the regeneration stream reached its steady-state operating temperature, the step change was accomplished by quickly (almost instantaneously) re-directing the regeneration stream to the wheel plenum through a wye section with blast gates (Figure 25).

87
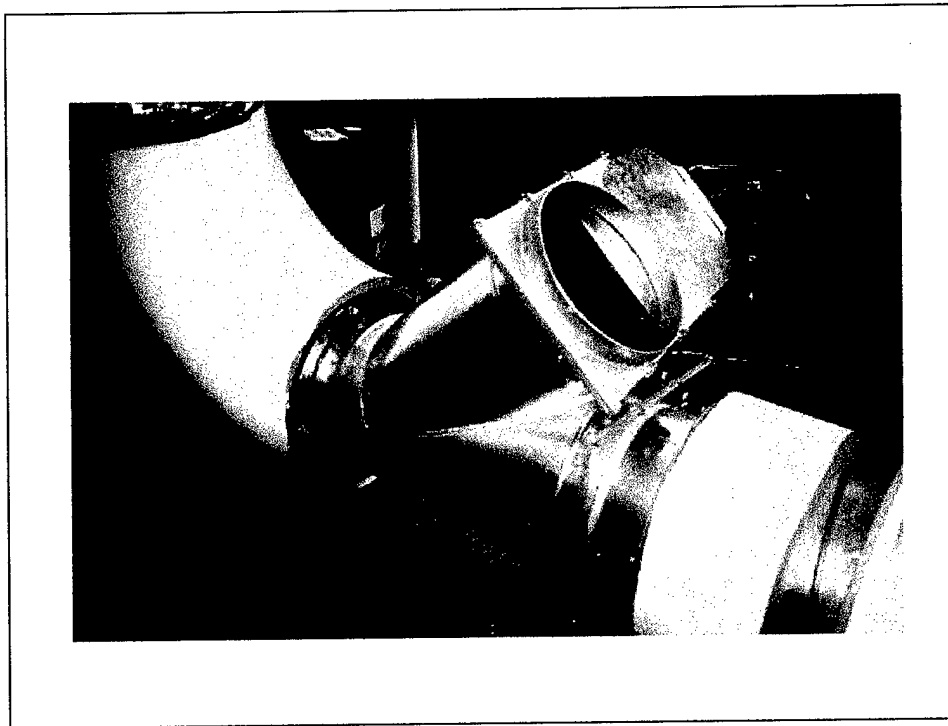
Figure 25. Flow Diverting Modification to Existing Desiccant Laboratory

Step Decrease To Regeneration Temperature. In order to achieve steady-state at the design operating conditions, the system must receive both process and regeneration streams since these are at different temperatures. Therefore, the flow switching strategy will not work exactly in reverse. Once steady-state was achieved at the design operating conditions, the step decrease was accomplished by an "instantaneous" shutdown of the heating system and then disconnection of the ductwork. The disconnected ductwork then used actual ambient air to return to "ambient" conditions. Because of the thermal mass in the system (heating coils, duct), the step change was actually less than instantaneous. The actual data

(temperature, flowrate, humidity ratio) from during the step change; however, can be

provided to the computer model for validation purposes.
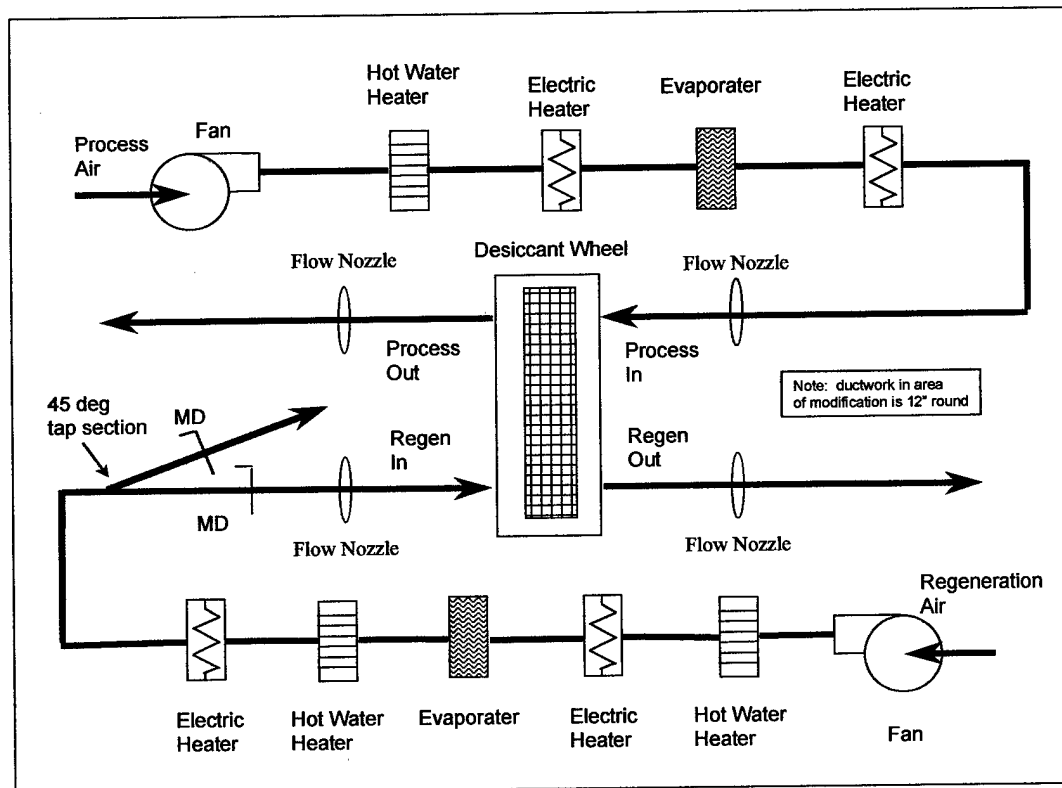
Figure 26. Experimental Configuration for Step Change to
Regeneration Temperature

Step Increase And Decrease To Process Flowrate. The configuration for

this step change is shown at Figure 27. The flow switching section used in the

regeneration temperature step change was moved to the process stream. The gate

dampers were adjusted for the steady-state conditions. Once the steady-state

conditions were achieved, the step change was made by quickly adjusting the

dampers to increase the flow to the step increase flowrate. Once steady-state was

achieved at the higher flowrate, the dampers were adjusted back to their original

position to achieve the step decrease.
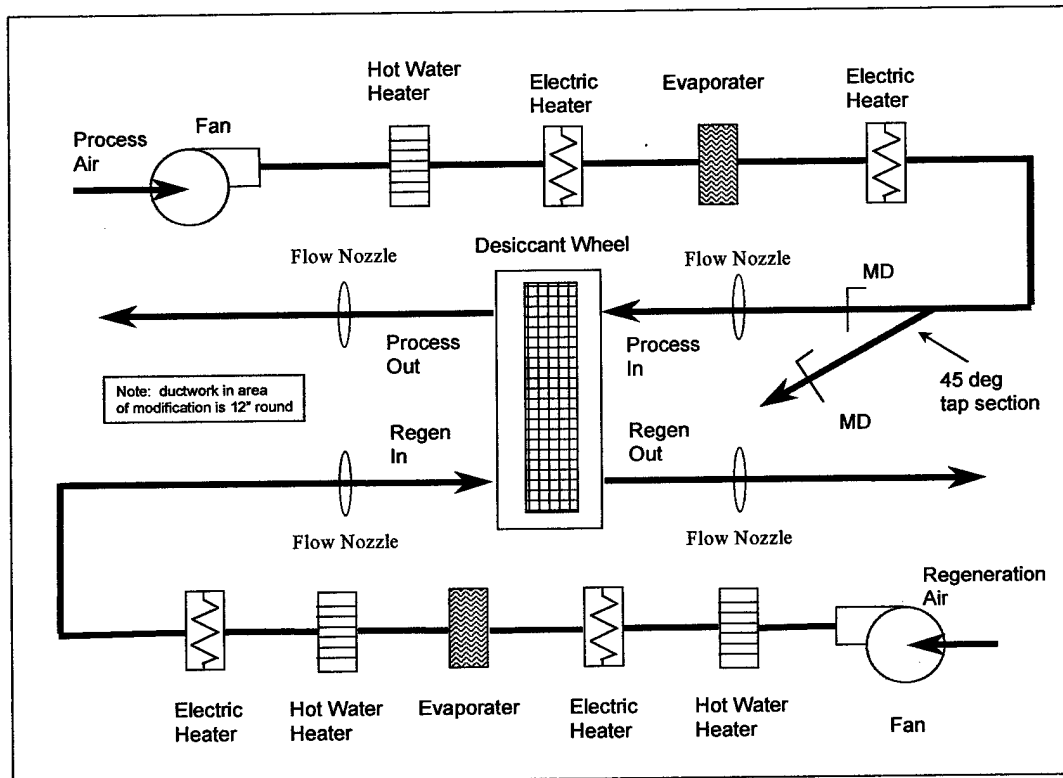
Figure 27. Experimental Configuration for Step Change to Process Flowrate

Step Increase And Decrease To Wheelspeed. The step change to the wheel speed is the easiest to physically implement and in fact can use the existing system (Figure 21) without modification. The motor turning the desiccant wheel can be directly and quickly tuned to the necessary wheelspeed. The time required for the change can be considered almost instantaneous.

CHAPTER 6. VALIDATION

The experimental results produced at NREL were used to validate the computer model. A validated model can produce accurate results relatively quickly and less expensively than experimental runs

Steady-state Validation

The actual input parameters for the experimental validation runs are shown in Table 7. There is some small deviation from recommended operational design values due to equipment configuration – however this does not impact the validation results.

Before doing an actual comparison of transient data from the experiment and numerical results, a steady-state analysis was performed using data from the runs that were in steady-state. In order to confirm that the experimental results were reasonable, a comparison was made with steady-state data for the WSG wheel published by the NovelAire company and the experimental data obtained at NREL. NovelAire has developed a computer program to calculate the steady-state characteristics of their wheels using curve-fits to actual historical data. The NovelAire program output is shown in Appendix G. The results of this comparison are shown in Table 8. The percent change column uses the difference between inlet and outlet states as the denominator. The steady-state results from the numerical runs are also presented in Table 8.

| | | Initial Steady-state | | | | | | Step Change (Transient phase) | | | | | | |
| | | Process | | | regen | | | | process | | | regen | | |
Run	Speed Revs/hr	Flow Rate (kg/s)	Temp, K	w, kg_w/kg_{da}	flow rate (kg/s)	Temp, F/C	w, kg_w/kg_{da}	Speed revs/hr	flow rate (kg/s)	Temp, K	w, kg_w/kg_{da}	flow rate (kg/s)	Temp, K	w, kg_w/kg_{da}
1	18	.469	308.15	.0178	.143	308.15	.0178	18	.469	308.15	.0178	.143	407.15	.0178
2	18	.469	308.15	.0178	.143	407.15	.0178	18	.460	308.15	.0177	.176	298.07	.009
3	9	.469	308.15	.01778	.157	407.15	.01778	18	.469	308.15	.01778	.157	407.15	.01778
4	18	.469	308.15	.01778	.157	407.15	.01778	9	.469	308.15	.01778	.157	407.15	.01778
5	18	.3127	308.15	.0178	.160	407.15	.0178	18	.471	308.15	.0178	.160	407.15	.0178
6	18	.471	308.15	.0178	.160	407.15	.0178	18	.3127	308.15	.0178	.160	407.15	.0178

Table 7. System Input Parameters for the Experimental Validation

		NovelAire Program		Experimental Runs		Comparison Percent (%) Difference		Numerical runs	
Run	Stream	Temp, K	w, kgw/kgda	Temp, K	w, kgw/kgda	Temp	w	Temp, K	w, kgw/kgda
1	process	333.2	0.011	333.15	0.01229	0.02	0.12	332.49	0.0120
1	regen	330.48	0.0381	320.75	0.03500	2.94	8.14	328.67	0.0368
2	process	333.2	0.011	334.00	0.01225	0.24	11.36	332.49	0.0120
2	regen	330.48	0.0381	321.05	0.03500	2.85	8.14	328.67	0.0368
3	process	333.2	0.011	334.02	0.01221	0.25	10.96	332.49	0.0120
3	regen	330.48	0.0381	321.10	0.03495	2.84	8.27	328.67	0.0368
4	process	333.2	0.011	333.29	0.01232	0.03	12.00	332.49	0.0120
4	regen	330.48	0.0381	320.85	0.03512	2.91	7.82	328.67	0.0368
5	process	334.53	0.01090	336.10	0.01179	0.47	8.17	336.10	0.0118
5	regen	332.37	0.03860	322.92	0.03559	2.84	7.80	322.92	0.0356
6	process	334.53	0.01090	336.25	0.01179	0.51	8.17	336.25	0.0118
6	regen	332.37	0.03860	322.60	0.03558	2.94	7.82	322.60	0.0356

Table 8. Validation Results for Experimental Data

It can be seen from Table 8 that the temperature values are relatively close to their predicted steady-state levels. The percent changes with humidity ratio is off a significantly higher amount than the percent changes with temperature. Even the worst case however is well within 10% of the actual value and close enough to say that the experimental data appears reasonably close to the historical performance.

A more interesting picture uses the psychometric chart for comparison, Figure 28. In this case, the steady-state values of the first run are used. The two profiles for heat and mass transfer, the rectangle and triangle, appear to follow a linear extension from the inlet conditions. This corresponds to their NTU values: the greater NTU magnitudes of the triangular profile translate into greater heat and mass transfer as one might expect.

Clearly, the process outlet values are in very good agreement with all three sources of data. Only the numerical solution with the triangular profile appears to deviate from the pack. On the regeneration side, the outlet states are close; however, there is significant separation between the experimental data and the numerical and/or historical. The triangular and rectangular points are about equidistant from the experimental data. The triangular point is closer in temperature while the rectangular point is closer in humidity ratio. The historical curve fit point is substantially closer to the numerical run with the rectangular profile.
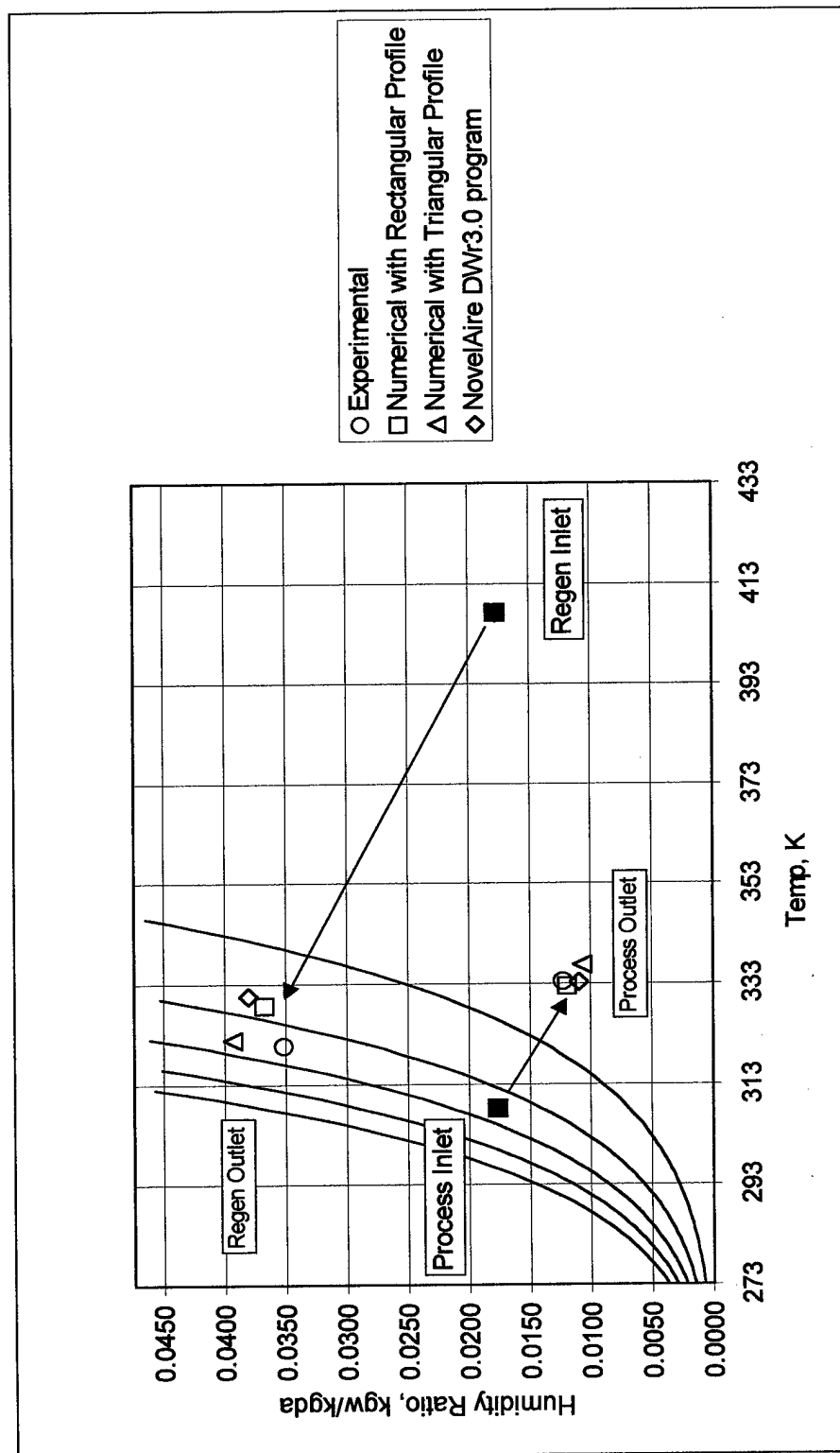
Figure 28. Steady-State Comparison of Process and Regeneration Outlet States Using Experimental, Numerical, and Historical Data (NovelAire DWr3.0)

Mass and energy balances, using Equation 87 and Equation 88, are much better for the numerical and historical points than with the experimental points for all cases. Specifically, the energy balances for the experimental runs give ratios of approximately 0.6-0.8. The numerical runs and the program based on historical data conserve mass and energy implicitly and their balances are typically between 0.98 and 1.0. Because the experimental runs do not appear to conserve both mass and energy well, the numerical results cannot be expected to validate perfectly with the experimental results.

The numerical runs represent the best case scenario where losses and inaccuracies are eliminated which can cause the mass and energy balance deviations.

There are several possible explanations for the deviation of the mass and energy balances of the experimental data. They will be reviewed here.

1. Incorrect sensor reading due to stratification of the airstream. This is unlikely because the thermocouple sensors are arranged in a grid to average the temperature distribution in the airflow. If there was stratification, then little variation in the outlet temperature would be seen and this was not the case. If stratification is a problem, then it is probably relatively small.

2. Incorrect sensor reading due to incorrect correlation equation. This error would occur if the equation correlating the electrical signal to a temperature were incorrect for the type of thermocouple used. The equation used by the NREL equipment was checked against the equation used by a major manufacturer of electrical sensing devices. Both were higher order polynomials and appeared to have the same basic curve. Therefore, the correlation equation appears correct. Previous

comparisons with other temperature sensing devices by NREL personnel have not indicated a discrepancy.

3. The inaccuracy associated with the sensors themselves. An analysis was performed using the accuracies provided by the laboratory as listed in Chapter 5 (Experimental Setup) with the steady-state inlet and outlet parameters (flowrate, temperature, and humidity ratio). A mass and energy balance was done on the wheel using the steady-state conditions from the step increase to regeneration temperature. Balances were done on the system to see the effect of using the upper and lower bound accuracy for each sensor individually. This is summarized in Table 9. The initial balances for the experimental, numerical, and historical results can be seen in the first three rows. The process flowrate sensor appears to have the greatest individual impact as it can alter the energy balance by 0.13.

An uncertainty analysis done using the procedure presented by Kline-McClintock [Holman, 1989] was done and is located in Appendix H. This analysis calculates a combined uncertainty error that takes into account the error of all variables. The result of this analysis is an absolute energy balance ratio error of 0.22. The accuracy bounds of the sensors can therefore significantly impact the energy balance and agreement with the numerical results

Case	Accuracy Bound	H20 mass balance	energy balance
Original Data Experimental		1.12	0.66
Original Data Numerical		1.00	1.00
Original Data Historical		1.00	1.00
Process Inlet Temperature	high	1.12	0.62
Process Inlet Temperature	low	1.04	0.86

Case	Accuracy Bound	H20 mass balance	energy balance
Regen Inlet Temperature	high	1.04	0.81
Regen Inlet Temperature	low	1.04	0.83
Process Outlet Temperature	high	1.12	0.69
Process Outlet Temperature	low	1.12	0.62
Regen Outlet Temperature	high	1.12	0.66
Regen Outlet Temperature	low	1.12	0.65
Process Inlet Flowrate	high	1.22	0.52
Process Inlet Flowrate	low	1.01	0.79
Regen Inlet Flowrate	high	1.16	0.60
Regen Inlet Flowrate	low	1.08	0.73
Process Outlet Flowrate	high	1.04	0.81
Process Outlet Flowrate	low	1.19	0.50
Regen Outlet Flowrate	high	1.05	0.71
Regen Outlet Flowrate	low	1.19	0.61
Process Inlet Humidity Ratio	high	1.22	0.58
Process Inlet Humidity Ratio	low	0.97	0.76
Regen Inlet Humidity Ratio	high	1.17	0.63
Regen Inlet Humidity Ratio	low	1.07	0.68
Process Outlet Humidity Ratio	high	1.02	0.73
Process Outlet Humidity Ratio	low	1.22	0.58
Regen Outlet Humidity Ratio	high	1.03	0.70
Regen Outlet Humidity Ratio	low	1.22	0.62

Table 9. Summary of Mass and Energy Balance Analysis with
Sensor Accuracies

4. Leakage. Leakage occurs when air from one stream enters the other stream

through openings between the casing and the wheel itself or releases air straight to the

atmosphere as shown in Figure 29. Some leakage does occur during normal

operation and previous researchers have quantified the leakage percentages for the

different pathways using other systems to be in the range of 1-4.3% [Schultz, 1987].

Experimental Pressure Readings indicate a difference of approximately 2.4

inWG between the Process Inlet and Regeneration Outlet Streams and 1.8 in WG

between the Regeneration Inlet and Process Outlet Streams. This pressure difference clearly indicates that some leakage must occur assuming there are any openings between the streams in the plenum.

Another indication of leakage within the experimental wheel runs are the mass flowrates. The input values used in Table 7 for the computer model indicate the mass flowrates are constant from inlet to outlet because the computer model uses a constant flowrate. The actual experimental values for inlet and outlet flowrates differed in some cases by as much as 6%. The values listed in Table 7 are the lower flowrates which were assumed to have made it through the wheel and were used by the numerical model. The difference in flowrates also indicate carryover and possible leakage to the atmosphere.

The disagreement in the energy balance of the experimental results and the discrepancy with numerical regeneration temperature is believed to be the result of combined sensor accuracy and carryover/leakage within the experimental apparatus.

Transient Validation

The statistical test used for the outlet validation portion of this research is the root mean square error or RMSE as shown in Equation 89. The RMSE statistic can be interpreted as the average error between the two curves over the range of interest. The range was selected to focus on the transient response and minimize steady-state impact. This statistic is used to compare the correlation of two curves.
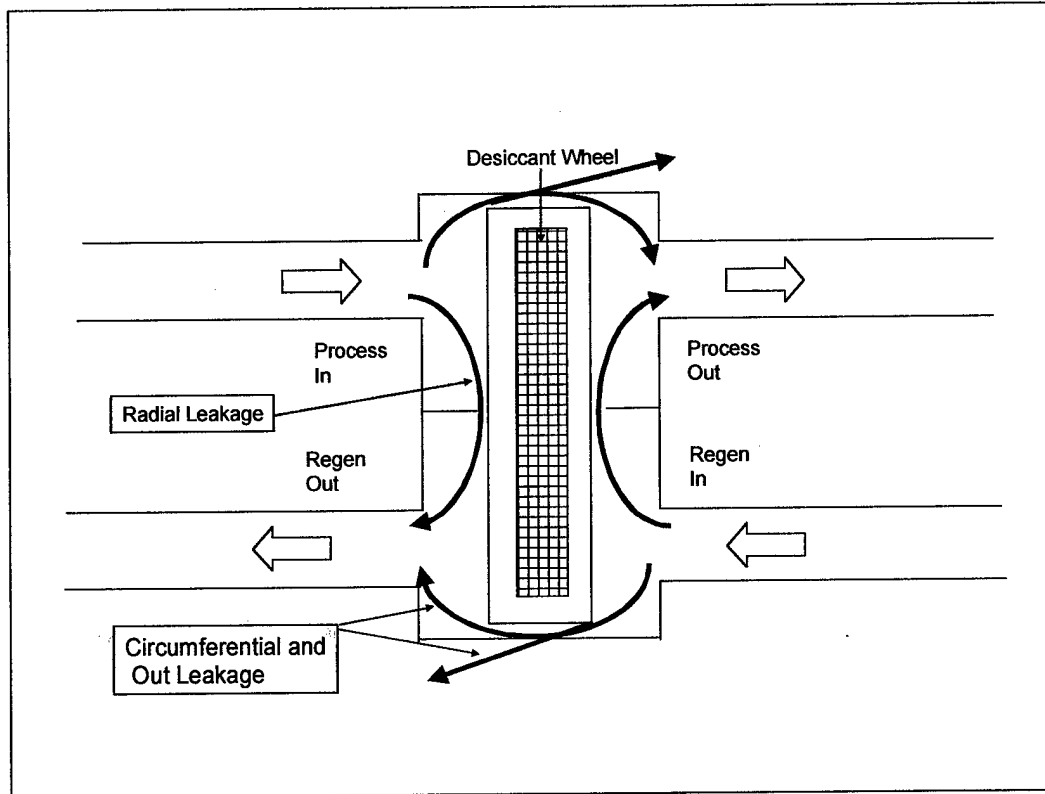
Figure 29. Schematic Showing Possible Leakage Sites

$$RMSE = \sqrt{\frac{\sum (y_{pred,\,i} - y_i)^2}{n}}$$

Equation 89

The initial validation focused on the step change to regeneration temperature because the difference in process and regeneration temperature is the primary driving potential for moisture removal. At this point, both transfer profiles (triangular and rectangular) were used in transient response runs. Looking at the change in process outlet temperature (Figure 30), it can be seen that the rectangular profile follows the experimental curve with much greater fidelity than the triangular. The triangular

profile clearly reached a steady-state much faster and at a much higher magnitude than the rectangular. Based on the steady-state graph (Figure 28) and the initial transient runs, the rectangular profile was chosen as the most representative of the average profile within the WSG wheel. The remainder of the runs were therefore done with the rectangular profile.

Looking at the figures, Figure 30 through Figure 33, the curves generally appear to be a close match. The RMSE (Table 11) for these runs look relatively good. Process temperature RMSE is within a degree and the RMSE for the humidity ratios are both within 10%. The regeneration temperature curve parallels the steady-state psychrometric chart offset shown earlier and has a correspondingly higher RMSE.

The numerical curve of the process humidity ratio has a slight initial bump that does not greatly affect the statistical value. Intuitively, it would appear that a surface layer of moisture is quickly evaporated; however, there is no similar response from the experimental side. An explanation is that the data collection period from the experiment is not short enough or the PCP numerical scheme needs some time to "set up" when there is excess moisture.

Although the steady-state response of the regeneration outlet temperature is a few degrees off (as seen earlier with the psychrometrics graph, Figure 28), the curves are still nearly identical. A normalized graphing of the response would show very good agreement as with the other parameters (process temperature, process humidity ratio, and regeneration humidity ratio).

101
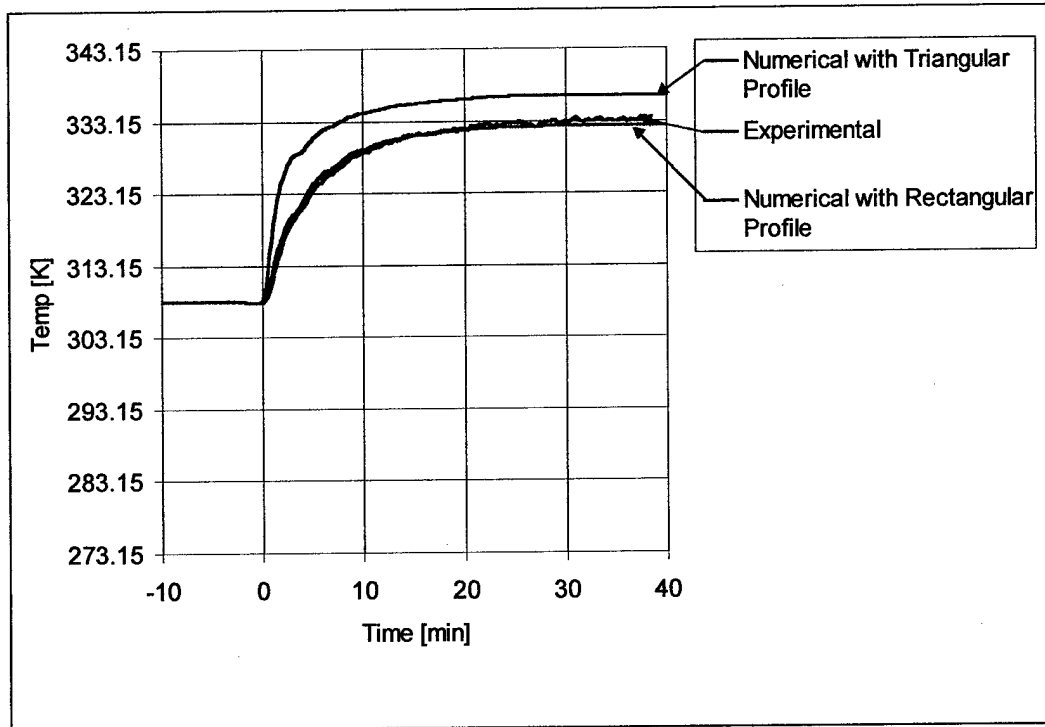
Figure 30. Process Outlet Temperature Versus Time With a Step
Increase to Regeneration Inlet Temperature
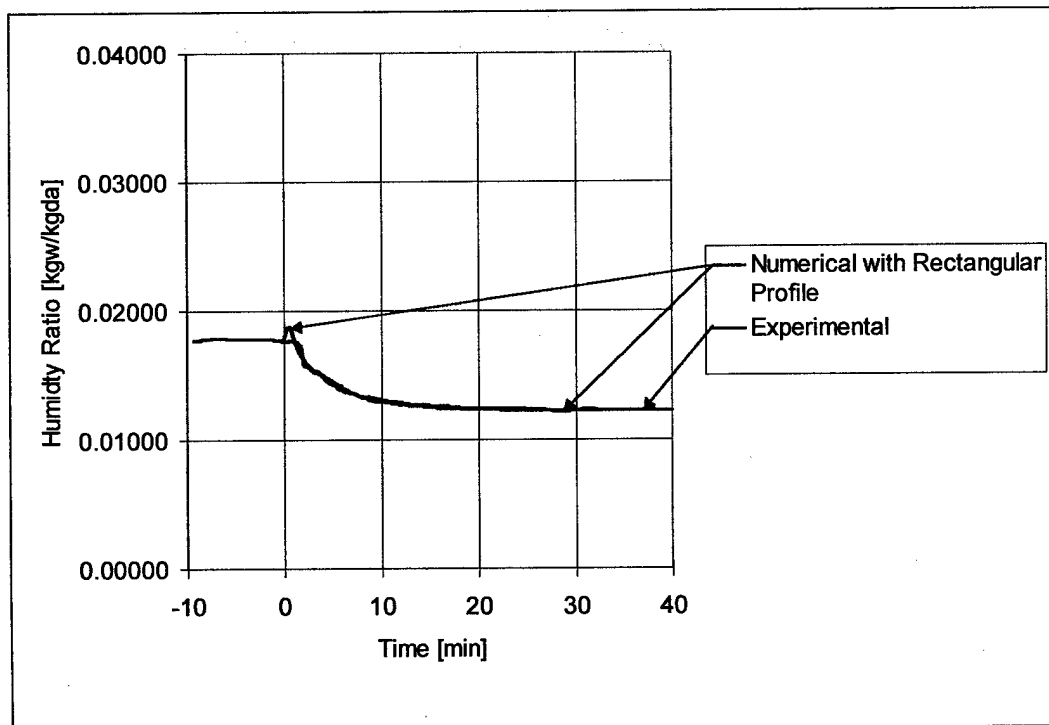
Figure 31. Process Outlet Relative Humidity Versus Time with a
Step Increase to Regeneration Inlet Temperature

102
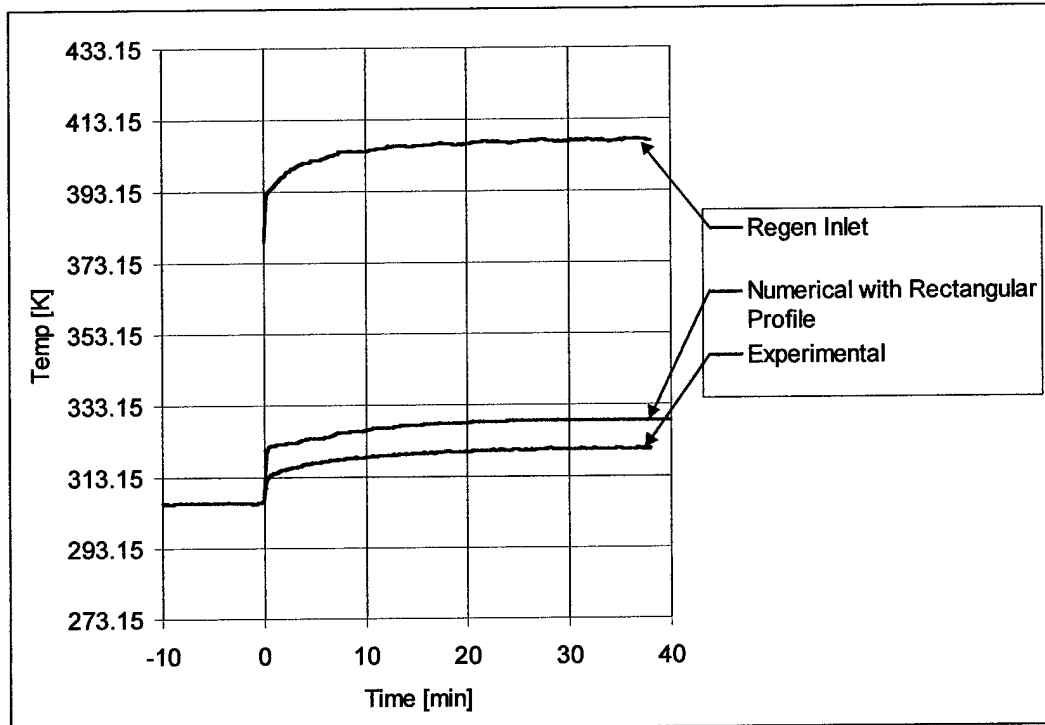
Figure 32. Regeneration Outlet Temperature Versus Time with a
Step Increase to Regeneration Inlet Temperature
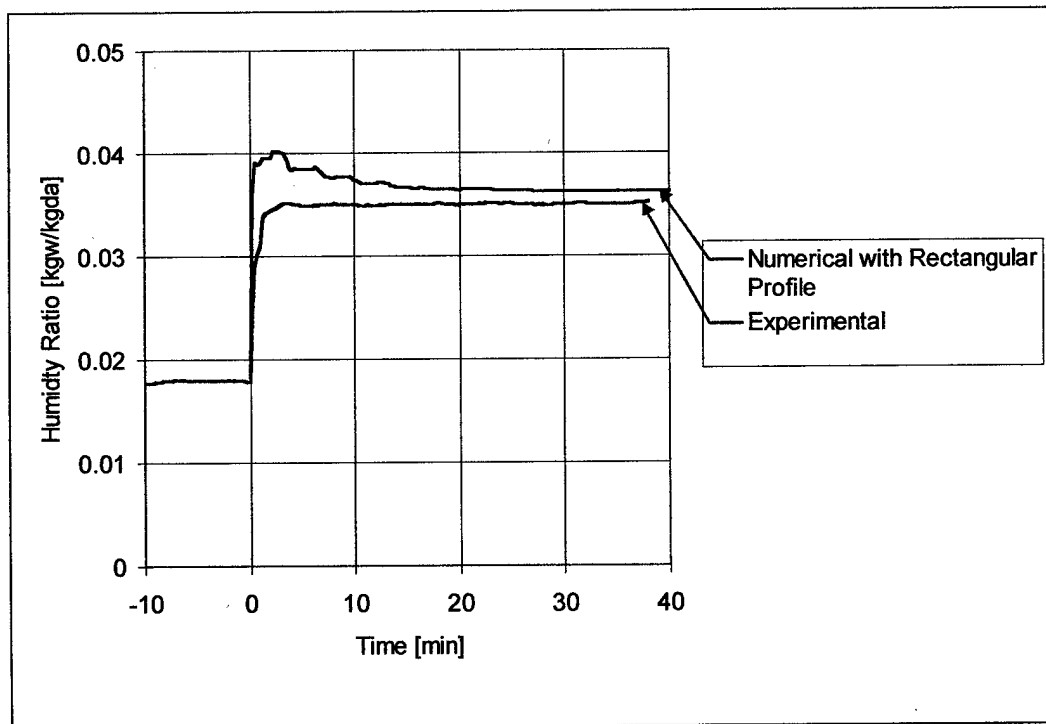
Figure 33. Regeneration Outlet Humidity Ratio Versus Time with
a Step Increase to Regeneration Inlet Temperature

103

The numerical results for the step decrease in regeneration temperature also exhibit very good agreement with the experimental results, Figure 34 through Figure 37. The RMSE values for the graphs also reflect good correlation as with the step increase to regeneration temperature except for regeneration temperature.

The numerical values for the regeneration stream show a curious initial "spike" both in temperature and humidity ratio. They are of a much shorter duration and greater amplitude than with the process humidity ratio in the step increase to regeneration temperature. The explanation for this discrepancy is not known. The experimental data does not exhibit this phenomena and the data collection frequency again may be too long.

The step increase and decrease to regeneration temperature clearly display a logarithmic response function. With this type of response, a time constant of the system can be determined using the transient response values. The time constant here is defined as the time required by the system to reach 63% of its steady-state.

Run	Stream	Prop	Initial value	SS value	Time (min)	63%	time (min)
step increase	process	temp	308.15	333.4	22.1	324.06	5
"	process	humidity ratio	0.0177	0.0122	22.1	0.0142	5
"	regen	temp	308.15	320.5	22.0	315.93	3.25
"	regen	humidity ratio	0.0177	0.035	5.0	0.0286	0.5
step decrease	process	temp	333.4	306	38.9	316.14	6
"	process	humidity ratio	0.0122	0.0177	38.9	0.0087	6
"	regen	temp	320.5	300	36.8	307.59	7
"	regen	humidity ratio	0.035	0.01	26.8	0.0193	1.25

Table 10. Summary of Time Constant Calculations for the Step Increase and Step Decrease to Regeneration Temperature

It may be quickly noticed that the transient times for the step decrease are significantly longer than the step increase. This is due to the temperature to which the regeneration stream was lowered. The step decrease was accomplished by using the ambient temperature as the step temperature, which was lower than the initial steady-state temperature for the step increase.
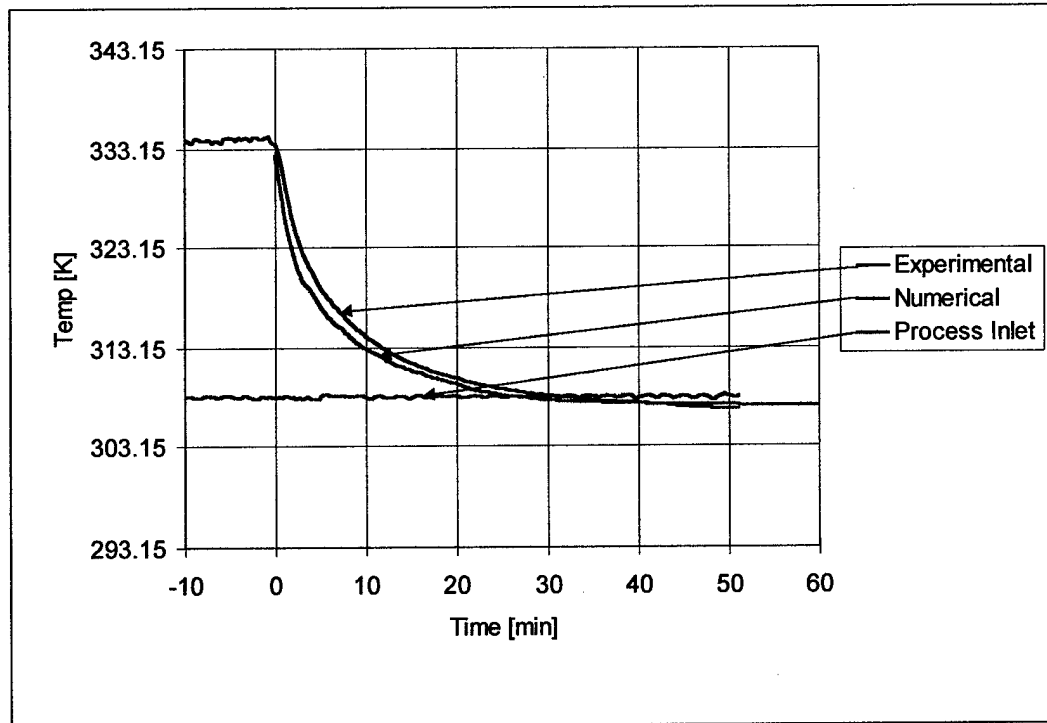
Figure 34. Process Outlet Temperature Versus Time with a Step
Decrease In Regeneration Inlet Temperature
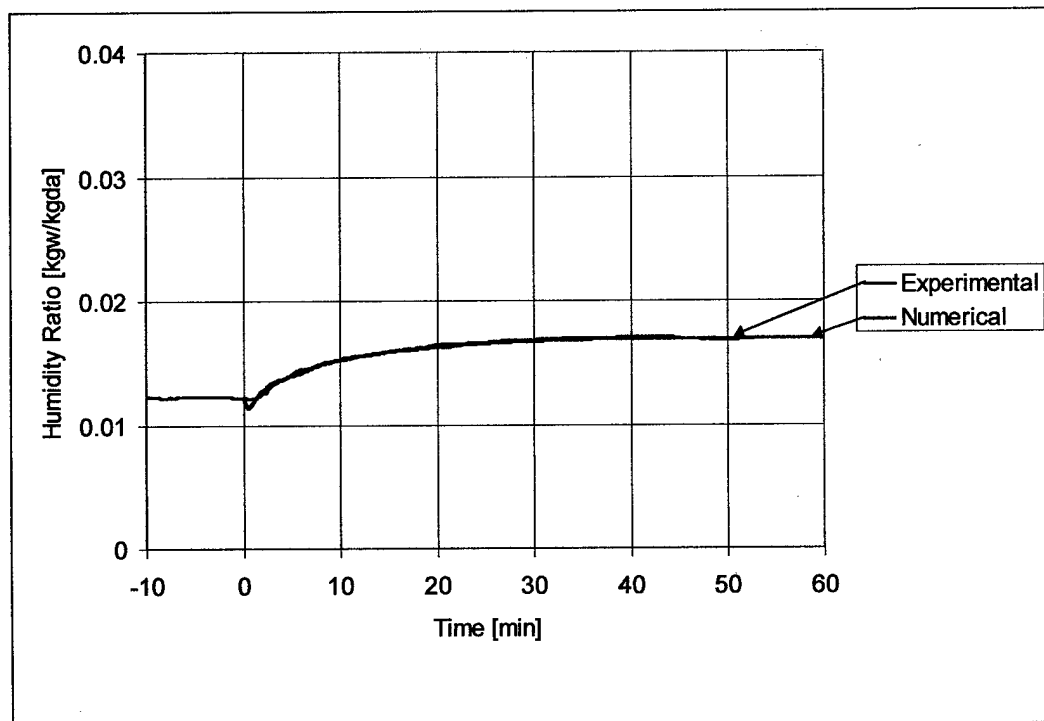
Figure 35. Process Outlet Humidity Ratio Versus Time with a
Step Decrease to Regeneration Inlet Temperature

106
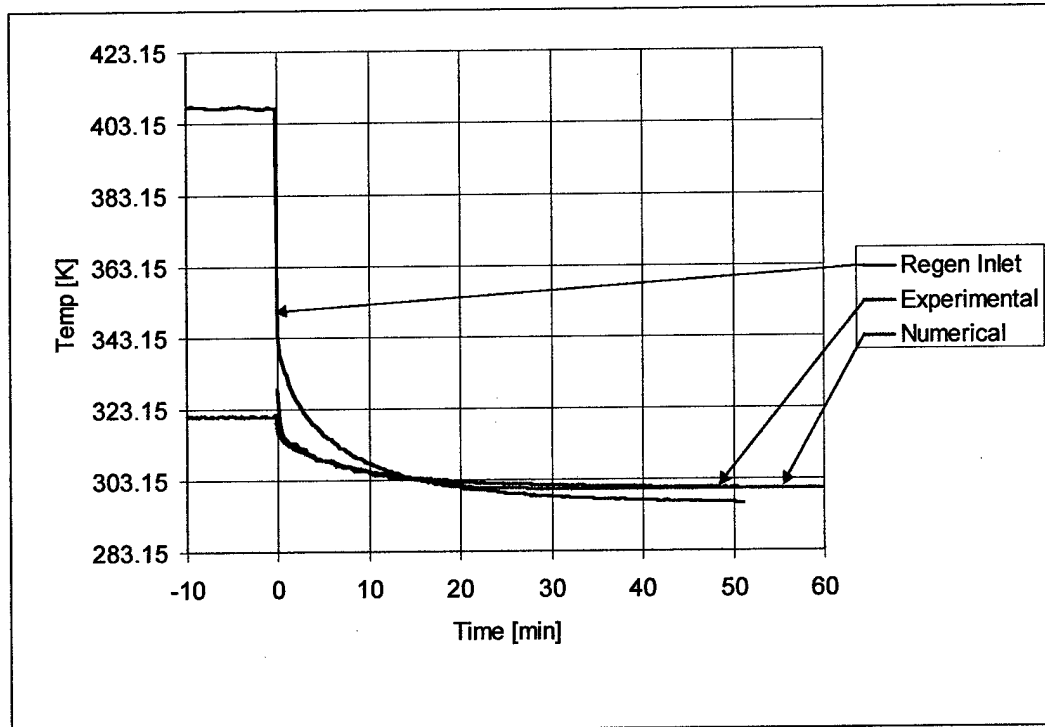
Figure 36. Regeneration Outlet Temperature Versus Time with a
Step Decrease to Regeneration Inlet Temperature
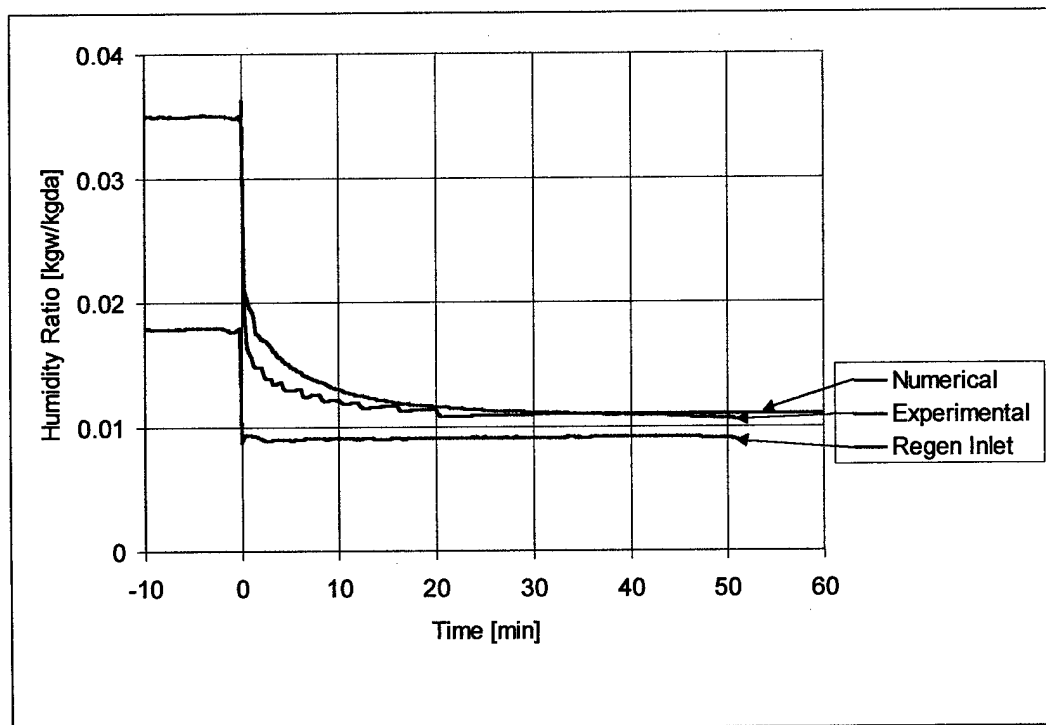
Figure 37. Regeneration Outlet Humidity Ratio Versus Time with
a Step Decrease to Regeneration Inlet Temperature

107

The graphs of the step increase to wheel speed are shown in Figure 38 through Figure 41. The numerical model curves generally look like those from the experiment. The RMSE (Table 11) values tend to reflect this exactly as with the previous runs. The process temperature and humidity ratios appear fine. The regeneration temperature again has a slight steady-state offset while the regeneration humidity ratio looks reasonable.

One interesting point, and these can most clearly be seen in Figure 40, are the sinusoidally converging oscillations. The sinusoidal period corresponds to the wheel rotation speed. The step increase wheel rotation speed of 18 revolutions per hour corresponds to 3.3 minutes per revolution. Examining the graph in Figure 40, it can be seen that the period of the oscillations is indeed about 3.3 minutes. The temperature and moisture distributions, which form inside the desiccant wheel, are clearly a function of the wheel speed. When the step change occurs, the desiccant temperature and moisture gradients within the wheel do not change as quickly as the wheel speed. They produce the sinusoidal effect on the airstream temperature and humidity ratio until the new temperature and humidity ratio gradients are formed. The sinusoidal response is "damped" out as the transformation occurs.

The step decrease to wheel speed (Figure 42 through Figure 45) also appears to show that the numerical curves are close approximations of the experimental results. Again, the RMSE values are consistent with previous runs.

The oscillations in the graphs for step decrease are muted relative to the step increase. The oscillations apparently do not appear because with the slower wheel speed, the new temperature and humidity distributions have time to set up and the previous distributions to fade.
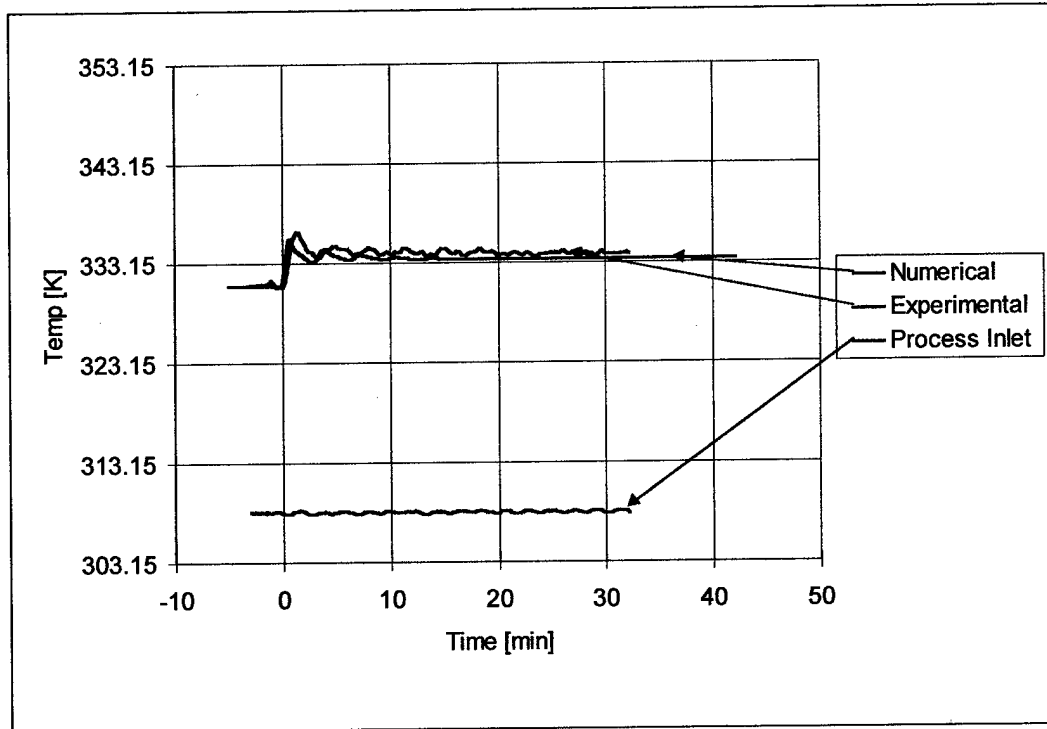
Figure 38. Process Outlet Temperature Versus Time with a Step
Increase to Wheel Speed
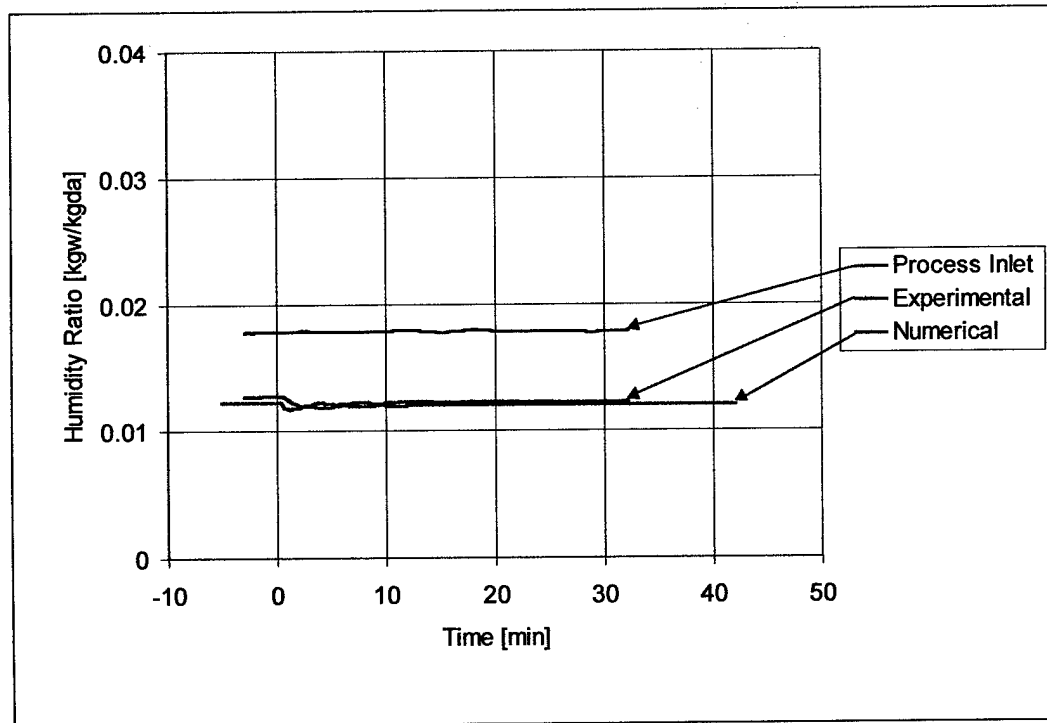
Figure 39. Process Outlet Humidity Ratio Versus Time with a
Step Increase to Wheel Speed

110
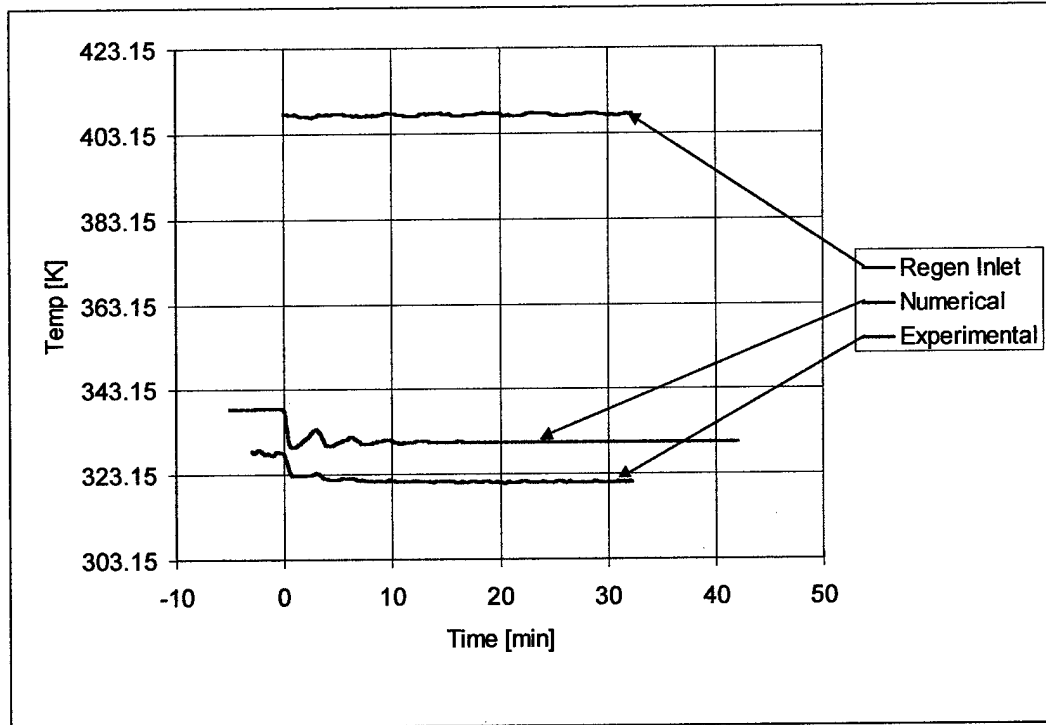
Figure 40. Regeneration Outlet Temperature Versus Time with a
Step Increase to Wheel Speed
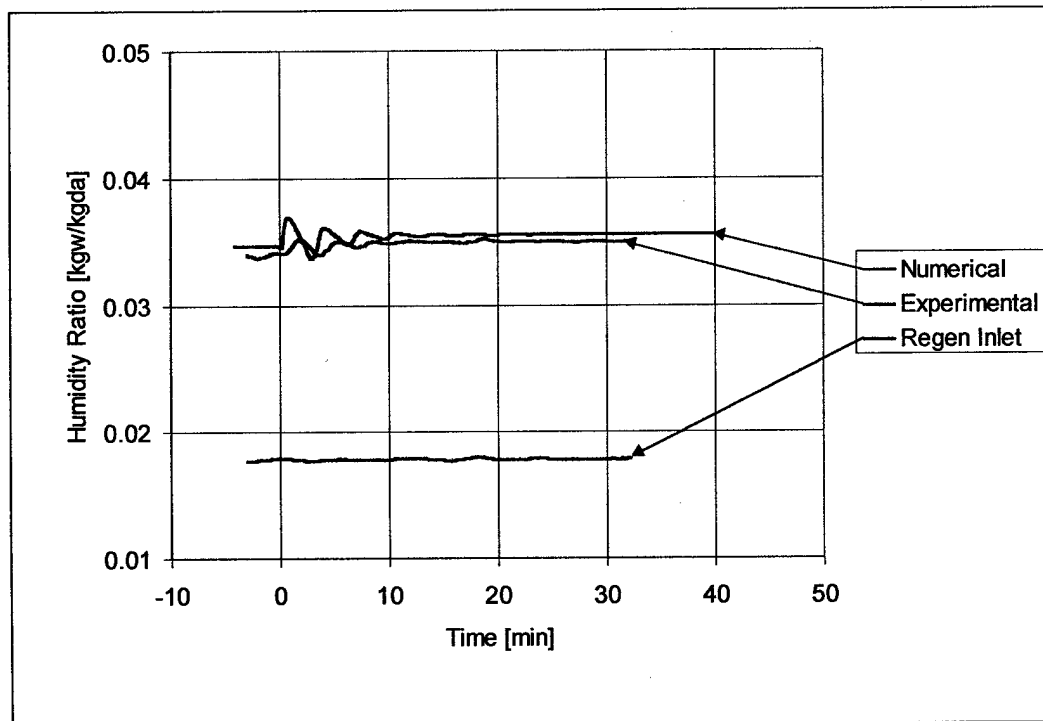
Figure 41. Regeneration Outlet Relative Humidity Versus Time
with a Step Increase to Wheel Speed

111
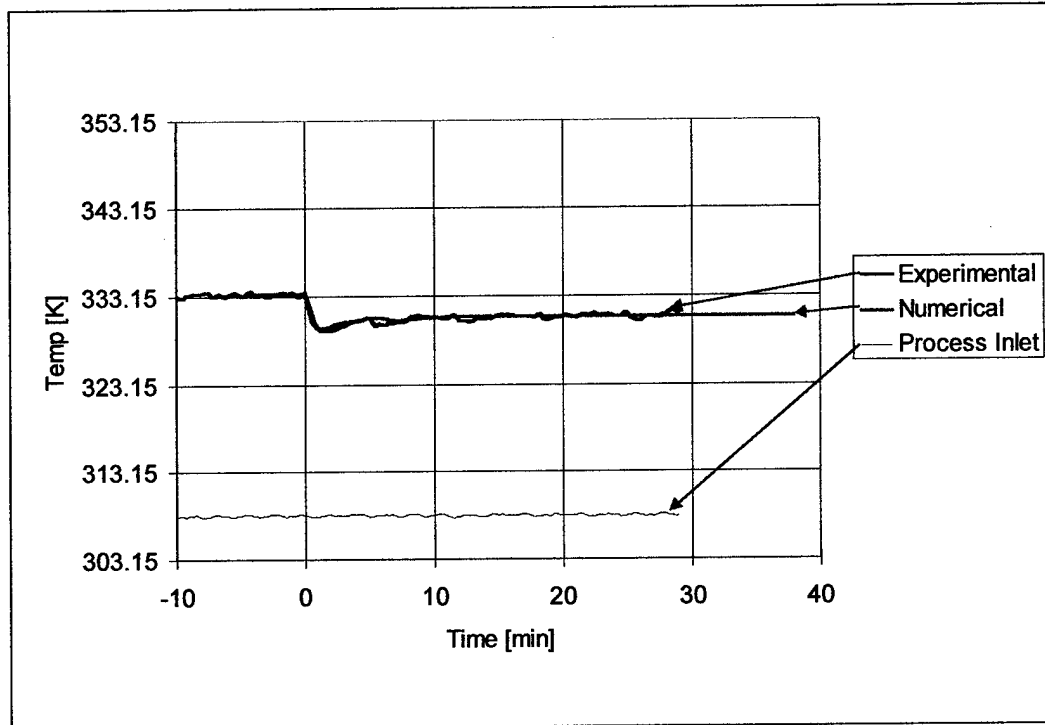
Figure 42. Process Outlet Temperature Versus Time with a Step Decrease to Wheel Speed
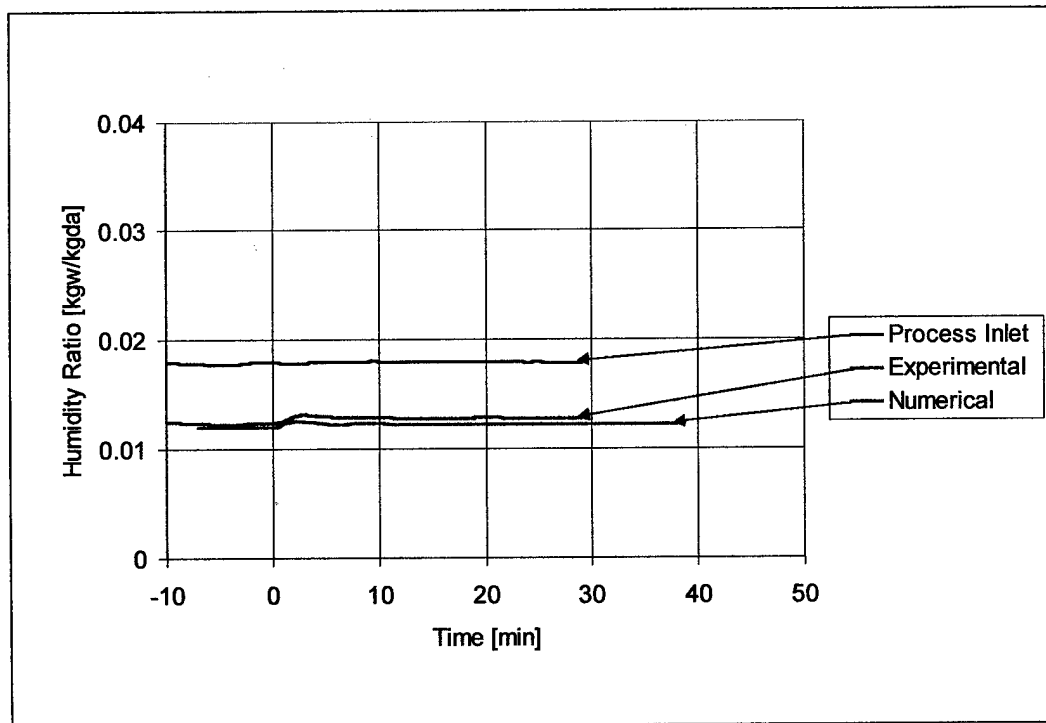
Figure 43. Process Outlet Humidity Ratio with a Step Decrease to Wheel Speed

112
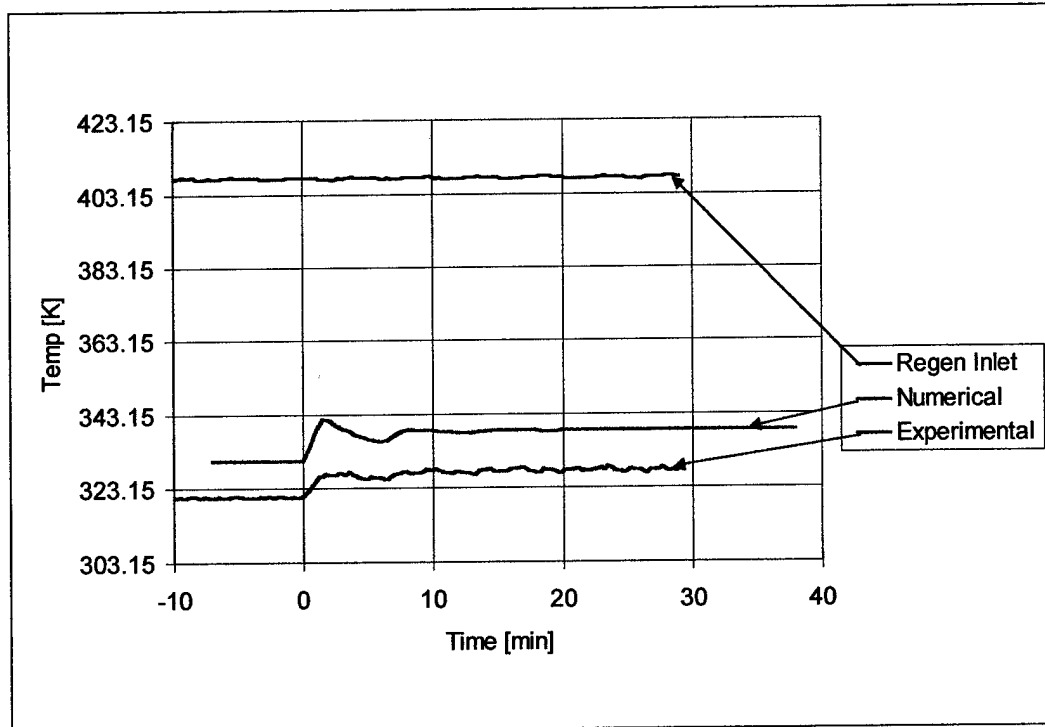
Figure 44. Regeneration Outlet Temperature Versus Time with a Step Decrease to Wheel Speed
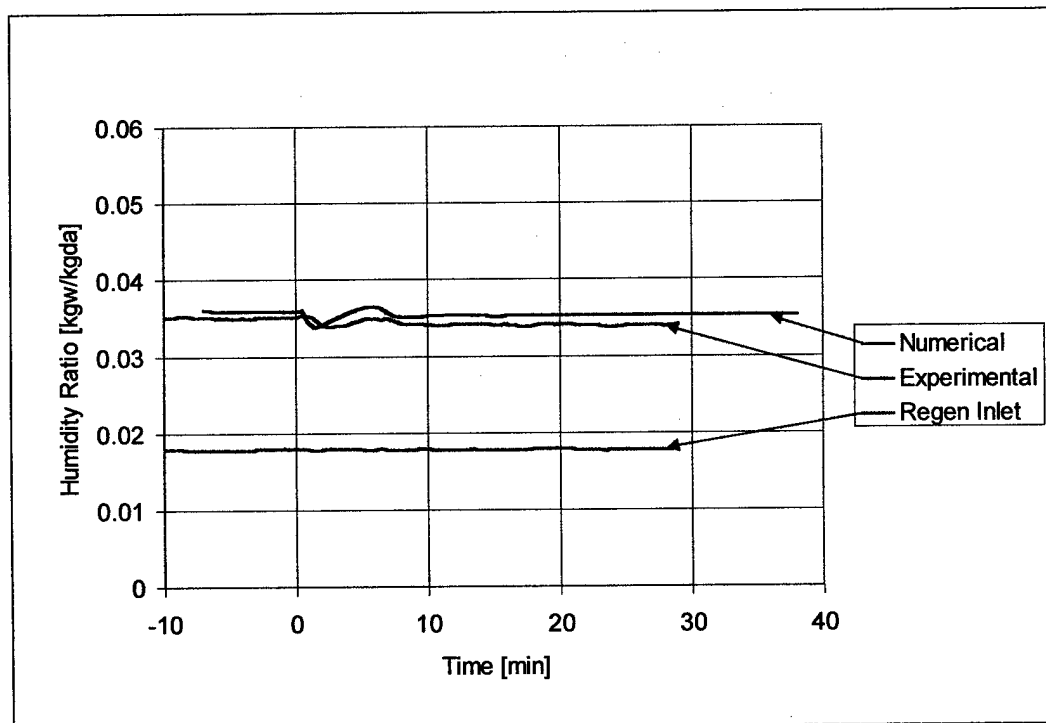
Figure 45. Regeneration Outlet Humidity Ratio Versus Time with a Step Decrease to Wheel Speed

113

The step increase to process flowrate (Figure 46 through Figure 49) also appears to show good agreement between the experimental and numerical solutions. The RMSE statistic (Table 11) also showed good agreement as with previous runs. The curves for these step changes also somewhat resemble a logarithmic function (in particular the process temperature) although there is significantly more fluctuation than the step change to regeneration temperature and the curve is less distinguishable. The fluctuation occurs as in the step change to wheel speed – without the oscillations. This would make sense as the airstream flowrate is delivered as a constant while the desiccant mass "flowrate" is sinusoidal.

The step decrease to process flowrate (shown in Figure 50 through Figure 53) also indicates good agreement visually and with the RMSE statistic. The step decrease to process flowrate also appeared to have the largest change in optimum grid size between the initial and step change conditions. The decreased flowrate produces larger NTU values which make the finite difference equations significantly stiffer.
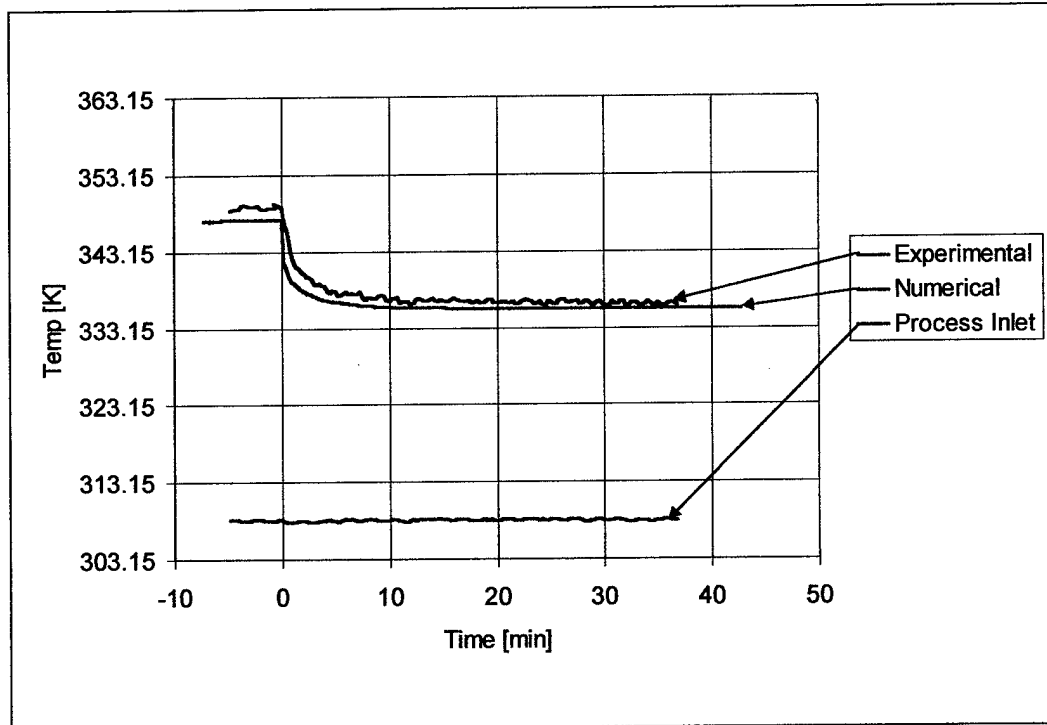
Figure 46. Process Outlet Temperature Versus Time with a Step
Increase to Process Flowrate
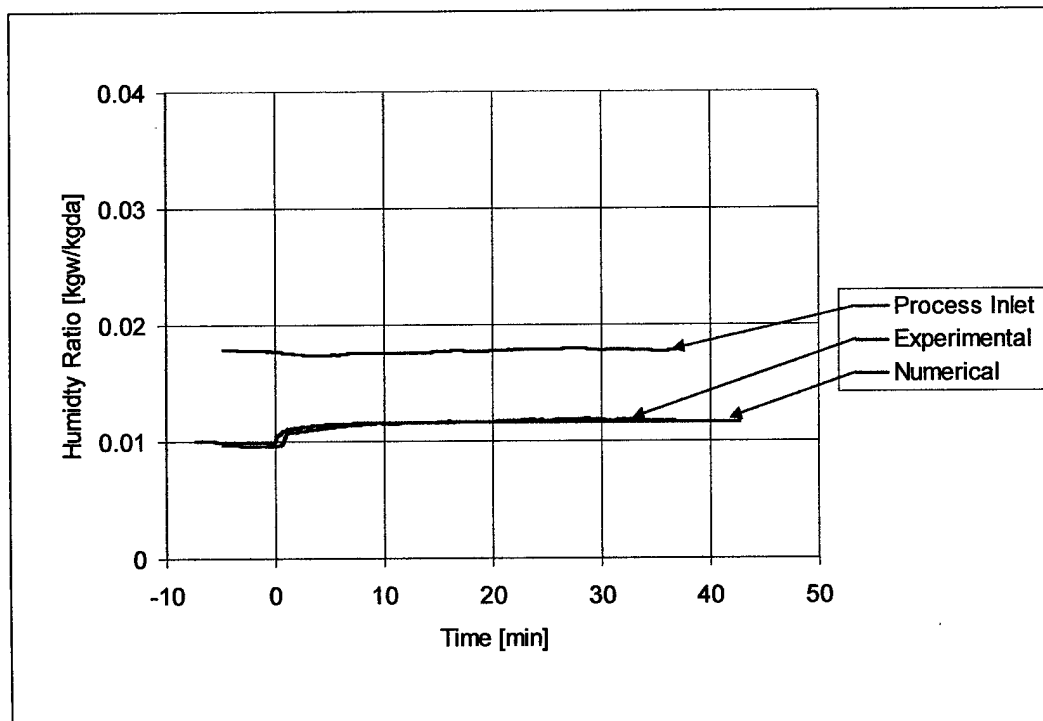
Figure 47. Process Outlet Humidity Ratio Versus Time with a
Step Increase to Process Flowrate

115
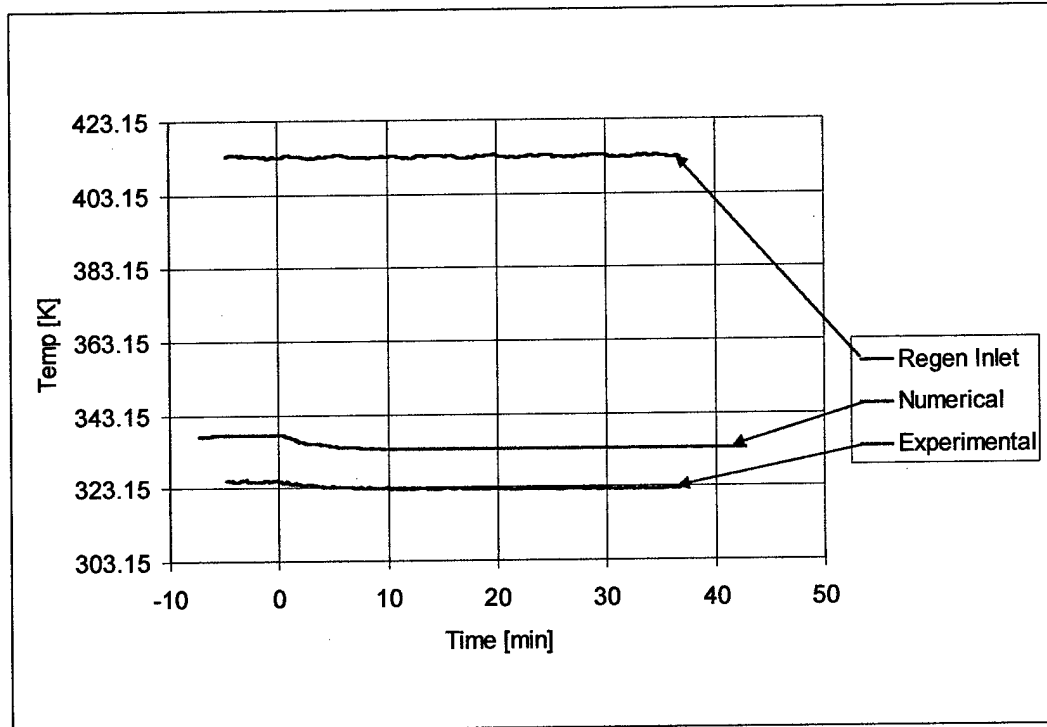
Figure 48. Regeneration Outlet Temperature Versus Time with a
Step Increase to Process Flowrate
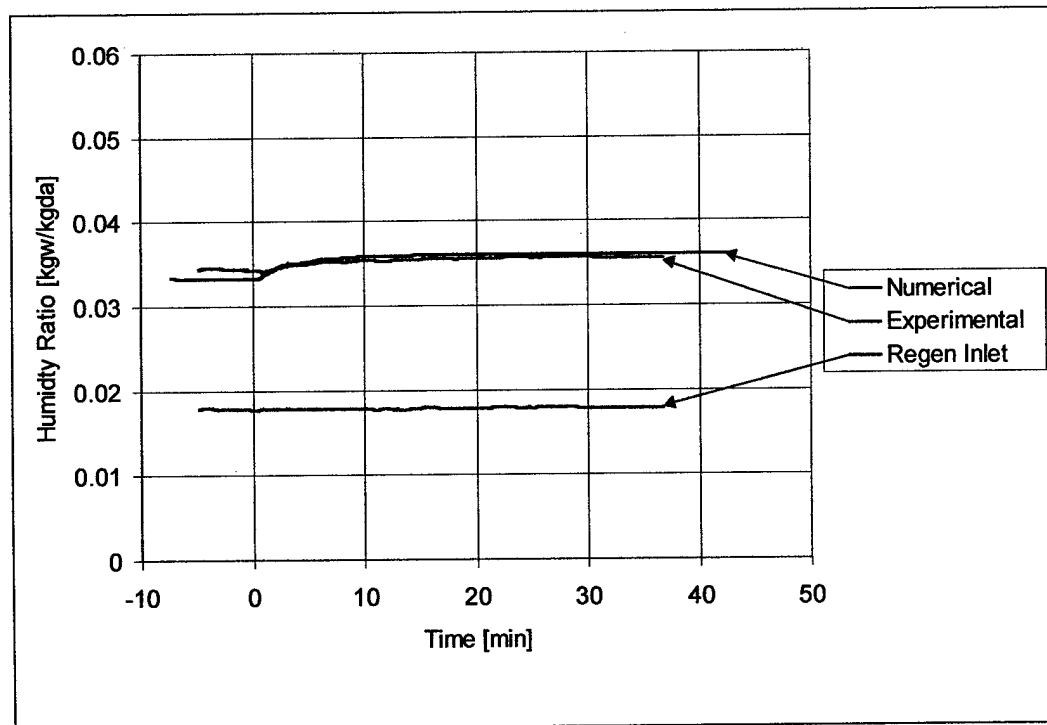
Figure 49. Regeneration Relative Humidity Versus Time with a
Step Increase to Process Flowrate

116
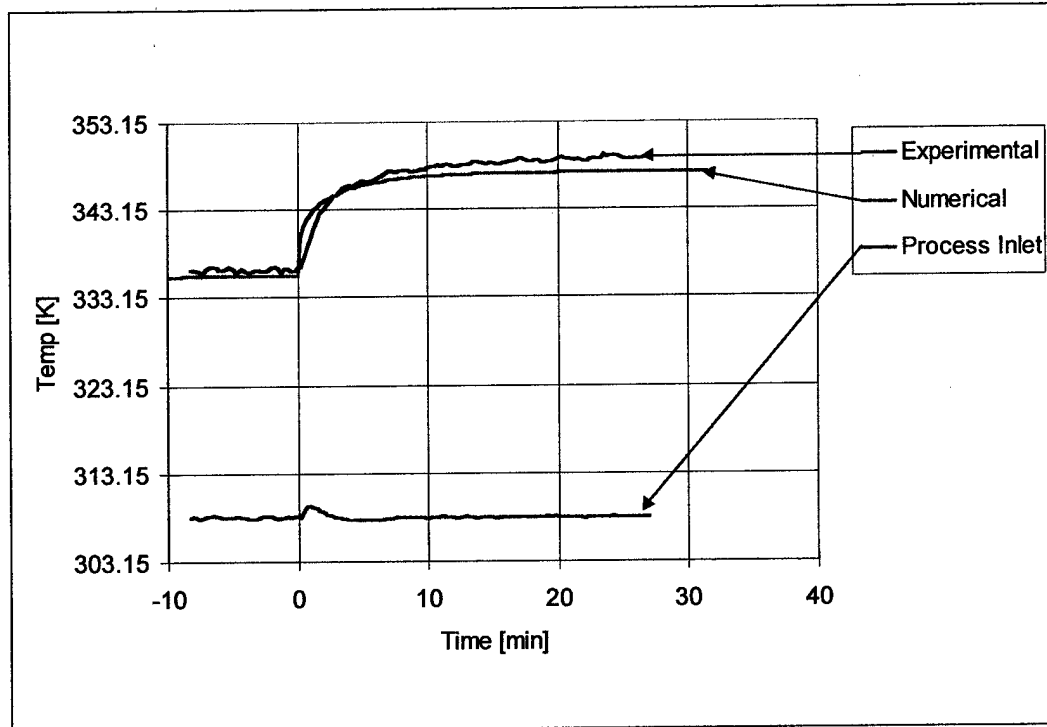
Figure 50. Process Outlet Temperature Versus Time with a Step
Decrease to Process Flowrate
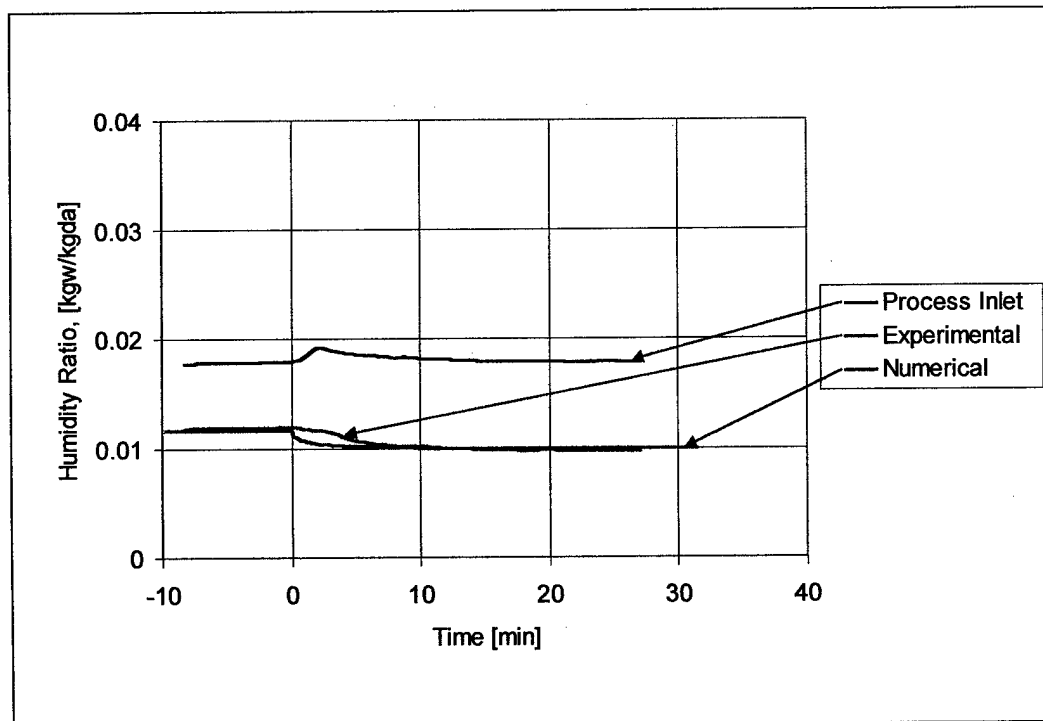
Figure 51. Process Outlet Humidity Ratio Versus Time with a
Step Decrease to Process Flowrate
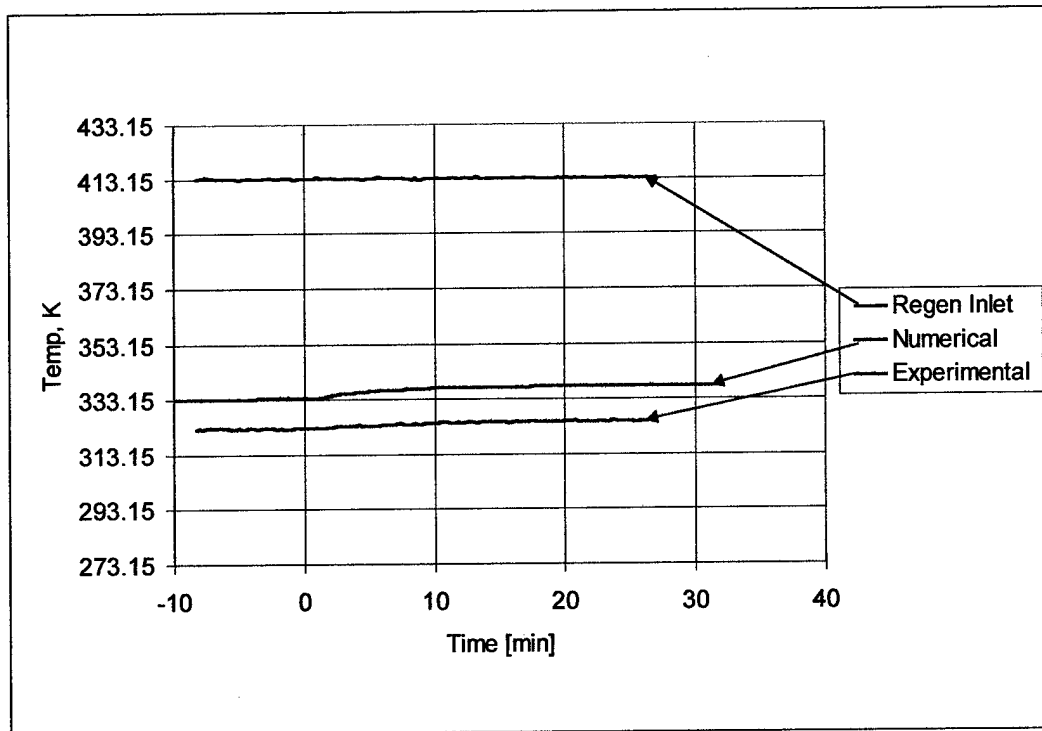
Figure 52. Regeneration Outlet Temperature Versus Time with a
Step Decrease to Process Flowrate
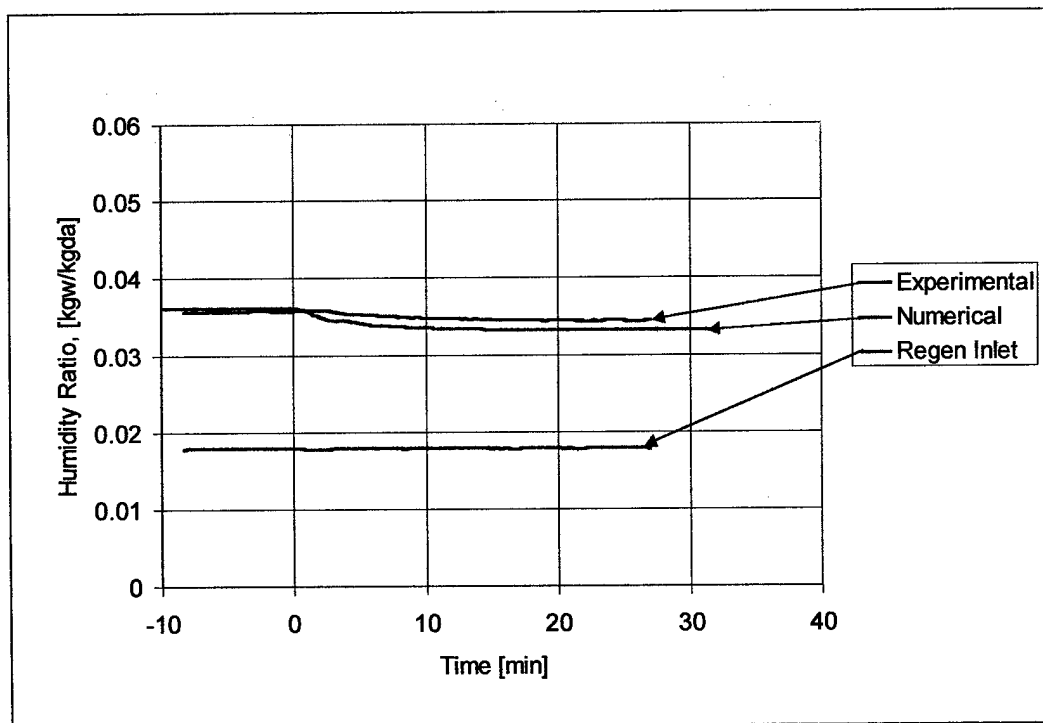
Figure 53. Regeneration Outlet Humidity Ratio Versus Time with
a Step Decrease to Process Flowrate

118

Validation Summary

It can be seen from the transient graphs and the summary (Table 11) that the numerical finite difference model does, in fact, accurately represent the transient response of a rotary heat and mass desiccant wheel. The numerical and experimental curves can be visually determined and the RMSE values can be checked to confirm that they are reasonably be close approximations of one another.

The summary of transient response times (Table 12) shows that the transient response of the WSG rotary desiccant wheel under these conditions is significant relative to the response time of a typical cooling coil. The steady-state values were calculated at a point removed from the transient phase. The transient times were essentially determined using 99% of the steady-state value or the full transient period. The step change to regeneration temperature required approximately 22 minutes whereas a typical cooling coil requires 1-2 minutes. The WSG wheel is fairly typical of current technology in this area and testing conditions were set to the manufacturer's design levels.

Run	Stream	Parameter	Av Value	RMSE
step increase to regen temp	process	temp	320.7	0.62
"	process	humidity ratio	0.0150	0.0003
"	regen	temp	314.5	7.77
"	regen	humidity ratio	0.0264	0.0030
step decrease to regen temp	process	temp	319.9	1.09
"	process	humidity ratio	0.0147	0.0001
"	regen	temp	308.4	1.13
"	regen	humidity ratio	0.0230	0.0010
step increase to wheel speed	process	temp	332.5	0.62
"	process	humidity ratio	0.0123	0.0003
"	regen	temp	324.5	9.55
"	regen	humidity ratio	0.0343	0.0010

119

Run	Stream	Parameter	Av Value	RMSE
step decrease to wheel speed	process	temp	332.1	0.50
"	process	humidity ratio	0.0123	0.0006
"	regen	temp	324.5	11.16
"	regen	humidity ratio	0.0345	0.0011
step increase to process flowrate	process	temp	342.4	1.28
"	process	humidity ratio	0.0105	0.0002
"	regen	temp	324.0	11.04
"	regen	humidity ratio	0.0340	0.0004
step decrease to process flowrate	process	temp	342.0	1.36
"	process	humidity ratio	0.0108	0.0005
"	regen	temp	323.8	12.49
"	regen	humidity ratio	0.0351	0.0012

Table 11. Summary of Root Mean Square Error for All Runs and Parameters

Run	Stream	Parameter	initial	SS value	time (min)
step increase to regen temp	process	temp	308.15	333.4	22.1
"	process	humidity ratio	0.0177	0.0122	22.1
"	regen	temp	308.15	320.5	22.0
"	regen	humidity ratio	0.0177	0.035	5.0
step decrease to regen temp	process	temp	333.4	306	38.9
"	process	humidity ratio	0.0122	0.0177	38.9
"	regen	temp	320.5	300	36.8
"	regen	humidity ratio	0.035	0.01	26.8
step increase to wheel speed	process	temp	330.7	334.1	5.0
"	process	humidity ratio	0.0126	0.011	3.5
"	regen	temp	327	321	12.5
"	regen	humidity ratio	0.034	0.035	10.0
step decrease to wheel speed	process	temp	333	331	10.0
"	process	humidity ratio	0.0117	0.0127	4.0
"	regen	temp	321	327	10.0
"	regen	humidity ratio	0.035	0.034	9.0
step increase to process flowrate	process	temp	348	336	12.0
"	process	humidity ratio	0.0096	0.011	10.0

Run	Stream	Parameter	initial	SS value	time (min)
"	regen	temp	325	323	10.0
"	regen	humidity ratio	0.034	0.035	10.0
step decrease to process flowrate	process	temp	336	348	15.0
"	process	humidity ratio	0.0118	0.0095	13.0
"	regen	temp	322.5	325.5	15.0
"	regen	humidity ratio	0.0357	0.0344	15.0

Table 12. Summary of Full Transient Time for All Runs And Parameters

CHAPTER 7. DESICCANT WHEEL VALIDATION

An additional form of validation maybe accomplished by looking at the temperature and moisture content of the desiccant wheel itself. Like the airstream, the wheel will have temperature and moisture gradients as well. Using infrared technologies and the numerical matrix data of the desiccant wheel, the experimental and numerical temperature distributions can be compared. Graphical representations of the temperature and moisture matrices can also aid in understanding the transient response.

The desiccant laboratory at NREL has a thermographic camera with which to look at the end surfaces of the desiccant wheel in operation. The camera is an Inframetrics, model PM-280 Thermacam. The range of the camera is from −10 to 450° C and it has a sensitivity of <0.1° C. The camera's optimal accuracy is +/- 2° C or 2% of the full temperature range, depending upon which value is the greater. The optimum accuracy, however, is dependent upon using the correct emissivity for the surface of interest. For most surfaces 0.93 is considered reasonable and was also used in this research.

The thermographic camera can view and take pictures of the wheel through an infrared lens. It can distinguish heat gradients of a surface and tell the approximate temperature of points on that surface. Pictures can also be taken over a period of time to observe the transient response of that surface

With the numerical matrix data from the computer model the wheel can be viewed in a two dimensional format: axial and circumferential. In this format, both

the external surfaces of the wheel (outlet) and the internal gradients can be observed. The numerical data was graphed for this research using Matrix Visualizer software by Digital Corp.

Methodology

In the next series of figures, graphical and photo representations of the desiccant matrix are shown at succeeding time steps. Figure 54 and Figure 55 show the initial state of the wheel at a constant temperature. Figure 66 and Figure 67 show the wheel after 34 minutes at steady-state. The figures in-between are the transient steps at the given times. For this validation, the step increase to regeneration temperature (run #1) was used. The axial direction of the wheel is vertical in the figures and the circumferential direction is horizontal. The regeneration-inlet/process-outlet side of the wheel corresponds to the axial position "5" on the matrix graph. The infrared photos of the regeneration-inlet/process-outlet side of the wheel are from the thermographic camera provided by NREL. Below the infrared photos are circular histograms of the temperature gradients as constructed by the thermographic camera software.

Time: 0 minutes

Axial and circumferential image views of desiccant matrix temperature and water content. Axial length is vertical and circumferential is horizontal.

Desiccant Water Content, kgw/kgda
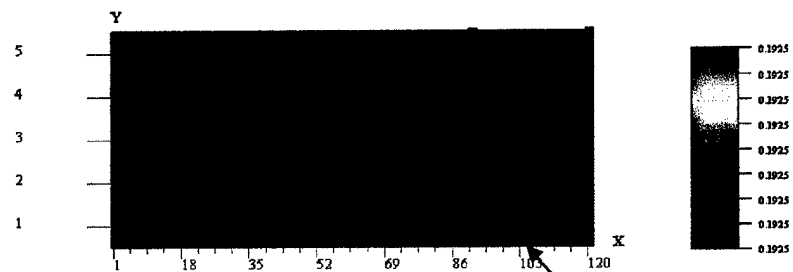
Regen

Desiccant Wheel Temperature, K
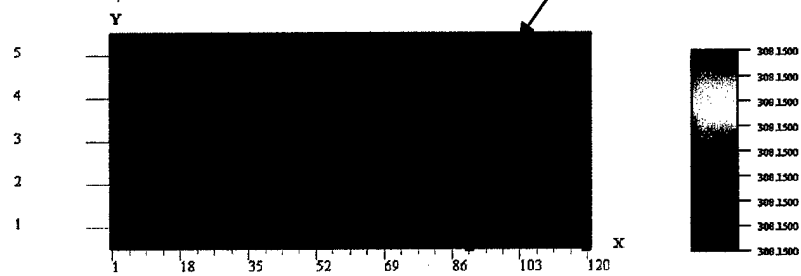
Figure 54. Graphic of Desiccant Moisture Content and Temperature at Time = 0.0 minutes.
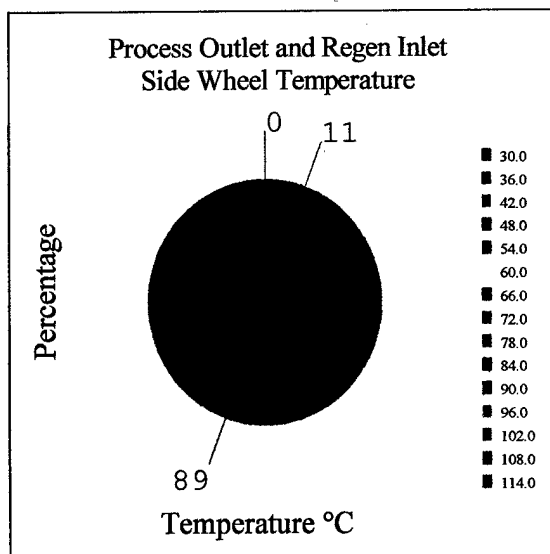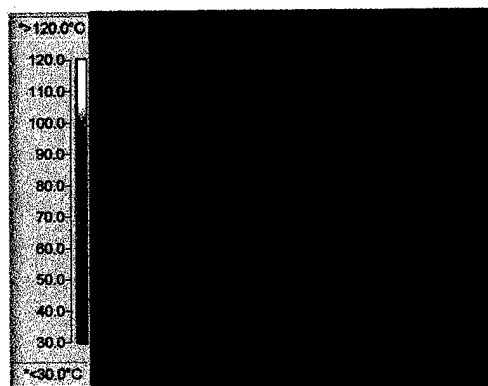
Figure 55. Thermographic Image and Histogram of Desiccant
Wheel at Time = 0.0 minutes.

Time: .5 minutes

Axial and circumferential image views of desiccant matrix temperature and water content. Axial length is vertical and circumferential is horizontal.

Desiccant Water Content, kgw/kgda
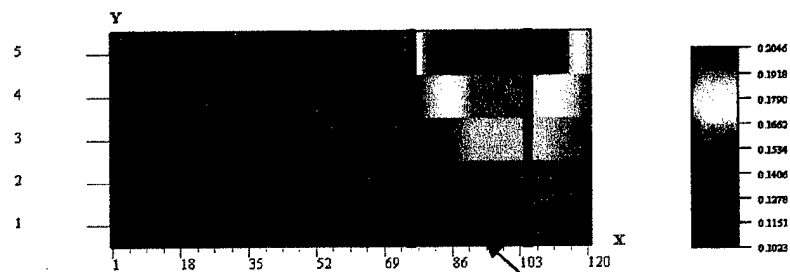
Regen

Desiccant Wheel Temperature, K
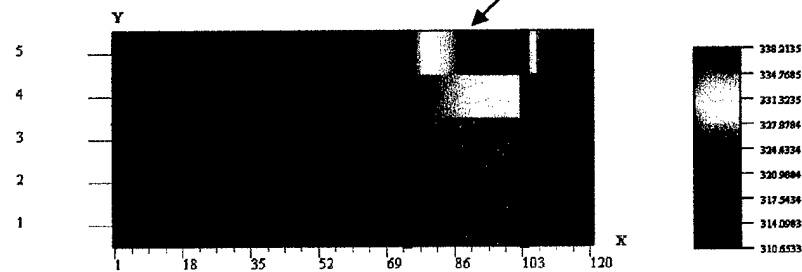
Figure 56. Graphic of Desiccant Moisture Content and Temperature at Time = .5 minutes.
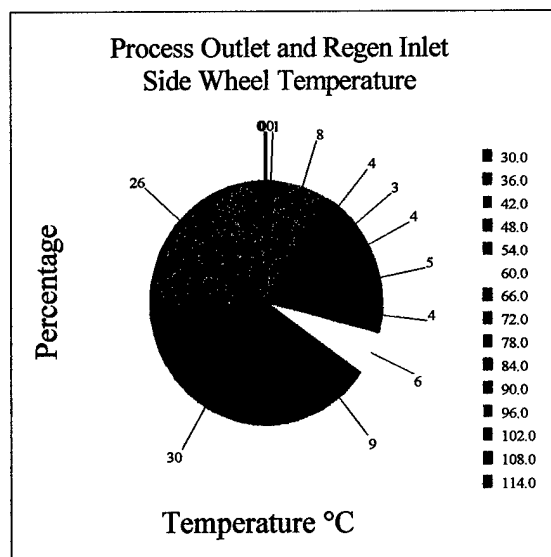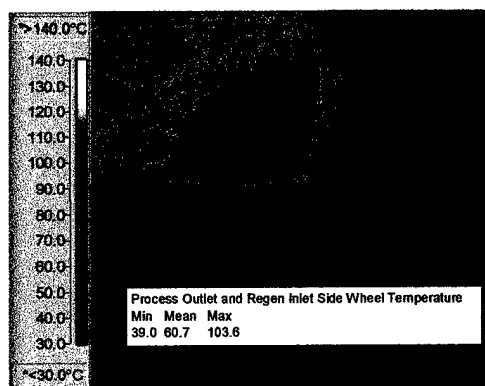
Figure 57. Thermographic Image and Histogram of Desiccant
Wheel at Time = 0.5 minutes.
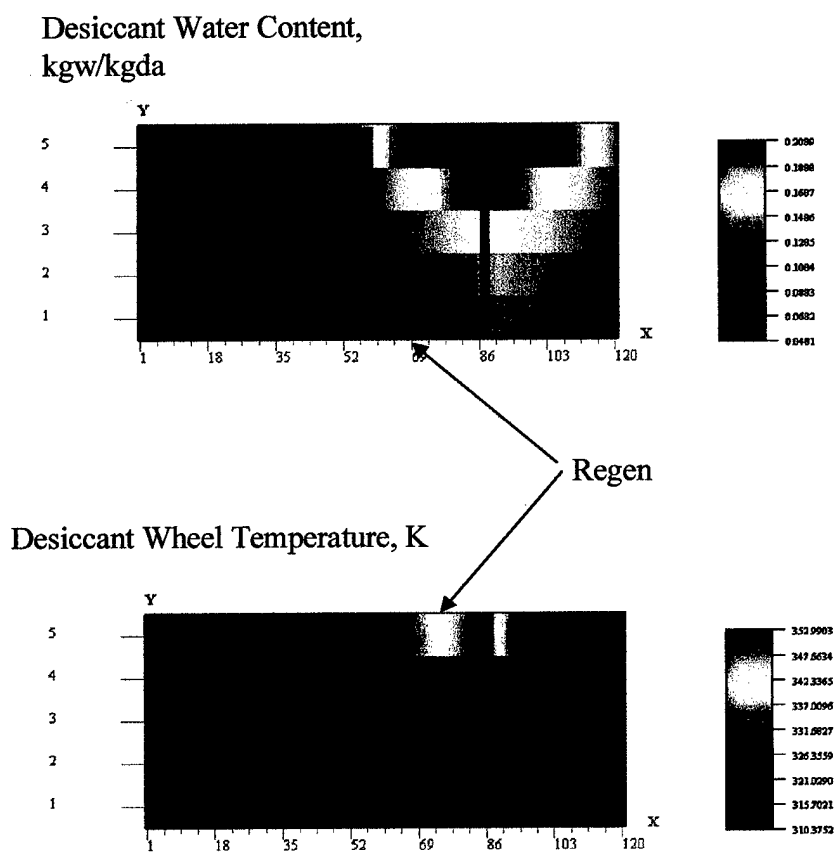
Figure 58. Graphic of Desiccant Moisture Content and
Temperature at Time = 2.0 minutes.

128

Time: 1 minute

Thermographic Image
(temperature in deg C)
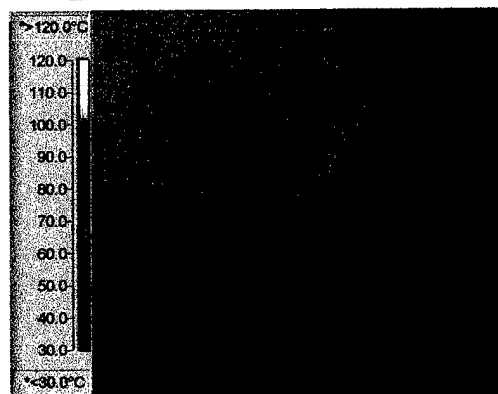
Process Outlet and Regen Inlet
Side Wheel Temperature
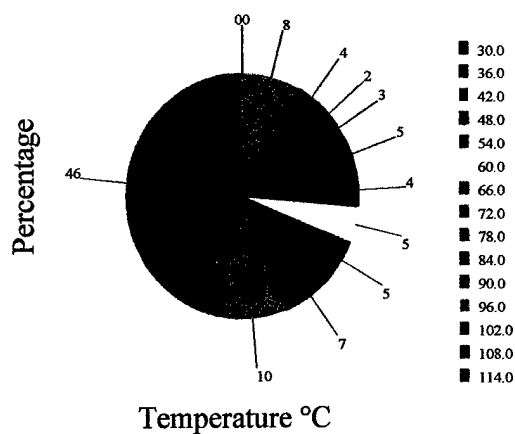
Figure 59. Thermographic Image and Histogram of Desiccant
Wheel at Time = 1.0 minutes.
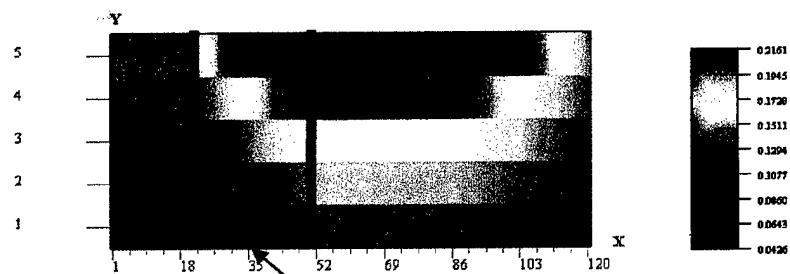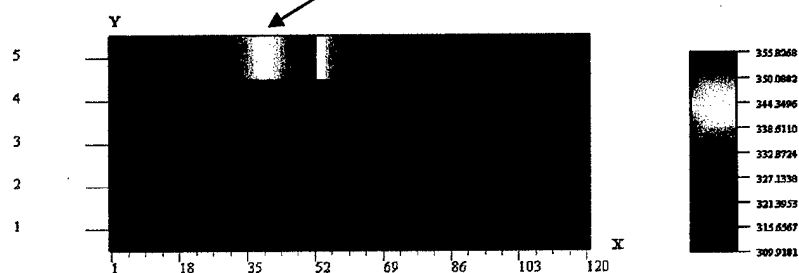
Figure 60. Graphic of Desiccant Moisture Content and
Temperature at Time = 2.0 minutes

Time: 2 minutes

Thermographic Image
(temperature in deg C)

Process Outlet and Regen Inlet
Side Wheel Temperature
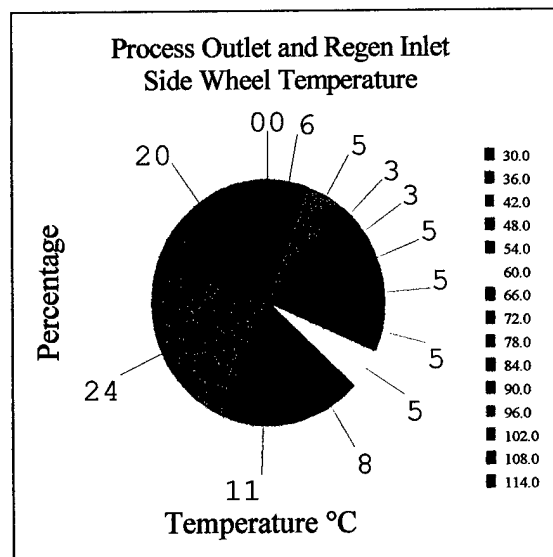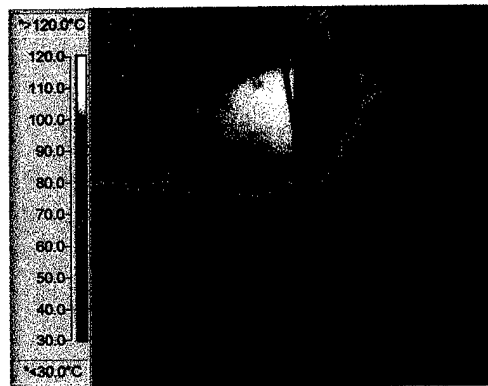
Figure 61. . Thermographic Image and Histogram of Desiccant
Wheel at Time = 2.0 minutes.

131
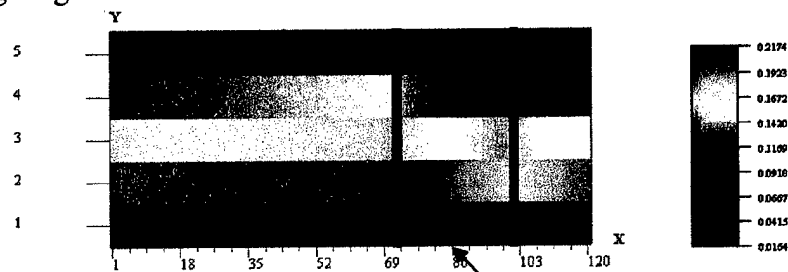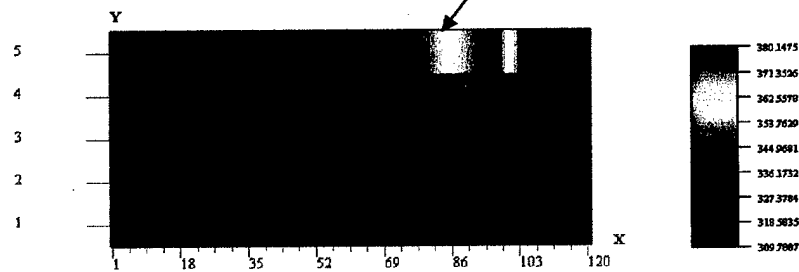
Figure 62. Graphic of Desiccant Moisture Content and
Temperature at Time = 4.0 minutes

Time: 4 minutes

Thermographic Image
(temperature in deg C)

Process Outlet and Regen Inlet
Side Wheel Temperature
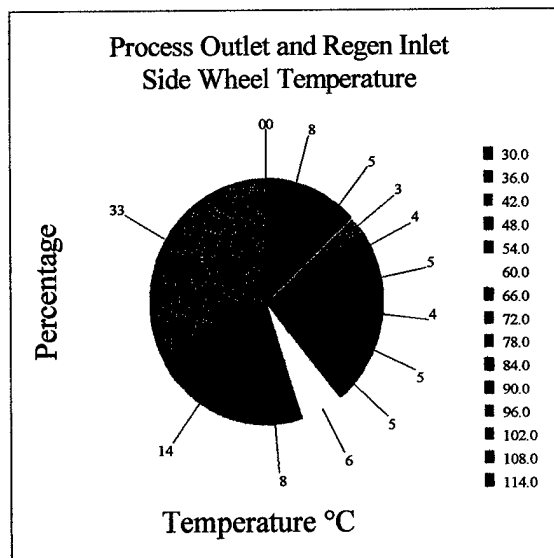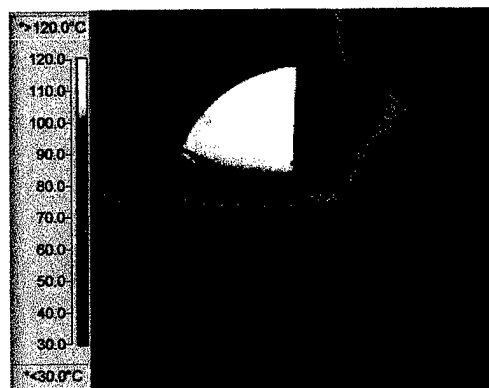
Figure 63. Thermographic Image and Histogram of Desiccant
Wheel at Time = 4.0 minutes.

Time: 8 minutes

Axial and circumferential image views of desiccant matrix
temperature and water content. Axial length is vertical and
circumferential is horizontal.

Desiccant Water Content,
kgw/kgda

Regen
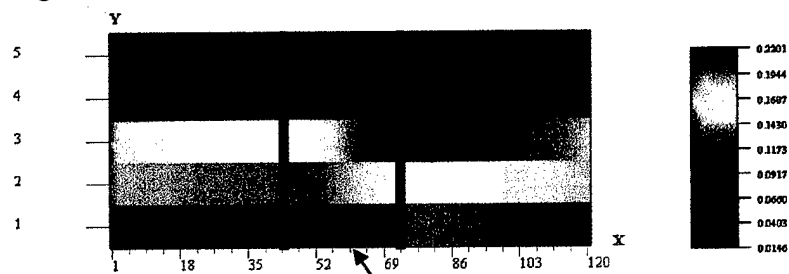
Desiccant Wheel Temperature, K
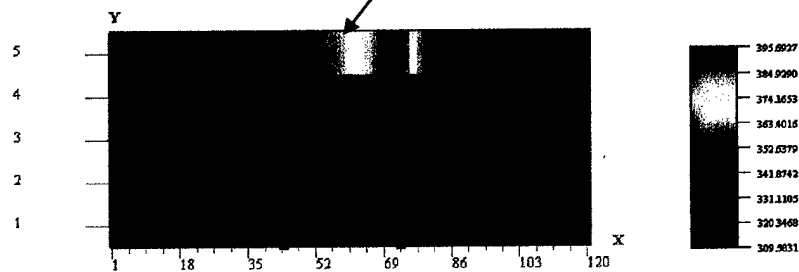
Figure 64. Graphic of Desiccant Moisture Content and
Temperature at Time = 8.0 minutes

134

Time: 8 minutes

Thermographic Image
(temperature in deg C)

Process Outlet and Regen Inlet
Side Wheel Temperature
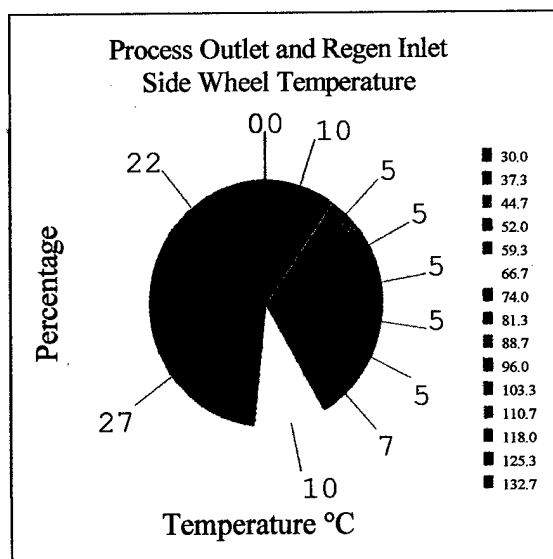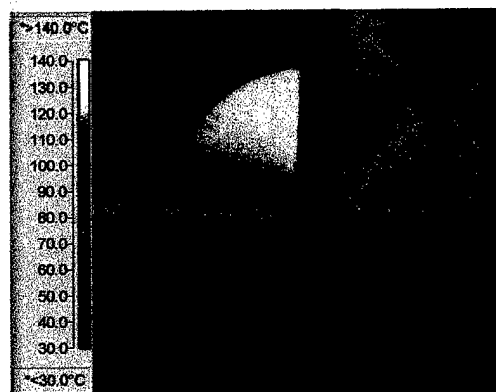
Figure 65. Thermographic Image and Histogram of Desiccant
Wheel at Time = 8.0 minutes.

135

Figure 66. Graphic of Desiccant Moisture Content and
Temperature at Time = 34.0 minutes

Time: 34 minutes

Thermographic Image
(temperature in deg C)

Process Outlet and Regen Inlet
Side Wheel Temperature
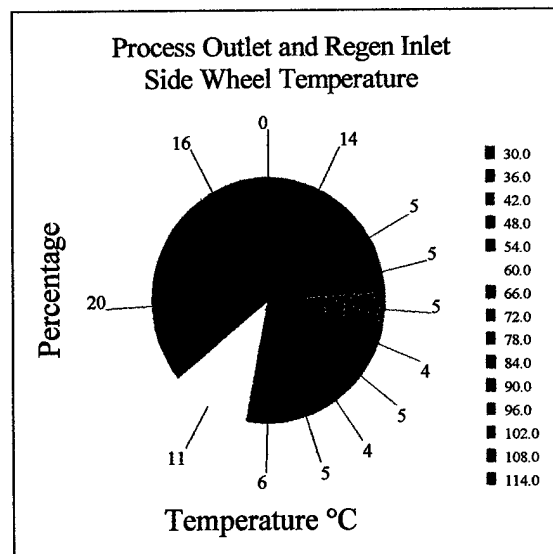
Figure 67. Thermographic Image and Histogram of Desiccant
Wheel at Time = 34.0 minutes.

The methodology used for comparing the experimental data (thermographic images) with the numerical (computer generated matrices) involved constructing their frequency distributions as shown in Figure 68 and Figure 69. Visual comparison of the referenced histograms show that, in general, the temperature ranges of the thermographic images appear fairly close to the predicted values from the numerical model.

After observing their distributions patterns, a statistical test was accomplished to compare their patterns and see if they are equivalent. The statistical test used was the Chi-Squared (χ^2) test which tests for the equality of two multinomial distributions.

Equation 90 shows the formula for the χ^2 statistic. The χ^2 test statistic was calculated for several points in time and these are located in Table 13.

$$\chi^2 = \sum \left[\frac{(n_i - E_i)^2}{E_i} \right]$$

Equation 90

The variables used in the χ^2 statistic are as follows: n is the number of occurrences for outcome i, and E is the number of trials expected to result in outcome i.

The distributions are equivalent (the null hypothesis is true) if the χ^2 calculated for the data sets is less than the critical χ^2 for a given confidence level. The calculated χ^2s are less than the critical values for time equal to 4 minutes and 34

minutes. At these times the numerical results are generally equivalent to the experimental.

When time is at one minute, the χ^2 does not show perfect agreement between the experimental and the numerical. Looking at Figure 68, the most significant disagreement between the data sets occurs in the last few bins (highest temperature) and the first bin (lowest temperature). The thermographic solution predicts several occurrences in the higher bins and the numerical solution does not. The numerical case in the lowest bin, on the other hand, significantly overpredicts the number of occurrences compared to the experimental. This can be readily explained by the structural members of the cassette: the wide rectangular member running vertically down the center of the wheel and a horizontal piece on the regeneration side of the wheel. These are made of galvanized steel and they cover a significant portion of the matrix face. Since they have a low specific heat and high thermal conductivity, they rise in temperature higher and faster than the desiccant matrix. The temperatures registered from the structural members would be significantly higher than the portion of the wheel they are covering. As the system reaches steady-state, the temperature difference between the structural members and the wheel should disappear. The improved statistical agreement over time indicates this to be true.
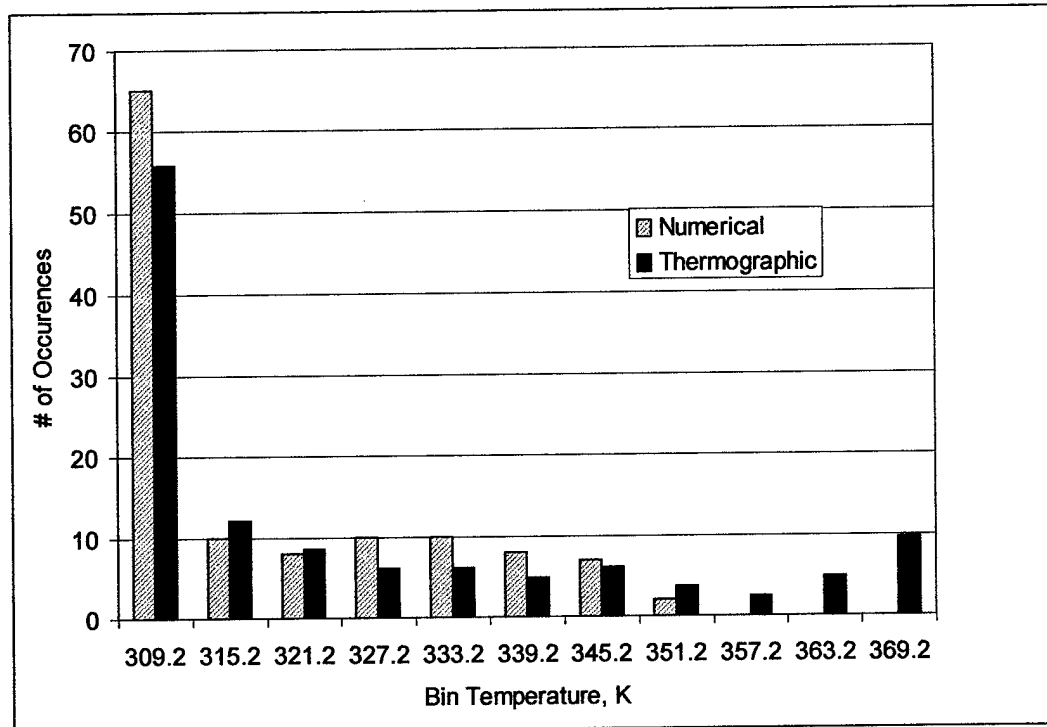
Figure 68. Temperature Distributions for the Regeneration-In,
Process-Out Side of the WSG Desiccant Wheel with a Step
Increase to Regeneration Temperature at Time Equals 1 Minute.

Temperature and Moisture Gradients

Looking at the two-dimensional numerical matrices (Figure 54 through Figure

67), a definite patterns for temperature and moisture develop over time. These

patterns or gradients proceed from the airstream inlet end and progress in the axial

direction toward the outlets. As the steady-state condition is approached, the

gradients change less and begin to maintain a constant position.

Looking closely at the differences between the temperature gradients and the

moisture gradients can help understand the long transient response of the rotary

desiccant wheel.

140
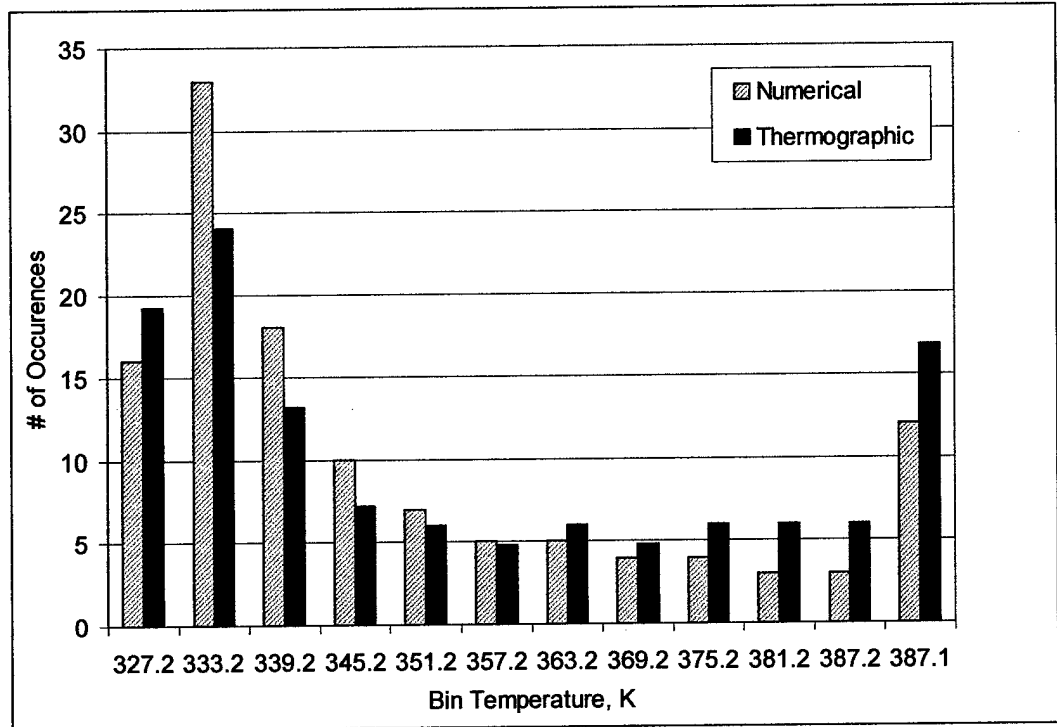
Figure 69. Temperature Distributions for the Regeneration-In,
Process-Out Side of the WSG Desiccant Wheel with a Step
Increase to Regeneration Temperature at Time Equals 34 Minutes.

Time (min)	n	df	α	χ^2 critical	α	χ^2 critcal	χ^2
1	12	11	0.05	19.68	0.01	24.72	26.95
4	12	11	0.05	19.68	0.01	24.72	17.51
34	12	11	0.05	19.68	0.01	24.72	12.25

Table 13. Summary of Statistical Comparison

The temperature gradients set up and reach steady-state within 4 minutes (they
essentially do not change after the 4 minute graph). The moisture content gradients
of the desiccant take longer – the graphs at 8 minutes and 34 minutes are significantly
different. This indicates that the moisture profile is not steady-state at the 8-minute
point. The desiccant moisture profile should coincide with the airstream moisture
outlet conditions. Since the airstream outlet conditions require approximately 22

141

minutes to reach steady-state, the desiccant wheel moisture profiles should require approximately the same amount of time. The graphical matrices of the desiccant moisture profile tend to exhibit this same phenomena because steady-state clearly requires longer than eight minutes.

Since the moisture profile is based on the average moisture content within a particle, the movement of the moisture is dependent upon the diffusion of the moisture through the particle itself. This agrees with previous researchers' evidence that the solid-side diffusion is a dominant resistance and the primary reason for the length of the transient response.

Summary

The matrix itself can be useful for examining and verifying the desiccant wheel's behavior. The numerical data from the desiccant matrix and the thermographic camera data, in particular, appear to be additional tools that can be used to validate simulation models. In this particular case, they have been used as a secondary form of validation. The results they gave tend to agree well and confirm earlier validation results. Significant deviations with this configuration can be explained. Additionally, graphical representations of the numerical matrix can quickly and intuitively help explain the behavior of the rotary desiccant wheel. In particular, the relatively slow development of the moisture gradients provides a quick, intuitive explanation for the long transient response.

CHAPTER 8. PARAMETRIC ANALYSIS

Variables

In order to determine the operating characteristics and factors affecting the transient response of a rotary desiccant wheel, a parametric analysis was performed using the NovelAire WSG wheel materials, dimensions, and operating characteristics as the basis. The parametric analysis was structured by initially dividing it into two categories based on fuel source: conventional and renewable. From this point, the conventional and renewable wheels were tested over four different categories: operational factors, ambient conditions, wheel geometry, and material properties. Within each category, a list of variables was considered. The list of variables within each category is shown in Table 14. Using the WSG wheel parameters, industry standards, and potential ambient conditions, a range of values was developed for each variable that is also shown in the table.

A review was also done of the types of step changes as shown in Table 15. The step change to regeneration temperature is the most significant because it is the primary driving potential for moisture transfer within the wheel. Experimental and numerical results also show the temperature difference generates the greatest change in steady-state value and has the longest transient response.

variables for parametric analysis			
Category	Variable	Range of Values	
Energy Source	regen temp	80C	140 °C
	wheel split	50/50	75/25
Operational	wheel speed	9 rph	36 rph

variables for parametric analysis			
Category	Variable	Range of Values	
	Airstream flowrate	400 fpm	800 fpm
	Initial Wheel Temperature	308.15 K	330 K
Ambient Conditions	Humidity	40% RH	70% RH
	Temperature	70	95
Wheel Geometry	transfer area – profile	rectangular	triangular
	desiccant mass	8.1 kg	9.9 kg
	wheel depth	.2 m	.1 m
Material Properties	particle size	3.5 microns	47.5 microns
	effective diffusivity	regular density (RD) silica gel	10x RD silica gel
	desiccant specific heat	1.824kJ/(kg-K)	3.6 kJ/(kg-K)

Table 14. Parametric Analysis Variables

types of step changes	
to wheel speed	very quick response
to flowrate	very small response
regen temps	most significant

Table 15. Types of Step Changes

Parametric Conventions

Several conventions were established for the parametric analysis and they are explained here.

The desiccant wheel industry typically bases their performance characteristics on the volumetric or airflow velocity of the stream entering the process and regeneration sides of the wheel. For this reason, during the parametric analysis a constant flowrate was done on a velocity or volumetric basis, not a mass basis. Therefore, in keeping with the performance characteristics of the NovelAire WSG wheel, 600 fpm, was kept as the base case flowrate.

144

For the parametric analysis, MRC, as defined in Chapter 2 was used as the main output standard. This is the industry standard term and, typically, moisture removal is the primary objective for desiccant wheels.

Several non-dimensional parameters were also observed as well to better assess the impact of the variables on the output. Specifically, the flowrate ratio (Γ), the inlet number of transfer units (NTU), and the inlet ratio of mass convection to mass solid-side diffusion, the Sherwood number (Sh). These were calculated for both streams as defined in Chapter 3 on mathematical modeling. The NTU and Sherwood numbers are dependent upon temperature and moisture; therefore, their values are different at every element. The NTU and Sherwood numbers shown in these tables are calculated at the inlets for each stream to obtain an estimate of the range of these variables.

The time to reach transient response for the parametric analysis was calculated by finding the average steady-state response and then determining 95% of this value. Using the numerical data, the time corresponding to the 95% of steady-state value was then determined. The transient time corresponding to the 95% value is approximately equal to three time constants. The value for a single time constant is also shown for reference purposes. The steady-state average was taken at a point well after the transient period to ensure the transient did not affect the steady-state value. This can be seen in Figure 70.

The parametric analysis runs were calculated at sea level. This typically is the most common elevation for HVAC analysis and most areas with high humidity are typically situated near sea level. The validation runs were done at the 5000 foot

elevation of the NREL lab in Golden, Colorado. The model takes elevation into

account through the atmospheric pressure and the saturation vapor pressure.

The specific input conditions for each run are located in Appendix I.
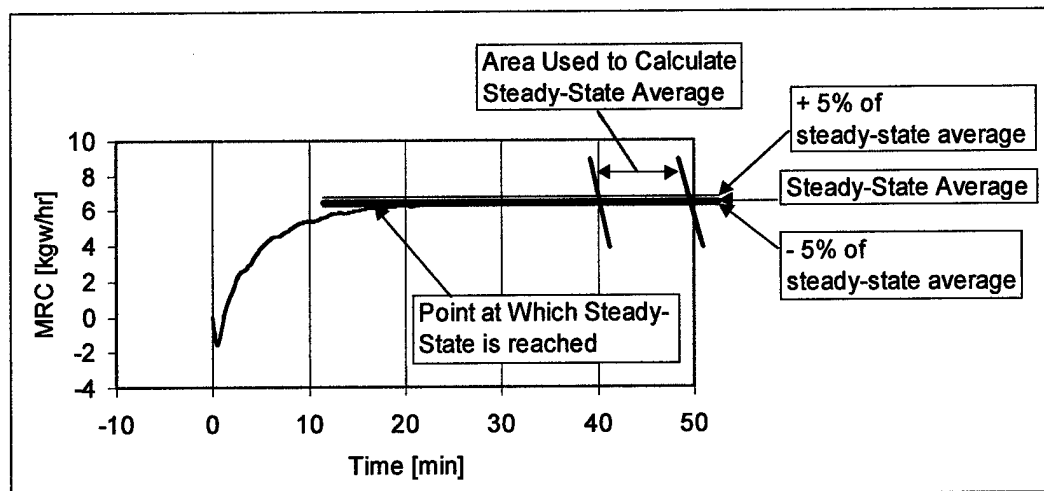
Figure 70. Schematic Showing Point Where Steady-State is
Reached

Wheel Split and Regeneration Temperature

The initial runs comparing regeneration temperature and wheel split are

shown in Figure 71, Table 16, and Table 17. The two variables altered in these runs

were the regeneration temperature and the wheel split. The <u>conventional</u> base case

was assumed to operate at a regeneration temperature of 140 °C with a wheel split of

75/25. The 140 °C temperature is a typical regeneration temperature for wheels using

heat generated by fossil fuel sources. The conventional case has an unbalanced wheel

split (75/25) precisely because of the high temperature. This is done to maximize

moisture removal and prevent thermal energy in the regeneration stream from being

wasted. The <u>renewable</u> case was assumed to operate at a regeneration temperature of

80 °C with a wheel split of 50/50. The 80 °C temperature corresponds to renewable

energy sources such as solar thermal. The balanced wheel split (50/50) maximizes

the moisture removal at the lower temperature and still has sufficient thermal

capacitance so that regeneration energy is not wasted. In other words, all the heat

capacity of the regeneration stream is used and not released to the atmosphere. This

would occur if the regeneration temperature were much higher than the inlet process

temperature.

The difference in regeneration temperature affects most of the non-

dimensional variables as can be seen in Table 16. Overall, increasing temperature

increases Γ and NTU and decreases the Sherwood number. The temperature of the

air directly affects the specific volume, which in turn directly affects the mass

flowrate. The mass flowrate in turn directly affects Γ and NTU. Increasing

temperature will also increase the heat and mass transfer coefficients and the effective

diffusivity slightly. Both the NTU and Sherwood number are directly related to the

transfer coefficients while the Sherwood number is inversely related to the effective

diffusivity.

Increasing the regeneration temperature (or increasing the temperature

difference between the process and regeneration streams) will significantly increase

the steady-state value and decrease the transient response time as shown in Table 17.

This is typical behavior as increasing NTUs will normally produce higher steady-state

transfer. The downside with the increased regeneration temperature is the higher

energy cost.

The unbalanced wheel split (75/25) produces both a lower steady-state output

and has a longer transient response (Table 17). As stated earlier, it can be effectively

used with the high temperature source (140 °C) to maximize moisture removal and

minimize thermal waste. Conversely, the balanced wheel split has a higher steady-state output and a shorter transient response time.

The slope of the transient curve for the 50/50 split at high temperature appears to "hit" a plateau (Figure 71) and then maintain this value as a steady-state. This can be readily explained because of the temperature, wheel split, and depth of the wheel. It can be seen in the steady-state 50/50 wheel split matrix, Figure 72, that the high temperature wave of the regeneration airstream has essentially "broken through" the matrix and is exiting the opposite axial end of the desiccant matrix. This is then wasted thermal energy. This is in contrast to the 75/25 wheel split matrix seen in Figure 73. The desiccant wheel temperatures in the outlet regeneration elements are only slightly higher than the process inlet values.

The 75/25 split with 140 °C regeneration temperature will herein be referred to as the conventional configuration and the 50/50 split with 80 °C regeneration temperature will be referred to as the renewable configuration. The "base" case is defined as the values for the NovelAire WSG wheel: 18 rph, 600 fpm, the rectangular profile, and the same material properties (adsorption isotherm, specific heats, etc.).
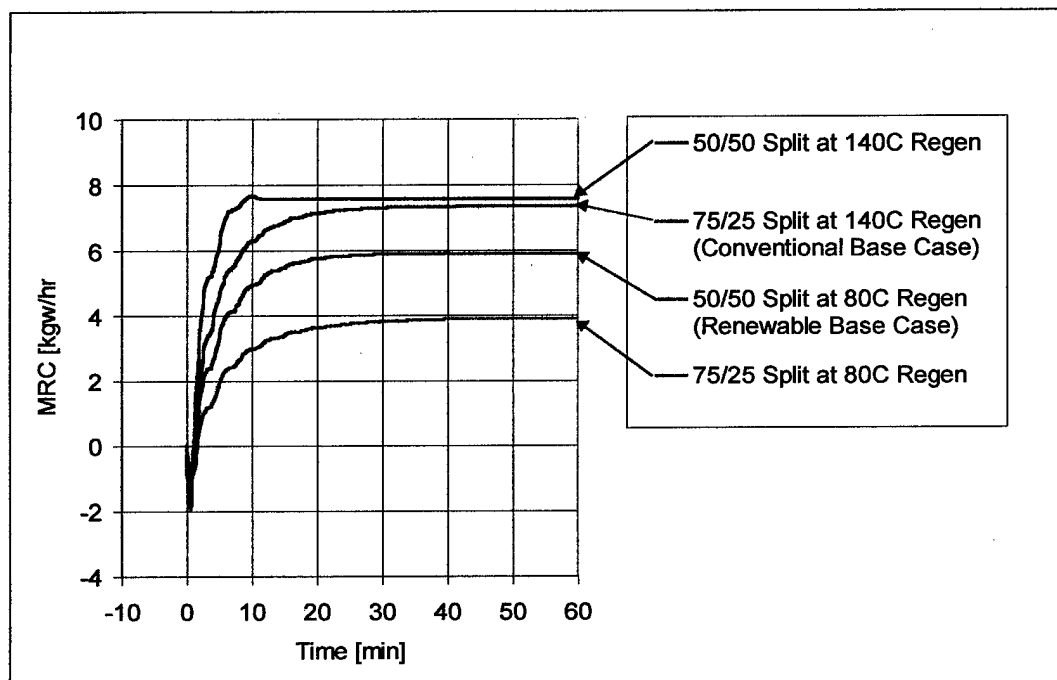
Figure 71. Transient Response Curves of Regeneration
Temperature and Wheel Split

RUN	DESCRIPTION	Γ_p	Γ_r	NTU$_p$	NTU$_r$	Sh$_p$	Sh$_r$
1	75/25 Split at 140 °C Regen (Conventional Base Case)	0.1161	0.4565	4.361	7.274	0.567	0.059
2	50/50 Split at 140 °C Regen	0.1742	0.2281	4.361	7.271	0.567	0.059
3	50/50 Split at 80C Regen (Renewable Base Case)	0.1742	0.1984	4.361	5.585	0.567	0.177
4	75/25 Split at 80C Regen	0.1161	0.3970	4.361	5.585	0.567	0.177

Table 16. Inlet Non-Dimensional Variables for Wheel Split and
Regeneration Temperature

	STEADY -STATE	CHANGE	TRANS TIME, 95%	CHANGE	TIME CONSTANT	CHANGE
RUN	MRC	(%)	(MIN)	(%)		(%)
1	7.36		16.36		5	
2	7.56	2.64	6.5	-60.27	2.75	-45.00
3	5.92	-19.65	16	-2.20	5.5	10.00
4	3.93	-46.68	23.57	44.07	7.47	49.40

Table 17. Comparison of Steady-State MRC and Transient
Response Time with Regeneration Temperature and Wheel Split

149
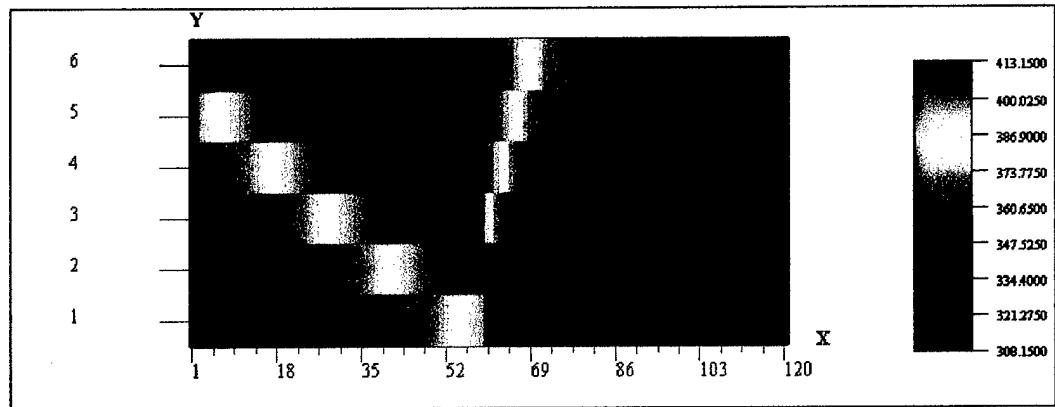
Figure 72. Graphic of the Airstream Temperature Matrix at 50/50
Wheel Split and 140 °C Regeneration Temperature
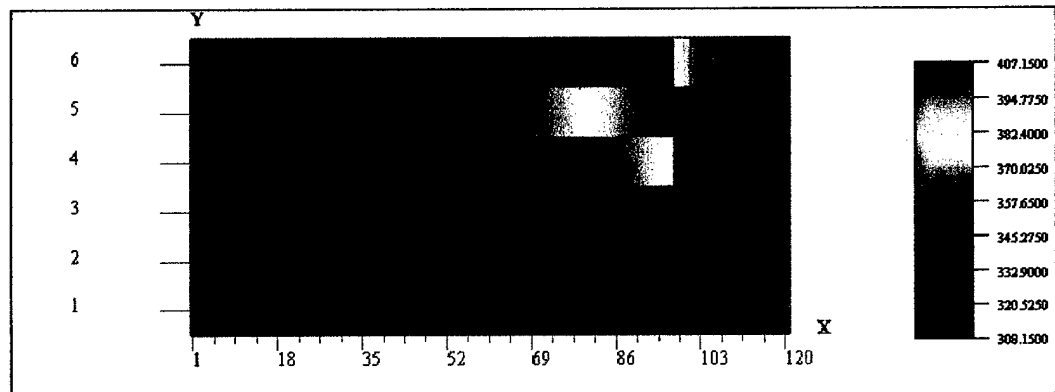
Figure 73. Graphic of the Airstream Temperature Matrix at 75/25
Wheel Split and 140 °C Regeneration Temperature

Comparison of Factors with the Conventional Configuration

The conventional configuration comparison for all variables will now be

presented and is shown in Figure 74 through Figure 80 and Table 18 through Table 31.

As mentioned in Chapter 4, (numerical technique), the NTU variable can be substantially dependent upon temperature and moisture. It can be observed most dramatically in the conventional configuration analysis (Table 16) that the inlet NTU values for regeneration streams are typically 67% higher than for process streams. This tends to justify calculating NTU at every element rather than using a constant value for a whole stream or wedge as previous researchers have done in order to minimize computational requirements.

The transient response for wheel speed in the conventional configuration is shown in Figure 74, Table 18, and Table 19. In this set of parametric runs the wheel speed was increased and decreased by a factor of two from the base case speed of 18 rph. The change in wheel speed is directly related to Γ through the desiccant mass flowrate. There is no change to NTU or the Sherwood number.

The change in wheel speed, hence Γ, has an inverse relation to the steady-state value and a direct relation to the transient time for MRC. This agrees with previous steady-state results that also show a strong relationship between wheel speed and heat and mass transfer. Typically, there is in fact an optimum wheel speed at which mass transfer is maximized for rotary desiccant wheels. And operating a desiccant wheel at a higher speed will increase the energy transfer and reduce the mass transfer. This can partially be seen in this analysis. The decrease in wheel speed by half from the base case produces a 9% increase in output; increasing the wheel speed by two from the base case drops the output by 25%.

Interestingly, the validation runs showed a higher output at 18 rph than 9 rph. The flowrates, temperatures and humidities are slightly different between these runs

while the major difference is the elevation. The change in relative humidity due to

elevation has apparently shifted the optimum wheel speed.

Figure 74. Transient Response Curves for Wheel Speed with
Conventional Configuration

RUN	DESCRIPTION	Γ_p	Γ_r	NTU_p	NTU_r	Sh_p	Sh_r
1	Conventional Base Case	0.1161	0.456	4.361	7.274	0.567	0.059
5	Wheel Speed = 36 rph	0.2321	0.913	4.361	7.274	0.567	0.059
6	Wheel Speed = 9 rph	0.058	0.228	4.361	7.274	0.567	0.059

Table 18. Non-Dimensional Inlet Variables for Wheel Speed with
the Conventinal Configuration

	STEADY-STATE	CHANGE	TRANS TIME	CHANGE	TIME CONSTANT	CHANGE
RUN	MRC	(%)	(MIN)	(%)		(%)
1	7.36		16.36		5	
5	5.36	-27.20	17.88	9.29	6.06	21.20
6	8.02	8.83	16.59	1.41	4.55	-9.00

Table 19. Comparison of Steady-State MRC and Transient
Response Times for Wheel Speed with the Conventional
Configuration

153

The transient response for flowrate with the conventional configuration is shown in Figure 75, Table 20, and Table 21. In this case, *both* process and regeneration volumetric flowrates were increased or decreased concurrently (to 400 fpm and 800 fpm). As discussed earlier, the flowrate tends to be worked in terms of air velocity or a volumetric basis.

The change in flowrate is inversely related to Γ and NTU as the flowrate occurs in the denominator of both variables. The Sherwood number is not affected.

Increasing the flowrate increases the steady-state response (+34%) and reduces the transient time (-23%). This would clearly be advantageous. There is an upper limit; however, due to the fan power required to move the air through the desiccant wheel at the higher velocities. The power required to move the air increases exponentially with increased flowrate.
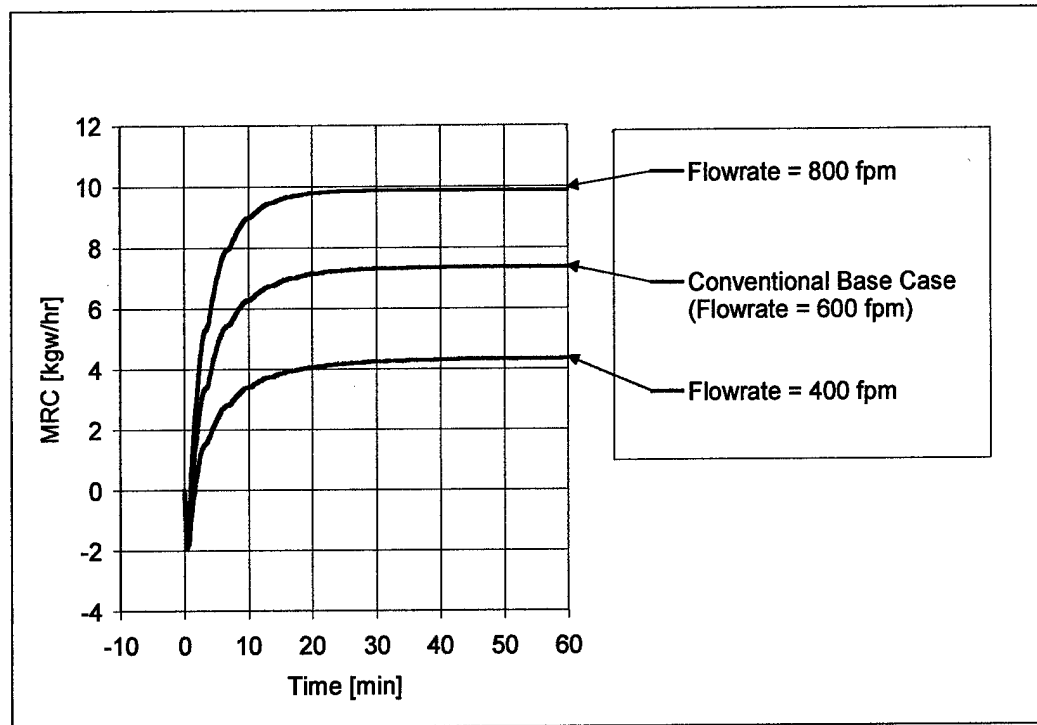
Figure 75. Transient Response Curves for Flowrate with the Conventional Configuration

RUN	DESCRIPTION	Γ_p	Γ_r	NTU_p	NTU_r	Sh_p	Sh_r
1	Conventional Base Case	0.1161	0.456	4.361	7.274	0.567	0.059
7	Flowrate = 800 fpm	0.0871	0.342	3.270	5.454	0.567	0.059
8	Flowrate = 400 fpm	0.1741	0.684	6.542	10.90	0.567	0.059

Table 20. Non-Dimensional Inlet Variables for Flowrate with the Conventional Configuration

	STEADY-STATE	CHANGE	TRANS TIME	CHANGE	TIME CONSTANT	CHANGE
RUN	MRC	(%)	(MIN)	(%)		(%)
1	7.36		16.36		5	
7	9.88	34.12	12.56	-23.23	4.49	-10.20
8	4.35	-40.97	22.25	36.00	6.5	30.00

Table 21. Comparison of Steady-State MRC and Transient Response Times for Flowrate with the Conventional Configuration

155

The parametric runs for initial wheel temperature are shown at Figure 76, Table 22, and Table 23. These runs were made in an effort strictly to reduce the transient phase by bringing the wheel up to temperature before turning on the process flow. This could be accomplished by simply running the regeneration stream at its operational temperature until the wheel reached a uniform temperature. At that point, the process stream could then be "turned on". The trade-off is that additional energy would be required to do this - energy that is not directly used for dehumidifying air.

Because the initial wheel temperature is just that - an initial condition - the non-dimensional variables (Γ, NTU, and Sherwood) are independent of this change and remain constant.

This procedure is clearly effective in reducing the transient response. In the best case, the transient was reduced by 83% from 16 minutes to 3 minutes.
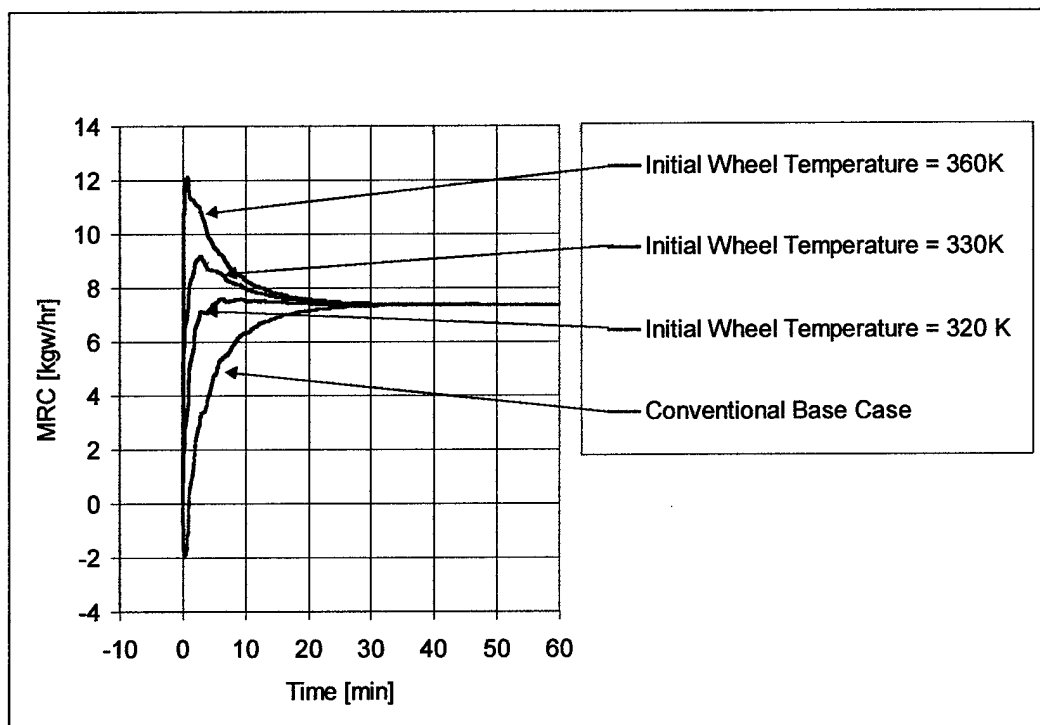
Figure 76. Transient Response Curves for Initial Wheel
Temperature with the Conventional Configuration

RUN	DESCRIPTION	Γ_p	Γ_r	NTU_p	NTU_r	Sh_p	Sh_r
1	Conventional Base Case	0.1161	0.4565	4.361	7.274	0.567	0.059
9	Initial Wheel Temp = 360K	0.1161	0.4565	4.361	7.274	2.495	0.163
10	Initial Wheel Temp = 330K	0.1161	0.4565	4.361	7.274	1.323	0.106
11	Initial Wheel Temp = 320K	0.1161	0.4565	4.361	7.274	0.864	0.079

Table 22. Inlet Non-Dimensional Variables for Initial Wheel
Temperature with the Conventional Configuration

	STEADY-STATE	CHANGE	TRANS TIME	CHANGE
RUN	MRC	(%)	(MIN)	(%)
1	7.36		16.36	
9	7.36	0.00	16.36	0.00
10	7.36	0.00	13.41	-18.03
11	7.36	0.00	2.73	-83.31

Table 23. Comparison of Steady-State MRC and Transient
Response Times for Initial Wheel Temperature with the
Conventional Configuration

157

The ambient humidity ratio is of concern because humidity levels can vary greatly over time and geography. This parametric run was arranged by keeping the air temperature constant with different humidity ratios.

The transient response with respect to ambient humidity conditions is shown in Figure 77, Table 24, and Table 25. The increasing humidity ratio causes small increases in Γ, small decreases in NTU, and small decreases in the Sherwood number. Like changes in temperature, this is predominantly due to the change in specific volume which affects the flowrate. Additionally, the specific heat of moist air is also increased with increasing moisture and this lowers the heat and mass transfer coefficients. The lower transfer coefficients cause the NTU and Sherwood number to reduce even more. The reduced Sherwood number also makes sense from an intuitive standpoint in that the effective diffusivity would be expected to decrease. The increased amount of water molecules would slow transport within the pore itself because of increased contact with other water molecules.

The effect of increasing humidity ratio is to increase the steady-state MRC and lengthen the transient response as can be seen in Table 25. The increasing steady-state values are caused by a greater magnitude of moisture in the ambient airstream to begin with. The longer transient, however, can be traced to the reduced NTU and Sherwood numbers. This evidence also supports previous findings that the solid-side mass resistance causes the slow development of the moisture gradients within the particle and hence the transient response time. This increase in time can be significant as shown in the 70% relative humidity case which is approximately 40% longer.
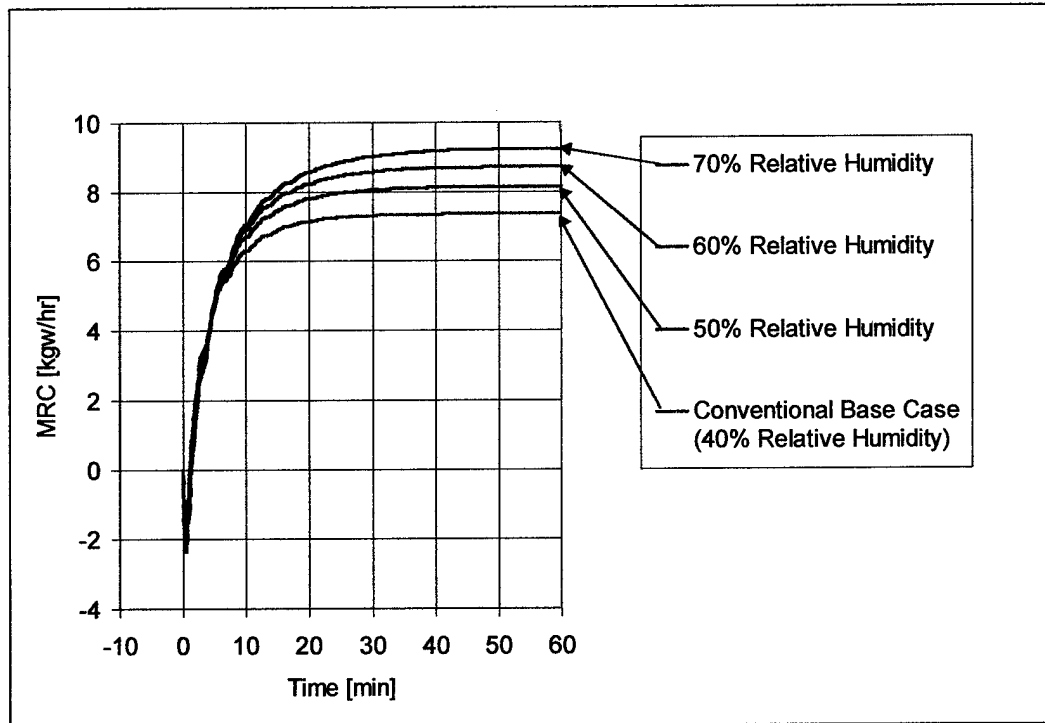
Figure 77. Transient Response Curves Comparing Ambient
Humidity Conditions for the Conventional Configuration

RUN	DESCRIPTION	Γ_p	Γ_r	NTU_p	NTU_r	Sh_p	Sh_r
1	Conventional Base Case	0.1161	0.4565	4.361	7.274	0.567	0.059
12	35C/50%RH	0.1173	0.458	4.377	7.242	0.502	0.054
13	35C/60%RH	0.1174	0.4601	4.348	7.221	0.466	0.051
14	35C/70%RH	0.1180	0.4623	4.347	7.200	0.443	0.049

Table 24. Non-Dimensional Inlet Variables for Ambient Humidity
Conditions with the Conventional Configuration

	STEADY-STATE	CHANGE	TRANS TIME	CHANGE	TIME CONSTANT	CHANGE
RUN	MRC	(%)	(MIN)	(%)		(%)
1	7.36		16.36		5	
12	8.15	10.61	18.75	14.61	5.5	10.00
13	8.73	18.56	21.5	31.42	6	20.00
14	9.23	25.35	23	40.59	7	40.00

Table 25. Comparison of Steady-State MRC and Transient
Response Times for Ambient Humidity Condition with the
Conventional Configuration

159

The transient response for ambient temperatures with the conventional configuration is shown at Figure 78, Table 26, and Table 27. As with the regeneration temperature, discussed in the first set of runs, the ambient temperature has the same effect upon the non-dimensional variables Γ, NTU, and the Sherwood number. (Γ and NTU will decrease, the Sherwood number will increase). The decrease in ambient temperature (or the temperature difference between process and regeneration) had the most significant increase in transient response time. The 70°F/21.1°C case, for example, had a transient period of over 32 minutes. As shown in Table 27, this is an increase compared to the base case of 97%.
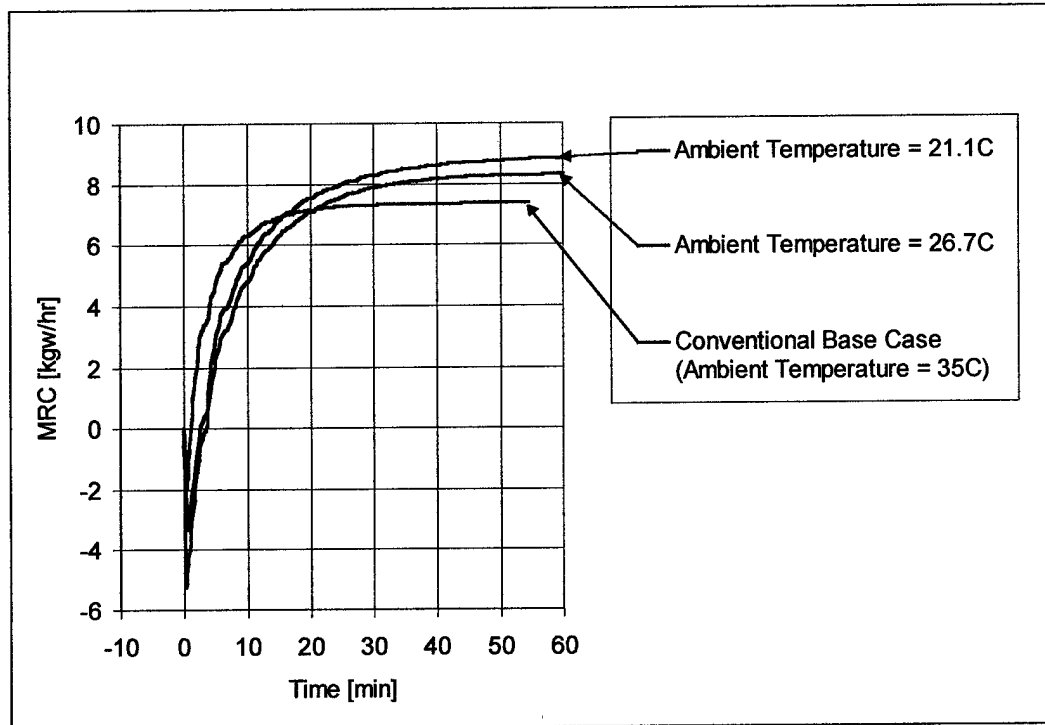
Figure 78. Transient Response Curves for Ambient Temperature
with the Conventional Configuration

RUN	DESCRIPTION	Γ_p	Γ_r	NTU$_p$	NTU$_r$	Sh$_p$	Sh$_r$
1	Conventional Base Case	0.1161	0.4565	4.361	7.274	0.567	0.059
15	80F/26.7C (64% RH)	0.1128	0.4565	4.139	7.274	0.563	0.050
16	70F/21.1C (90%RH)	0.1108	0.4565	3.997	7.274	0.659	0.049

Table 26. Non-Dimensional Inlet Variables for Ambient
Temperature with the Conventional Configuration

	STEADY-STATE	CHANGE	TRANS TIME	CHANGE	TIME CONSTANT	CHANGE
RUN	MRC	(%)	(MIN)	(%)		(%)
1	7.36		16.36		5	
15	8.32	12.91	30.75	87.96	11.25	125.00
16	8.82	19.78	32.25	97.13	10.75	115.00

Table 27. Comparison of Steady-State MRC and Transient
Response Times for Ambient Temperatures with the Conventional
Configuration

For the parametric runs with changes made to the wheel itself, the parameters were limited to a higher or lower value for the variable to be compared against the base case. The transient response with respect to geometric factors is shown in Figure 79, Table 28, and Table 29. The three runs in this set consist of using the triangular profile, lower desiccant mass, and shorter wheel depth.

The triangular profile maximizes the transfer surface area and minimizes the hydraulic diameter and desiccant mass. The effects are increased transfer coefficients, increased NTU, and a reduction in Γ. The triangular profile represents optimal heat and mass transfer because of the much larger surface area that it generates and this translates into a substantially higher NTU. The result is an increased steady-state MRC and a shorter transient period, Table 29. This makes sense because the improved transfer should, in fact, improve the magnitude and rate of the response.

The lower desiccant mass run uses the rectangular profile as in the base case but with the desiccant mass as used in the triangular profile (8.1 vs 9.9 kg). The net effect on the non-dimensional variables is a reduction in Γ and no reduction in NTU or Sherwood number. The output result is a higher steady-state MRC and a faster transient response. The lower desiccant mass apparently provides less thermal capacitance which increases the rate and amount of mass transfer. This output may therefore be a little misleading. The model bases convective heat and mass upon surface area. As long as the heat and mass transfer surface is provided, it assumes the desiccant mass provided is sufficient to cover it. The program cannot tell if the desiccant mass is sufficient to actually cover the area, but clearly there is minimal

amount of mass that is required. The lesson here is that the wheel should use the minimum amount of desiccant mass that will cover a particular surface and meet structural (thickness) requirements in order to optimize performance.

The wheel depth run was designed to see the impact when the wheel depth is reduced by half to 0.1 m. The non-dimensional variables Γ and NTU are reduced dramatically because of the reduced surface area. The Sherwood number is unaffected. The result is a lower steady-state MRC and shorter transient response time. Inspection of the steady-state numerical matrix for the desiccant reveals that, like the 50/50 split at 140 °C regeneration, the regeneration temperature wave has extended through the axial end of the matrix. There is insufficient thermal capacitance in the wheel for the regeneration stream flowrate as indicated by the lower Γ and NTU. The inlet NTUs for this run were approximately 2.1-3.6 versus 4.3-7.2 for the base case run.

Clearly there is an optimum axial length for a given set of inlet conditions: the leading edge of the temperature wave should fall just shy of exiting the wheel. Otherwise, the heated air is rejected to the atmosphere as waste heat. A production desiccant wheel must be designed to handle a variety of design conditions. It will therefore will probably use the worst case scenario which would mean an axial distance *slightly* longer than that called for by design conditions.

Structural requirements might also determine the axial length if the desiccant and substrate are used as part of the structure.
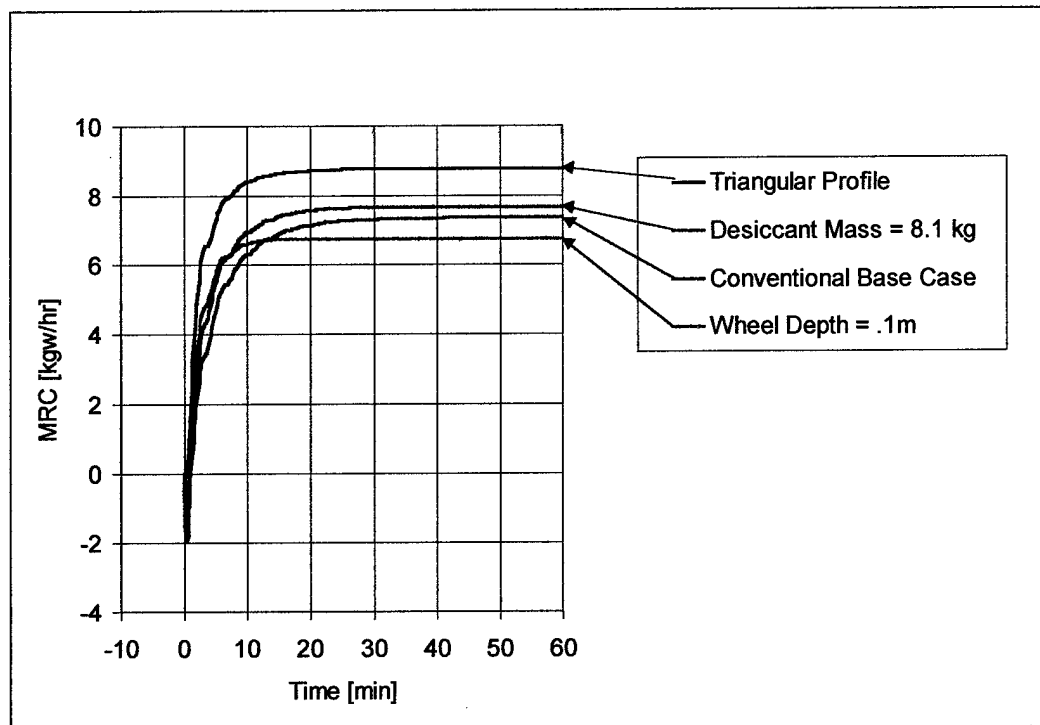
Figure 79. Transient Response Curves Comparing Wheel
Geometry Factors for the Conventional Configuration

RUN	DESCRIPTION	Γ_p	Γ_r	NTU_p	NTU_r	Sh_p	Sh_r
1	Conventional Base Case	0.1161	0.4565	4.361	7.274	0.567	0.059
17	Triangular profile	0.0887	0.3485	11.169	18.618	0.619	0.065
18	Desiccant Mass = 8.1kg	0.0947	0.3722	4.361	7.274	0.567	0.059
19	Wheel Depth = .1m	0.0579	0.2275	2.184	3.643	0.567	0.059

Table 28. Inlet Non-Dimensional Variables for Wheel Geometry
Factors with the Conventional Configuration

	STEADY-STATE	CHANGE	TRANS TIME	CHANGE	TIME CONSTANT	CHANGE
RUN	MRC	(%)	(MIN)	(%)		(%)
1	7.36		16.36		5	
17	8.78	19.22	9.5	-41.93	2.25	-55.00
18	7.69	4.39	13.75	-15.95	4.25	-15.00
19	6.75	-8.30	8	-51.10	2.75	-45.00

Table 29. Comparison of Steady-State MRC and Transient
Response Times for Wheel Geometry Factors with the
Conventional Configuration

164

A parametric run for material properties is shown in Figure 80, Table 31, and Table 31.

The first run consisted of using a larger particle size of the desiccant silica gel. In this case, the particle size selected was that from the SERI microbead wheel which has a radius of 47.5 microns or a little over ten times the size of the particle used for the NovelAire WSG, (3.5 microns). The silica gels used in the SERI microbead wheel and the NovelAire WSG are both regular density silica gels with the same particle density (1129 kg/m^3) and pore size (22 Å). The adsorption isotherm data used by Brandemuehl and the adsorption isotherm data provided by Grace Davison Co. (the maker of the 3 micron size silica gel) are exactly the same. Therefore the isotherm equation developed by Brandemuehl [1982] should apply to both. The adsorption properties are predominantly a function of the pore radius and, as a result, the density as well. Adsorption properties are independent of the particle size for this material.

For all of the matrix property runs, the only non-dimensional variable affected was the Sherwood number. The radius size contributes directly to the Sherwood number and, as expected, the Sherwood number is much larger. This indicates that the convection transfer is much greater relative to the solid-side diffusivity. This would produce a much higher surface water content and, incidentally, a higher equilibrium moisture content. On the process side, this will prevent the desiccant from picking up additional moisture. Looking at the results, this is shown to be correct with a lower steady-state MRC than the base case. The transient response is also slightly longer for the larger particle radius.

The second run consisted of increasing the specific heat of the matrix by a factor of two. This could occur, for example, if different structural materials or a different filler material were used. The matrix specific heat does not affect any of the non-dimensional variables. Logically, however, the transient response should be longer because of the matrix's greater thermal capacity. Table 31 indicates that this is the case. More interestingly perhaps, the steady-state MRC is also much lower than the base case. Apparently, because a wedge moving around the wheel is always in a state of transition between two inlet conditions, the increased matrix specific heat keeps an individual wedge farther from it's potential steady-state. Consequently, an individual wedge has acquired less or removed less moisture (than with a base case wedge) before it moves into the next inlet condition. The overall effect is less transfer and a lower steady-state MRC.

The last run for material properties was to increase the effective diffusivity by a factor of ten. A more appropriate analysis would probably be to have found a different desiccant material with a higher effective diffusivity and a new adsorption isotherm as well. Increasing the effective diffusivity inversely affects the Sherwood number. The NTU and Γ are independent of effective diffusivity. Increasing the effective diffusivity should speed the transient response as well. This is indeed the case (Table 31); however, it is not affected very much at all.
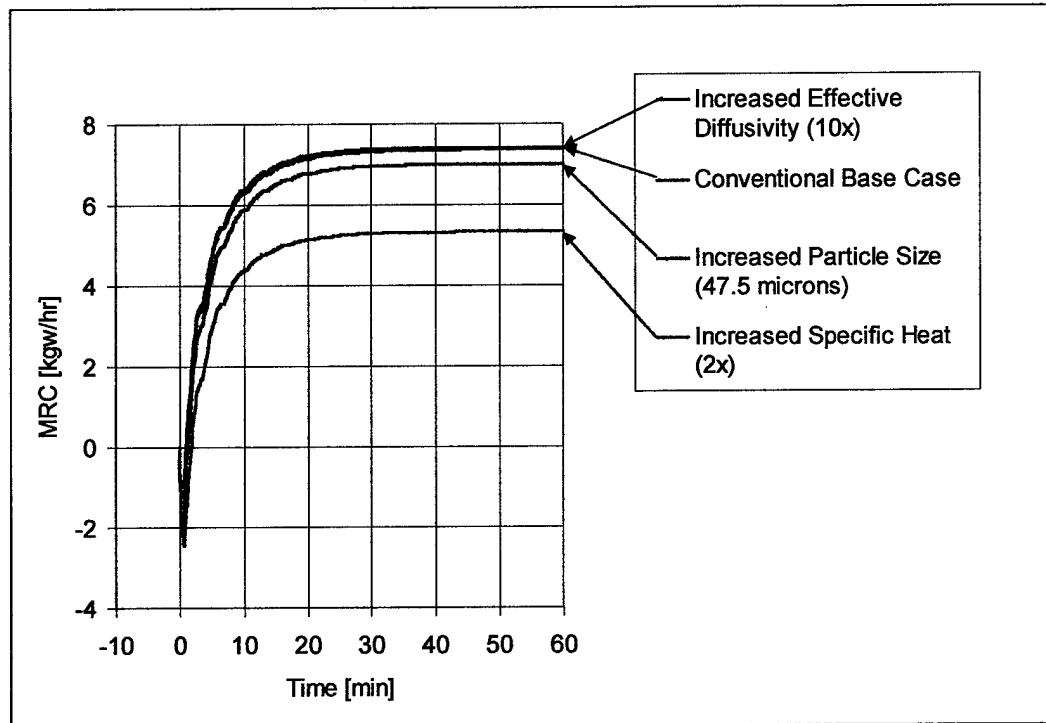
Figure 80. Transient Response Curves of Material Properties with
the Conventional Configuration

RUN	DESCRIPTION	Γ_p	Γ_r	NTU_p	NTU_r	Sh_p	Sh_r
1	Conventional Base Case	0.1161	0.4565	4.361	7.274	0.567	0.059
20	Particle Size = 47.5 microns	0.1161	0.4563	4.361	7.274	7.700	0.801
21	Increased Diffusivity (10x)	0.1161	0.4563	4.361	7.274	0.057	0.006
22	Increased Specific Heat (2x)	0.1161	0.4563	4.361	7.274	0.567	0.059

Table 30. Non-Dimensional Inlet Variables for Material Properties
with the Conventional Configuration

	STEADY-STATE	CHANGE	TRANS TIME	CHANGE	TIME CONSTANT	CHANGE
RUN	MRC	(%)	(MIN)	(%)		(%)
1	7.36		16.36		5	
20	7.01	-4.83	17.5	6.97	5.5	10.00
21	7.41	0.65	16.25	-0.67	5	0.00
22	5.34	-27.48	18.25	-69.44	6	20.00

Table 31. Comparison of Steady-State MRC and Transient
Response Time for Material Properties with the Conventional
Configuration

167

In general, the parametric runs for the renewable configuration follow the same response patterns as shown in the initial comparison between the conventional and renewable configuration. The parametric runs for the renewable configuration are shown in Figure 81 through Figure 87 and Table 32 through Table 45.
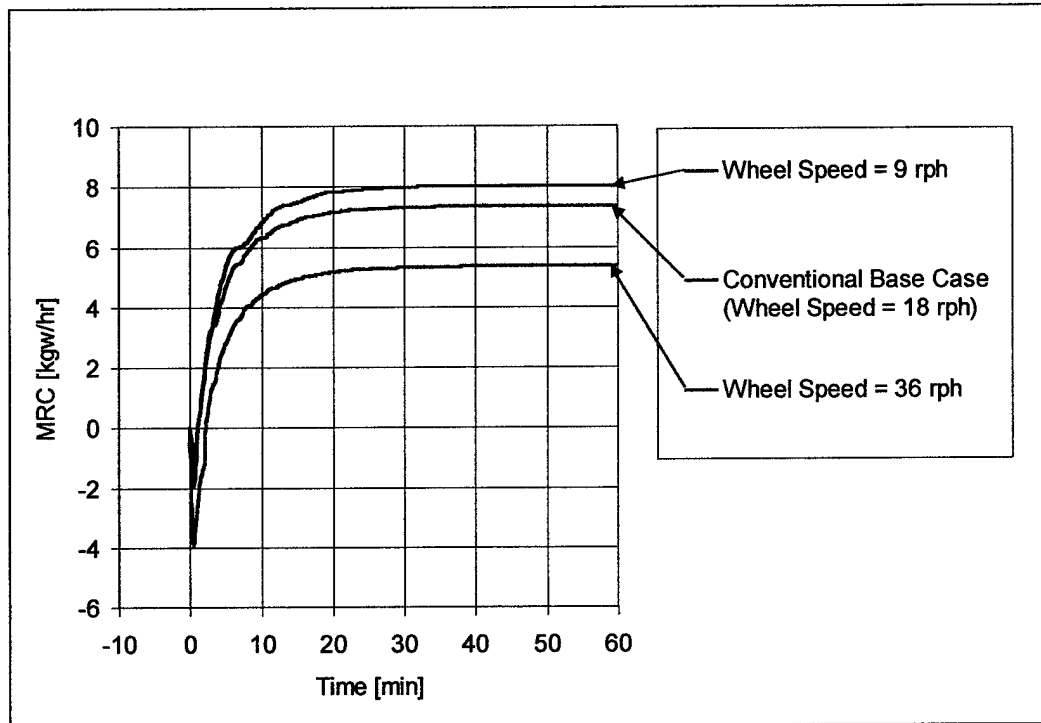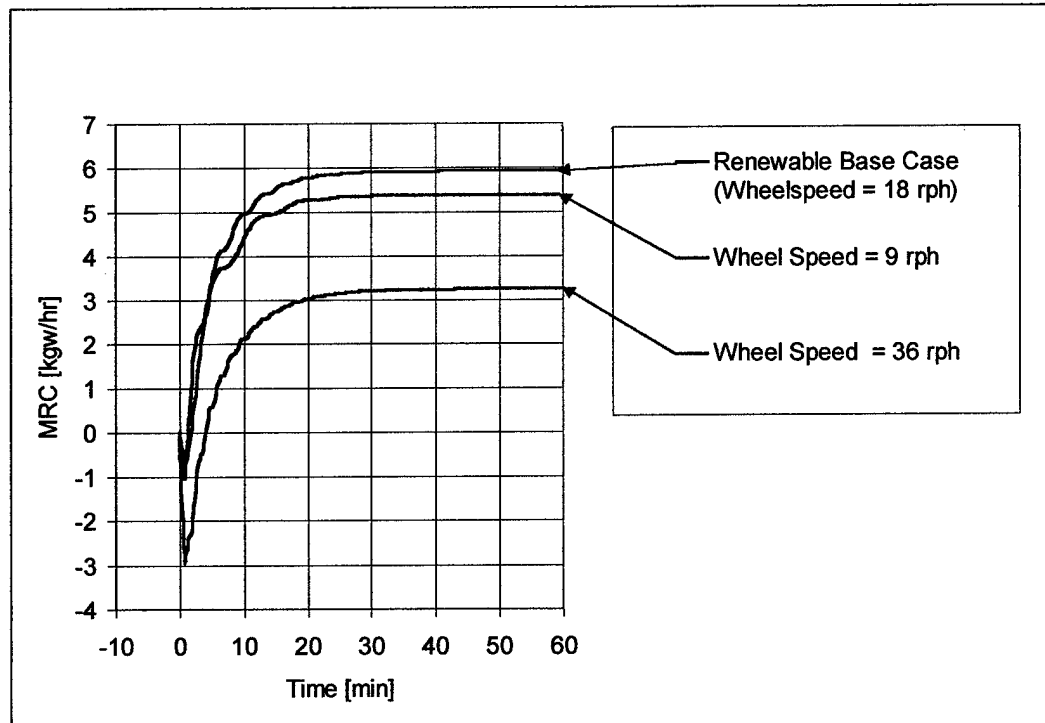
Figure 81. Transient Response Curves for Wheel Speed with Renewable Configuration

RUN	DESCRIPTION	Γ_p	Γ_r	NTU_p	NTU_r	Sh_p	Sh_r
3	Renewable Base Case	0.174	0.198	4.364	5.585	0.567	0.177
23	Wheel Speed = 36 rph	0.348	0.397	4.361	5.585	0.567	0.177
24	Wheel Speed = 9 rph	0.087	0.099	4.361	5.584	0.567	0.177

Table 32. Non-Dimensional Inlet Variables for Wheel Speed with the Renewable Configuration

	STEADY-STATE	CHANGE	TRANS TIME	CHANGE	TIME CONSTANT	CHANGE
RUN	MRC	(%)	(MIN)	(%)		(%)
3	5.92		16		5.5	
23	3.25	-45.00	22.5	40.63	9.5	72.73
24	5.38	-9.03	16.79	4.94	5.19	-5.64

Table 33. Comparison of Steady-State MRC and Transient Response Times for Wheel Speed with the Renewable Configuration

169
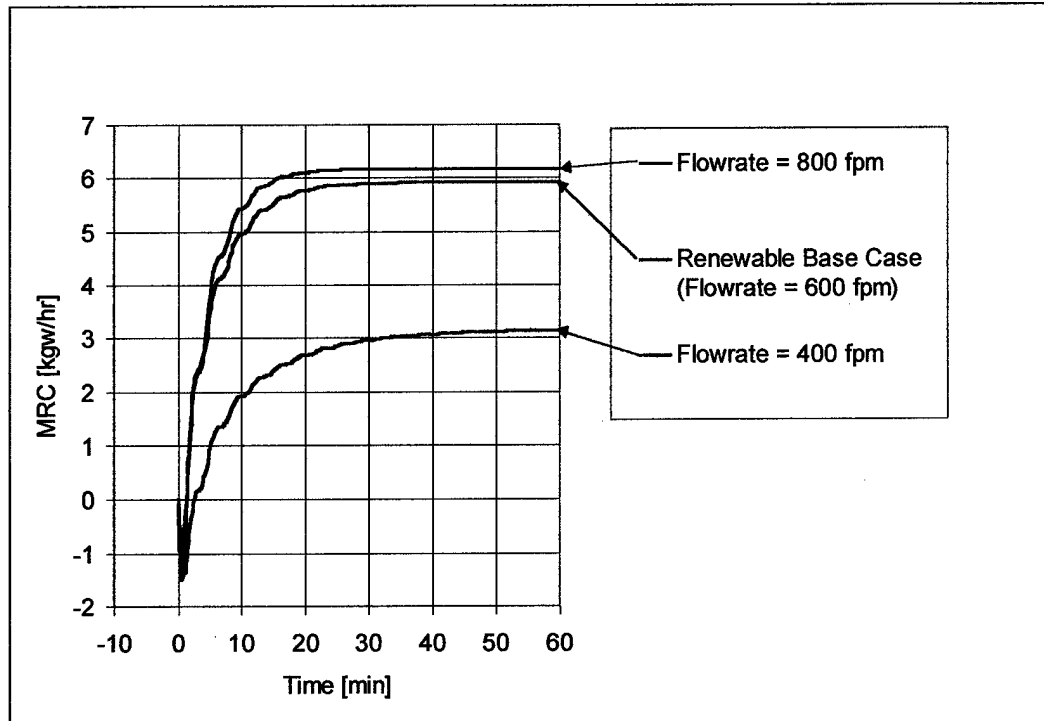
Figure 82. Transient Response Curves for Flowrate with
Renewable Configuration

RUN	DESCRIPTION	Γ_p	Γ_r	NTU_p	NTU_r	Sh_p	Sh_r
3	Renewable Base Case	0.1742	0.198	4.364	5.585	0.567	0.177
25	Flowrate = 800 fpm	0.1315	0.151	3.293	4.240	0.567	0.177
26	Flowrate = 400 fpm	0.2612	0.298	6.543	8.377	0.567	0.177

Table 34. Non-dimensional Inlet Variables for Flowrate with the
Renewable Configuration

	STEADY-STATE	CHANGE	TRANS TIME	CHANGE	TIME CONSTANT	CHANGE
RUN	MRC	(%)	(MIN)	(%)		(%)
3	5.92		16		5.5	
25	6.16	4.12	14.09	-11.94	5.28	-4.00
26	3.13	-47.03	31.18	94.88	10.97	99.45

Table 35. Comparison of Steady-State MRC and Transient
Response Times for Flowrate with the Renewable Configuration
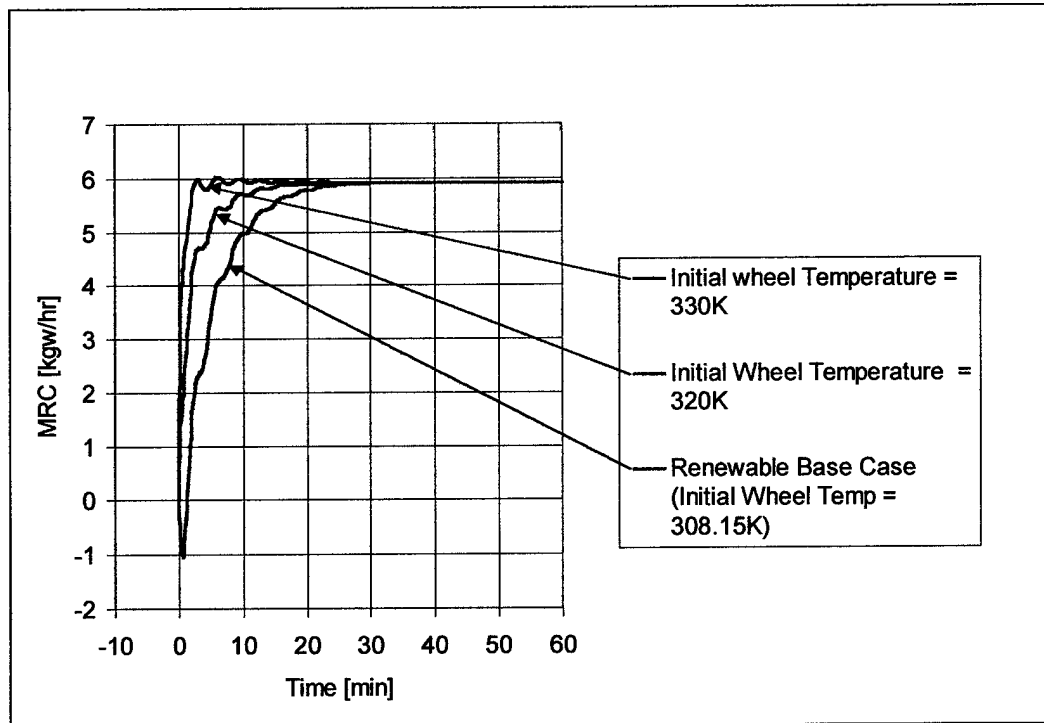
Figure 83. Transient Response Curves for Initial Wheel
Temperature with the Renewable Configuration

RUN	DESCRIPTION	Γ_p	Γ_r	NTU_p	NTU_r	Sh_p	Sh_r
3	Renewable Base Case	0.1742	0.1984	4.364	5.585	0.567	0.177
27	Initial Wheel Temp = 330K	0.1742	0.1984	4.364	5.585	1.323	0.360
28	Initial Wheel Temp = 320K	0.1742	0.1984	4.364	5.585	0.8635	0.251

Table 36. Inlet Non-Dimensional Variables for Initial Wheel
Temperature with the Renewable Configuration

	STEADY-STATE	CHANGE	TRANS TIME	CHANGE
RUN	MRC	(%)	(MIN)	(%)
3	5.92		16	
27	5.92	0.00	2	-87.50
28	5.92	0.00	8.75	-45.31

Table 37. Comparison of Steady-State MRC and Transient
Response Times for Initial Wheel Temperature with the
Renewable Configuration

171
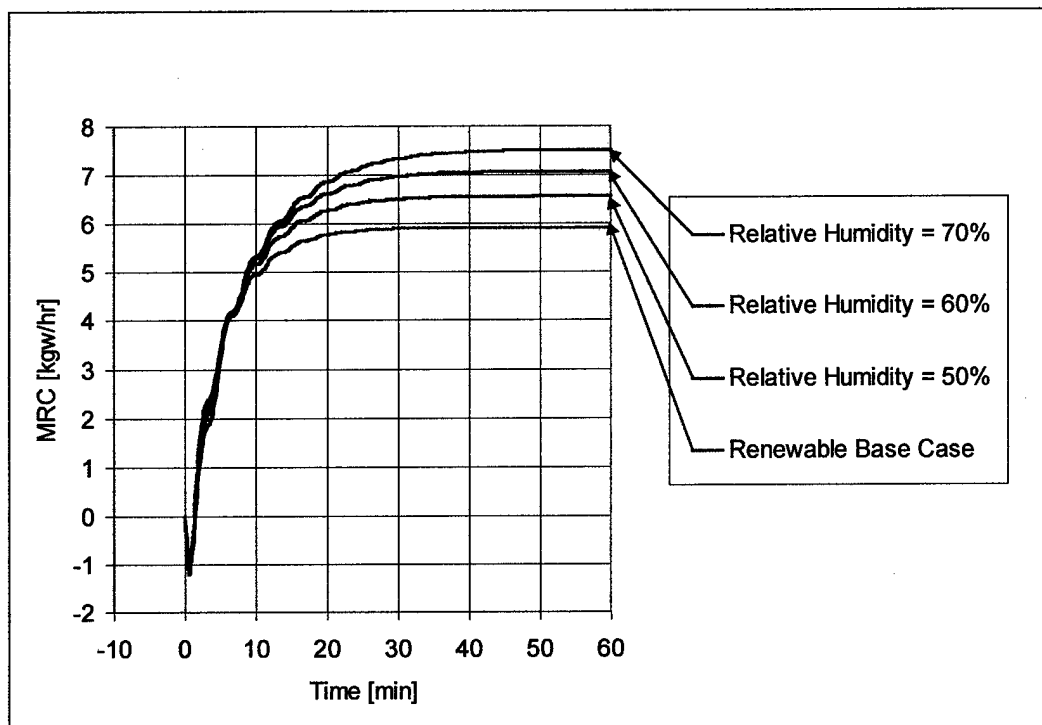
Figure 84. Transient Response Curves With Ambient Humidity
Conditions with the Renewable Configuration

RUN	DESCRIPTION	Γ_p	Γ_r	NTU_p	NTU_r	Sh_p	Sh_r
3	Renewable Base Case	0.1742	0.1984	4.364	5.585	0.567	0.177
29	35C/50%RH	0.1753	0.2009	4.135	5.323	0.502	0.159
30	35F/60%RH	0.1759	0.2021	4.347	5.609	0.466	0.149
31	35F/70%RH	0.177	0.2027	4.347	5.587	0.443	0.143

Table 38. Inlet Non-Dimensional Variables for Ambient Humidity
Conditions with the Renewable Configuration

	STEADY-STATE	CHANGE	TRANS TIME	CHANGE	TIME CONSTANT	CHANGE
RUN	MRC	(%)	(MIN)	(%)		(%)
3	5.92		16		5.5	
29	6.56	10.93	19	18.75	6.25	13.64
30	7.08	19.63	22	37.50	7.75	40.91
31	7.51	26.92	24.75	54.69	8.50	54.55

Table 39. Comparison of Steady-State MRC and Transient
Response Time for Ambient Humidity Conditions with the
Renewable Configuration

172
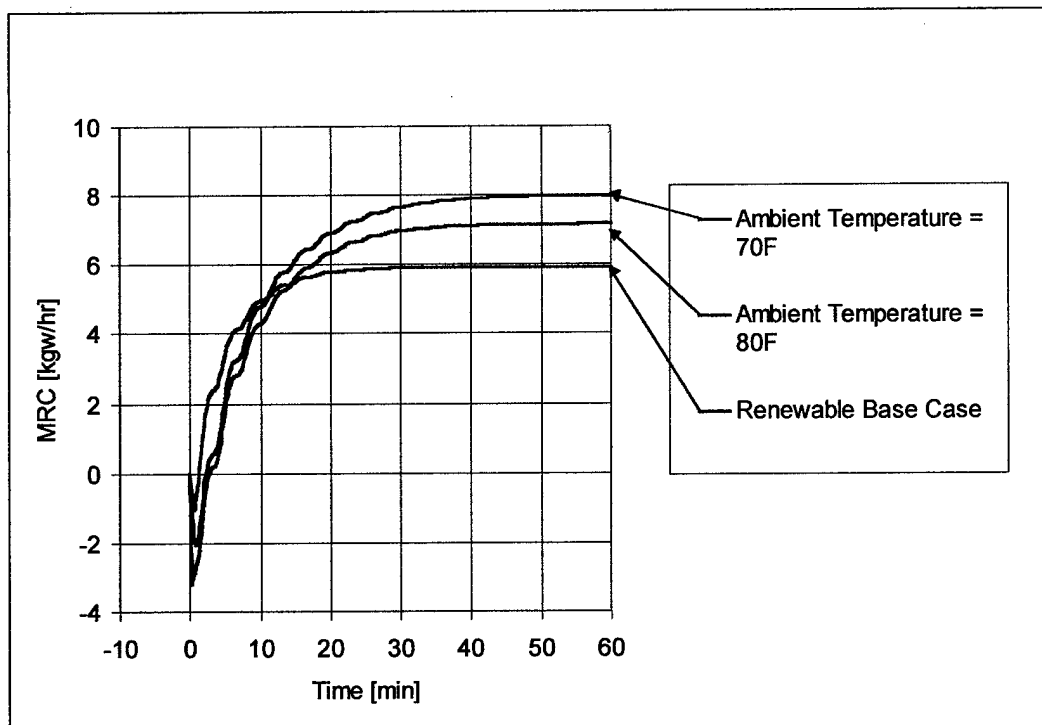
Figure 85. Transient Response Curves for Ambient Temperature with Renewable Configuration

RUN	DESCRIPTION	Γ_p	Γ_r	NTU_p	NTU_r	Sh_p	Sh_r
3	Renewable Base Case	0.1742	0.198	4.364	5.585	0.567	0.177
32	80F/26.7C (64% RH)	0.1693	0.199	4.131	5.585	0.563	0.142
33	70F/21.1C (90%RH)	0.1662	0.199	3.997	5.585	0.659	0.140

Table 40. Non-Dimensional Inlet Variables for Ambient Temperature with the Renewable Configuration

	STEADY-STATE	CHANGE	TRANS TIME	CHANGE	TIME CONSTANT	CHANGE
RUN	MRC	(%)	(MIN)	(%)		(%)
3	5.92		16		5.5	
32	7.16	20.95	25.71	60.69	10.95	99.09
33	7.98	34.81	28.57	78.56	11.19	103.45

Table 41. Comparison of Steady-State MRC and Transient Response Times for Ambient Temperature with Renewable Configuration

173
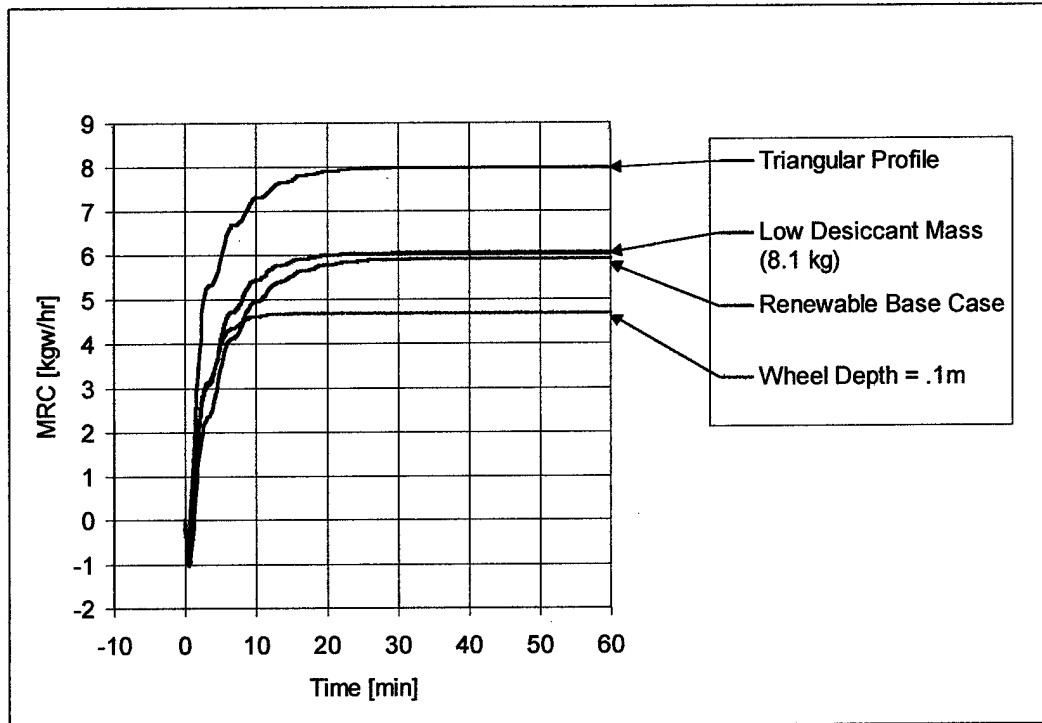
Figure 86. Transient Response Curves for Wheel Geometry with
the Renewable Configuration

RUN	DESCRIPTION	Γ_p	Γ_r	NTU_p	NTU_r	Sh_p	Sh_r
3	Renewable Base Case	0.174	0.1984	4.364	5.585	0.567	0.177
34	Triangular Profile	0.133	0.1516	11.169	14.300	0.619	0.193
35	Low Desiccant Mass (8.1kg)	0.142	0.1619	4.361	5.585	0.567	0.177
36	Wheel Depth = .1m	0.087	0.0991	2.184	2.797	0.567	0.177

Table 42. Inlet Non-Dimensional Variables for Wheel Geometry
with the Renewable Configuration

	STEADY-STATE	CHANGE	TRANS TIME	CHANGE	TIME CONSTANT	CHANGE
RUN	MRC	(%)	(MIN)	(%)		(%)
3	5.92		16		5.5	
34	7.98	34.81	12.6	-21.25	2.8	-49.09
35	6.04	2.04	12.6	-21.25	4.8	-12.73
36	4.68	-20.87	7.89	-50.69	2.7	-50.91

Table 43. Comparison of Steady-State MRC and Transient
Response Times for Wheel Geometry with the Renewable
Configuration
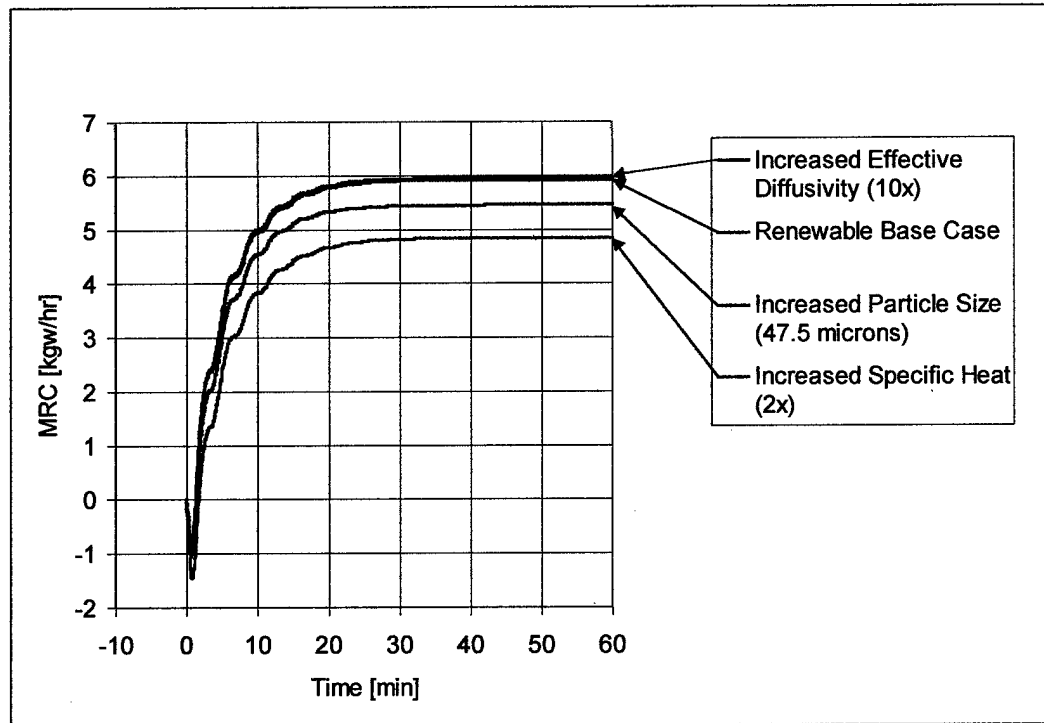
Figure 87. Transient Response Curves for Material Properties with the Renewable Configuration

RUN	DESCRIPTION	Γ_p	Γ_r	NTU_p	NTU_r	Sh_p	Sh_r
3	Renewable Base Case	0.1742	0.1984	4.364	5.585	0.567	0.177
37	Particle Size = 47.5 microns	0.1741	0.1984	4.361	5.585	7.700	2.399
38	Increased Diffusivity (10x)	0.1741	0.1984	4.361	5.585	0.312	0.303
39	Increased Specific Heat (2x)	0.1741	0.1984	4.361	5.585	0.567	0.176

Table 44. Inlet Non-Dimensional Variables for Material Properties with the Renewable Configuration

	STEADY -STATE	CHANGE	TRANS TIME	CHANGE	TIME CONSTANT	CHANGE
RUN	MRC	(%)	(MIN)	(%)		(%)
3	5.92		16		5.5	
37	5.45	-7.88	15.83	-1.06	5.38	-2.18
38	5.95	0.61	16	0.00	5.42	-1.45
39	4.85	-18.05	18.5	15.63	7.08	28.73

Table 45. Comparison of Steady-State MRC and Transient Response Times for Material Properties with the Renewable Configuration

175

Worst Case

A run was created with conditions from several variables that will produce the longest transient response or "worst case." Specifically, the wheel split, regeneration temperature, wheel speed, flowrate, and ambient conditions were used. The 75/25 wheel split was used as well as the lower regeneration (80C) temperature. For operational factors, the faster wheel speed (36 rph) and the lower flowrate (400 fpm) produce the longest transient response. For ambient conditions, a low temperature (70C) and a high relative humidity (90%) were selected. The output is shown in Figure 88, Table 46, and Table 47.

The worst case produced a transient response time of 92.3 minutes or an increase of over 450% compared to the conventional base case. While this system is clearly not configured for optimum performance, it could be duplicated by a modulating system. It simply indicates that the rotary desiccant wheel transient response can be quite substantial under the right conditions.
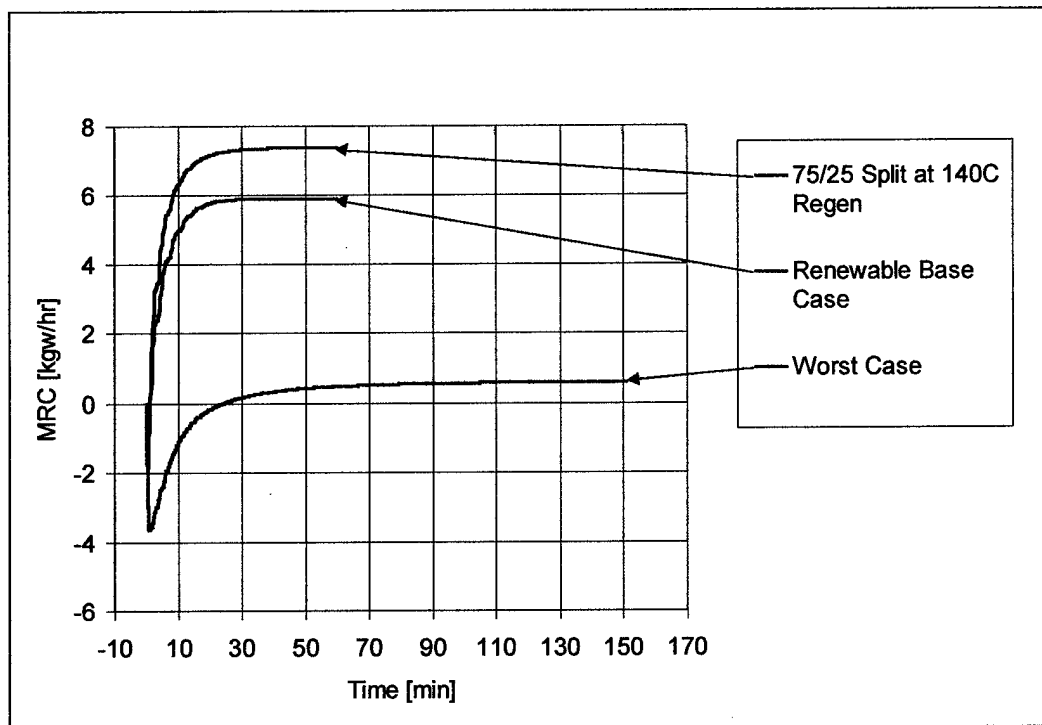
Figure 88. Transient Response of Worst Case Scenario

RUN	DESCRIPTION	Γ_p	Γ_r	NTU_p	NTU_r	Sh_p	Sh_r
1	Conventional Base Case	0.1161	0.456	4.361	7.274	0.567	0.059
3	Renewable Base Case	0.1742	0.198	4.364	5.585	0.567	0.177
40	Worst Case	0.3483	1.368	6.2809	9.623	0.659	0.140

Table 46. Non-Dimensionalized Inlet Variables for the Worst Case Scenario

	STEADY-STATE	CHANGE	TRANS TIME	CHANGE	TIME CONSTANT	CHANGE
RUN	MRC	(%)	(MIN)	(%)		(%)
1	7.36		16.36		5.23	
3	5.92		16		5.75	
40	0.58	-92.07	92.3	464.18	44.17	744.55

Table 47. Comparison of Steady-State and Transient Response Time for the Worst Case Scenario

177

Comparison with Previous Research

Previous research from Brandemuehl [1982] has indicated that the transient response is quite long: sometimes in the neighborhood of an hour. This is within the range of some of the previous parametric runs. However, it would interesting to see if the parameters used by the earlier research can produce the same transient response if they are roughly duplicated with the WSG wheel. The parameters used on pages 292 and 293 of Brandemuehl [1982] and gleaned from interviews with Dr. Brandemuehl are:

Parameter	Value
Λ, NTU	3.7
Γ	.3
Le	3.6
Wheel Split	50/50
Wheelspeed	20 rph
Regeneration Temperature	60C
Ambient Humidity Ratio	.01
Ambient Temperature	25C

Table 48. List of Parameters for Transient Runs by Brandemuehl [1982]

The correct NTU was calculated by using the NTU listed above and the Lewis number with the Lewis analogy. A comparable NTU value for the PCP model was reached by adjusting the transfer area. The Lewis number is set for the model in this research because of the parabolic concentration profile. The psuedo-gas side model uses a combined heat and mass transfer coefficient. The rest of the values are input directly into the model.

The results are shown in Figure 89 and Figure 90. Overall, the transient response time looks comparable to the runs by Brandemuehl, approximately 65 minutes. The process and regeneration temperature graphs as well as the process humidity ratio look fairly accurate. The initial upswing on the regeneration humidity ratio graph is slightly higher (2.1 versus 1.75) than the result shown by Brandemuehl. For a rough approximation, the result appears to be in the ballpark. The two models differ significantly in how the transfer coefficients are calculated and this could easily account for the difference.
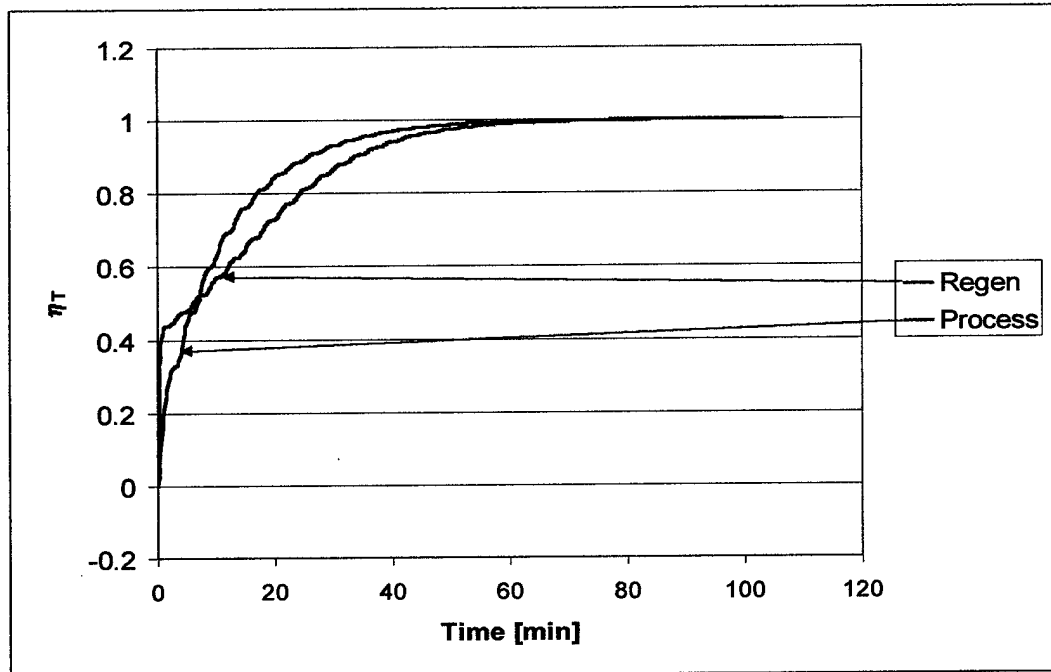
Figure 89. Transient Response Curves for Temperature of the NovelAire WSG Wheel with the Parameters from Brandemuehl [1982]
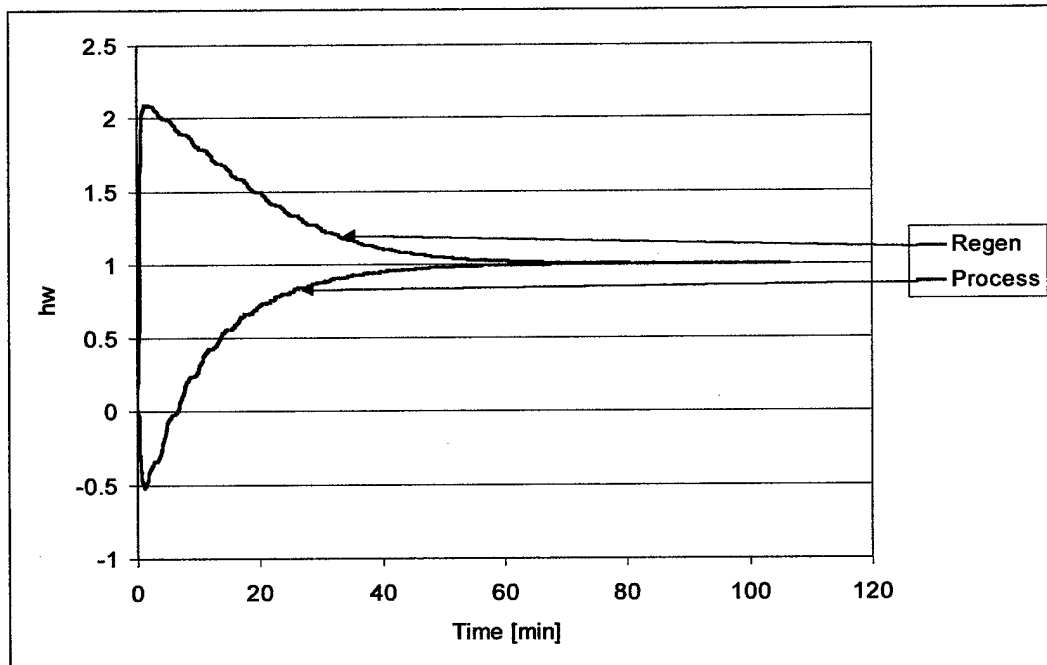
Figure 90. Transient Response Curves for Humidity Ratio of the NOvelAire WSG Wheel with the Parameters from Brandemuehl [1982]

Summary

The parametric analysis just completed shows that the ambient conditions, operational characteristics, and the wheel hardware parameters can significantly affect both the steady-state and transient response time of the rotary desiccant wheel. Depending upon how these factors are combined, the transient response time can be decreased or increased by several orders of magnitude.

Operational factors. Lowering the regeneration temperature can decrease the steady-state MRC by as much as 47% and increase the transient response time by 44% for a properly designed and efficient system. Optimized wheelspeed and flowrate can improve steady-state performance and lower transient response as well. A possible option to decrease the transient response is to "pre-heat" the wheel which can reduce the transient response by 83% as compared to the conventional case.

Ambient Conditions. Increasing the humidity ratio and increasing the temperature difference between the process and regeneration streams both improve the steady-state performance (increased MRC) of the rotary desiccant wheel. Increases in ambient humidity ratio can extend the transient response by as much as 41%. Lowering the ambient temperature can extend the transient response up to 97%.

Wheel Characteristics. The two most significant items learned from changes to the wheel itself are with the transfer profile and the desiccant particle size for regular density silica gel. Optimizing the transfer characteristics (large surface area, small hydraulic diameter, profile shape) can substantially improve the steady-state

(+19%)and transient response time(-32%). It is readily apparent that smaller particle size also improves steady-state performance (+5%) and reduces transient response time (-7%)

Most of the improvements to operational settings and wheel design to minimize the transient will also improve the steady-state response. Individual parameters can also be incorporated into non-dimensional variables for cross comparison of heat and mass transfer devices.

Clearly design of the wheel can be accomplished using these characteristics to optimize its performance.

- Maximizing transfer area while minimizing excess desiccant mass (minimum necessary material thickness for structure).

- Optimizing the wheel depth can also get the most out of the wheels performance without wasting material. Of course, this must be balanced against structural and durability considerations.

- Using the smallest practicable desiccant particle

Comparison of the non-dimensional variables such as NTU indicates a large difference between the process and regeneration inlet values due to the temperature and moisture effects on various air and matrix properties. This indicates a strong dependence on temperature and moisture content and indicates that a constant value for NTU for stream or wedge will be less accurate.

CHAPTER 9. CONTROL STRATEGIES

While the parametric analysis allows one to see the effect of various factors on the steady-state and transient response, the value of the model and the transient information it can generate is to apply it towards an actual problem. This chapter will illustrate how the model can be used to analyze various control strategies incorporating the transient response of the rotary desiccant wheel.

The primary driving requirement in determining the type of rotary desiccant wheel needed and how it is operated is the airflow required and the amount of moisture removal or MRC. In some cases, it is helpful to put the MRC in terms of the airflow for comparison, (MRC/(m³/s).

These two requirements can be met with the proper combination of wheel size, wheel split, and regeneration temperature.

Assuming the correct size of wheel and correct wheel split to handle the flowrate, the MRC can be met by optimization of the regeneration temperature and wheel speed. Figure 92 shows that an optimum regeneration temperature and wheel speed exists for a given wheel model and wheel split based on the MRC per the energy consumed. This must be balanced against the required MRC to ensure that the point at which the wheel is most efficient also has sufficient moisture removal capacity.
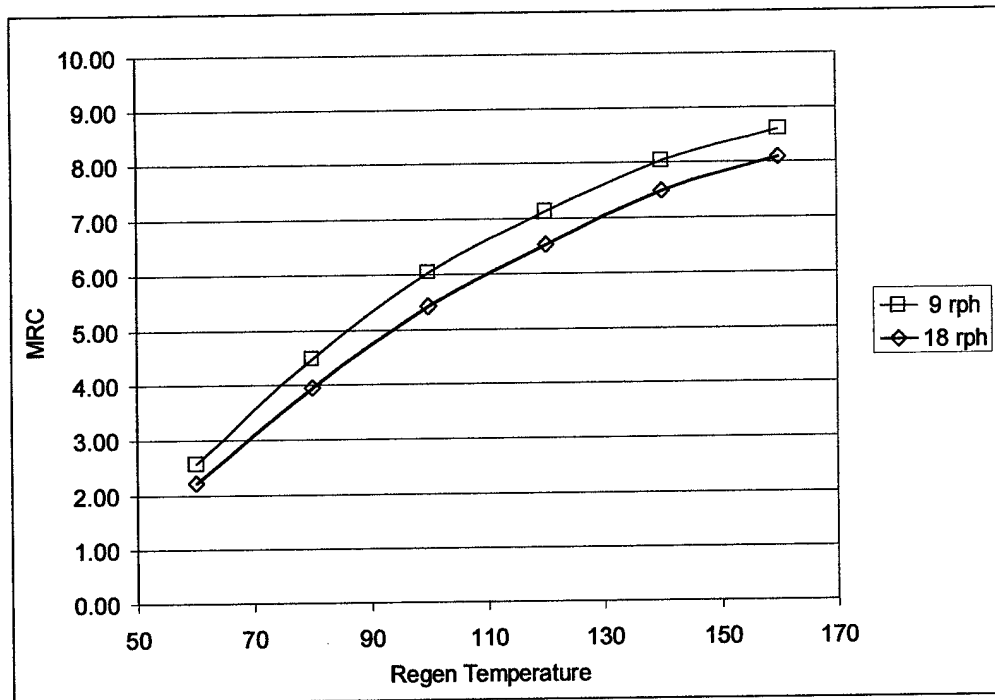
Figure 91. Graph of MRC Versus Regeneration Temperature for Different Wheelspeeds
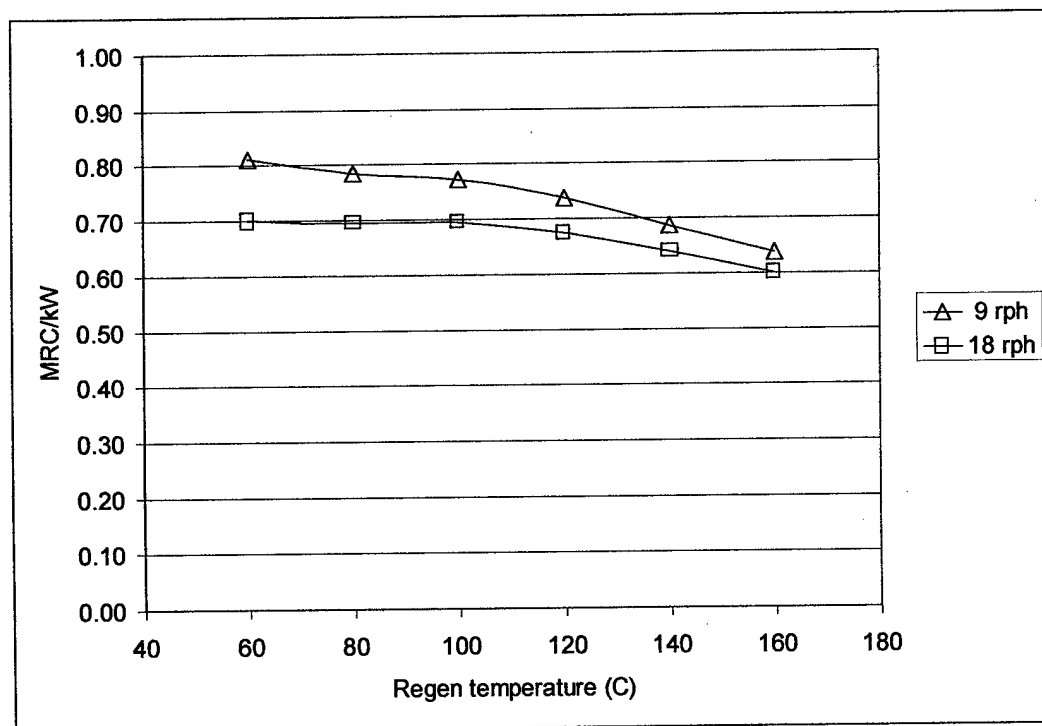
Figure 92. MRC Efficiency for a Rotary Desiccant Wheel over Various Regeneration Temperatures and Wheel Speeds

184

Regen Temp	Airflow (m³/s)	MRC (kg/hr)	MRC/airflow (MRC/m³/s)	Regen Energy (kW)	(MRC/kW)
at 18 rph					
60	0.381	2.21	5.79	3.151	0.70
80	0.381	3.95	10.35	5.690	0.69
100	0.381	5.40	14.18	7.779	0.69
120	0.381	6.51	17.10	9.659	0.67
140	0.381	7.49	19.67	11.732	0.64
160	0.381	8.09	21.23	13.492	0.60
at 9 rph					
60	0.381	2.55	6.70	3.1508	0.81
80	0.381	4.46	11.72	5.6904	0.78
100	0.381	6.01	15.77	7.7786	0.77
120	0.381	7.12	18.69	9.6589	0.74
140	0.381	8.037	21.10	11.732	0.69
160	0.381	8.585	22.53	13.492	0.64

Table 49. Tabular MRC Efficiency over Various Regeneration Temperatures and Wheel Speed

Comparison of Control Strategies with the Transient Response

Another current practice to reduce the energy consumption of the wheel is to cycle the heat added to the regeneration stream to change its temperature from full-on to full-off. In this case, the MRC requirement for a facility would have to be met by the average MRC over a period of time.

A sample of this cycling strategy at a 10 minute period with the transient response is shown at Figure 93. It can be seen that there is a significant variation through the cycle and this would have to be acceptable to the facility's occupants and

materials. The average MRC was calculated at the end of the run to avoid start-up

effects and is also shown on Figure 93.

A variation of this cycling strategy is to alter the ratio at which the

regeneration heat is off or on. This is referred to as an unbalanced cycling period.

For example, the regeneration energy could be added for twice as long as the energy

is turned off (10 minutes on, 5 minutes off).

The following comparison of various dehumidification strategies takes into

account the transient response of the rotary desiccant wheel. The heat that is directly

added to the regeneration stream is the energy addition of concern. Energy required

to turn the wheel is ignored as minimal. The summary of the comparison is shown in

Table 50.
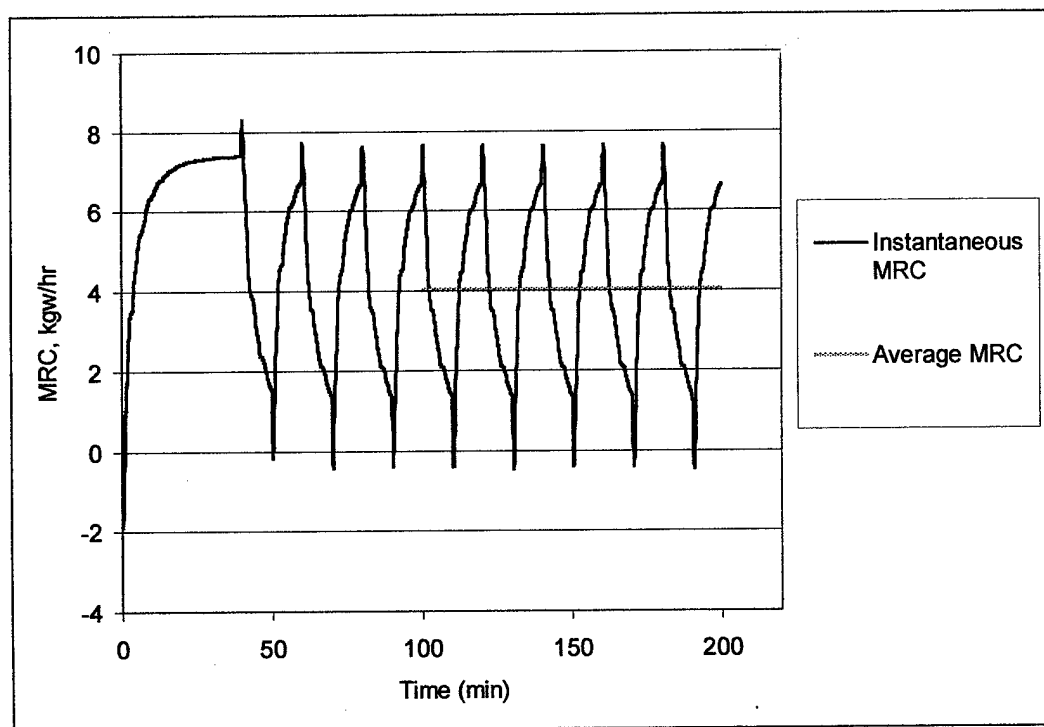
Figure 93. Cycling Strategy with 10 Minute Period and Transient
Response

186

The strategies consist of continuous regeneration at high and low temperatures, cycling without the transient response taken into account, cycling at various intervals with the transient response, and cycling with unbalanced periods with the transient response. The airflow is constant for all strategies for purposes of analysis.

The average MRC column quickly shows that continuous regeneration at the higher temperature yields the highest MRC. If the requirement, for example, is for 7 kg_w/hr, then the only alternative is to run the high temperature, continuous operation strategy.

If the MRC requirement is lower, perhaps around 3.5-4.0, then the other options are available. Specifically, running continuously with the lower regeneration temperature or cycling of the unit at a higher temperature will also work.

The next item of interest is the efficiency, or the MRCs per kilowatt. This is the amount of water removed per unit of energy. Looking at the high and low temperature continuous operation, it can be seen that the lower temperature actually has the higher moisture removal efficiency (0.69 vs 0.55). As pointed out in Figure 92, there is an optimum efficiency regeneration temperature for a given setup. Increasing the regeneration temperature beyond this optimum point will increase the MRC capacity but at a higher energy cost per unit of moisture removal.

Run	Airflow	Average MRC	Average MRC per Flowrate	Average Regen Energy	MRC/ Regen Energy
	m³/s	(kgw/hr)	(MRC/m³/s)	(kW)	(MRC/kW)
High Regen Temperature – 140C (continuous operation)	0.381	7.36	19.32	11.732	0.63
High Regen Temperature - 140C (cycled but with no transient)	0.381	3.68	9.66	5.87	0.63
Low Regen Temperature - 80C (continuous operation)	0.381	3.93	10.31	5.69	0.69
Periodic Regeneration - 5 minute cycle	0.381	4.08	10.71	5.87	0.70
Periodic Regeneration - 10 minute cycle	0.381	4.02	10.55	5.87	0.69
Periodic Regeneration - 20 minute cycle	0.381	3.91	10.27	5.87	0.67
Cycle Ratio - 10 min on and 5 min off	0.381	5.24	13.75	7.85	0.67
Cycle Ratio - 5 min on and 10 min off	0.381	2.81	7.39	3.94	0.71

Table 50. Summary Comparison of Control Strategies
Incorporating the Transient Response

If the lower temperature, continuous operation is compared with the balanced

cycling strategies, the moisture removal and the efficiencies are in the same range.

Both strategies have an MRC of approximately 4 kgw/hr. The largest difference in

efficiency (MRC/hr) between these two is approximately 3% (0.69 versus 0.67). The

cycling strategy with a very short period (5 minutes) actually has a higher efficiency

than the continuous operation at low temperature (0.70 versus 0.69). Again assuming

the moisture removal requirement is met, the system could operate at a lower

temperature continuously or at a higher temperature with cycling and with roughly

the same efficiency and effectiveness.

As mentioned above decreasing the cycle period (with balanced periods) produces an increase in efficiency. Intuitively, as the cycling period decreases, the system begins to approach continuous operation and the MRC level rises accordingly. Because the energy requirement remains the same, the efficiency improves. The limiting factor, in this case, maybe fatigue on the system with the short cycle period. For example, cycling the burner switch or hot water valve too frequently may cause prematurely failure.

Altering the cycling ratio can also have interesting effects. The ratio with longer regeneration time (10 minutes on, 5 minutes off) can produce even higher average MRC values than the balanced ratio and with a slight drop in efficiency (0.67). The ratio with longer recovery time (5 minutes on, 10 minutes off) actually had the highest efficiency (0.71) but also the lowest MRC (2.81).

There are numerous configurations that can be tested to optimize the effectiveness and efficiency of a given system. In order to achieve meaningful results, this must start with an accurate moisture removal requirement for the facility and its occupants.

Cooling Coil Comparison

It makes sense to roughly compare the effectiveness and the efficiency of the desiccant wheel to a cooling coil for dehumidification to have a feel for its performance. This comparison will use a "typical" cooling coil, the NovelAire desiccant wheel used in this research, and the ARI standard inlet condition (35 °C / 40% RH / 0.0142 $kg_{water}/kg_{dry\ air}$). Using a standard coil with an SHR = 0.75 and the standard inlet conditions listed above, the cooling coil can drop the humidity ratio to

approximately 0.011. The NovelAire wheel operating under its manufacturer's recommended settings can achieve a humidity ratio of 0.094. From a theoretical standpoint, the cooling coil can remove moisture down to the humidity ratio corresponding to the dry bulb temperature at freezing or 0.004. The desiccant wheel can achieve a humidity ratio of almost zero with higher regeneration temperature and cascading.

Looking at efficiency, the typical coil will use a COP of 3.0. Looking strictly at moisture removal, MRC, divided by the energy input or kilowatts will be the parameter to compare the systems. For a typical cooling coil, the MRC/kw is equal to about 1.2. The desiccant wheel from this research has a ratio range of about 0.63 to 0.71.

This indicates that the desiccant wheel can be more effective at moisture removal (especially with increased regeneration temperature) while the cooling coil is generally more efficient. Because the desiccant wheel uses lower quality thermal energy and the cooling coil uses higher quality electrical energy, the operational cost of the desiccant wheel may be comparable to the cooling coil. It needs to be remembered this analysis only takes the moisture removal into account. Additional energy will be required to bring the outlet stream to a particular temperature and relative humidity.

CHAPTER 10. CONCLUSIONS AND RECOMMENDATIONS

Conclusions

The primary objective of this research was to predict and characterize the transient response of rotary desiccant wheels for dehumidification. This was accomplished by development of a computer model to predict the transient response with improvements to previous efforts. Secondly, experiments were done to observe the transient response of a current, commercially available rotary desiccant wheel. The model was then validated using the experimental results both from the airstream outlet states and thermographically from the desiccant wheel surfaces. After validation, the model was used to characterize the desiccant wheel transient response through a parametric analysis. Finally, some control strategies were attempted in order to see if the transient could be applied more efficiently.

Model Development. This research developed a computer model for observing the transient response of the rotary desiccant wheel. The model is based on fundamental thermodynamic and heat and mass transfer principles to ensure correct prediction of physical phenomena. The computer routines were designed to be robust for a variety of conditions and yet computer performance was kept in mind to optimize user convenience. It was written in Fortran 90 and developed with modularity in mind in order to make it flexible for use by future researchers.

The model differs from previous models in several different respects. The first is the successful use of the parabolic concentration profile (PCP) for the transient response of the rotary desiccant wheel with the finite difference method. The PCP

assumes that the moisture profile within a particle is parabolic. It uses the readily available effective diffusivity (D_s) property as the means to take into account the solid side diffusion resistance of water into the desiccant. This allows calculation of the equilibrium humidity ratio at the surface of the particle. Convective heat and mass transfer coefficients can then be determined analytically. The PCP concept has been proven a valid profile for the moisture content within a desiccant particle by previous researchers. The PCP profile is fundamentally more correct than the PGS, or pseudo-gas side, model which uses a combined gas and solid-side transfer coefficient much like a lumped capacitance approach. This transfer coefficient must be experimentally determined which reduces the flexibility of the model. Unlike the most rigorous gas and solid side or GSS model, the PCP does not require the solution of an additional second order differential equation accounting for moisture diffusivity within the particle.

Additionally, previous researchers have used an average NTU for an entire stream or wedge. The model from this research calculates NTU at *every* element. The difference in NTU between inlet states for the process and regeneration streams can be as high as 67% making it relatively substantial.

Several improvements were also made from a numerical standpoint. It was recognized that the set of finite difference equations fit the tri-diagonal matrix pattern. Solution of the tri-diagonal matrix is much faster and more efficient than simple matrix inversion techniques. This is then solved iteratively until convergence is achieved. The solution of the non-linear a2 coefficient equation was also improved

by the use of the bisection method with bracketing. This highly stable and robust technique avoided the instabilities of other previous methods.

Experimental Results. Experiments were conducted within the desiccant lab facilities at the National Renewable Energy Laboratory (NREL) in Golden, CO. This facility is normally designed for steady-state analysis of rotary desiccant wheels and some alteration was required in order to handle transient changes. Experiments were performed on a NovelAire WSG (wound silica gel) desiccant wheel. The transient response was observed through six tests using step increases and decreases to regeneration temperature, wheelspeed, and flowrate. The most significant step change was for regeneration temperature and the time to complete the step increase was approximately 22 minutes.

Validation. The experimental results were used to validate the computer model by using input data from the experimental runs and running it through the model. The experimental data was also compared with historical data with curve fits from the NovelAire Company. The steady-state results were relatively close for all parameters and within 10 percent of each other.

The transient response curves exhibited some interesting characteristics. The change in regeneration temperature exhibited the classic logarithmic curve which could be used to determine the time constant of the system. The change in wheelspeed produced converging oscillations corresponding to the rotational period of the wheel.

The root mean square error statistic was used as the basic quantitative parameter to evaluate the equality of the experimental and numerical transient. The

predicted transient response for the experiments was reasonably good in most cases including the all-important step change to regeneration temperature.

Discrepancies with energy balances in the experimental data can be explained by a combination of sensor accuracies and carryover/leakage within the experimental apparatus.

Desiccant Wheel Validation. The infrared thermographic camera and numerical matrices for the desiccant temperature were also used to validate the model. This was done by using a temperature histogram provided with the thermographic output combined with the numerical results of the desiccant matrix. The process-out, regeneration-in side of the wheel was used for temperature comparison. Using a χ^2 statistic, these two multinomial distributions were compared. The comparison showed the temperature distributions to be relatively close ($\chi^2 < \chi^2$ critical for a given confidence level) and therefore the experimental results validate the numerical. While the distributions were clearly equivalent in the steady-state mode; the early transient period showed less agreement. This can be explained; however, by metal structural members blocking portions of the matrix. The structural members' higher thermal conductivity and lower specific heat would present a higher temperature to the thermographic camera. The structural members would also reach a higher temperature faster.

The numerical matrix can also be put in a visual graphic form that can be used to observe the temperature and moisture gradients during the transient period. For the graphs accompanying the validation runs the temperature gradients set up fairly quickly (approximately 4 minutes) relative to the desiccant moisture gradients. This

supports the theory and evidence that the solid side mass resistance is the dominant resistance mechanism and primarily responsible for the long transient period.

Parametric Runs. A parametric analysis was performed using the NovelAire WSG parameters to see the effect different variables had upon the moisture removal capacity (MRC) after the model had been validated. The parametric analysis was divided into two distinct types: conventional and renewable. This initial comparison showed higher regeneration temperature speeds the transient response. The more balanced the wheel split, the shorter the transient response.

From this, four categories of variables were tested: operational factors, ambient conditions, wheel geometries, and wheel material properties.

- The operational factors. Increasing the regeneration temperature from 80C to 140 °C can substantially increase steady-state MRC and lower the transient response time by as much as 44%. Increasing the wheel temperature is also the predominate means of control within the desiccant wheel industry. Optimized wheelspeed and flowrate can significantly improve steady-state MRC performance and reduce the transient the same time as well.

- Ambient Conditions. The ambient conditions can have a dramatic effect upon the steady-state and transient respone as well. Decreases in temperature from 35° C to 21.6° C can increase the transient response by 97%. Increasing the humidity ratio from 40% to 70% can increase the transient response up to 41%.

    - Wheel Characteristics. The two most significant items learned from changes to the wheel itself are with the transfer profile and the desiccant

particle size for regular density silica gel. Optimizing the transfer characteristics (larger surface area, smaller hydraulic diameter, profile shape) can substantially improve the steady-state (+19%) and transient response (-42%). It is readily apparent that smaller particle size also improves steady-state performance (+5%) and reduces transient response time (-7%)

The model was also used to compare control strategies that incorporate the transient response. Although increasing regeneration temperature will produce greater moisture removal, there is an optimal regeneration temperature for a given configuration and that increasing beyond this temperature will reduce the system efficiency. Cycling the wheel can also have useful results if the MRC requirement can be met and low temperature heat is unavailable. The efficiency with cycling the wheel is comparable to using lower temperatures.

Recommendations

There are several areas where additional work on the transient response of rotary desiccant wheels can be achieved.

1. Determine the transient response of desiccant wheels with other materials such as zeolytes and molecular sieves

2. Optimize control strategies incorporating the transient response

3. Integrate other components (cooling coil, heat pipe, etc.) with the model to see the combined effects

APPENDIX A. AIR AND

MOISTURE RELATIONS

T, K	Cpwv, kJ/(kg*K)
273.15	1.854
275	1.855
280	1.858
285	1.861
290	1.864
295	1.868
300	1.872
305	1.877
310	1.882
315	1.888
320	1.895
325	1.903
330	1.911
335	1.92
340	1.93
345	1.941
350	1.954
355	1.968
360	1.983
365	1.999
370	2.017
373.15	2.029
375	2.036
380	2.057
385	2.08
390	2.104
400	2.158
410	2.221
420	2.291
430	2.369
440	2.46
450	2.56
460	2.68
470	2.79
480	2.94

T, K	cp	k
100	1.032	9.34E-06
150	1.012	1.38E-05
200	1.007	1.81E-05
250	1.006	2.23E-05
300	1.007	2.63E-05
350	1.009	3.00E-05
400	1.014	3.38E-05
450	1.021	3.73E-05
500	1.03	4.07E-05
550	1.04	4.39E-05
600	1.051	4.69E-05
650	1.063	4.97E-05
700	1.075	5.24E-05
750	1.087	5.49E-05
800	1.099	5.73E-05

The tabular data listed here are

the basic air and moisture values used

for curve fitting. They are from

[Incropera and Dewitt, 1986].
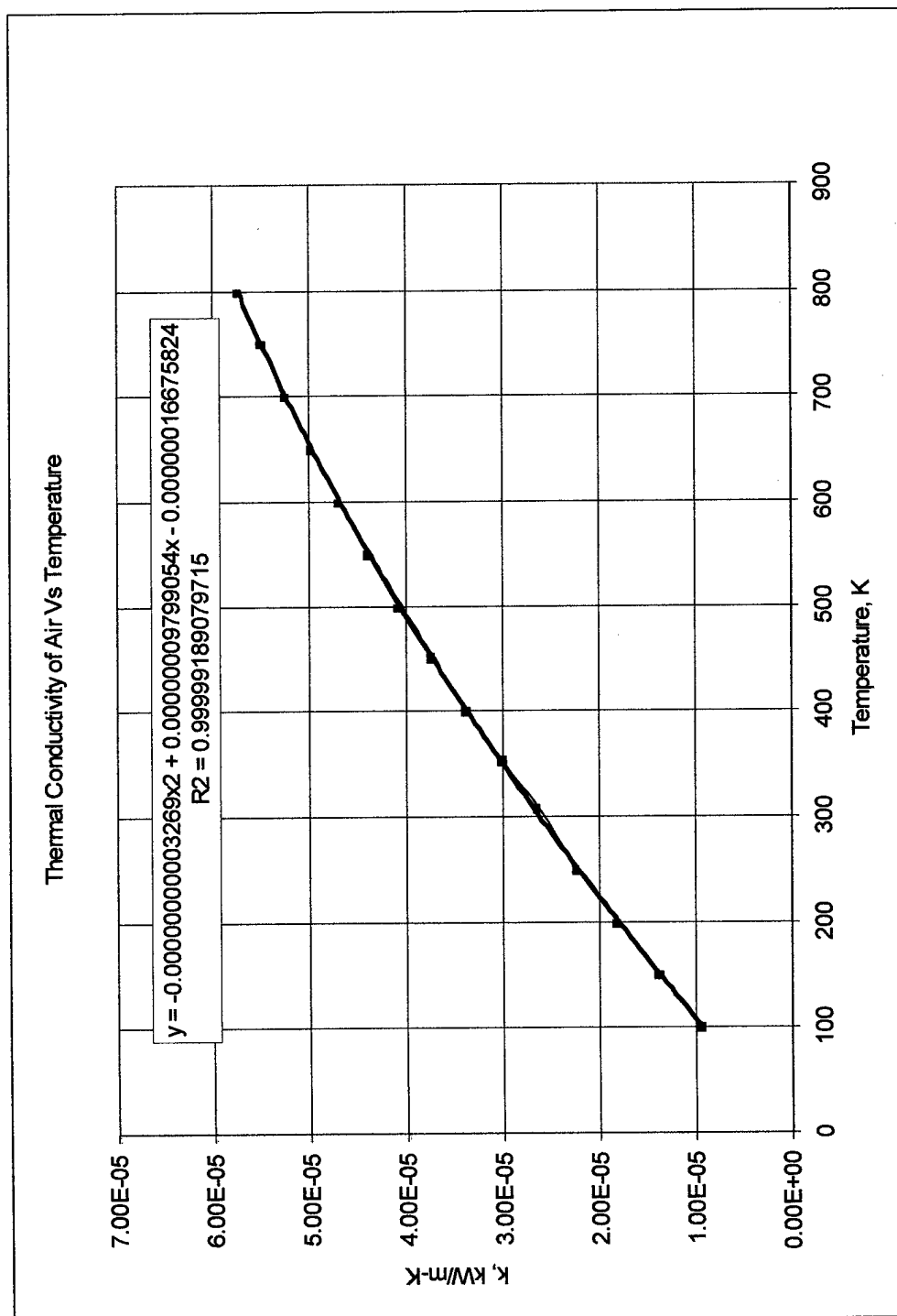
Figure 94. Graph and Equation of the Thermal Conductivity of Air Versus Temperature

198
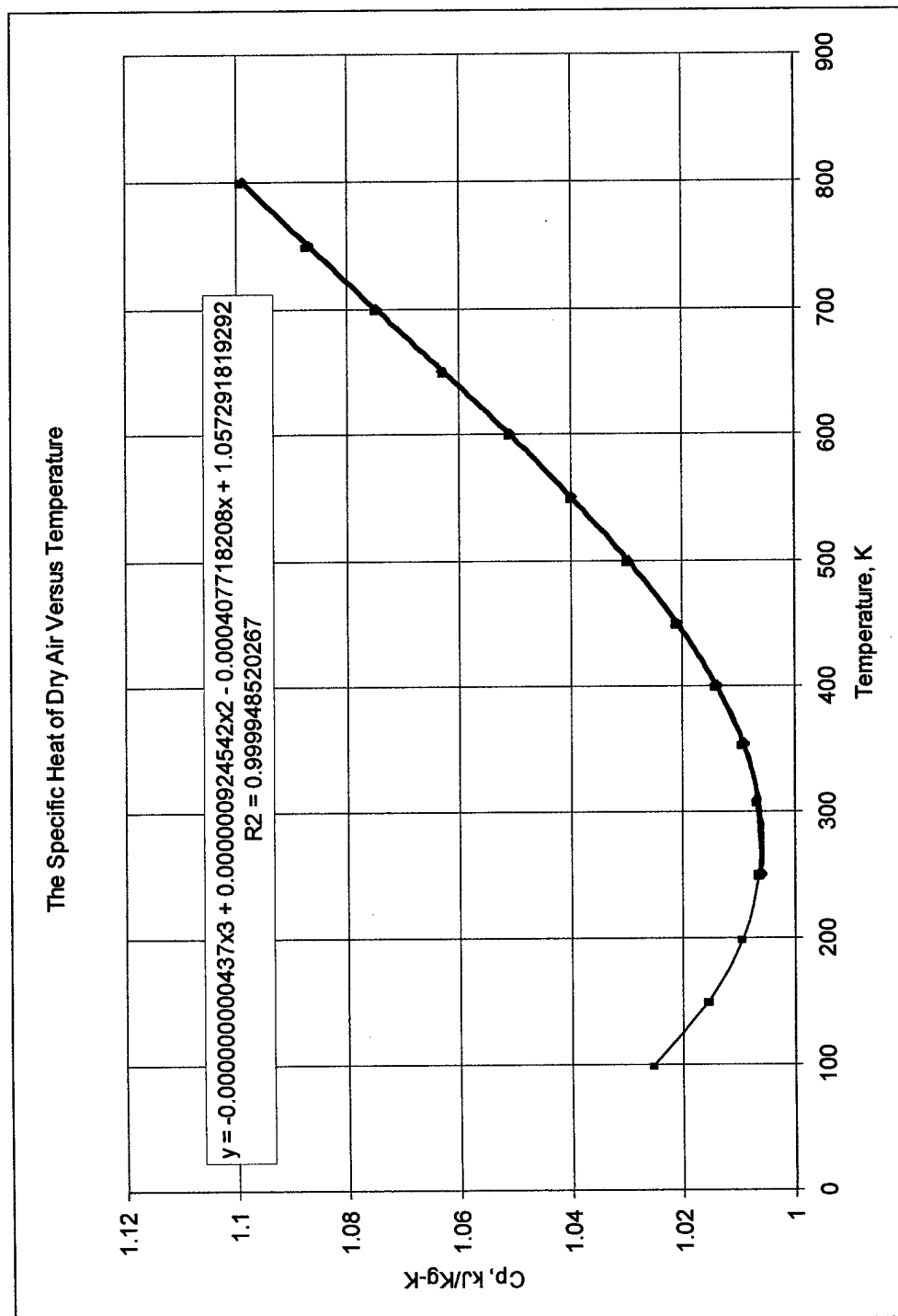
Figure 95. The Graph and Equation of the Specific Heat of Dry Air Versus Temperature
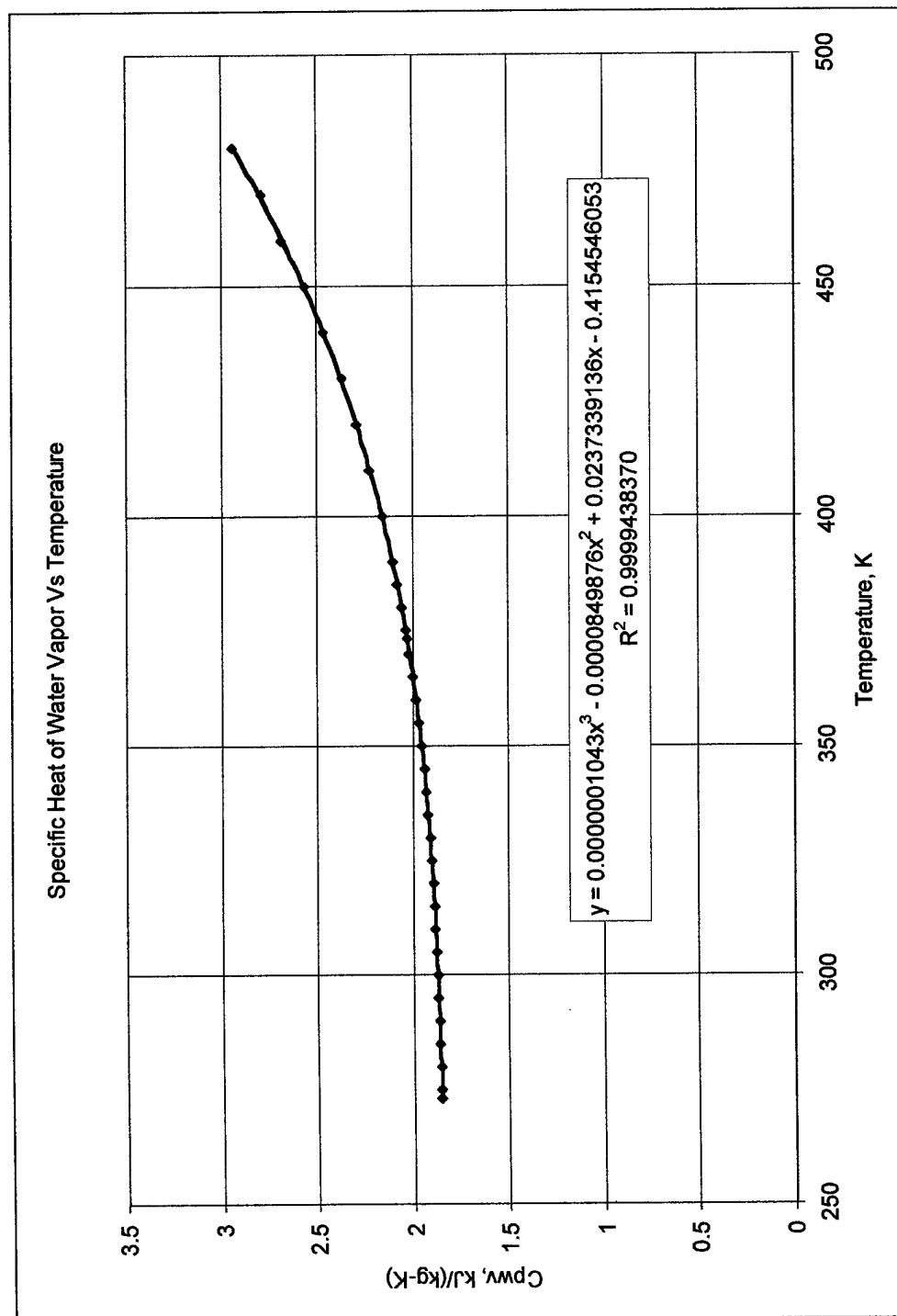
Figure 96. Graph and Equation of the Specific Heat of Water Vapor Versus Temperature

APPENDIX B. PARABOLIC CONCENTRATION PROFILE (PCP)

This appendix shows the process for defining the relationships used with the parabolic concentration profile. This derivation was essentially done by Chant [1991]. It is included here to provide a complete understanding of the parabolic concentration concept.

The basic parabolic profile for the local moisture content is defined as:

$$W_l = a1 + (r/R)^2 a2$$

Equation 91

The conservation of mass equation for spherical coordinates assuming radial symmetry was originally from Pesaran and is shown here, Equation 92. This is the second order equation that the parabolic concentration profile relation replaces in order to save computational time.

$$\frac{\partial W_l}{\partial t} = \frac{1}{r^2} \frac{\partial}{\partial r} \left(r^2 De \frac{\partial W}{\partial r} \right)$$

Equation 92

The initial condition is as follows:

$$W(r, t = 0) = W_0(r)$$

Equation 93

The first boundary condition is for symmetry:

$$\left. \frac{\partial W}{\partial r} \right|_{r=0} = 0$$

Equation 94

The second boundary condition is for conservation of energy at the surface:

$$-\rho PD_e \left.\frac{\partial W}{\partial r}\right|_{r=R} = h_m(we - w)$$

Differentiating the parabolic profile equation, Equation 91, and inserting the surface boundary condition, Equation 95, into the result:

$$\left.\frac{\partial W_l}{\partial r}\right|_{r=R} = 2a2(R/R^2) = 2a2/R = -h_m(we(W_s,T) - w)/(\rho_P D_e)$$

To obtain the local moisture content at the surface, the relation is:

$$W_s = W_l(r = R) = a1 + a2$$

The function relating the average moisture content and the parabolic concentration profile coefficients can be found by integrating the parabolic profile over the volume of the particle and dividing by the total volume of the particle and is:

$$W = a1 + 3/5a2$$

Rearranging to solve for a1:

$$a1 = W - 3/5a2$$

Substituting the expression above into the local moisture content expression, Equation 97, to get the local moisture content at the surface as a function of a2:

$$W_s = W_l(r = R) = W + 2/5a2$$

Equation 100

To obtain for the surface moisture content, the PCP coefficient a2 must be solved for. This can be done by substituting the surface moisture expression, Equation 100, into the rate equation at the surface of the particle, Equation 96. The result is a non-linear expression for a2:

$$a2 = \frac{-h_m R}{2 \rho_P D_e} \left(we(W = 2/5a2, T) - w \right)$$

Equation 101

The surface moisture content Ws can be solved by using an iterative or convergence routine using equations Equation 101 and Equation 100. The equilibrium humidity ratio can then be found using the adsorption isotherm.

APPENDIX C. ADSORPTION ISOTHERM CHARTS FOR RD SILICA GEL
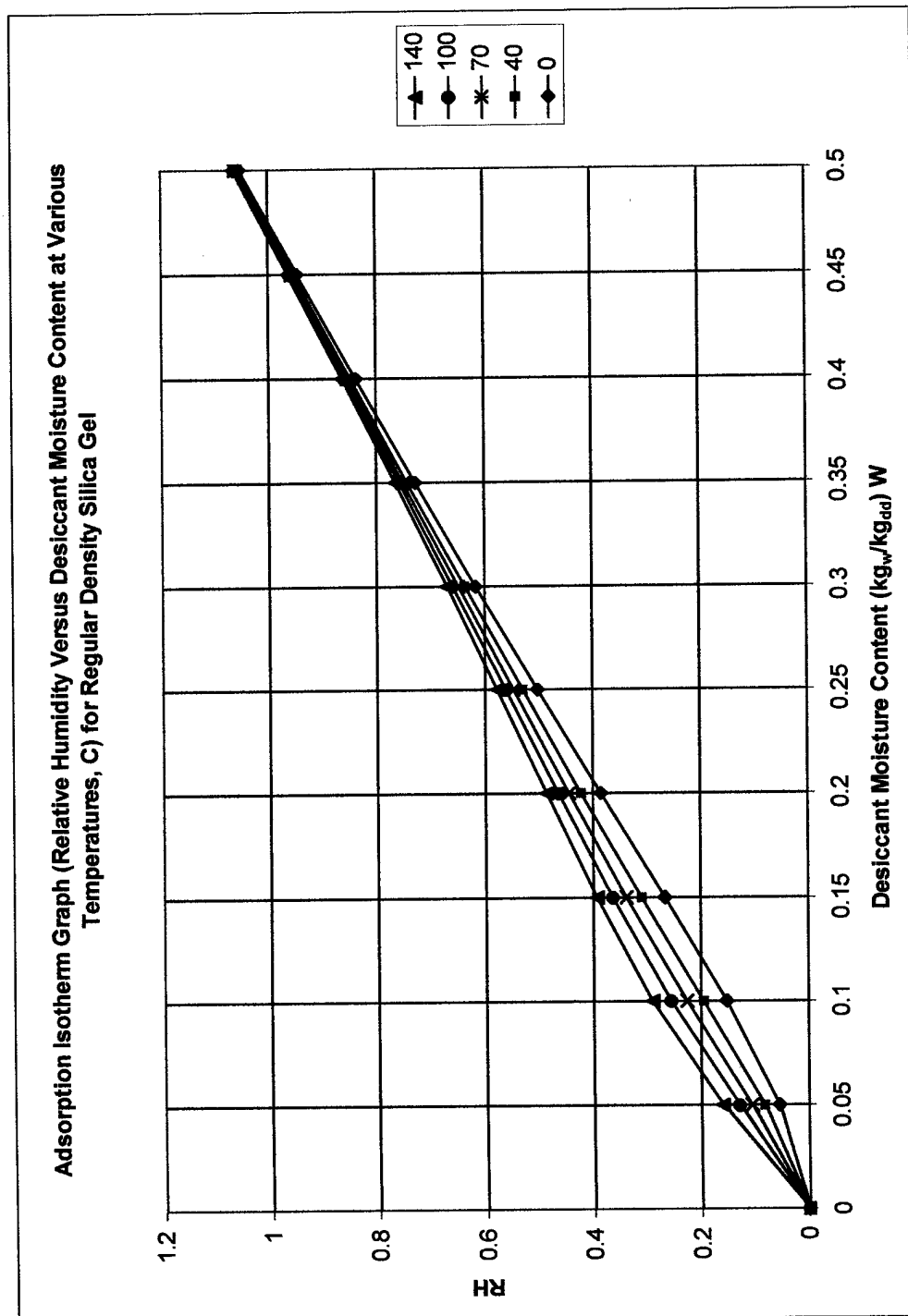
Figure 97. Adsorption Isotherm Chart in Terms of Relative Humidity for Regular Density Silica Gel

APPENDIX D. NUSSELT CURVE FIT
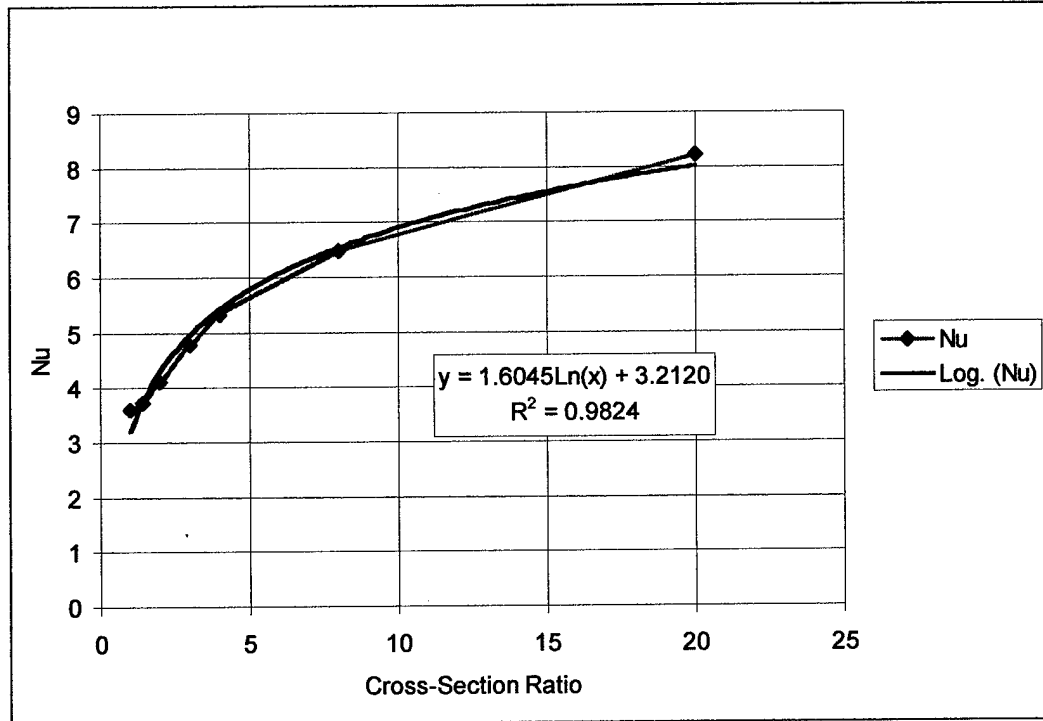
Figure 98. Graph of Nusselt Number Versus Cross Section Ratio

Cross Section Ratio	Nu
1	3.61
1.43	3.73
2	4.12
3	4.79
4	5.33
8	6.49
20	8.23

Table 51. Data Values for Nusselt Number Versus Cross Section Area [Incropera]

APPENDIX E. IMPLICIT FINITE DIFFERENCING

These are the finite difference and matrix format equations for the fully implicit method (backward differencing the time equation and central differencing across the space direction.

Mass Rate Transfer

$$w(j+1, k+1) - w(j, k+1) = NTU_{m, j}\Delta x(w_e - w)_{av}$$

where

$$(w_e - w)_{av} = [(w_e(Td(j, k+1), Wd(j, k+1), tdavg] - \frac{1}{2}[(wf(j+1, k+1) + w(j, k+1)]$$

<div align="right">Equation 102</div>

Conservation of Mass

$$3W(j, k+1) - 4W(j, k) + W(j, k-1) = -\frac{2\Delta\theta}{\beta_j\Gamma_j\Delta x}[w(j+1, k+1) - w(j, k+1)]$$

<div align="right">Equation 103</div>

Energy Transfer Rate

$$t(j+1, k+1) - t(j, k+1) = NTU_{q, j}\Delta x(T - t)_{av}$$

where

$$(Td - tf)_{av} = [Td(j, k+1)] - \frac{1}{2}[tf(j+1, k+1) - tf(j, k+1)]$$

<div align="right">Equation 104</div>

Conservation of Energy

$$3T(j,k+1) - 4T(j,k) + T(j,k-1) =$$

$$= -\frac{2\Delta\theta}{\Delta x \beta_j \Gamma_j c_{p,m}}[c_{p,ma}(t(j+1,k+1) - t(j,k+1)) + i_{ad}(w(j+1,k+1) - w(j,k+1))]$$

<div align="right">Equation 105</div>

Matrix Format

In order to use various numerical solution techniques, a convenient way of expressing the equations is in a matrix format. The finite difference equations are first placed in a format where

j ,k (+1 step) = current j,k

Mass Rate

$$(1 + \frac{NTU_m\Delta x}{2})w(j+1,k+1) = NTU_{m,j}\Delta x w_e + (1 - \frac{NTU_m\Delta x}{2})w(j,k+1)$$

<div align="right">Equation 106</div>

Mass Conservation

$$3W(j,k+1) + \frac{2\Delta\theta}{\beta_j\Gamma_j\Delta x}w(j+1,k+1) = 4W(j,k) - W(j,k-1) + \frac{2\Delta\theta}{\beta_j\Gamma_j\Delta x}w(j,k+1)$$

<div align="right">Equation 107</div>

Energy Rate

$$(\frac{NTU_q\Delta x}{2} + 1)t(j+1,k+1) - NTU_q\Delta x T(j,k+1) = (1 - \frac{NTU_q\Delta x}{2})t(j,k+1)$$

<div align="right">Equation 108</div>

208

Energy Conservation

$$3T(j,k+1)+\frac{2\Delta\theta}{\Delta x\beta_j\Gamma_jc_{p,m}}c_{p,mat}(j+1,k+1)+\frac{2\Delta\theta}{\Delta x\beta_j\Gamma_jc_{p,m}}i_{ad}w(j+1,k+1)=$$

$$=4T(j,k)-T(j,k-1)+\frac{2\Delta\theta}{\Delta x\beta_j\Gamma_jc_{p,m}}[c_{p,mat}(j,k+1)+i_{ad}w(j,k+1)]$$

Equation 109

These equations are then placed in a matrix notation:

Ax=b

A is the matrix of coefficients, x is the current solution, and b is the remainder on the right side of the equations. For the current set of finite difference equations, the arrangement is shown in Figure 99. By moving the order of the variables and the equations around, the matrix format is still sparse yet banded

$$A$$

$$\begin{bmatrix} 3 & \dfrac{2\Delta\theta}{\beta\Gamma_j\Delta x} & 0 & 0 \\[2ex] 0 & (1+\dfrac{NTU_m\Delta x}{2}) & 0 & 0 \\[2ex] 0 & \dfrac{2\Delta\theta}{\Delta x\beta_j\Gamma_jc_{p,m}}i_{ad} & 3 & \dfrac{2\Delta\theta}{\Delta x\beta_j\Gamma_jc_{p,m}}c_{p,ma} \\[2ex] 0 & 0 & -NTU_q\Delta x & (\dfrac{NTU_q\Delta x}{2}+1) \end{bmatrix} \begin{matrix} MassConservation \\[2ex] MassRate \\[2ex] EnergyConservation \\[2ex] EnergyRate \end{matrix}$$

$$x$$

$$\begin{bmatrix} W(j,k+1) \\ \\ w(j+1,k+1) \\ \\ T(j,k+1) \\ \\ t(j+1,k+1) \end{bmatrix}$$

$$b$$

$$\begin{bmatrix} 4W(j,k) - W(j,k-1) + \dfrac{2\Delta\theta}{\beta_j\Gamma_j\Delta x}w(j,k+1) \\ \\ NTU_m\Delta x w_e + (1 - \dfrac{NTU_m\Delta x}{2})w(j,k+1) \\ \\ 4T(j,k) - T(j,k-1) + \dfrac{2\Delta\theta}{\Delta x\beta_j\Gamma_j c_{p,m}}((c_{p,mat}(j,k+1) + i_{ad}w(j,k+1)) \\ \\ (1 - \dfrac{NTU_q\Delta x}{2})t(j,k+1) \end{bmatrix}$$

Figure 99. Completed Matrix

APPENDIX F. DETAILED NOVELAIRE WSG WHEEL DATA
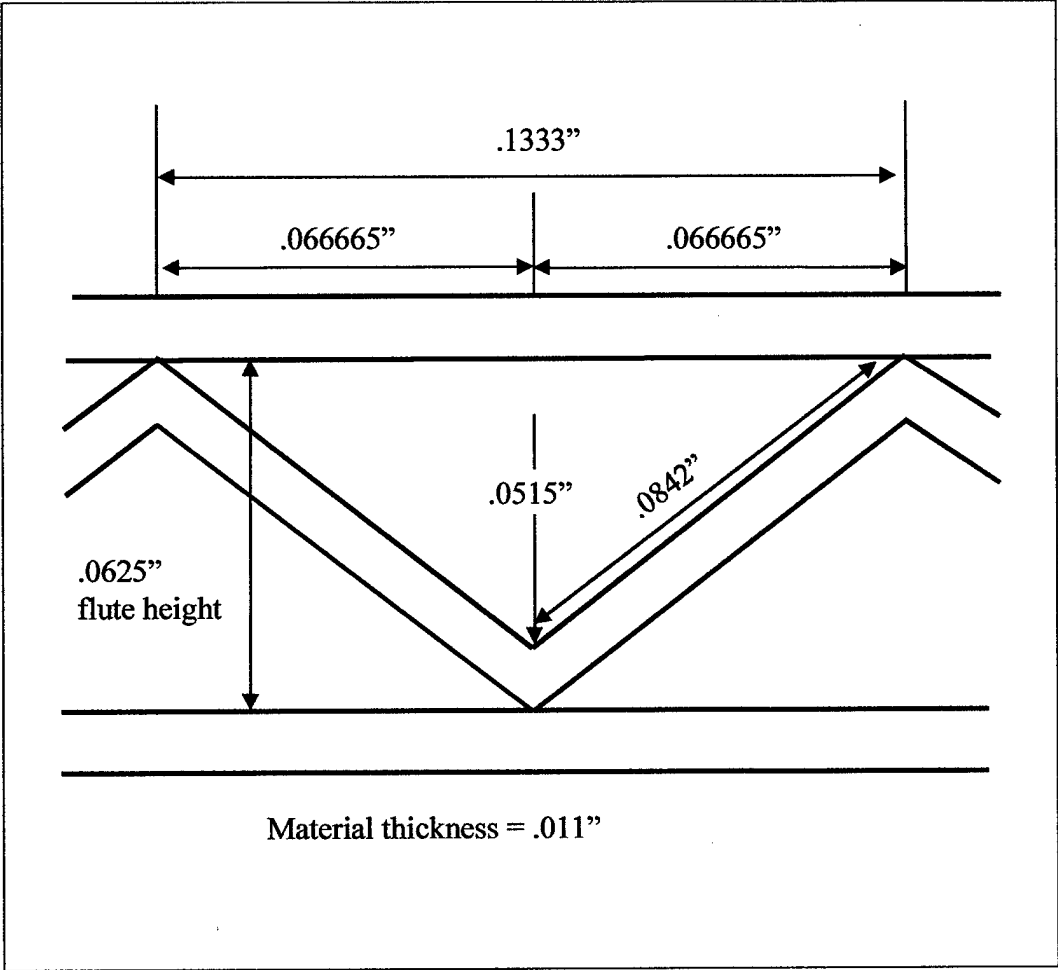
Figure 100. Triangular Profile
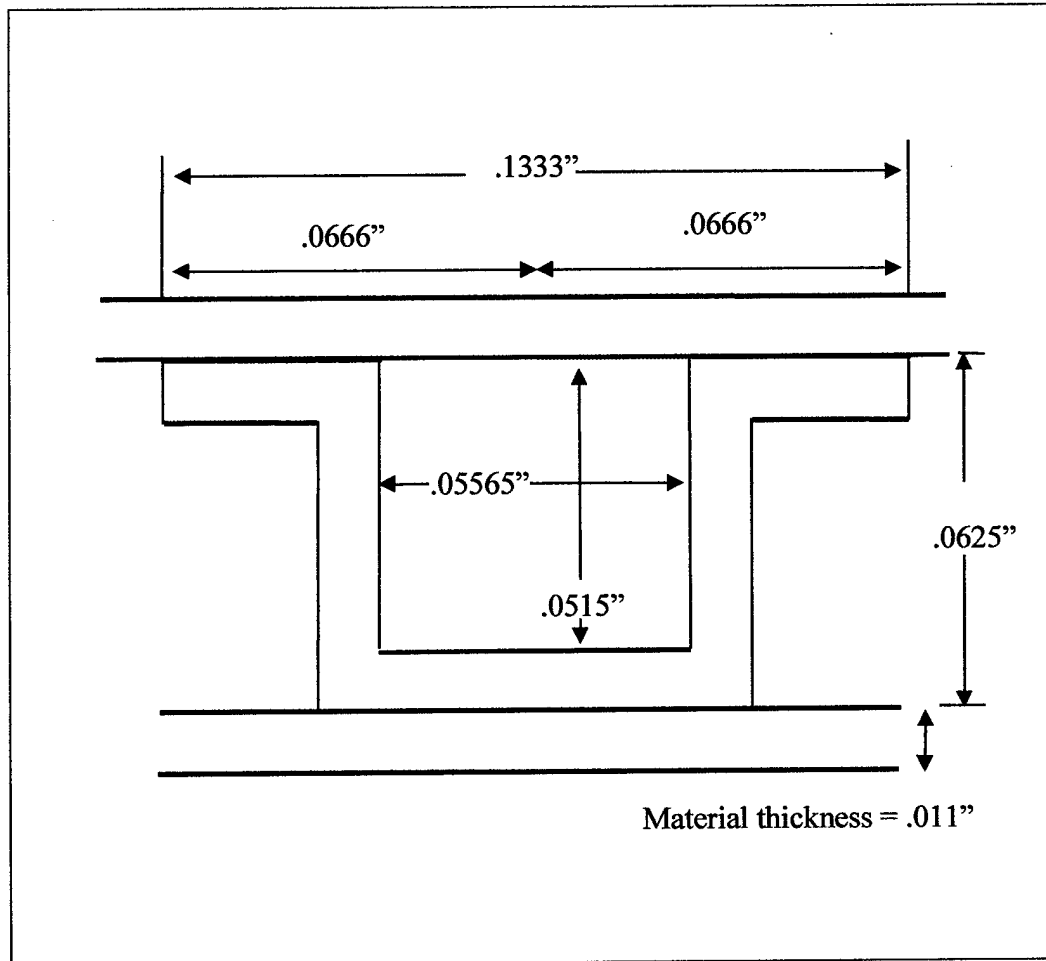
Figure 101. Rectangular Profile

ITEM	VALUE	UNIT	VALUE	UNIT
	TRIANGULAR FLUTE		RECTANGULAR FLUTE	
external wheel dimensions				
depth	0.2	m	0.2	m
diameter	0.55	m	0.55	m
radius	0.275	m	0.275	m
total face area	0.23758	m2	0.237582	m2
total face area	2.55639	ft2	2.556392	ft2

ITEM	VALUE	UNIT	VALUE	UNIT
	TRIANGULAR FLUTE		RECTANGULAR FLUTE	
volume	0.047516	m3	0.047516	m3
volume	1.678034	ft3	1.678034	ft3
hub diameter	0.08890	m	0.088900	m
hub radius	0.044450	m	0.0444500	m
hub diameter	3.5	in	3.5	in
hub radius	1.75	in	1.75	in
hub area	0.006207	m2	0.006207	m2
hub area	0.06678	ft2	0.06678	ft2
hub volume	0.00124	m3	0.001241	m3
hub volume	0.04384	ft3	0.043841	ft3
width of spoke	0.12	in	0.12	in
width of spoke	0.003048	m	0.003048	m
length of spoke	0.22737	m	0.227501	m
number of spokes	4	ea	4	ea
area covered by spokes	0.00277	m2	0.002773	m2
area covered by spokes	0.02982	ft2	0.029845	ft2
depth of spoke	1	in	1	in
depth of spoke	0.08333	ft	0.08333	ft
depth of spoke	0.02540	m	0.025400	m
volume of spokes	7.041E-05	m3	7.0452E-05	m3
volume of spokes	0.002486	ft3	0.002488	ft3
volume of area between spokes	0.000413	m3	0.000413	m3
volume of area between spokes	0.014606	ft3	0.014614	ft3
thickness of band	0.125	in	0.12	in
thickness of band	0.003175	m	0.003048	m
face area of band	0.058688	ft2	0.056354	ft2
face area of band	0.005454	m2	0.00523	m2
depth of band	0.2	m	0.2	m
volume of band	0.03852	ft3	0.036991	ft3
volume of band	0.00109	m3	0.001047	m3
face area of wheel without band, spokes, hub	0.22314	m3	0.223364	m3
face area of wheel without band, spokes, hub	7.8804	ft3	7.888055	ft3
volume of wheel without band, spokes, hub	0.04511	m3	0.04515	m3

ITEM	VALUE	UNIT	VALUE	UNIT
	TRIANGULAR FLUTE		RECTANGULAR FLUTE	
volume of wheel without band, spokes, hub	1.59318	ft3	1.594713	ft3
volume of wheel without above and space between spokes	0.04470	m3	0.044743	m3
volume of wheel without above and space between spokes	1.578576	ft3	1.580099	ft3
internal wheel dimensions				
flute height	0.0625	in	0.0625	in
material or base thickness	0.011	in	0.011	in
corrugation height (base+flute)	0.0735	in	0.0735	in
flutes per foot	90	fl/ft	90	fl/ft
flute base	0.13333	in	0.133333	in
half flute base	0.06666	in	0.066666	in
internal flute height	0.0515	in	0.0515	
internal flute diagonal	0.084241	in	N/A	in
(using pythagorean theorem)				
internal flute width	N/A		0.055666	in
area of flute for hydraulic diam	0.00343	in2	0.002866	in2
perimeter of flute for hydraulic diam	0.301817	in	0.214333	in
hydraulic diameter, 4*area/perimeter	0.045502	in	0.053502	in
hydraulic diameter, 4*area/perimeter	0.00115	m	0.001358	m
length of fluted material per flute	0.16848	in	0.236333	in
length of transfer area per flute		in	0.214333	in
length of fluted material per foot	15.16353	in	21.27	in
(# flutes in foot * 2 * length)				
length of fluted material per foot	1.26362	ft/lin ft matrix	1.7725	ft/lin ft matrix
total length of layer per ft (flute+1ft base)	2.26362	ft material/ ft matrix	2.7725	ft material/ ft matrix
length of transfer area per foot		ft	19.29	in
length of transfer area per foot			1.6075	ft
total number of "layers" in a vertical	163.2653	layers	163.2653	layers
foot of material (12 in / flute height)				
total lf or sf of all material in a cubic ft	369.5719	sf/ft3	452.6530	sf/ft3
total transfer area in a cubic foot	0	ft2/ft3	262.4489	ft2/ft3

214

ITEM	VALUE	UNIT	VALUE	UNIT
	TRIANGULAR FLUTE		RECTANGULAR FLUTE	
foot, (# of layers * length of layer)				
total sf of material in the wheel	588.795	sf/wheel	721.1590	sf/wheel
total transfer area in the wheel	1177.591	sf	414.6954	sf tr/wheel
total sm of material in the wheel	54.7207	m2	67.02221	m2
total heat and mass transfer area in wheel	109.44	m2	38.54046	m2
glue area	139.297	ft2	N/A	
glue area	12.9458	m2	N/A	
total heat and mass transfer area in wheel	96.4957	m2	38.54046	m2
flow area				
area covered by thickness of matrix	0.53972	ft2	0.66106	ft2
area covered by thickness of matrix	0.05016	m2	0.06143	m2
total flow area	1.92004	ft2	1.79869	ft2
total flow area	0.17844	m2	0.167165	m2
flow area in process period	0.13383	m2	0.12537	m2
flow area in regen period	0.0446	m2	0.041791	m2
flow area in process period	1.44003	ft2	1.349021	ft2
flow area in regen period	0.48001	ft2	0.449673	ft2
process area percent of total	0.75	%	0.75	%
regen area percent of total	0.25	%	0.25	%
matrix properties				
density of material, lbs/pt, basis wt	10	lbs/pt, lbs/mil	10	lbs/pt
"point"	1	mil	1	mil
mil	0.001	in	0.001	in
weight of material, basis	130	lb	130	lb
"basis" weight	3000	sf	3000	sf
thickness of material	11	mil	11	mil
thickness of material	0.011	in	0.011	in
density of sheet of material	0.04333	lbm/sf	0.043333	lbm/sf
density of ft3	16.0147	lbm/ft3	19.61496	lbm/ft3
density of m3	256.556	kg/m3	314.2317	kg/m3

ITEM	VALUE	UNIT	VALUE	UNIT
	TRIANGULAR FLUTE		RECTANGULAR FLUTE	
mass of wheel excluding hub, spokes, band	25.51447	lbm	30.99359	lbm
mass of wheel excluding hub, spokes, band	11.5742	kg	14.18983	kg
density of steel spokes	490.089	lbm/ft3	490.0896	lbm/ft3
density of steel spokes	7854	kg/m3	7854	kg/m3
wheel composition by mass				
mass percentage of desiccant	0.7		0.7	
percentage of binder	0.15		0.15	
percentage of fiber	0.15		0.15	
mass of desiccant	8.10199	kg	9.932882	kg
mass of binder	1.736140	kg	2.128474	kg
mass of fiber	1.736140	kg	2.128474	kg
mass of spokes	0.55302	kg	0.553332	kg
mass of hub				
mass of band				
secific heats				
specific heat of hub	0.434	kj/(kg-k)	0.434	kj/(kg-k)
specific heat of band	0.434	kj/(kg-k)	0.434	kj/(kg-k)
specific heat of spokes	0.434	kj/(kg-k)	0.434	kj/(kg-k)
specific heat of desiccant	0.921	kj/(kg-k)	0.921	kj/(kg-k)
specific heat of fiber		kj/(kg-k)		kj/(kg-k)
25c	1.42	kj/(kg-k)	1.42	kj/(kg-k)
100c	2.01	kj/(kg-k)	2.01	kj/(kg-k)
180c	2.515	kj/(kg-k)	2.515	kj/(kg-k)
use specific heat at 100c	2.01	kj/(kg-k)	2.01	kj/(kg-k)
specific heat of binder	2.093	kj/(kg-k)	2.093	kj/(kg-k)
specific heat of binder	0.5	btu/(lbm-f)	0.5	btu/(lbm-f)
matrix specific heat	1.80021	kj/(kgdd-k)	1.824391	kj/(kgdd-k)

Table 52. Detailed Wheel Data

APPENDIX G. NOVELAIRE DWR3.0 OUTPUT

Title:	Diss Model: WSG 550x200
Date: 31-Mar-99	Custom Model
Wheel Diameter: 550 mm	Face Velocity
Wheel Depth 200 mm	Process Side 462 sfpm
	Regeneration Side 453 sfpm
Drive Motor 1/3 HP	
Wheel Speed 18 RPH	Pressures
Hub Diameter 4.5 in	OA Static 331.60 in. W.G.
Cassette Dimensions	IA Static 331.60 in. W.G.
Height 42 in.	Process Side Loss 1.40 in. W.G.
Width 42 in.	Regen. Side Loss 1.69 in. W.G.
Depth 6.5 in.	
	Flow Ratio
Heat Values	Regen/Process 0.327
Regen Heat 54,460 BTU/h	
per lb H2O 2160 BTU/lb H2O	Regeneration Fraction 25%
Proc. Sens. Gain 40,825 BTU/h	Regen Temperature 273 °F
per lb H2O 1619 BTU/lb H2O	Water Adsorption
Energy Cost $613 @ 2000 h/yr	Dynamic Capacity 25.2 lb/h
	Grain Depression 46.8 gr/lb

Altitude 5000 ft.	Temp °F	W.B. Temp °F	Flow Rate Cfm	Flow Rate scfm	Mass Flow lb/min	Hum Ratio lb/lb	Hum Ratio gr/lb	Dew Point °F	RH %	Enth-alpy BTU/lb
1 Process In	95.0	74.4	1,104	835	62.92	.01770	123.9	67.5	40.9	42.33
2 Process Out	140.1	78.0	1,181	835	62.92	.01102	77.1	54.5	7.2	45.99
3 Regen In	95.0	74.4	361	273	20.57	.01770	123.9	67.5	40.9	42.33
4 Heater Out	273.0		477	273	20.57	.01770	123.9	67.5	0.8	86.45
5	135.	96.7	399	273	20.57	.03813	266.	89.8	27.3	75.1

Regen Out	2						9			9

WHEEL

WHEEL: Unitary rotor design with six (6) galvanized steel spokes equally spaced, 4.5 in. aluminum center hub, 3/4 in. diameter shaft, 14 ga. outer band

MEDIA: WSG (Wound Silica Gel) Desiccant Media, corrugated synthetic fibrous matrix

CASSETTE

FRAME: 14 ga. galvanized steel with two (2) removable side panels

BEARINGS: Sealed roller bearings

AIR SEALS: Inner and outer bulb contact seals

DRIVE: Perimeter driven chain drive

APPENDIX H. UNCERTAINTY ANALYSIS

Uncertainty Analysis of the Experimental Output

An uncertainty analysis was performed on the experimental data using the accuracies provided by NREL to see what the total error could be. The error analysis was performed using the Kline-McClintock relationship [Holman, 1989] as shown:

$$ErrorR = \left[\left(\frac{\partial R}{\partial x_1} err_1 \right)^2 + \left(\frac{\partial R}{\partial x_2} err_2 \right)^2 + ... + \left(\frac{\partial R}{\partial x_3} err_3 \right)^2 \right]^{1/2}$$

Equation 110

where R is the function is question, x is one of the variables of the function, and *err* is the error associated with that variable.

The uncertainty was measured in the energy balance using a form of the energy balance ratio defined in Chapter 4 as follows:

$$EnergyBalanceRatio = \frac{\dot{m}_{p,out,da} i_{p,out} - \dot{m}_{p,in,da} i_{p,in}}{\dot{m}_{r,out,da} i_{r,out} - \dot{m}_{r,out,da} i_{r,in}}$$

Equation 111

where p and r represent the process streams at the inlet or outlet points.

There are a total of 12 variables: 4 temperatures, 4 humidity ratios, and 4 flowrates. The enthalpy used in the energy balance equation is a function of the temperature and humidity ratio. Because of the number of variables and their relationships, the uncertainty analysis was broken into two parts. The first part

219

consisted of calculating the error for the enthalpy. The enthalpy error was then used to calculate the overall energy balance error along with the mass flowrate error. The enthalpy equation used is the same as Equation 15.

Using the steady-state conditions from the step increase to regeneration temperature, the following errors were calculated for the enthalpy and overall energy balance:

Enthalpy	0.18
Energy Balance Ratio	0.22

Discussion of Uncertainty in the Computer Model

In Chapter Five the uncertainty associated with measuring different variables in the experimental setup is provided. This is necessary to ensure the accuracy of the results and make sure that the data from the experiment is close enough to reflect reality. This is also a concern of the computer model as well. Since the model output is dictated by input, the accuracy of the input data must be confirmed. The purpose of this section is to review the input data and try to establish its reliability. Therefore, the input data has been divided into various types and the uncertainty of this data is discussed.

Air and Water Properties. The thermal properties of air and water are basic to the study of thermodynamics and heat and mass transfer. The tables for these properties are readily available in most textbooks on the subject. They have been experimentally confirmed by various researchers and laboratories and are thought to be very accurate. The relations used for these values in the model are not constants

but higher order polynomials with very good fidelity to the tabular values. Therefore it is expected that their uncertainty is very low.

Desiccant Density and Specific Heat. There are three materials used in the desiccant matrix: the desiccant itself, a filler, and a binder. The density of each material is necessary in order to determine its mass. The specific heat of each material is necessary to determine the thermal capacitance of the matrix as a whole.

The various manufacturers of that particular material provided the density and specific heat of the individual components. Except for the specific heat of the filler material, all values provided by the manufacturers were constants. Since these are relatively specialized materials, there very few other sources of information on them and no other could be found with the properties as a function of temperature.

Because these materials are solids, the constants provided for density were considered relatively accurate and it is not expected that the density will change significantly with temperature.

For most materials, specific heat is a function of temperature and not just a constant. For two of the three materials, constants for specific heat were all that could be obtained. The specific heats of the desiccant materials used in this research were constants for all three materials in order to treat all three materials consistently. Therefore, there is some inaccuracy in the model associated with this. However, because the materials are solids and the temperature range is relatively small ($\approx 105°C$), it is hoped that the specific heats for the desiccant and binder should be relatively small.

The data for the filler material can be found in the appendix for the NovelAire Desiccant wheel. This does have a significant change in specific heat with respect to temperature. Using a roughly "average" value of Cp=2.0 which occurs at 100°C, the maximum values from this average can be +/- 25%. This could be relatively significant, but the filler mass percentage of the total matrix is only 15% and so its impact is minimized.

Another aspect to consider is that more and more materials are being used for rotary desiccant wheels (zeolites, molecular sieves, etc..). For more exotic materials there is less likelihood that detailed thermal data will be available. Clearly, the output would be more accurate with more accurate thermal data for the matrix. It is beneficial; however, to see how accurate the model can be without this level of detail because it is not always possible to find. For these materials under these conditions, the validation results indicate that the use of constants is probably acceptable.

Adsorption Isotherm. The adsorption isotherm relation has the potential for significant inaccuracy. The original data used by Brandemuehl [Hubbard, 1954] was developed with temperatures up to 200°F (93°C). The validation modeling and the conventional runs in the parametric analysis had regeneration temperatures at 140°C. The temperature used in the adsorption isotherm is actually the desiccant temperature; however, the airstream energy is quickly transferred to the desiccant and there are desiccant temperatures well above 200°F (93°C). Looking at the adsorption isotherm in Appendix C, the temperature dependence looks relatively consistent for all temperatures.

Complications can occur if the calculated equilibrium relative humidity (from the adsorption isotherm equation) is too high and the desiccant temperature is also high (hence the high saturation pressure). The equation referenced in the mathematical modeling chapter and also presented (Equation 112) here will "blow" up when the vapor pressure (RH*pvsat) is greater than the total pressure, pa. The result will be a negative humidity ratio which is impossible.

$$w_e = 0.62198 \frac{RH * p_{v,\,sat}}{p_t - RH * p_{v,\,sat}}$$

Equation 112

In using the PCP subroutines combined with the secant solution methodology, this condition would in fact occur as discussed in the chapter on numerical technique.

Effective Diffusivity. The equation used for effective diffusivity is a "mechanistic hopping" correlation which uses the heat of adsorption to capture the effect of concentration and temperature upon the surface diffusion. This relation plays a significant role primarily in determining the equilibrium humidity ratio. The effective diffusivity is highly dependent upon concentration and temperature

Pesaran [1987] gave a generalized operational range for this relationship with silica gels for temperatures of 20<T<50°C and humidities <0.03 kg$_w$/kg humid air. Looking at his results, this appears to be the range of temperatures and humidities that he performed his experiments in rather than disagreement between numerical and experimental output. He displays transient graphical output and states that, in general, there is "reasonable agreement" between his experimental and numerical results.

223

He also observed a significant difference between the effective diffusivity for desorption versus adsorption by approximately a factor of two. Specifically, he found $D_o = 0.8 * 10^{-6}$ m^2/s to work better for desorption than $D_o = 1.6 * 10^{-6}$ m^2/s. He concludes that there is an apparent dynamic hysteresis effect that causes this discrepancy. The model in this research did not include hysteresis effects in order to keep the model relatively simple. Pesaran focused on the effective diffusivity for fixed beds.

The original developer of the simplified mechanistic hopping model, [Sladek], found the equation to predict within 5-10% of the experimental results for material pairs other than silica gel and water.

APPENDIX I. PARAMETRIC INPUTS

run	description	wheel split	profile	depth m	wheel temp K	wheel moisture kg_w/kg_dd	wheel speed rph	process flowrate kg/s	temp C	hum ratio kg_w/kg_dd	regen flowrate kg/s	temp C	hum ratio kg_w/kg_dd
								step conditions					
	Regeneration Temperature and Wheel Split												
1	75/25 Split at 140 C Regen (Conventional Base Case)	75/25	rect	0.2	308.15	0.1925	18	0.4278	35	0.0142	0.1089	140	0.0142
2	50/50 Split at 140 C Regen	50/50	rect	0.2	308.15	0.1925	18	0.2852	35	0.0142	0.2177	140	0.0142
3	50/50 Split at 80C Regen (Renewable Base Case)	50/50	rect	0.2	308.15	0.1925	18	0.2852	35	0.0142	0.2502	80	0.0142
4	75/25 Split at 80C Regen	75/25	rect	0.2	308.15	0.1925	18	0.4278	35	0.0142	0.1251	80	0.0142
			rect										
			rect										
	Conventional, Control Factors: wheel speed		rect										

run	description	wheel split	profile	depth (m)	wheel temp (K)	wheel moisture (kg$_w$/kg$_{dd}$)	wheel speed (rph)	process flowrate (kg/s)	process temp (C)	process hum ratio (kg$_w$/kg$_{dd}$)	regen flowrate (kg/s)	regen temp (C)	regen hum ratio (kg$_w$/kg$_{dd}$)
1	18 rph and 600 fpm (Conventional Base Case)	75/25	rect	0.2	308.15	0.1925	18	0.4278	35	0.0142	0.1089	140	0.0142
5	Wheel Speed = 36 rph	75/25	rect	0.2	308.15	0.1925	36	0.4278	35	0.0142	0.1089	140	0.0142
6	Wheel Speed = 9 rph	75/25	rect	0.2	308.15	0.1925	9	0.4278	35	0.0142	0.1089	140	0.0142
			rect										
			rect										
	Conventional, Control Factors: flowrate		rect										
1	Conventional Base Case	75/25	rect	0.2	308.15	0.1925	18	0.4278	35	0.0142	0.1089	140	0.0142
7	Flowrate = 800 fpm	75/25	rect	0.2	308.15	0.1925	18	0.5704	35	0.0142	0.1451	140	0.0142
8	Flowrate = 400 fpm	75/25	rect	0.2	308.15	0.1925	18	0.2852	35	0.0142	0.0726	140	0.0142
			rect										
			rect										
	Conventional, Initial Wheel Temperature		rect										
1	Conventional Base Case	75/25	rect	0.2	308.15	0.1925	18	0.4278	35	0.0142	0.1089	140	0.0142
9	Initial Wheel Temp = 360K	75/25	rect	0.2	360	0.0196	18	0.4278	35	0.0142	0.1089	140	0.0142
10	Initial Wheel Temp = 330K	75/25	rect	0.2	330	0.06241	18	0.4278	35	0.0142	0.1089	140	0.0142

		initial conditions					step conditions						
		wheel		depth	wheel temp	wheel moisture	wheel speed	process flowrate	temp	hum ratio	regen flowrate	temp	hum ratio
run	description	split	profile	m	K	kg$_w$/kg$_{dd}$	rph	kg/s	C	kg$_w$/kg$_{dd}$	kg/s	C	kg$_w$/kg$_{dd}$
11	Initial Wheel Temp = 320K	75/25	rect	0.2	320	0.1076	18	0.4278	35	0.0142	0.1089	140	0.0142
			rect										
			rect										
	Conventional, Ambient Relative Humidity		rect										
1	Conventional Base Case	75/25	rect	0.2	308.15	0.1925	18	0.4278	35	0.0142	0.1089	140	0.0142
12	35C/50%RH	75/25	rect	0.2	308.15	0.23946	18	0.4234	35	0.018	0.1084	140	0.018
13	35C/60%RH	75/25	rect	0.2	308.15	0.2841	18	0.4221	35	0.0216	0.1079	140	0.0216
14	35C/70%RH	75/25	rect	0.2	308.15	0.331	18	0.4207	35	0.0252	0.1075	140	0.0252
			rect										
			rect										
	Conventional, Ambient Temperature		rect										
1	Conventional Base Case	75/25	rect	0.2	308.15	0.1925	18	0.4278	35	0.0142	0.1089	140	0.0142
15	80F/26.7C (64% RH)	75/25	rect	0.2	299.85	0.3795	18	0.4401	26.7	0.0142	0.1089	140	0.0142
16	70F/21.1C (90%RH)	75/25	rect	0.2	294.24	0.4272	18	0.4482	21.1	0.0142	0.1089	140	0.0142
			rect										
			rect										
	Conventional, Wheel Geometry		rect										

run	description	initial conditions					step conditions						
		wheel split	profile	depth m	wheel temp K	wheel moisture kg_w/kg_dd	wheel speed rph	process flowrate kg/s	process temp C	process hum ratio kg_w/kg_dd	regen flowrate kg/s	regen temp C	regen hum ratio kg_w/kg_dd
1	Conventional Base Case	75/25	rect	0.2	308.15	0.1925	18	0.4278	35	0.0142	0.1089	140	0.0142
17	Triangular profile	75/25	tri	0.2	308.15	0.1925	18	0.4567	35	0.0142	0.1162	140	0.0142
18	Desiccant Mass = 8.1kg	75/25	rect	0.2	308.15	0.1925	18	0.4278	35	0.0142	0.1089	140	0.0142
19	Wheel Depth = .1m	75/25	rect	0.2	308.15	0.1925	18	0.4278	35	0.0142	0.1089	140	0.0142
			rect										
			rect										
	Conventional, Material Properties		rect										
1	Conventional Base Case	75/25	rect	0.2	308.15	0.1925	18	0.4278	35	0.0142	0.1088	140	0.0142
20	Particle Size = 47.5 microns	75/25	rect	0.2	308.15	0.1925	18	0.4278	35	0.0142	0.1088	140	0.0142
21	Increased Diffusivity (10x)	75/25	rect	0.2	308.15	0.1925	18	0.4278	35	0.0142	0.1088	140	0.0142
22	Increased Specific Heat (2x)	75/25	rect	0.2	308.15	0.1925	18	0.4278	35	0.0142	0.1088	140	0.0142
			rect										
			rect										
	Renewable, Control Factors: Wheel Speed		rect										
3	Renewable Base Case	50/50	rect	0.2	308.15	0.1925	18	0.2852	35	0.0142	0.2502	80	0.0142
23	Wheel Speed = 36 rph	50/50	rect	0.2	308.15	0.1925	36	0.2852	35	0.0142	0.2502	80	0.0142

run	description	initial conditions					wheel speed	step conditions			regen		
		wheel split	profile	depth m	wheel temp K	wheel moisture kg$_w$/kg$_{dd}$	rph	process flowrate kg/s	temp C	hum ratio kg$_w$/kg$_{dd}$	flowrate kg/s	temp C	hum ratio kg$_w$/kg$_{dd}$
24	Wheel Speed = 9 rph	50/50	rect	0.2	308.15	0.1925	9	0.2852	35	0.0142	0.2502	80	0.0142
			rect										
			rect										
	Renewable, Control Factors: Flowrate		rect										
3	Renewable Base Case	50/50	rect	0.2	308.15	0.1925	18	0.2852	35	0.0142	0.2502	80	0.0142
25	Flowrate = 800 fpm	50/50	rect	0.2	308.15	0.1925	18	0.3777	35	0.0142	0.3296	80	0.0142
26	Flowrate = 400 fpm	50/50	rect	0.2	308.15	0.1925	18	0.1901	35	0.0142	0.1668	80	0.0142
			rect										
			rect										
	Renewable, Initial Wheel Temperature		rect										
3	Renewable Base Case	50/50	rect	0.2	308.15	0.1925	18	0.2852	35	0.0142	0.2502	80	0.0142
27	Initial Wheel Temp = 330K	50/50	rect	0.2	330	0.06241	18	0.2852	35	0.0142	0.2502	80	0.0142
28	Initial Wheel Temp = 320K	50/50	rect	0.2	320	0.1076	18	0.2852	35	0.0142	0.2502	80	0.0142
			rect										
			rect										
	Renewable, Ambient Humidity Conditions		rect										

		initial conditions					wheel speed	step conditions					
		wheel split	profile	depth	wheel temp	wheel moisture		process flowrate	temp	hum ratio	regen flowrate	temp	hum ratio
run	description			m	K	kg$_w$/kg$_{dd}$	rph	kg/s	C	kg$_w$/kg$_{dd}$	kg/s	C	kg$_w$/kg$_{dd}$
3	Renewable Base Case	50/50	rect	0.2	308.15	0.1925	18	0.2852	35	0.0142	0.2502	80	0.0142
29	35C/50%RH	50/50	rect	0.2	308.15	0.23946	18	0.2832	35	0.018	0.2472	80	0.018
30	35F/60%RH	50/50	rect	0.2	308.15	0.2841	18	0.2823	35	0.0216	0.2457	80	0.0216
31	35F/70%RH	50/50	rect	0.2	308.15	0.331	18	0.2805	35	0.0252	0.2450	80	0.0252
			rect										
			rect										
	Renewable, Ambient Temperature		rect										
3	Renewable Base Case	50/50	rect	0.2	308.15	0.1925	18	0.2852	35	0.0142	0.2502	80	0.0142
32	80F/26.7C (64% RH)	50/50	rect	0.2	299.85	0.3795	18	0.2934	26.7	0.0142	0.2502	80	0.0142
33	70F/21.1C (90%RH)	50/50	rect	0.2	294.24	0.4272	18	0.2988	21.1	0.0142	0.2502	80	0.0142
			rect										
			rect										
	Renewable, Wheel Geometry		rect										
3	Renewable Base Case	50/50	rect	0.2	308.15	0.1925	18	0.2852	35	0.0142	0.2502	80	0.0142
34	Triangular profile	50/50	tri	0.2	308.15	0.1925	18	0.3045	35	0.0142	0.2671	80	0.0142
35	Low Desiccant Mass (8.1kg)	50/50	rect	0.2	308.15	0.1925	18	0.2852	35	0.0142	0.2502	80	0.0142
36	Wheel Depth = .1m	50/50	rect	0.1	308.15	0.1925	18	0.2852	35	0.0142	0.2502	80	0.0142
			rect										

| run | description | initial conditions | | | | | | step condtions | | | | | |
		wheel split	profile	depth m	wheel temp K	wheel moisture kg_w/kg_dd	wheel speed rph	process flowrate kg/s	temp C	hum ratio kg_w/kg_dd	regen flowrate kg/s	temp C	hum ratio kg_w/kg_dd
	Renewable, Material Properties		rect										
			rect										
3	Renewable Base Case	50/50	rect	0.2	308.15	0.1925	18	0.2852	35	0.0142	0.2502	80	0.0142
37	Particle Size = 47.5 microns	50/50	rect	0.2	308.15	0.1925	18	0.2852	35	0.0142	0.2502	80	0.0142
38	Increased Diffusivity (10x)	50/50	rect	0.2	308.15	0.1925	18	0.2852	35	0.0142	0.2502	80	0.0142
39	Increased Specific Heat (2x)	50/50	rect	0.2	308.15	0.1925	18	0.2852	35	0.0142	0.2502	80	0.0142
	Worst Case												
1	Conventional Base Case	75/25	rect	0.2	308.15	0.1925	18	0.4278	35	0.0142	0.1089	140	0.0142
3	Renewable Base Case	50/50	rect	0.2	308.15	0.1925	18	0.2852	35	0.0142	0.2502	80	0.0142
40	Worst Case	75/25	rect	0.2	294.24	0.4272	36	0.2852	21.1	0.0142	0.0726	80	0.0142

APPENDIX J. COMPUTER PROGRAM

```
!        Program hmxsystem
!        description: this program calculates the average outgoing air states
!        of the process and regeneration streams entering a heat and mass rotary
!        regenerator.  It solves for an individual element and then proceeds to the
!        next using the tridiagonal matrix solver numerical scheme.
!        The units for this program are: meters(m), seconds(s), Kelvins(K),
!        kilograms(kg), kiloJoules(kJ)
!        variables are described before their delaration statements

         program hmxsystem

         USE global
         CHARACTER*50 RUNNAME
         OPEN(unit=10,file='hmxrun.out',status='unknown')

!        setup for multiple runs
!        Loop1: DO run=2,1
         run=1

!        initialize time and circumferential position
         tau=0.
         dtau=0.
         pa=1.0

         WRITE(*,9)
         WRITE(10,9)
9        FORMAT(/,7x,'HMX',4x,'output',6x,'data',/,/)

         WRITE (*,*) 'Please Input the Run Title'

      READ(*,*) RUNNAME

         WRITE(*,5) RUNNAME
         WRITE(10,5) RUNNAME
5        FORMAT(/,A50,/)

         WRITE (*,*) 'Please input the atmospheric pressure in kPa'
□
      READ(*,*) atmp
□

         WRITE(*,1)
         WRITE(10,1)
1        FORMAT(/,4x,'heat &',6x,'mass',4x,'coeffs',/)

         WRITE(*,2)cplw,tref,muair,atmp,epstri
         WRITE(10,2)cplw,tref,muair,atmp,epstri
2        FORMAT(/,'cplw, kj/kglw-K =  ',F10.6,  &
                /,'tref, K =        ',F10.6,  &
                /,'muair, (N-s)/m2  = ',F10.6,  &
```

232

```fortran
                /,'amb pressure, kPa = ',F10.6,      &
                /,'epstri =          ',F10.6)


100 CONTINUE

!       input/read airstream conditions
!       (temperatures, humidity ratios, volumetric flowrate)


        CALL inlet

!       get subroutine to solve for rotary desiccant wheel
        CALL hmx


!       increment time
        tau=tau+dtau
        taum=tau/60.0

!       season=30000.0

        IF(tau.le.season)GOTO 100

        DEALLOCATE(Wd,Td,wf,tf)

!       END DO Loop1

        STOP
        END PROGRAM hmxsystem




        MODULE global
        IMPLICIT none
!       k1 - circumferential position of the first wedge
!       kpr - wedge position between process and regeneration
!       nx - number of axial positions
!       ntheta - number of circumferential positions
!       shape - the shape of the transfer profile in the desiccant wheel
!       n - the wedge number
!       j - the axial position
!       k - the circumferential position
        INTEGER k1,kpr,nx,ntheta,shape,n,j,k,d
!       maxite - the maximum number of iterations for a numerical solution
!       iter - the count of the number of iterations for a solution
!       ss - steady-state identifier
!       pp - counter for printing of results at a time step
!       pt - counter for printing of reuslts at a time step
!       run - counter for runs under different conditions
        INTEGER maxite,iter,ss,pp,pt,run
!       dim - size of matrix for tridiagonal numerical solution
        INTEGER ::dim=4
!       Wd - desiccant water content, kgw/kgdd
        REAL(8),ALLOCATABLE::Wd(:,:,:)
```

```fortran
!          Td - desiccant temperature, K
           REAL(8),ALLOCATABLE::Td(:,:,:)
!          wf - air humidity ratio, kgw/kgda
           REAL(8),ALLOCATABLE::wf(:,:)
!          tf - air temperature, K
           REAL(8),ALLOCATABLE::tf(:,:)
!          A1,2,3 - coefficient matrices for solution of tridiagonal matrix
           REAL(8) A1(4)
           REAL(8) A2(4)
           REAL(8) A3(4)
!          b(4) - right hand side matrix for solution of tridiagonal matrix
           REAL(8) b(4)
!          x(4) - solution matrix for tridiagonal matrix
           REAL(8) x(4)
!          ac - cross sectional area, m2
!          acp - process cross sectional area, m2
!          acr - regeneration cross sectional area, m2
!          asurf - total transfer surface area, m2
!          asurfp - process transfer surface area, m2
!          asurfr - regeneration transfer surface area, m2
!          atmp - atmospheric pressure. kpa
!          betap - process period fraction, dimensionless
!          betar - regeneration period fraction, dimensionless
           REAL(8) ac,acp,acr,asurf,asurfp,asurfr,atmp,betap,betar
!          cpdd - dry desiccant matrix heat capacity (includes support structure), kJ/(kgdd-K)
!          cplw - liquid water constant pressure specific heat, 4.186 kJ/(kglw-K)
!          cpda - dry air constant pressure specific heat, 1.007 kJ/(kgda-K)
!          cpwv - water vapor constant pressure specific heat, 1.872 kJ/(kgwv-K)
!          cpm - specific heat of matrix (desiccant + water), kJ/(kgm-K)
!          cpma - specific heat of moist air, kJ/(kgda-K)
           REAL(8) cpdd,cplw,cpda,cpwv,cpma,cpm
!          cross - ratio of length to heigth for square profiles
           REAL(8) cross
!          the change in axial position, m
!          dtheta - the change in non-dimensional time
!          dh - hydraulic diameter, m
!          dtau - the change in time, s
!          Dseffo - effective diffusivity, m2/s
           REAL(8) dx,dtheta,dh,dtau,Dseffo
!          epstri - the epsilon criteria for the tridiagonal matrix
           REAL(8) ::epstri=.000001
!          errmax - the
           REAL(8) errmax
!          effpt - effectiveness in terms of process temperature
!          effrt - effectiveness in terms of regen temperature
!          effpw - effectiveness in terms of process humidity ratio
!          effrw - effectiveness in terms of regen humidity ratio
!          effmrc - effectiveness in terms of mrc
           REAL(8)         effpt,effrt,effpw,effrw,effmrc
!          effenthp - effectiveness in terms of process enthalpy
!          effenthr - effectivess in terms of regen enthalpy
           REAL(8) effenthp,effenthr
!          enthpi - process inlet enthalpy, kJ/kg
!          enthri - regen inlet enthalpy, kJ/kg
!          enthpo - process outlet enthaply, kJ/kg
!          enthro - regen outlet enthalpy, kJ/kg
```

```fortran
      REAL(8) enthpi,enthri,enthpo,enthro
!     Epi - total process inlet enthalpy, kJ/s
!     Eri - total regen inlet enthalpy, kJ/s
!     Epo - total process outlet enthalpy, kJ/s
!     Ero - total regen outlet enthaply, kJ/s
!     energybal - the ratio Epi-Epo/Eri-Ero
      REAL(8) Epi,Eri,Epo,Ero,energybal
!     gamp - process mass capacity fraction, dimenionless
!     gamr - regeneration mass capacity fraction, dimensionless
      REAL(8) gamp,gamr
!     H20massbal - mass balance, process mass transferred/regen mass trasferrred
      REAL(8)      H20massbal
!     h - height of transfer profile
!     hqfd - fully developed convection heat transfer coefficient,
!     hmfd - mass transfer coefficient
!     kf - thermal conductivity of moist air,  kJ/(m-s-K)
!     L - depth of desiccant wheel, m
!     Le - the Lewis number
      REAL(8) h,hmfd,hqfd,kf,L,Le
!     mda - total mass flowrate of dry air, kgda/s
!     mdap - process mass flowrate of dry air, kgda/s
!     mdar - regen mass flowrate of dry air, kgda/s
!     mdd - mass of dry desiccant, kg
!     muair - dynamic viscosity of moist air, 184.6 E-7 (N-s)/m2
!     mrc - moisture removal capacity, kgwater/hr
      REAL(8) mda,mdap,mdar,mdd,muair,mrc
!     nrev - desiccant wheel speed, revs/hr
!     nrevl - nrev last, tracking variable
!     nufd - fully developed flow Nusselt number
      REAL(8) nrev,nrevl,nufd,nle,indx
!     NTUhp - NTU number convective heat transfer, process
!     NTUhr - NTU number convective heat transfer, regen
!     NTUmp - NTU number convective mass transfer, process
!     NTUmr - NTU number convective mass transfer, regen
      REAL(8) NTUmp,NTUmr,NTUhp,NTUhr
!     Pr - Prandtl number
!     pa - atmospheric pressure, atmospheres
!     rad - desiccant particle radius, m
!     rhop - density of desiccant particle, kg/m3
!     reyp - Reynolds number for process
!     reyr - Reynolds number for regeneration
!     Rwv - gas constant for water vapor,
!     RH - relative humidity
      REAL(8) Pr,pa,rad,rhop,reyp,reyr,Rwv,RH
!     season - length of run, s
!     Sherwoodp - Sherwood number for inlet process conditions
!     Sherwoodr - Sherwood number for inlet regen conditions
      REAL(8) Sc,season,Sherwoodp,Sherwoodr
!     tfpi - temperature of the process inlet airstream, K
!     tfri - temperature of the regeneration inlet airstream, K
!     tfpo - temperature of the process outlet airstream, K
!     tfro - temperature of the regeneration outlet airstream, K
!     tfamb - ambient temperature, K
      REAL(8)      tfpi,tfri,tfpo,tfro,tfamb
!     tau - time, s
!     taum - time, m
```

235

```fortran
!          Tdi - initial wheel temperature, K
!          tref - reference temperature for enthalpy calcs (273.15 K)
!          thetap - dimensionless time corresponding to end of processing period
!          thetar - dimensionless time corresponding to end of regeneration period
!          TotH20bal - total mass balance, h20in/h20out
           REAL(8) tau,taum,Tdi,tref,thetap,thetar,TotH20bal
!          wfpi - process inlet humidity ratio of the air, kgw/kgda
!          wfri - regeneration inlet humidity ratio of the air, kgw/kgda
!          wfpo - process inlet humidity ratio of the air, kgw/kgda
!          wfro - regeneration outlet humidity ratio of the air, kgw/kgda
!          wfamb - ambient humidity ratio, kgw/kgda
           REAL(8) wfpi,wfri,wfpo,wfro,wfamb
!          Wdi - initial desiccant wheel humidity content
           REAL(8) w,Wdi
           DATA cplw/4.3/,tref/273.15/
           DATA Pr/.707/,muair/197.34E-7/,Rwv/.462/
           DATA Sc/0.6/,maxite/50/,pa/1.0/
           END MODULE global




           SUBROUTINE inlet
!          subroutine to retrieve the system conditions

           USE global
           INTEGER inc,incc,intot

!          step change to temperature
           IF(run.eq.1)THEN
           IF(taum.lt.90.0)THEN
           nrev=20.0
           mdap=0.1839
           mdar=0.1839
!          temps are in degrees Kelvin; humidity ratios are in kgw/kgdd
           tfpi=298.15
           wfpi=.01
           tfri=333.15
           wfri=.01
           END IF

!          set variable to indicate change to input variables



           RETURN
           END SUBROUTINE inlet




           SUBROUTINE hmx

!          this subroutine represents the rotary heat and mass exchanger and
!          its affect upon the two airstreams:  process and regeneration

           USE global
```

```
!          for time=0, call subroutine to initialize wheel
           IF(tau.eq.0.)THEN

           CALL wheel

           CALL syspar

!          set step size
           CALL step

           ALLOCATE(Wd(ntheta,nx,2))
           ALLOCATE(Td(ntheta,nx,2))
           ALLOCATE(wf(ntheta,nx+1))
           ALLOCATE(tf(ntheta,nx+1))

!          initialize all matrix locations
           Wd=Wdi
           Td=Tdi

!          initialize time/position integers
           k=0
           k1=1

!          print instantaneous input/output

           WRITE (*,*)
           WRITE (*,*) 'Approximately, what time interval would you like the output data printed?'
         WRITE (*,*) '(in seconds)'

       READ(*,*) interval

           pt=INT(interval/dtau)
           IF(pt.lt.1)pt=1
           pp=pt

           WRITE(*,4)
           WRITE(10,4)
4          FORMAT(/,/,/,3x,'primary',4x,'output',6x,'data',/)

!          print column headings
           WRITE(*,5)
           WRITE(10,5)
5          FORMAT(6x,'taum',7x,'rph',6x,'mdap',6x,'mdar',6x,'tfpi',6x,'tfri', &
                  6x,'wfpi',6x,'wfri',6x,'tfpo',6x,'tfro',6x,'wfpo',6x,'wfro',7x,'mrc', &
                  4x,'enthpi',4x,'enthri',4x,'enthpo',4x,'enthro',3x,'massbal',1x,'energybal', &
         & 1x,'TotH20bal',5x,'effpt',5x,'effrt',5x,'effpw',5x,'effrw',4x,'effmrc', &
              & 2x,'effenthp',2x,'effenthr',5x,'state')
           END IF

!          set system parameter conditions
           IF(tau.gt.0.0)THEN
           CALL syspar
           END IF

!          write initial output air conditions
           IF(tau.eq.0.)THEN
```

237

```fortran
        tfpo=tfpi
        tfro=tfri
        wfpo=wfpi
        wfro=wfri
        END IF


        IF(pp.eq.pt)THEN
!       print instantaneous input/output
        WRITE(*,6)taum,nrev,mdap,mdar,tfpi,tfri,wfpi,wfri,tfpo,tfro,wfpo, &
        wfro,mrc,enthpi,enthri,enthpo,enthro,H20massbal,energybal, &
        TotH20bal,effpt,effrt,effpw,effrw,effmrc,effenthp,effenthr,ss
        WRITE(10,6)taum,nrev,mdap,mdar,tfpi,tfri,wfpi,wfri,tfpo,tfro,wfpo, &
        wfro,mrc,enthpi,enthri,enthpo,enthro,H20massbal,energybal, &
        TotH20bal,effpt,effrt,effpw,effrw,effmrc,effenthp,effenthr,ss
6
        FORMAT(2x,F8.2,2x,F8.3,2x,F8.5,2x,F8.5,2x,F8.2,2x,F8.2,2x,F8.6,2x,F8.6,2x,F8.3,2x,F8.3,
2x,F8.6, &
        2x,F8.6,2x,F8.4,2x,F8.3,2x,F8.3,2x,F8.3,2x,F8.3,2x,F8.5,2x,F8.5, &
        2x,F8.5,2x,F8.4,2x,F8.4,2x,F8.4,2x,F8.4,2x,F8.4,2x,F8.4,2x,F8.4,8x,I2)
        pp=0
        END IF
        pp=pp+1




!       obtain a unique wedge
        Loop1: DO n=1,ntheta


!       determine the circumferential position of each wedge
!   based on the n=1 (k1) wedge
        k=k1+(n-1)

!       reset k back if greater than ntheta
        IF(k.gt.ntheta)THEN
        k=k-ntheta
        END IF

!       determine whether each wedge is in process or regen stream
        IF(k.le.kpr)THEN
        CALL process
        ELSE
        CALL regen
        END IF

        END DO Loop1


!       solve for average outlet conditions
        CALL outlet

        CALL effect

        CALL balance
```

```fortran
!        advance the #1 wedge circumferential position
         k1=k1+1

!        reset k1 back to one if greater than ntheta
         IF(k1.gt.ntheta)THEN
         k1=1
         END IF

         RETURN
         END SUBROUTINE hmx



         SUBROUTINE wheel
!        this subroutine inputs information about the desiccant wheel

         USE global
         INTEGER q
         CHARACTER*12 Filename

         WRITE (*,*) 'Please Input Wheel Data File Name'

         READ(*,*) FILENAME

         OPEN(1,FILE=FILENAME)

         READ(1,*) rad,rhop,asurf,mdd,cpdd,thetap,thetar,ac,dh,L,h,w,shape,Tdi,Wdi
         CLOSE(1)

!        calculate the period fraction, beta
         betap=thetap
         betar=thetar-thetap

!        set process and regen flow areas
         acp=ac*betap
         acr=ac*betar

!        calculate transfer area per period
         asurfp=asurf*betap
         asurfr=asurf*betar

!        calculate transfer coefficients from geometry
         Check_Shape: SELECT CASE (shape)
         CASE(1)
                 nufd=4.36
!        shape 1 is a circle
         CASE(2)
                 nufd=3.11
!        shape 2 is a triangle
         CASE(3)
                 cross=w/h
                 nufd=1.4437*DLOG(cross)+3.262
!                nufd=3.61
!        shape 3 is a recangle
```

```fortran
          END SELECT Check_Shape

!         print out wheel and initial values
          WRITE(*,25) filename
          WRITE(10,25) filename
25        FORMAT(/,/,2x,'contents',8x,'of',5x,'wheel',6x,'data',5x,'file:',2x,A12,/)

          WRITE(*,2)rad,rhop,asurf,mdd,cpdd,thetap,thetar,betap,betar,ac,dh,L,h,w,shape,Wdi,Tdi,acp,
acr,asurfp,asurfr
          WRITE(10,2)rad,rhop,asurf,mdd,cpdd,thetap,thetar,betap,betar,ac,dh,L,h,w,shape,Wdi,Tdi,ac
p,acr,asurfp,asurfr
2         FORMAT(/,'rad, m =          ',F10.7,  &
                /,'rhop, kg/m3 =      ',F10.3,  &
                /,'asurf, m2 =        ',F10.3,  &
                /,'mdd, kg =          ',F10.3,  &
                /,'cpdd, kJ/kg-K=     ',F10.5,  &
                /,'thetap, non dim =  ',F10.3,  &
                /,'thetar, non dim =  ',F10.3,  &
                /,'betap, non dim =   ',F10.3,  &
                /,'betar,non dim =    ',F10.3,  &
                /,'ac, m2 =           ',F10.4,  &
                /,'dh, m =            ',F10.6,  &
                /,'L, m =             ',F10.3,  &
                /,'h, m =             ',F10.3,  &
                /,'w, m =             ',F10.3,  &
                /,'shape, non dim =   ',7x,I3,  &
                /,'Wdi, kgw/kgdd =    ',F10.6,  &
                /,'Tdi, K =           ',F10.3,  &
                /,'acp, m2 =          ',F10.3,  &
                /,'acr, m2 =          ',F10.3,  &
                /,'asurfp, m2 =       ',F10.3,  &
                /,'asurfr, m2 =       ',F10.3)

          RETURN
          END SUBROUTINE wheel




          SUBROUTINE syspar
!         this subroutine calculates the current desiccant and airstream conditions
!         using data from wheel and the latest system airflow readings

          USE global
          REAL(8) kfda,cpwvT,cpdaT,Dseff,Dtempp,Dtempr
          EXTERNAL kfda,cpwvT,cpdaT,Dseff

!         in case there is a change in speed
          dtau=dtheta*(1./nrev)*3600

!         determine gamma for each side
          gamp=mdd*nrev/(3600*mdap)
          gamr=mdd*nrev/(3600*mdar)

!         Reynolds numbers
          reyp=mdap*dh/(muair*acp)
```

```fortran
        reyr=mdar*dh/(muair*acr)

!       is reyp and reyr less than 2300?
        IF(reyp.gt.2300.)THEN
        WRITE(*,1)reyp
        WRITE(10,1)reyp
1       FORMAT(/,'Reynolds No. says flow is non-laminar',2x,'Reyp= ',F10.3)
        STOP
        END IF

        IF(reyr.gt.2300.)THEN
        WRITE(*,2)reyr
        WRITE(10,2)reyr
2       FORMAT(/,'Reynolds No. appears flow is non-laminar',2x,'Reyr= ',F10.3)
        STOP
        END IF

!       determine the Lewis number
        Pr=.705
        Sc=.6
!       Le=Sc/Pr
        Le=1.0
        nle=.3


        NTUhp=(nufd*kfda(tfpi)/dh)*asurfp/(mdap*(cpdaT(tfpi)+wfpi*cpwvT(tfpi)))
        NTUmp=(nufd*kfda(tfpi)/dh*asurfp/((cpdaT(tfpi)+wfpi*cpwvT(tfpi))*mdap))
        NTUhr=(nufd*kfda(tfri)/dh*asurfr/(mdar*(cpdaT(tfri)+wfri*cpwvT(tfri))))
        NTUmr=(nufd*kfda(tfri)/dh*asurfr/((cpdaT(tfri)+wfri*cpwvT(tfri))*mdar))
!       determine Sherwood number for process
kf=kfda(tfpi)
hqfd=nufd*kf/dh
cpda=cpdaT(tfpi)
cpwv=cpwvT(tfpi)

cpma=cpda+wfpi*cpwv

        hmfd=hqfd/(cpma*Le**(1-nle))

        Dtempp=Dseff(Wdi,tfpi)

        Sherwoodp=hmfd*rad/(2*rhop*Dtempp)


!       determine Sherwood number for regen

        kf=kfda(tfri)

        hqfd=nufd*kf/dh

        cpda=cpdaT(tfri)
        cpwv=cpwvT(tfri)

        cpma=cpda+wfri*cpwv
```

```fortran
        hmfd=hqfd/(cpma*Le**(1-nle))

        Dtempr=Dseff(Wdi,tfri)

        Sherwoodr=hmfd*rad/(2*rhop*Dtempr)

!       print out syspar variables if there is a change in the input conditions
        IF(tau.eq.0.0)THEN
        WRITE(*,43)
        WRITE(10,43)
43      FORMAT(/,/,4x,'Syspar',6x,'data')

        WRITE(*,8)dtau,gamp,gamr,reyp,reyr,NTUhp,NTUmp,NTUhr,NTUmr,Le,Sherwoodp,Sher
woodr,Dtempp,Dtempr
        WRITE(10,8)dtau,gamp,gamr,reyp,reyr,NTUhp,NTUmp,NTUhr,NTUmr,Le,Sherwoodp,Sher
woodr,Dtempp,Dtempr
8       FORMAT(/,'dtau, non dim =    ',F10.4,   &
                /,'gamp, non dim =    ',F10.4,   &
                /,'gamr, non dim =    ',F10.4,   &
                /,'reyp, non dim =    ',F10.4,   &
                /,'reyr, non dim =    ',F10.4,   &
                /,'NTUhp, non dim =   ',F10.4,   &
                /,'NTUmp, non dim =   ',F10.4,   &
                /,'NTUhr, non dim =   ',F10.4,   &
                /,'NTUmr, non dim =   ',F10.4,   &
                /,'Le, non dim =      ',F10.4,       &
                /,'Sherwoodp, non dim=',F10.4,   &
                /,'Sherwoodr, non dim=',F10.4,   &
                /,'Dtempp,m2s =            ',F20.16  &
                /,'Dtempr,m2s =   ',F20.16)

        END IF

        RETURN
        END SUBROUTINE syspar




        SUBROUTINE step
!       this subroutine calculates the step required for the rotary heat and
!       mass exchanger

        USE global


        WRITE(*,5)
        WRITE(10,5)
5       FORMAT(/,/,6x,'Step',6x,'data')


!       prompt screen for wheel rotation speed (nrev) in RPH
!       WRITE(*,*)'Please input wheel rotation speed (RPH)'
!       READ(*,*)nrev

        gamp=mdd*nrev/(3600*mdap)
        gamr=mdd*nrev/(3600*mdar)
```

242

```fortran
!         determine number of axial and circumferential (time) steps (grid size)
          WRITE(*,*)'How would you like to input the axial and circumferential grid steps?'
          WRITE(*,*)'The automatic step size includes correction for stability'
          WRITE(*,*)'1=manual, 2=automatic computer algorithm'
          READ(*,*)input

!         select the right procedure
          Check_input: SELECT CASE(input)
          CASE(1)
          WRITE(*,*)'Please input number of axial grid steps'
          READ(*,*)nx
          WRITE(*,*)'Please input number of circumferential grid steps'
          READ(*,*)ntheta
          CASE(2)


          nx=NINT(2.8*(MAX(NTUmp,NTUmr))**.5+5.6)
          ntheta=NINT(nx/(MIN(gamp,gamr)*MIN(betap,betar)))


!         make sure the time step is compatible with the process/regen split of the wheel
          Loop1: DO q=1,1000
          nth=ntheta
          nth=INT(thetap*ntheta)+INT((1-thetap)*ntheta)
          IF(nth.eq.ntheta)THEN
          nx=NINT(ntheta*(MIN(gamp,gamr)*MIN(betap,betar))/2)
          GOTO 22
          END IF
          ntheta=ntheta+1
          END DO Loop1

22        continue

          END SELECT Check_input

          dx=1./real(nx)
          dtheta=1./real(ntheta)
          dtau=dtheta*(1./nrev)*3600
          kpr=thetap*ntheta

          WRITE(*,6)nrev,nx,ntheta,dx,dtheta,nufd,kpr,dtau,gamp,gamr
          WRITE(10,6)nrev,nx,ntheta,dx,dtheta,nufd,kpr,dtau,gamp,gamr
6         FORMAT(/,'nrev, rph =      ',F10.3, &
                 /,'nx, =            ',6x,I4, &
                 /,'ntheta, =        ',6x,I4, &
                 /,'dx, =            ',F10.5, &
                 /,'dtheta, =        ',F10.5, &
                 /,'nufd, non dim =  ',F10.5, &
                 /,'kpr, =           ',6x,I4, &
                 /,'dtau, sec =      ',F10.5, &
                 /,'gamp, non dim =  ',F10.6, &
                 /,'gamr, non dim =  ',F10.6)

!         nrevl=nrev
```

```fortran
      RETURN
      END SUBROUTINE step




      SUBROUTINE process
!     this subroutine sets up the matrix for wedges in the process stream.

      USE global
      REAL(8) iadso,iads,cpwvT,cpdaT,kfda
      REAL(8) Wdavg,Tdavg,wfavg,tfavg,weo,a2c
      EXTERNAL iads,cpwvT,cpdaT,kfda

!     establish do loop to solve for every axial position
      Loop3: DO j=1,nx

      IF(tau.gt.49.9 .AND. n.eq.91 .AND. k.eq.1 .AND. j.eq.2)THEN
      pa=pa+0
      END IF



!     apply appropriate boundary condition
      IF(j.eq.1)THEN
      tf(n,j)=tfpi
      wf(n,j)=wfpi
      END IF

!     make initial guess across next element to evaluate coefficients
      tf(n,j+1)=tf(n,j)
      wf(n,j+1)=wf(n,j)
      Td(n,j,2)=Td(n,j,1)
      Wd(n,j,2)=Wd(n,j,1)

      iter=0




101   CONTINUE

!     calculate differential coefficients
      Wdavg=.5*(Wd(n,j,1)+Wd(n,j,2))
      Tdavg=.5*(Td(n,j,1)+Td(n,j,2))
      wfavg=.5*(wf(n,j)+wf(n,j+1))
      tfavg=.5*(tf(n,j)+tf(n,j+1))

      kf=kfda(tfavg)

      hqfd=nufd*kf/dh



      cpda=cpdaT(tfavg)
      cpwv=cpwvT(tfavg)

      CALL eqhr(Wdavg,Tdavg,wfavg,tfavg,weo)
```

```
        iadso=iads(Wdavg,Tdavg)

        cpm=cpdd+Wdavg*cplw
        cpma=cpda+wfavg*cpwv

        hmfd=hqfd/(cpma*Le**(1-nle))

        NTUhp=hqfd*asurfp/(mdap*(cpma))
        NTUmp=hmfd*asurfp/mdap


!       put in matrix notation

!       the "remainder" matrix, b
        b(1)=Wd(n,j,1)+(dtheta*wf(n,j))/(betap*gamp*dx)
        b(2)=NTUmp*dx*weo+(1-NTUmp*dx/2)*wf(n,j)
        b(3)=Td(n,j,1)+(dtheta)/(dx*betap*gamp*cpm)*(cpma*tf(n,j)+&
        iadso*wf(n,j))
        b(4)=(1.-NTUhp*dx/2.0)*tf(n,j)+NTUhp*dx/2.0*Td(n,j,1)

!       the coefficient "A" matrix
!       mass conservation equation
        A2(1)=1.0
        A3(1)=dtheta/(betap*gamp*dx)

!       mass rate
        A1(2)=0.
        A2(2)=(1+NTUmp*dx/2)
        A3(2)=0.


!       energy conservation

        A1(3)=(dtheta*iadso)/(dx*betap*gamp*cpm)
        A2(3)=1.0
        A3(3)=(dtheta*cpma)/(dx*betap*gamp*cpm)

!       energy rate
        A1(4)=-NTUhp*dx/2.
        A2(4)=(1.+NTUhp*dx/2.)

!       possible solution
        x(1)=Wd(n,j,2)
        x(2)=wf(n,j+1)
        x(3)=Td(n,j,2)
        x(4)=tf(n,j+1)

!       solve matrix
        CALL tridag


!       make sure variables do no go below zero
        IF(x(1).lt.1E-10)x(1)=1E-10
        IF(x(2).lt.1E-10)x(2)=1E-10
        IF(x(3).lt.1E-10)x(3)=1E-10
```

245

```fortran
        IF(x(4).lt.1E-10)x(4)=1E-10


        Wd(n,j,2)=x(1)
        wf(n,j+1)=x(2)
        Td(n,j,2)=x(3)
        tf(n,j+1)=x(4)

        iter=iter+1
        IF(iter.ge.maxite)GOTO 102

!       check for convergence
        IF(errmax.gt.epstri)GOTO 101

!       otherwise, convergence has been reached


!       set future (2) desiccant conditions (Wd & Td) equal to be new current(1)
!       conditions
        Wd(n,j,1)=Wd(n,j,2)
        Td(n,j,1)=Td(n,j,2)

        END DO loop3


        RETURN

102     continue

        IF(errmax.gt.0.0001)THEN
        WRITE(*,103)maxite,tau,n,j,k,errmax,Wdavg
        WRITE(10,103)maxite,tau,n,j,k,errmax,Wdavg
103     FORMAT('*** process convergence not reached',I4,1x,'iterations',2x,'tau=
     ',F8.3,2x,'n=',1x,I3, &
        'j= ',1x,I3,2x,'k= ',1x,I3,2x,'errmax= ',F8.5,2x,'Wdavg= ',F8.5)
        END IF

        END SUBROUTINE process



        subroutine regen
!       this subroutine sets up the matrix for wedges in the process stream.

        USE global
        REAL(8) iads,iadso,kfda
        REAL(8) Wdavg,Tdavg,wfavg,tfavg,weo,Wds
        EXTERNAL iads,cpwvT,cpdaT,kfda

!       establish do loop to solve for every axial position
        Loop4: DO j=nx,1,-1

!       apply appropriate boundary condition
        IF(j.eq.nx)THEN
        tf(n,j+1)=tfri
        wf(n,j+1)=wfri
```

```
        END IF

!       make initial guess across element
        tf(n,j)=tf(n,j+1)
        wf(n,j)=wf(n,j+1)
        Td(n,j,2)=Td(n,j,1)
        Wd(n,j,2)=Wd(n,j,1)

        iter=0

201     CONTINUE

!       calculate differential coefficients
        Wdavg=.5*(Wd(n,j,1)+Wd(n,j,2))
        Tdavg=.5*(Td(n,j,1)+Td(n,j,2))
        wfavg=.5*(wf(n,j)+wf(n,j+1))
        tfavg=.5*(tf(n,j)+tf(n,j+1))

        kf=kfda(tfavg)

        hqfd=nufd*kf/dh

        cpda=cpdaT(tfavg)
        cpwv=cpwvT(tfavg)

!       solve for equilibrium humidity ratio
        CALL eqhr(Wdavg,Tdavg,wfavg,tfavg,weo)

!       solve for enthalpy of adsorption
        iadso=iads(Wdavg,Tdavg)

        cpm=cpdd+Wdavg*cplw
        cpma=cpda+wfavg*cpwv

        hmfd=hqfd/(cpma*Le**(1-nle))

        NTUhr=hqfd*asurfr/(mdar*(cpma))
        NTUmr=hmfd*asurfr/mdar


!       put in matrix notation

!       the remainder matrix
        b(1)=Wd(n,j,1)+(dtheta*wf(n,j+1))/(betar*gamr*dx)
        b(2)=NTUmr*dx*weo+(1-NTUmr*dx/2.)*wf(n,j+1)
        b(3)=Td(n,j,1)+(dtheta)/(dx*betar*gamr*cpm)*(cpma*tf(n,j+1)+&
        iadso*wf(n,j+1))
        b(4)=(1.-NTUhr*dx/2.)*tf(n,j+1)+NTUhr*dx/2*Td(n,j,1)

!       the "A" matrix
!       mass conservation equation
        A2(1)=1.0
        A3(1)=dtheta/(betar*gamr*dx)

!       mass rate
```

```
      A1(2)=0.
      A2(2)=(1.+NTUmr*dx/2)
      A3(2)=0.

!     energy conservation
      A1(3)=(dtheta*iadso)/(dx*betar*gamr*cpm)
      A2(3)=1.0
      A3(3)=(dtheta*cpma)/(dx*betar*gamr*cpm)

!     energy rate
      A1(4)=-NTUhr*dx/2.
      A2(4)=(NTUhr*dx/2.+1.)

!     possible solution
      x(1)=Wd(n,j,2)
      x(2)=wf(n,j)
      x(3)=Td(n,j,2)
      x(4)=tf(n,j)

!     solve the matrix
      CALL tridag

!     make sure variables do no go below zero
      IF(x(1).lt.1E-10)x(1)=1E-10
      IF(x(2).lt.1E-10)x(2)=1E-10
      IF(x(3).lt.1E-10)x(3)=1E-10
      IF(x(4).lt.1E-10)x(4)=1E-10


      Wd(n,j,2)=x(1)
      wf(n,j)=x(2)
      Td(n,j,2)=x(3)
      tf(n,j)=x(4)

      iter=iter+1
      IF(iter.ge.maxite)GOTO 202

!     check for convergence
      IF(errmax.gt.epstri)GOTO 201

!     convergance has been reached


!     set future (2) desiccant conditions (Wd & Td) equal to be new current(1)
!     conditions

      Wd(n,j,1)=Wd(n,j,2)
      Td(n,j,1)=Td(n,j,2)

      END DO Loop4

      RETURN

202   continue

      IF(errmax.gt.00001)THEN
```

```fortran
      WRITE(*,203)maxite,tau,n,j,k,errmax
      WRITE(10,203)maxite,tau,n,j,k,errmax
203   FORMAT('*** regen convergence not reached',i4,5x,'iterations',2x,'tau= ',F10.3,2x,'n= ',I3, &
      2x,'j= ',I3,2x,'k= ',1x,I3,2x,'errmax= ',F8.5)
      END IF

      END SUBROUTINE regen




      SUBROUTINE eqhr(Wdavg,Tdavg,wfavg,tfavg,weo)
!     this subroutine returns the equilibrium humidity ratio for a given
!     point using the parabolic concentration profile (PCP)

      USE global
      REAL(8) Wdavg,Tdavg,wfavg,tfavg,weo,a2c,xacc
      REAL(8) Wds,Dseff,we,RHe,cpdaT,cpwvT,succes,x1,x2
      EXTERNAL Dseff,we,RHe,cpdaT,cpwvT

      xacc=1E-6
      x1=0.0
      x2=.01
      biter=0
      Dseffo=Dseff(Wdavg,Tdavg)
      cpda=cpdaT(tfavg)
      cpwv=cpwvT(tfavg)



      CALL bracket(Wdavg,Tdavg,wfavg,weo,x1,x2,succes)


       a2c=bis(Wdavg,Tdavg,wfavg,weo,x1,x2,xacc)

      CALL a2sub(Wdavg,Tdavg,wfavg,weo,a2c)

!     check coefficients



      RETURN
      END SUBROUTINE eqhr




      SUBROUTINE bracket(Wdavg,Tdavg,wfavg,weo,x1,x2,succes)
!     this subroutine puts the solution root in a bracket

      USE global

      INTEGER NTRY
      REAL(8) Tdavg,wfavg,Wdavg,weo
      REAL(8) x1,x2,a2sub,FACTOR
      EXTERNAL a2sub
      PARAMETER (FACTOR=1.6,NTRY=50)
```

```fortran
      INTEGER pj
      REAL(8) f1,f2
      LOGICAL succes


      IF(x1.eq.x2)pause 'you have to guess an initial range'
      f1=x1-a2sub(Wdavg,Tdavg,wfavg,weo,x1)
      f2=x2-a2sub(Wdavg,Tdavg,wfavg,weo,x2)
      succes=.true.
      Loop1:  DO pj=1,NTRY

!

            IF(f1*f2.lt.0.0 .AND. ABS(f1).gt.1E-4 .AND. ABS(f2).gt.1E-4)THEN
            RETURN
            END IF
            IF(ABS(f1).lt.ABS(f2))THEN
                  x1=x1+FACTOR*(x1-x2)
                  f1=x1-a2sub(Wdavg,Tdavg,wfavg,weo,x1)
            ELSE
                  x2=x2+FACTOR*(x2-x1)
                  f2=x2-a2sub(Wdavg,Tdavg,wfavg,weo,x2)
            END IF

      END DO Loop1
      succes=.false.

      WRITE(*,1) pj,x1,x2,f1,f2
      WRITE(10,1) pj,x1,x2,f1,f2
1     FORMAT('bracket did not find the range',3x,'pj=',I3,2x,'x1=',F8.4,2x, &
      'x2=',2x,F8.4,'f1=',F8.4,'f2=',F8.4)



      RETURN
      END SUBROUTINE bracket



      FUNCTION bis(Wdavg,Tdavg,wfavg,weo,x1,x2,xacc)

!     this function uses the bisection method to locate the root
!     between a known interval

      USE global

      INTEGER BJMAX
      REAL(8) x1,x2,xacc,a2sub,bis
      REAL(8) Wdavg,Tdavg,wfavg,weo
      EXTERNAL a2sub
      PARAMETER (BJMAX=40)
      INTEGER bj
      REAL(8) dxb,f,fmid,xmid

      fmid=x2-a2sub(Wdavg,Tdavg,wfavg,weo,x2)
```

```fortran
        f=x1-a2sub(Wdavg,Tdavg,wfavg,weo,x1)
        IF(f*fmid.ge.0.0)pause 'root must be bracketed'
        IF(f.lt.0.0)THEN
                bis=x1
                dxb=x2-x1
        ELSE
                bis=x2
                dxb=x1-x2
        ENDIF

!       bisection loop
        Loop1: DO bj=1,BJMAX
                dxb=dxb*.5
                xmid=bis+dxb
                fmid=xmid-a2sub(Wdavg,Tdavg,wfavg,weo,xmid)
                IF(fmid.le.0.0)bis=xmid
                IF(ABS(dxb).lt.xacc .OR. fmid.eq.0.0)RETURN

        ENDDO Loop1


        END FUNCTION bis



        FUNCTION a2sub(Wdavg,Tdavg,wfavg,weo,a2x)
!       this function calculates the a2 coefficient

        USE global
        REAL(8) Tdavg,wfavg,Wdavg,weo,a2x,a2sub
        REAL(8) Wds,we
        EXTERNAL we

        cpma=cpda+weo*cpwv
        hmfd=hqfd/((cpma)*Le**(1-nle))

!       spherical model
        a2coeff=-((hmfd*rad)/(2.0*rhop*Dseffo))

        Wds=Wdavg+0.4*a2x
        weo=we(Wds,Tdavg)
        a2sub=a2coeff*(weo-wfavg)



        RETURN
        END FUNCTION a2sub



        FUNCTION cpdaT(tfavg)
!       this functions calculates the specific heat of dry air at
!       ambient pressure given the dry air temperature

        USE global
        REAL(8) cpdaT,tfavg
```

```fortran
cpdaT=-4.37E-10*(tfavg)**3+9.24542E-7*(tfavg)**2-0.0004077182*tfavg+1.05729181


RETURN
END FUNCTION cpdaT




FUNCTION cpwvT(tfavg)
!       this function calculates the specific heat of water vapor at low
!       pressures given the temperature of the water vapor

REAL(8) cpwvT,tfavg

cpwvT=1.043E-7*(tfavg)**3-8.4987E-5*(tfavg)**2+0.02373391*tfavg-0.41545460


RETURN
END FUNCTION cpwvT


FUNCTION Dseff(Wdds,Tdavg)
!       effective diffusivity of RD silica gel, grade 03
!       inputs:
!       Wd-bulk mass fraction of water to desiccant (kgw/kgdd)
!       Td-temperature
!       output:
!       Dseff - effective diffusivity (sq-m/s)

USE global
REAL(8) Wdds,Tdavg
REAL(8) iadso,iads,Dseff
REAL(8) Dso,tort
EXTERNAL iads

DATA Dso,tort/1.6E-6,2.8/

iadso=iads(Wdds,Tdavg)
Dseff=Dso/tort*DEXP(-.974*iadso/(Tdavg))


RETURN
END FUNCTION Dseff




FUNCTION iads(Wdavg,Tdavg)
!       this function calculates the enthalpy of adsorption
!       using the Clausis-clapeyron equation and the adsorption isotherm
!       for RD silica gel No.3
!       input:
!       Wd-bulk mass fraction of water to desiccant (kgw/kgdd)
!       Td-desiccant temperature
!       output:
!       iad-enthalpy of adsorption (kJ/kg)
```

```fortran
      REAL(8) Wdavg,Tdavg
      REAL(8) iads,ifgo,ifg
      EXTERNAL ifg

      ifgo=ifg(Tdavg)
      iads=ifgo*(1.+.2843*dexp(-10.28*Wdavg))

      RETURN
      END FUNCTION iads




      FUNCTION ifg(Tdavg)
!     calculates the enthalpy of vaporization as a function of temperature
!     using the Clausius-clapeyron equation
!     input:
!     Tdavg - temperature
!     ouput:
!     ifg - enthalpy of vaporization (kJ/kg)

      USE global
      REAL(8) Tdavg
      REAL(8) ifg,dpvsdT,pvsat
      EXTERNAL dpvsdT,pvsat
!     convert temp to celsius for this equation and divide by 1000 to convert
!     to kJ
      ifg=dpvsdT(Tdavg)*Rwv*(Tdavg**2)/pvsat(Tdavg)




      RETURN
      END FUNCTION ifg




      FUNCTION we(Wds,Tdavg)
!     this function calculates the equilibrium air humidity ratio
!     given the equilibrium relative humidity and saturation vapor pressure

      USE global
      REAL(8) Wds,Tdavg,PV,PVp,RHe,psat
      EXTERNAL pvsat,PVp,RHe

!     PV=PVp(Wds,Tdavg)

      psat=pvsat(Tdavg)
      IF(psat.gt.0.95)psat=0.95


      RH=RHe(Wds,Tdavg)
      we=(.622*RH*psat)/(pa-RH*psat)
      IF(we.lt.1.0E-15)we=1.0E-15


      RETURN
```

```fortran
        END FUNCTION we




        FUNCTION pvsat(Tdavg)
!       this function calculates the saturation vapor pressure in atmospheres for a
!       given temperature in degrees Kelvin using the Hyland-Wexler equations in ASHRAE,1993

        USE global
        REAL(8) Tdavg
        REAL(8) c8,c9,c10,c11,c12,c13
        DATA c8,c9,c10,c11,c12,c13/-5.8002206E3,-5.5162560,-4.8640239E-2, &
        4.1764768E-5,-1.4452093E-8,6.545973/

        atmp=82.5
        pvsat=DEXP(c8/Tdavg+c9+c10*Tdavg+c11*Tdavg**2+c12*Tdavg**3+c13*DLOG(Tdavg)
)/atmp

        RETURN
        END FUNCTION pvsat




        FUNCTION dpvsdT(Tdavg)
!       derivative of the Heyland-Wexler saturation curve wrt Temperature
!       inputs:
!       temp(K)
!       outputs:
!       dPwsat/dT
        USE global
        REAL(8) Tdavg,dpvsdT
        REAL(8) c8,c9,c10,c11,c12,c13
        DATA c8,c9,c10,c11,c12,c13/-5.8002206E3,-5.5162560,-4.8640239E-2, &
        4.1764768E-5,-1.4452093E-8,6.545973/


        atmp=82.5
        dpvsdT=EXP(c8/Tdavg+c9+c10*Tdavg+c11*Tdavg**2+c12*Tdavg**3+c13*DLOG(Tdavg)
)/atmp* &
    (-c8*Tdavg**-2+c10+2*c11*Tdavg+3*c12*Tdavg**2+c13/Tdavg)

        IF(dpvsdT.lt.1E-25)dpvsdT=1E-25
!       WRITE(*,1)Tdavg,dpvsdT
!       WRITE(10,1)Tdavg,dpvsdT
!1      FORMAT(/,'dPvsdT subroutine',2x,'Tdavg=',F8.3,2x,'dpvsdT=',F8.3)
!       STOP
!       END IF



        RETURN
        END FUNCTION dpvsdT
```

```fortran
      FUNCTION RHe(Wds,Tdavg)
!     this function uses the adsorption isotherm to calculate the
!     equilibrium relative humidity from the desiccant water content W, and
!     desiccant temperature, Td
!     RD silica gel grade 03

      USE global
      REAL(8) Wds,Tdavg
      REAL(8) RHe
      REAL(8) hstar,psat,pvsat
      EXTERNAL pvsat

      psat=pvsat(Tdavg)
      IF(psat.gt.0.95)psat=0.95

      hstar=1.0+.2843*DEXP(-10.28*Wds)
      RHe=((2.112*Wds)**hstar)*((29.91*psat)**(hstar-1))

      IF(RHe.lt.1.0E-15)RHe=1.0E-15
      IF(RHe.gt.0.95)RHe=0.95


      RETURN
      END FUNCTION Rhe



      FUNCTION kfda(temp)
!     this subroutine provides the thermal conductivity of air
!     given the air temperature.  It uses a second order curve fit to
!     the air properties data from Incropera and Dewitt.
      USE global
      REAL(8) kfda,temp

      kfda=-3.269E-11*(Temp)**2+9.799051E-8*Temp-1.6675824E-7


      RETURN
      END FUNCTION kfda



      SUBROUTINE tridag
!     Solves for a vector x(1:n) of length n the tridiagonal linear set
!     given by equation (2:4:1).  A1(1:n), A2(1:n), A3(1:n), and b(1:n) are
!     input vectors and are not modified.  Parameter: NMAX is the maximum
!     expected value of s.

      USE global
      INTEGER s
      REAL(8) bet,gam(4),err,errcnv
      REAL(8) xl(4)
!     one vector of workspace, gam is needed.
      IF(A2(1).eq.0)PAUSE 'tridag: rewrite equations'
```

```fortran
!       If this happens then you should rewrite your equations as a set of
!       order 4-1, with u2 trivially eliminated.

        bet=A2(1)
        x(1)=b(1)/bet
Loop1:  DO s=2,4
                gam(s)=A3(s-1)/bet
                bet=A2(s)-A1(s)*gam(s)
                IF(bet.eq.0.)PAUSE 'tridag failed'
                x(s)=(b(s)-A1(s)*x(s-1))/bet




END DO Loop1
Loop2: DO s=4-1,1,-1
                x(s)=x(s)-gam(s+1)*x(s+1)
END DO Loop2

IF(tau.eq.45.0 .AND. n.eq.157 .AND. j.eq.16)THEN
!       check to see what matrix looks like
        iter=iter+0
        END IF

        errmax=0.0

!       calculate error relative to last iteration
        Loop3: DO r=1,4
        err=DABS(2*(xl(r)-x(r))/(xl(r)+x(r)))
        errmax=DMAX1(err,errmax)
        END DO Loop3

        xl=x

        RETURN
        END SUBROUTINE tridag




        subroutine outlet
!       this subroutine calculates the average output of the process and
!       regeneration streams.

        USE global
        EXTERNAL enthalpy

!       initialize outlet variables
        tfpo=0.0
        wfpo=0.0
        tfro=0.0
        wfro=0.0

!       obtain a unique wedge
        Loop2: DO n=1,ntheta
```

```
!        determine the circumferential position of each wedge
!        based on the n=1 (k1) wedge
         k=k1+(n-1)


!        reset k back to one if greater than ntheta
         IF(k.gt.ntheta)THEN
         k=k-ntheta
         END IF


!        determine whether each wedge is in process or regen stream
         IF(k.le.kpr)THEN
!        wedge is in the process stream
         tfpo=tf(n,nx+1)+tfpo
         wfpo=wf(n,nx+1)+wfpo
         ELSE
!        if k>kpr, wedge is in the regen stream
         tfro=tf(n,1)+tfro
         wfro=wf(n,1)+wfro
         END IF

         END DO Loop2

!        average the outlet values of each wedge for each period

         tfpo=tfpo/kpr
         wfpo=wfpo/kpr
         tfro=tfro/(ntheta-kpr)
         wfro=wfro/(ntheta-kpr)


!        mrc is expressed in terms of kgw/hr as per ARI Std 940
         mrc=mdap*3600*(wfpi-wfpo)


         enthpi=enthalpy(tfpi,wfpi)
         enthri=enthalpy(tfri,wfri)
         enthpo=enthalpy(tfpo,wfpo)
         enthro=enthalpy(tfro,wfro)


         Epi=mdap*enthpi
         Eri=mdar*enthri
         Epo=mdap*enthpo
         Ero=mdar*enthro



         RETURN
         END SUBROUTINE outlet




         Subroutine effect
!        subroutine to calculate the effectiveness of the rotary heat
!        and mass exchanger in terms of temperature only, moisture only, and
!        enthalpy.  It uses the inlet and outlet conditions of the process and
!        regen streams from subroutine outlet.
```

```fortran
      USE global
      REAL(8) cpmap,cpmar

      cpmap=cpda+((wfpi+wfpo)/2.)*cpwv
      cpmar=cpda+((wfri+wfro)/2.)*cpwv

!     temperature effectiveness
      IF(tfri.eq.tfpi)GOTO 1
      effpt=(mdap*cpmap*(tfpo-tfpi))/((MIN(mdap,mdar)*cpmap)*(tfri-tfpi))
      effrt=(mdar*cpmar*(tfro-tfri))/((MIN(mdap,mdar)*cpmar)*(tfpi-tfri))
1     continue

!     humidity ratio effectiveness
      effpw=(wfpo-wfpi)/wfpi
      effrw=(wfro-wfri)/wfri

!     MRC effectiveness
      effmrc=mrc/(3600*mdap*wfpi)

!     enthalpy effectiveness
      IF(Epi.eq.Eri)GOTO 2
      effenthp=(Epi-Epo)/DABS(Epi-Eri)
      effenthr=(Eri-Ero)/DABS(Epi-Eri)
2     continue

      RETURN
      END SUBROUTINE effect




      SUBROUTINE balance
!     this subroutine is for checking the H20 mass and energy balance
!     where the mass or energy out is in the numerator and the mass or
!     energy in is in the denominator

      USE global

      H20massbal=DABS((mdap*(wfpo-wfpi))/(mdar*(wfro-wfri)))

      TotH20bal=DABS((mdap*wfpo+mdar*wfro)/(mdap*wfpi+mdar*wfri))

      energybal=DABS((Epo-Epi)/(Ero-Eri))

      RETURN
      END SUBROUTINE balance




      FUNCTION enthalpy(tfx,wfx)
!     this subroutine calculates the enthalpy of an airstream using
!     the temperature and moisture content of the air.

      USE global
      REAL(8) ifg,tfx,wfx,cpdaT,cpwvT
      EXTERNAL ifg,cpdaT,cpwvT
```

258

```
cpda=cpdaT(tfx)
cpwv=cpwvT(tfx)
enthalpy=(cpda*(tfx-tref)+wfx*(cpwv*(tfx-tref)+ifg(tfx)))

RETURN
END FUNCTION enthalpy
```

BIBLIOGRAPHY

ARI Standard 410-91, Forced Circulation Air Cooling And Air-Heating Coils, 1991, Air Conditioning And Refrigeration Institute, Arlington, VA.

ARI Standard 940, Desiccant Dehumidification Components, 1998, Air Conditioning And Refrigeration Institute, Arlington, VA.

ASHRAE 62-1989, Indoor Air Quality Standards, ASHRAE, Atlanta, GA.

ASHRAE Fundamentals, 1993, ASHRAE, Atlanta, Georgia.

ASHRAE Standard 139P (draft), 1995, ASHRAE, Atlanta, Georgia.

Banks, N.J., 1992, "Field Test of a Desiccant-Based HVAC System for Hotels," ASHRAE Transactions, Vol 98, Pt. 2, AN-92-19-4, pp. 1303-1310.

Banks, P. J.; 1985, "Prediction of Heat and Mass Regenerator Performance Using Nonlinear Analogy Method: Part 1 -Basis", Journal of Heat Transfer, Vol. 107, pp. 222-229.

Banks, P. J.; Feb 1985, "Prediction of Heat and Mass Regenerator Performance Using Nonlinear Analogy Method: Part 2 - Comparison of Methods", Journal of Heat Transfer, Vol. 107, No. 1; pp. 230-238.

Banks, P.J., 1972, "Coupled Equilibrium Heat and Single Adsorbate Transfer in Fluid Flow Through a Porous Medium-I. Characteristic Potentials and Specific Capacity Ratios," Chemical Engineering Science, Vol 27, pp 1143-1155.

Barker, J.M.; Kettleborough, C.F.; 1980, "Adiabatic Adsorption-Desorption Characterisitics of Silica Gel Beds—2. Curve Fits, ASME Winter Annual Meeting, Nov 1980. New York, NY: American Society of Mechanical Engineers, pp. 80-WA/Sol-30.

Barlow, R.S.; Dec 1982, Analysis of the Adsorption Process and of Desiccant Cooling Systems: A Pseudo-Steady-State Model for Coupled Heat and Mass Transfer, SERI/TR-631-1330. Solar Energy Research Inst, Golden, CO (USA).

Burns, P.R., Mitchell, J.W., Beckman, W.A., 1985, "Hybrid Desiccant Cooling Systems in Supermarket Applications," ASHRAE Transactions, Vol 91, CH-85-09, No. 5, pp. 457-467.

Bullock, C. E., Threlkeld, J. L., 1966, "Dehumidification of Moist Air by Adiabatic Adsorption," ASHRAE Transactions, 1966, vol 72, No. 1986, pp 301-313.

Brandemuehl, M.J., 1982, Analysis of Heat and Mass Transfer Regenerators with Time Varying or Spatially Non-uniform Inlet Conditions, Ph.D. Thesis, Department of Mechanical Engineering, University of Wisconsin, Madison, Wisconsin.

Carter, J.W., 1966, "A Numerical Method for Prediction of Adiabatic Adsorption in Fixed Beds," Transactions Institution of Chemical Engineers, Vol 44, pp. T253-259.

Cassie, A.B., 1940, "Absorption of Water Vapor by Wool Fibers, Part II—Theory of Propagation of Temperature Change," Trans. Faraday Soc., Vol A229, 281.

Chant, E.,E., 1991, Transient and Steady-State Simulations of an Advanced Desiccant Enhanced Cooling Cycle, Ph.D. Thesis, Georgia Institute of Technology, Atlanta, Georgia.

Collier, R.K., Cale, T.C., and Lavan, Z., 1986, "Advanced Desiccant Materials Assessment," GRI-8610181, Chicago Gas Research Institute.

Coppage, J.E., London, A.L., "The Periodic-Flow Regenerator-A Summary of Design Theory", Transactions of the ASME, July 1953, pp 779-787.

Cromer, C.J., 1988, "Experimental Determination of the Performance of Desiccant-Enhanced Electric Air Conditioning," Florida Solar Energy Center, Cape Canaveral, FL, FSSEC-CR-349-90.

Cromer, C.J., 1988 "Dehumidification Enhancement of Air Conditioners by Desiccant Moisture Exchange," Florida Solar Energy Center, Cape Canaveral, FL., June 1988, DOE #DE-FC03-865F16305.

Cromer, C.J., August 1998, phone conversation.

Do, D.D., Rice, R.G., 1986, "Validity of the Parabolic Profile in Adsorption Studies," AICHE Journal, Vol 32, No. 1, pp. 149-154.

Gatley, D.P., 1992, "Designing for Comfortable Cooling Season Humidity in Hotels," ASHRAE Transactions: Symposia, Vol 98, Pt 2, AN-92-18-3, pp 1293-1302.

Gilliland, E.R., Baddour, R..F., Perkinson, G.P., and Sladek, K., J., 1974, "Diffusion on Surfaces. I. Effect of Concentration on the Diffusivity of Physically Adsorbed Gases," Industrial Engineering and Chemistry Fundamentals, Vol 13, No. 2, pp. 95-100.

Hausen, H., 1929, "Uber die Theorie des Warmeastausches in Regenetorem, " Z. agnew. Math. Mech., Vol 9, 173.

Henry, P. S., "Diffusion in Absorbing Media," Proc. R. Soc. ser. A, Vol. 171, 215 (1939)

Holman, J.P, 1976, Heat Transfer, McGraw-Hill, New York.

Homan, J.P., 1989, Experimental Methods for Engineers, McGraw-Hill, New York.

Holmberg, R.B., 1979, "Combined Heat and Mass Transfer in Regenerators with Hygroscopic Materials," ASME Journal of Heat Transfer, Vol 101, pp. 205-210.

Hougen, O.A., Watson, K.M., 1943, Chemical Process Principles, John Wiley & Sons, Inc., London.

Hubbard, S. H., 1954, "Equilibrium Data for Silica Gel and Water Vapor," Industrial and Engineering Chemistry, February 1954, Vol 46, No. 2, pp. 356-358.

Incropera, F. P., DeWitt, D.P.,1986, Fundamentals of Heat and Mass Transfer, Wiley, NewYork.

Jurinak, J.J., 1982, Open Cycle Desiccant Cooling-Component Models and System Simulations, Ph.D. Thesis, University of Wisconsin at Madison, Wisconsin.

Kays, W.M., London, A.L., 1984, Compact Heat Exchangers, 3rd Edition, McGraw-Hill, NY.

Kosar, D.,R., Witte, M.J., Ph.D., Shirey, D.B. III, Hedrick, R.L., 1998, "Dehumidification Issues of Standard 62-1989," ASHRAE Journal, Vol. 40, No. 3, pp. 71-75.

Lambertson, T.J., "Performance Factors for a Periodic-Flow Heat Exchanger," 1958, Transactions of the ASME, April 1958, pp 586-592.

Lavan, Z., Monnier, J.B., Worek, W.M., 1982, "Second Law Analysis of Desiccant Cooling Systems," Journal of Solar Energy Engineering, Vol 104, pp. 229-236.

Maclaine-cross, I.L., Banks, P.J., 1972, A theory of Combined Heat and Mass Transfer in Regenerators, Ph.D. dissertation, dept. of Mech. Engr., Monash University (1974).

Maclaine-cross, I.L., Banks, P.J., 1972, "Coupled Heat and Mass Transfer in Regenerators-Predictions Using an Analogy with Heat Transfer," International Journal of Heat and Mass Transfer, Vol 15, pp 1225-1242.

Maclaine-cross, I.L., 1988, "Proposal for a Hybrid Desiccant Air-Conditioning System," ASHRAE Transactions, OT-88-19-1, pp. 1997-2009.

Mathiprakasam, B., Lavan, Z, 1980, Performance Predictions for Adiabatic Desiccant Dehumidifiers Using Linearized Solutions," Journal of Solar Energy Engineering, Vol 102, pp. 73-79.

Meckler, Milton, "Integrated Desiccant Cold Air Distribution System," ASHRAE Transactions, Vol. 95, Pt. 2, VA-89-21-1, pp. 1085-1097.

Moeller, T., Bailar, J.C., Kleinberg, J., Guss, C.O., Castellion, M.E., Metz, C., 1980, Chemistry with Inorganic Analysis, Academic Press, NY.

Nimmo, B.G., Collier, R.K., Renegarajan, K., 1993, "DEAC: Desiccant Enhancement of Cooling-Based Dehumidification," ASHRAE Transactions, Vol 99, Pt. 1, CH-93-4-4, pp. 842-848.

Odom III, J.D., and Dubose, G.H., Nelson, N.L., "Designing and Constructing Mildew-Free Hotels," ASHRAE Transactions, Vol. 98, AN-92-18-1, pp. 1275-1281.

Ozisik, M. Necati, 1994, Finite Difference Methods in Heat Transfer, CRC Press, Ann Arbor, MI

Pesaran, A.A., and Mills, A.F., 1984, "Modeling of Solid-side Mass Transfer Desiccant Particle Beds," Solar Engineering, 1984, Proceedings of the ASME Solar Division Sixth Annual Conference, Las Vegas, ASME New York, pp. 177-185.

Pesaran, A.A., Mills, A.F., 1987, "Moisture Transport in Silica Gel Packed Beds –II. Experimental Study," International Journal of Heat and Mass Transfer, Vol 30, No 6, pp 1051-1060.

Pesaran, A.A., Mills, A. F., 1987, "Moisture Transport in Silica Gel Packed Beds-I. Theoretical Study," International Journal of Heat and Mass Transfer, Vol 30, No. 6, pp 1037-1049.

Pesaran, A. A., and Bingham, C.E., 1989, "Testing of Novel Desiccant Materials and Dehumidifier Matrices for Desiccant Cooling Applications," ASHRAE Transactions, VA-89-21-3, pp. 1109-1115.

Pesaran, A. A., Penney, T.R., Czanderna, A.W., 1992, Desiccant Cooling: State-of-the-Art Assessment, National Renewable Energy Laboratory, contract DE-AC02-83CH10093.

Pla-Barby, F. E., 1978, Solid Desiccant Air Conditioning with Silica Gel Using Solar Energy, PhD Thesis, Austin, TX: University of Texas.

Press, William H., et. al., 1992, <u>Numerical Recipes in Fortran</u>: The Art of Scientific Computing, 2nd ed., Cambridge University Press.

Relwani, S.M., 1986, "Indoor Pollution Control Capabilities of Desiccant Dehumidifier System," ITT Research Institute, GRI-86/0200.

Rosen, J.B., 1951, "Kinetics of a Fixed Bed System for Solid Diffusion into Spherical Particles," The Journal of Chemical Physics, Vol 20, No 3., p 387.

Ruthven, 1984, <u>Principles of Adsorption and Adsorption Processes</u>, Wiley and Sons, New York.

Ryan, J., "Summary Sheet of Advanced HVAC Test Facility at NREL Thermal Test Facility, Golden, CO."

Slayzak, S.J., Pesaran A.A., Hancock, C.E., "Experimental Evaluation of Commercial Desiccant Dehumidifier Wheels," NREL paper NREL/TP-471-21167, May 1996.

Slayzak, Steven J. and Ryan, Joseph P., "Instrument Uncertainty Effect on Calculation of Absolute Humidity Using Dewpoint, Wet-bulb, and Relative Humidity Sensors," NREL paper NREL/CP-550-24523, April 1998.

Schultz, K.J., 1987, <u>Rotary Solid Desiccant Dehumidifier</u>, Ph.D. Thesis, University of Wisconsin at Madison.

Slaydek, K.J., Gilliland, E.R., Baddour, R., F., 1974, "Diffusion on Surfaces. II Correlation of Diffusivities of Physically and Chemically Adsorbed Species," Industrial Engineering Chemistry Fundamentals, Vol 13, No. 2, pp. 100-105.

Shakun, W., 1992, "The Causes and Control of Mold and Mildew in Hot and Humid Climates," ASHRAE Transactions, Vol. 98, Pt 1, AN-92-18-2, pp. 1282-1291.

Van Den Bulck, E., Mitchell, J.W., and Klein, S.A., 1985, "Design theory for Rotary Heat and Mass Exchangers-I. Wave Analysis of Rotary Heat and Mass Exchangers with Infinite Heat Transfer Coefficients," International Journal of Heat and Mass Transfer, Vol 28, pp 1575-1586.

Van Den Bulck, E., Mitchell, J.W., and Klein, S.A., 1985, "Design theory for Rotary Heat and Mass Exchangers-II. Number of Transfer Units Method for Rotary Heat and Mass Exchangers," International Journal of Heat and Mass Transfer, Vol 28, pp 1587-1595.

Van Wylen , G.J., and Sonntag, R.E., 1976, <u>Fundamentals of Classical Thermodynamics</u>, Wiley, New York.

West, M.K., Iyer, S.V., 1995, "Analysis of a Field-Installed Hybrid Solar Desiccant Cooling System," ASHRAE Transactions, Vol 101, Pt. 2, CH-95-5-2, pp. 686-695.

Wilmott, A.J., Burns, A., 1977, "Transient Response of Periodic Flow Regenerators," International Journal of Heat and Mass Transfer, Vol. 20, pp. 753-761, Pergamon Press.

VITA

Stephen Delbert Grumbach was born on January 22, 1962 in Charleston, South Carolina. He graduated from Summerville High School in South Carolina in 1980. In 1984, he received his Bachelor of Science degree in Mechanical Engineering from Clemson University in South Carolina. He joined the United States Air Force in 1984 and completed an assignment at Nellis AFB, Nevada doing base level engineering design, analysis, and management from 1984 to 1988. In 1989 he completed a Master of Science Degree in Engineering Management from the Air Force Institute of Technology located in Dayton, Ohio. Following this, he completed Air Force assignments in Spangdahlem, Germany and San Antonio doing engineering supervision and management from 1989 to 1996. Stephen arrived at the University of Colorado, Boulder in August 1996 where he has completed the required coursework, exams, and the research described in this thesis to earn a doctorate of engineering degree.